Two-Loop Five-Point Amplitudes for Bosons and Partons in QCD

Dissertation

zur Erlangung des Doktorgrades der Fakultät für Mathematik und Physik der

Albert-Ludwigs-Universität
Freiburg im Breisgau

vorgelegt von

Maximilian Klinkert

November 2022

Research Group
Quantum Fields and
Particle Phenomenology

Dekan: Prof. Dr. Michael Thoss
Referent: Prof. Dr. Harald Ita
Koreferent: Prof. Dr. Stefan Dittmaier
Tag der mündlichen Prüfung: 23. Februar 2023

Abstract

In this thesis, we develop and apply methods which allow to compute multi-scale two-loop amplitudes in analytic form. These amplitudes are an important ingredient for precise theoretical predictions for scattering processes at the Large Hadron Collider. We develop new approaches to construct unitarity compatible integration-by-parts relations through generating vectors by using an embedding space formulation of the problem and combining methods from algebraic geometry with linear algebra. With these methods, we obtain relations that can be used to reduce planar and non-planar two-loop amplitudes with up to one external mass to master integrals. We use these relations together with the method of numerical unitarity to numerically obtain master integral decompositions of the planar two-loop amplitudes contributing to $W(\to \ell\nu)$-production in association with two jets, the planar and non-planar amplitudes contributing to three-photon production and the amplitudes contributing to Higgs-production in association with two jets at leading colour and in the heavy-top-loop approximation. Furthermore, the W+jets amplitudes and the 3γ amplitudes are obtained analytically via functional reconstruction in a finite field together with some physically motivated improvements.

Contents

1 Introduction **1**

1.1 Motivation . . . 1

1.2 Short Introduction to the Standard Model . . . 4

1.2.1 Lagrangian Mechanics & Gauge Theories . . . 4

1.2.2 The Gauge-Group & Field Content of the SM . . . 7

1.2.3 Spontaneous Symmetry Breaking . . . 9

1.3 Quantisation . . . 11

2 Scattering Amplitudes & Feynman Rules **15**

2.1 Correlation Functions . . . 15

2.1.1 Feynman-Rules . . . 17

2.2 Lehmann-Symanzik-Zimmermann Reduction Formula . . . 18

2.3 Loop-Integrals . . . 21

2.3.1 Dimensional Regularisation . . . 22

2.4 Renormalisation . . . 25

2.4.1 Renormalisation of QCD . . . 25

2.4.2 Choice of the Renormalisation Scale & Running Couplings . . . 29

2.5 Cross-Sections from Scattering Amplitudes . . . 30

2.5.1 Final State Radiation . . . 30

2.5.2 Fixed-Order Computations . . . 31

2.5.3 Parton Model . . . 32

3 Multi-Loop Feynman-Integrals **34**

3.1 Integral Reduction . . . 34

3.1.1 Passarino-Veltmann Reduction . . . 36

3.1.2 Integral-Level Reduction . . . 38

3.2 The Differential Equation Approach to Master Integrals . . . 41

3.2.1 Differential Equations in Canonical Form 42

4 Integral Reduction via Generating Vectors 45
4.1 Integration-by-Parts Generating Vectors 45
4.1.1 Fixed Propagator Powers 45
4.1.2 Fixed Dimension in Baikov Coordinates 48
4.1.3 Embedding-Space Formulation 50
4.2 Constructing IBP-Vectors 56
4.2.1 Generic IBP-Vectors from Cramer's Rule 56
4.2.2 Gröbner Basis and Syzygies 57
4.2.3 Syzygies from Linear Algebra 66
4.2.4 Semi-Numeric IBP-Vectors 67
4.2.5 Semi-Numeric Power Reduction 68
4.3 Properties of IBP-Vectors 70
4.3.1 IBP-Vectors as Polynomial Tangent Vector Fields 71
4.3.2 IBP-Vectors at Extrema & Singularities of the Baikov Polynomial . 73
4.3.3 Gauge-Transformations of IBPs 75
4.4 Implementation & Validation 76

5 Multi-Loop Amplitude Computation 77
5.1 Colour-Ordering & Recursion Relations 77
5.1.1 Unitarity and Factorisation 79
5.2 Heavy-Top-Loop Approximation 80
5.3 Leading-Colour Approximation 81
5.4 Finite Remainders 83
5.5 Two-Loop Numerical Unitarity 85
5.5.1 Dimensions of Internal States 87
5.5.2 Remainders and Pentagon Functions 88
5.6 Analytic Reconstruction 88
5.6.1 Parametrisation in Terms of Mandelstam Invariants 89
5.6.2 Denominators from Univariate Slices 89
5.6.3 Linear Dependencies of Coefficients 91
5.6.4 Partial-Fraction Ansatz 92
5.6.5 Vandermonde Sampling Procedure 94
5.6.6 Spinor Reconstruction 96

6 Results 99
6.1 W-Boson + Four Partons 99
6.1.1 Notation & Conventions 100

6.1.2 Reduction to Five-Point One-Mass Kinematics . . . 101
6.1.3 Analytic Reconstruction . . . 104
6.1.4 Results and Validation . . . 106
6.2 Tri-Photon Production . . . 108
6.2.1 Helicity Amplitudes . . . 108
6.2.2 Results & Validation . . . 111
6.3 Surface-Terms for Higgs + Four Partons . . . 112
6.3.1 Notation and Conventions . . . 112
6.3.2 Surface Terms & Master-Integral Decomposition . . . 114

7 Conclusions and Outlook **115**
7.1 Conclusions . . . 115
7.2 Outlook . . . 116

Appendices

A QCD Feynman-Rules **118**

B Treatment of γ_5 in Dimensional Regularisation **120**

C Finite Fields **122**
C.1 Rational Reconstruction . . . 123
C.1.1 The Chinese Remainder Theorem . . . 123
C.1.2 Denominator Guessing & Integer Reconstruction . . . 124

D Interpolation Formulae **126**
D.1 Thieles Interpolation Formula . . . 126
D.2 Multivariate Newton Interpolation . . . 127

E Spinor Helicity Formalism **128**

F Rationalization of Momenta & tr_5 **130**
F.1 Five-Point Zero-Mass . . . 130
F.2 Five-Point One-Mass . . . 131

G Bibliography **132**

List of Abbreviations **155**

List of Figures **157**

List of Tables **160**

List of Publications **161**

Abstract in German **162**

Acknowledgements **163**

Chapter 1

Introduction

1.1 Motivation

The Standard Model of Particle Physics (SM) describes the fundamental forces of the electromagnetic, weak and strong interactions together with the fundamental constituents of matter, the quarks, leptons and neutrinos. It has demonstrated huge success in providing predictions for experiments. For instance, the existence and properties of the Higgs-, W- and Z-bosons and the running of coupling constants have been first predicted by the SM and then later were confirmed experimentally [1]. Nonetheless, observations e.g. from astrophysics have shown phenomena which are not explained by the SM, such as Dark Matter [2, 3], neutrino oscillations [4] and the matter-antimatter asymmetry in the universe [5]. Moreover, collider experiments have lead to a few experimental results which appear to differ from the SM prediction, such as the anomalous magnetic dipole moment of muons [6]. Furthermore, the SM includes a few ad hoc features such as the mass hierarchy of the fermions or the absence of a CP-violating term in QCD [7]. These features, although they are not problematic per se, hint towards an underlying structure which is not understood. These concerns and the so-far lacking description of gravity and dark energy within the SM demonstrate that the SM is not yet a complete description of nature and therefore, its predictions should be violated. These violations could either be pronounced but only visible at energies which are inaccessible for current collider experiments (energy frontier) or subtle deviations which can only be found via extremely accurate measurements and predictions (precision frontier).

The strongly interacting gluons and quarks form hadrons with binding energies of ≈ 1 GeV, which appear as point-like particles at lower energies. The W-, Z-, and Higgs bosons, on the other hand, have masses ranging from $80 - 125$ GeV and are therefore usually negligible at lower energies (β-decays are an exception). Hence, at the MeV-scale, physical phenomena are usually well-described by electromagnetic interactions. In order to reveal the full structure of fundamental interactions, experiments thus have to

be carried out with an energy transfer at GeV or higher scales[1]. Experiments in particle physics therefore typically involve accelerators which collide particles with large kinetic energy[2].

The current collider experiments at the Large Hadron Collider (LHC), in particular ATLAS and CMS have confirmed the SM including the Higgs boson and several predicted hadrons [1]. They did, however, not find clear violations of the SM predictions. Therefore, we are now in the *precision era* of the LHC, where theoretical predictions are compared to cross-section measurements with very low uncertainties.

Such precision comparison, even if it should not directly lead to discoveries of physics beyond the SM (BSM), can also constrain the energy scales where BSM physics can be expected. These can then in turn be used to plan future colliders at certain energy scales. For example, the LEP experiment at CERN permitted to conclude that the Higgs boson was heavier than 114 GeV (see e.g. [8]). At the beginning of the third run of the LHC, the statistical errors for many cross-section measurements are as small as a few percent (see e.g. [1] and the references therein), which is expected to further improve within this run and, even more, with the planned High-Luminosity LHC. Theory predictions should therefore reach a comparable level of accuracy. In order to achieve this, higher-order corrections in the perturbative expansion of cross-section predictions have to be taken into account. The electromagnetic coupling constant $\alpha_{\text{em}}(0) = 1/137$, or $\alpha_{\text{em}}(1\text{TeV}) = 1/125$ is relatively small at the energy scales of current colliders. Thus, predictions with next-to-leading-order (NLO) corrections are often sufficient in the electroweak sector[3]. However, in the expansion of the strong interaction, at least next-to-next-to-leading-order (NNLO) corrections are required, due to the relatively large coupling constant $\alpha_{\text{s}}(91\text{GeV}) = 0.118$ or $\alpha_s(1\text{TeV}) = 0.089$. While today the computation of next-to-leading-order corrections is largely automatised (see e.g references [10–21]), next-to-next-to-leading-order corrections still remain an active area of research, although many $2 \to 2$ (see e.g. [22–26]) processes and some $2 \to 3$ processes [27, 28] have been calculated during the last years.

One of the most intricate problems in the process of providing higher order QCD predictions is the computation of two-loop scattering amplitudes. In recent years, this field experienced substantial progress on the two fundamental aspects of the calculation. First, there have been important advances in computing the required master integrals, specifically using the methods of differential equations [29,30] in their canonical form [31]. Combining this method with Ansatz techniques [32] has led to the computation of all five-point massless and all planar five-point one-mass master integrals [33–36] as well as most of the non-planar five-point one-mass master integrals [37]. Furthermore, there now exist

[1] Therefore particle physics is often also called *high energy physics*.

[2] A complementary branch of particle physics called *astro-particle physics* instead studies particles from astronomical origins.

[3] In some kinematic regions, *Sudakov logarithms* $\log s/M_W$ can enhance EW corrections [9], making additional corrections necessary.

multiple frameworks for the numerical evaluation of master integrals, such as generalized series expansions [34,38–40], or iterated integral methods in the form of so-called *pentagon functions* [41–43].

On the second front, there have been important technical advances in the reduction of scattering amplitudes to master integrals through so-called integration-by-pars (IBP) reduction [44, 45], both in a simplified approach to the construction of IBP relations with unitarity-compatible techniques [46–48], as well as reconstructing the results from numerical evaluations over a finite field [49–53]. An improvement of these techniques is to build ansätze from studying the divergences of master integral coefficients near singular surfaces using $p-$adic numbers [54]. The direct numeric solution of IBP-systems can be computationally intense. As an alternative, the development of the multi-loop numerical unitarity method [48, 55–57], where loop amplitudes are numerically computed by exploiting their analytic properties has been an important step forward.

The focus of this thesis is to discuss methods of finding suitable sets of IBPs and their usage within the context of numerical unitarity, as well as methods of functional reconstruction of master integral coefficients. These methods are applied to cutting edge cases of two-loop amplitude computation, in particular the amplitudes contributing to W+2-jet production, 3γ production at the LHC. Furthermore, we present important steps towards computing amplitudes contributing to H+2-jet production.

The thesis is organised as follows: In the first chapter, we will review the Standard Model as a gauge theory, starting with the principles of relativistic field-theories before introducing the gauge group and field-content of the SM and spontaneous symmetry breaking via the Higgs mechanism. Furthermore, we will review the quantisation of gauge theories with Fadeev-Popov ghosts, leading to a gauge fixed effective SM-Lagrangian.

In the second chapter, we will review how scattering amplitudes are computed in the SM and how they are related to cross-sections. The discussion of amplitudes involves the computation of correlation functions from Feynman diagrams and -rules and the Lehmann-Symanzik-Zimmermann reduction formula. Furthermore, we will discuss how Feynman integrals arise in amplitude computations and how their divergences can be handled through dimensional regularisation and renormalisation. Finally, we will briefly review other aspects required for cross-section computations, such as defining infrared-save observables and parton-distribution functions.

In the third chapter, we will review modern methods for multi-loop integral computation, discussing their reduction both at integrand level through Passarino-Veltmann reduction and at integral level through integration-by-parts relations. Then, we will discuss how the remaining integrals can be computed with the method of differential equations.

In the fourth chapter, we discuss the construction of unitarity compatible IBPs. We will review aspects of algebraic geometry and discuss technical advances which allow to

construct sets of IBP-relations for challenging multi-scale integrals. Moreover, we will discuss some interesting properties of IBP vectors and the relations generated by them which are relevant for the study of Feynman integrals.

In the fifth chapter, we will discuss the computational setup we used for the computation of multi-loop amplitudes. As technical tools, we will review colour-decomposition and recurrence relations of tree-level amplitudes, before discussing the numerical unitarity method and functional reconstruction together with some physically motivated improvements.

We present two amplitude computations and first steps towards a third using these methods together with some process-dependent features in chapter 6 before coming to conclusions and an outlook.

1.2 Short Introduction to the Standard Model

Before discussing the computations of cross-sections and scattering amplitudes, we will review some basic principles of the underlying theory. In particular, we will review the gauge group and field content of the SM including spontaneous symmetry breaking and discuss its functional quantization in the path integral formalism. For further details, we refer the reader to the many excellent textbooks on the matter, such as [58, 59].

1.2.1 Lagrangian Mechanics & Gauge Theories

The SM is a local quantum field theory (QFT), whose interactions are governed by gauge principles. Relativistic QFT's can be described through a Lagrangian density $\mathcal{L}(x)$, which is a Poincaré-invariant and hermitian function of a set of fields $\{\varphi_i(x)\}$ and its derivatives[4] $\{\partial_\mu\varphi_i(x)\}$. Conventionally, the Lagrangian density is abbreviated as the Lagrangian. The time-evolution of the fields is then described by the Euler-Lagrange equations

$$\partial_\mu\left(\frac{\partial\mathcal{L}}{\partial(\partial_\mu\varphi_i)}\right)-\frac{\partial\mathcal{L}}{\partial\varphi_i}=0. \tag{1.1}$$

Poincaré invariance of $\mathcal{L}$ guarantees conservation of four momentum and angular momentum. For physical theories such as the SM, it is usually required that appearing ultraviolet (UV) divergencies can be absorbed into a redefinition of the fields and constants, so that predictions remain finite (see section 2.4). In natural units (i.e. $\hbar = 1$, $c = 1$, where $\hbar$ is the reduced Planck constant and c is the speed of light) this requires coupling constants to have mass dimensions greater than or equal to zero. In the following, we will briefly review the field content and the gauge structure of the SM.

[4] In principle a dependence on higher derivatiaves is also possible, however, we omit them here since first derivatives are sufficient to describe the SM.

The Lorentz group is described by six generators, three boosts K and three rotations L. This group can be represented using two commuting $SU_{\mathbb{C}}(2)$ subgroups, whose generators are given by

$$J_+^i = \frac{1}{2}(L^i + iK^i), \quad J_-^i = \frac{1}{2}(L^i - iK^i), \tag{1.2}$$

which fulfil the Lie-Algebra

$$[J_+^i, J_-^j] = 0, \ [J_\pm^i, J_\pm^j] = i\epsilon^{ijk} J_\pm^k. \tag{1.3}$$

Lorentz transformations are then expressed as $\Lambda = \mathrm{e}^{i(\theta_i^+ J_+^i + \theta_j^- J_-^j)}$, with $\theta^+ = (\theta^-)^*$. In the SM, there are four types of fields which can be classified according to their transformation properties under such a transformation:

- spin 0, scalar: $\phi(x) \to \phi(\Lambda^{-1}x)$,
- spin 1/2, *left-chiral* Weyl fermion [60]: $\xi^a \to \mathrm{e}^{i\theta_i^+ \frac{\sigma_i^{a\tilde{b}}}{2}} \xi_{\tilde{b}}(\Lambda^{-1}x)$, where $\xi_{\tilde{b}} = \delta_{a\tilde{b}}\xi^a$,
- spin 1/2, *right-chiral* Weyl fermion: $\chi^{\tilde{b}}(x) \to \mathrm{e}^{i\theta_i^- \frac{\sigma_i^{a\tilde{b}}}{2}} \chi_a(\Lambda^{-1}x)$, where $\chi_a = \delta_{a\tilde{b}}\chi^{\tilde{b}}$,
- spin 1, vector boson: $A_\mu(x) \to \Lambda_\mu^{\ \nu} A_\nu(\Lambda^{-1}x)$,

where σ_i are the Pauli matrices, which are conventionally chosen as

$$\sigma_1 = \begin{pmatrix} 0 & 1 \\ 1 & 0 \end{pmatrix}, \quad \sigma_2 = \begin{pmatrix} 0 & -i \\ i & 0 \end{pmatrix}, \quad \sigma_3 = \begin{pmatrix} 1 & 0 \\ 0 & -1 \end{pmatrix}. \tag{1.4}$$

Lorentz-vectors can also be expressed as a tensor product of left- and right-chiral Weyl-spinors via [61]

$$A_\mu = \sigma_\mu^{a\tilde{b}} \xi_a \chi_{\tilde{b}}, \tag{1.5}$$

where σ_0 is the identity matrix. Higher-dimensional representations of the Lorentz group, as they appear e.g. in theories of gravity, can be constructed from these lower dimensional representations in a similar way. Conventionally, a left- and right-chiral Weyl spinor are grouped together to a Dirac spinor[5]

$$(\psi_\alpha) = \begin{pmatrix} \xi^a \\ \chi_{\tilde{a}} \end{pmatrix} \qquad (\bar{\psi}^\alpha) = \begin{pmatrix} \chi_a & \xi^{\tilde{a}} \end{pmatrix}. \tag{1.6}$$

[5]In the literature, Dirac spinors are often defined in other representations, however, we stick to this so called *chiral representation* to keep the chiral structure of the SM as clear as possible.

In analogy to non-relativistic quantum mechanics, an equation of motion should result in $p\psi \propto \frac{\partial}{\partial x}\psi$, while at the same time preserving the relativistic condition that $p^2 = m^2$. In terms of Dirac-spinors, this is possible through the Dirac equation [62], which is the equation of motion for a relativistic spin 1/2 particle

$$i\gamma_\mu^{\alpha\beta}\partial^\mu\psi_\beta - m\delta^{\alpha\beta}\psi_\beta = 0, \tag{1.7}$$

using the Dirac-matrices which (in the chiral basis) are given by

$$\gamma^0 = \begin{pmatrix} 0 & \mathbb{1} \\ \mathbb{1} & 0 \end{pmatrix} \qquad \gamma^i = \begin{pmatrix} 0 & \sigma^i \\ -\sigma^i & 0 \end{pmatrix}. \tag{1.8}$$

These matrices fulfil the anti-commutation relations $\{\gamma_\mu, \gamma_\nu\} = 2g_{\mu\nu}$. The Dirac equation corresponds to the Lagrangian

$$\mathcal{L} = \bar{\psi}(i\not{\partial} - m)\psi, \tag{1.9}$$

where we used Feynman-slash notation, i.e. for any Lorentz vector A^μ, $\not{A} = \gamma_\mu A^\mu$. The basic principle of gauge theories is to start from such a Lagrangian of free fermionic fields which contains a global symmetry and then impose that this symmetry also holds locally, which can only be fulfilled by introducing additional bosonic fields [63, 64]. Such a symmetry transformation is described by a Lie group with generators T_a acting on the fields which transform as a representation of that group

$$\psi \to \mathrm{e}^{i\phi_a T^a}\psi, \quad \bar{\psi} \to \bar{\psi}\mathrm{e}^{-i\phi_a T^a}, \tag{1.10}$$

so that the Lagrangian remains constant $\mathcal{L} \to \mathcal{L}$. Locality of the symmetry is then imposed by making the transformation parameter space-time dependent

$$\psi \to \mathrm{e}^{i\phi_a(x) T^a}\psi, \quad \bar{\psi} \to \bar{\psi}\mathrm{e}^{-i\phi_a(x) T^a}. \tag{1.11}$$

This transformation is then referred to as a *gauge transformation*. Under such a transformation, the kinetic term is not left invariant but transforms as

$$\mathcal{L} \to \bar{\psi}(i\not{\partial} - m)\psi - \bar{\psi}\mathrm{e}^{-i\phi_a(x)T^a}(\partial_\mu\phi_a(x))T^a\mathrm{e}^{i\phi_a(x)T^a}\psi \neq \mathcal{L}. \tag{1.12}$$

The symmetry, however, can be restored by introducing an additional field A_μ^a which transforms as $A_\mu^a \to A^a + \frac{i}{g}\partial_\mu\phi_\mu^a T^a$ and replacing the derivative ∂_μ by the *covariant derivative*

$$D_\mu = \partial_\mu - igA_\mu^a T^a. \tag{1.13}$$

The resulting Lagrangian is invariant under gauge transformations. The Euler-Lagrange equations for A^a_μ, however, would require that $\bar{\psi}\psi = 0$. Hence it is necessary to include a gauge invariant kinetic term for the boson. This is achieved through the definition of antisymmetric field-strength tensors

$$F^a_{\mu\nu} = \partial_\mu A^a_\nu - \partial_\nu A^a_\mu + g f^{abc} A_{\mu,b} A_{\nu,c}, \tag{1.14}$$

where f^{abc} are the structure constants defining the Lie algebra of the group

$$[T^b, T^c] = i f^{abc} T_a. \tag{1.15}$$

This tensor is constructed in such a way that the derivatives of ϕ_a cancel out in gauge transformations. There are then two gauge invariant choices for the kinetic term in the Lagrangian

$$-\frac{1}{4} F^a_{\mu\nu} F^{\mu\nu}_a, \quad -\frac{1}{4} \epsilon_{\mu\nu\rho\sigma} F^{\mu\nu}_a F^{\rho\sigma}_a. \tag{1.16}$$

The second term, however, appears to have a vanishing coefficient in the strong interaction[6].

1.2.2 The Gauge-Group & Field Content of the SM

The gauge group of the SM is given by

$$SU(3)_C \otimes SU(2)_L \otimes U(1)_y. \tag{1.17}$$

The three parts of the SM associated to the three sub-groups are called quantum chromodynamics (QCD) [66], quantum flavourdynamics (QFD) [67] and quantum electrodynamics (QED) [68–70]. The first corresponds to the strong force, while the second and third can be combined to the electro-weak theory (EW) [71, 72], which contains the weak and electromagnetic interactions. We will denote the gauge fields and field-strength tensors of the three groups by G^a_μ and $G^a_{\mu\nu}$, W^a_μ and $W^a_{\mu\nu}$, respectively B_μ and $B_{\mu\nu}$. The group generators of the first and second group are denoted λ^a and τ^a, respectively.

Gauge theories, as they were introduced above, do not permit a mass term of the form

$$m^2 A_\mu A^\mu, \tag{1.18}$$

[6]Although this is not an inconsistency, this fact implies a lack of understanding, which goes by the name of *strong CP-problem*. An interesting solution, the Peccei-Quinn mechanism, implies the existence of an additional scalar field whose pseudo Nambu-Goldstone boson couples to this term anomalously and thereby dynamically sets it to zero [65].

because such a term would not be invariant under gauge transformations. This is problematic, since the bosons of the weak force are known to be massive. In addition, the $SU(2)_L$ gauge symmetry group only transforms left-chiral fermions, such that a Dirac mass term for fermions $m^2\bar{\psi}\psi$ would violate this symmetry. Both these problems are solved in the SM by introducing a scalar field ϕ which carries hypercharge (i.e. transforms in the $U(1)_y$ group) and transforms as a doublet under the $SU(2)_L$ group [73–75], i.e.

$$(D_\mu\phi) = \partial_\mu\phi - ig_1 B_\mu\phi - ig_2 W^a_\mu \tau_a \phi, \tag{1.19}$$

where τ_a are the generators of $SU(2)_L$, conventionally represented by the Pauli-matrices.

The Lagrangian permits a potential term for this field, which takes the form

$$V_\phi = -\mu^2\phi^\dagger\phi + \frac{\lambda}{4}(\phi^\dagger\phi)^2, \tag{1.20}$$

where $\phi^\dagger = (\phi^T)^*$.

It is also permitted to couple this field to the fermion fields via Yukawa interactions

$$\mathcal{L}_{\text{Yukawa}} = \sum_{f_L,f_R} G_{f_L,f_R}\bar{\psi}_{f_L}\phi^*\psi_{f_R} + G^*_{f_L,f_R}\bar{\psi}_{f_R}\phi^T \begin{pmatrix} 0 & -1 \\ 1 & 0 \end{pmatrix} \psi_{f_L}, \tag{1.21}$$

where ψ_{f_L} are (left-chiral) $SU(2)_L$ doublets while ψ_{f_R} are (right chiral) $SU(2)_L$ singlets, and the G_{f_L,f_R} are coupling constants describing the strength of the interaction and the matrix acts on the space defined by the $SU(2)_L$ doublet representation. These terms have to involve both left- and right-chiral fields, since the $SU(2)_L$ index of the ϕ-field has to be contracted with a left-chiral doublet, while the spinor indices of that doublet have to be contracted with spinors that do not transform under $SU(2)_L$.

The full SM Lagrangian (before symmetry breaking) is then given by

$$\begin{aligned} \mathcal{L}_{SM} = &-\frac{1}{4}G^{\mu\nu}_a G^a_{\mu\nu} - \frac{1}{4}W^{\mu\nu}_b W^b_{\mu\nu} - \frac{1}{4}B^{\mu\nu}B_{\mu\nu} \\ &+ i\sum_f \bar{\psi}_f \not{D}\psi_f \\ &+ (D_\mu\phi)^\dagger(D^\mu\phi) + V_\phi + \mathcal{L}_{\text{Yukawa}}, \end{aligned} \tag{1.22}$$

using the covariant derivative

$$D_\mu = \left(\partial_\mu - ig_s c_f G^a_\mu \lambda^a - i\frac{g_1}{2}t^f W^b_\mu \tau^b - i\frac{g_2}{2}y_f B_\mu\right), \tag{1.23}$$

where $c_f, t_f \in \{0, 1\}$ specify if the field f on which the derivative acts carries colour, respectively weak iso-spin and y_f is the weak hypercharge of the particle. The fermion-field content of the SM with charges is given in table 1.1.

Fermion family	Members	Colour-triplet	Isospin doublet	Hyper-charge
Left-chiral lepton doublets	$\ell_1 = \begin{pmatrix}\nu_e\\ e_L\end{pmatrix}$, $\ell_2 = \begin{pmatrix}\nu_\mu\\ \mu_L\end{pmatrix}$ $\ell_3 = \begin{pmatrix}\nu_\tau\\ \tau_L\end{pmatrix}$	no	yes	-1
Right-chiral leptons	e_R, μ_R, τ_R	no	no	-2
Left-chiral quark doublets	$q_1 = \begin{pmatrix}u_L\\ d_L\end{pmatrix}$, $q_2 = \begin{pmatrix}c_L\\ s_L\end{pmatrix}$, $q_3 = \begin{pmatrix}t_L\\ b_L\end{pmatrix}$	yes	yes	$\frac{1}{3}$
Right-chiral up-type quarks	u_R, c_R, t_R	yes	no	$\frac{4}{3}$
Right-chiral down-type quarks	d_R, s_R, b_R	yes	no	$-\frac{2}{3}$

Table 1.1: Fermion field content of the SM.
The fermions are organized into left-chiral doublets with and without strong interaction, which are called quarks and leptons, resepectively. Additionally, there are two types of strongly interacting right-chiral fermions and one type of right-chiral fermions without strong interaction. Each of these particles appears in three generations which differ by their Yukawa interactions. Remarkably, the values of the hypercharge cannot be chosen arbitrarily but are constrained by requiring a cancellation of $U(1)_y$ anomalies [76].

1.2.3 Spontaneous Symmetry Breaking

With $\mu^2 > 0$ in eqn. (1.20), the scalar field ϕ acquires a vacuum expectation value (VEV) $\frac{v}{\sqrt{2}} = \sqrt{\frac{2\mu^2}{\lambda}}$. By choosing an $SU(2)_L$-gauge, the doublet can be rewritten as

$$\phi(x) = \frac{1}{\sqrt{2}} \begin{pmatrix} 0 \\ (v + H(x)) \end{pmatrix}, \tag{1.24}$$

where $H(x)$ is the field corresponding to the Higgs boson [74]. ϕ has two complex, i.e. four real degrees of freedom, out of which only one corresponds to the Higgs boson while the others are Goldstone-bosons corresponding to gauge symmetries of $SU(2)\otimes U(1)$. Their physical degrees of freedom reappear as the additional polarization states of the three massive vector-bosons. Considering only terms including the vacuum expectation value, $(D_\mu\phi)^\dagger(D^\mu\phi)$ becomes

$$\frac{v^2}{2}\left(g_2^2 W_\mu^a W_a^\mu - 2ig_2^2 W_1^\mu W_\mu^2 + g_1^2 B_\mu B^\mu + 2g_1 g_2 W_3^\mu B_\mu\right) \tag{1.25}$$

and thus gives masses to the gauge-bosons. The mass eigenstates corresponding to physical particles are given by

$$W_\mu^\pm = \frac{1}{\sqrt{2}}(W_\mu^1 \pm iW_\mu^2), \qquad m_W = g_2\frac{v}{2}, \tag{1.26}$$

$$Z_\mu = \frac{1}{\sqrt{g_2^2+g_1^2}}(g_2W_\mu^3 + g_1B_\mu), \qquad m_Z = \frac{v}{2}\sqrt{g_1^2+g_2^2}, \tag{1.27}$$

$$A_\mu = \frac{1}{\sqrt{g_2^2+g_1^2}}(-g_1W_\mu^3 + g_2B_\mu), \qquad m_A = 0 \tag{1.28}$$

and describe the bosons of the electroweak interaction, i.e. the $W^\pm$- and Z-bosons and the (massless) photon A_μ. The ratio of the boson masses is a parameter of particular interest and is often abbreviated as $\cos\theta_W = m_W/m_Z$. Due to the VEV, the fermions also acquire masses through the Yukawa interactions. The physical particles again correspond to mass eigenstates, which are combinations of left- and right-chiral fields and whose Yukawa terms are given by

$$\frac{Y^f}{2}\bar{\psi}_f(v+H)\psi_f, \tag{1.29}$$

which attributes a mass $m_f\frac{-Y^f v}{2}$ to them. Since there is only one type of right-chiral lepton-fields, each of the lepton doublets contains one eigenstate with zero mass, corresponding to the neutrinos[7]. It is possible to extract the left-chiral components of such a mass eigenstate by the chirality projector $\frac{1-\gamma_5}{2}$, where γ_5 anticommutes with all other Dirac γ matrices and $\gamma_5^2 = 1$. In the chiral basis, it is given by

$$\gamma_5 = \frac{i}{4!}\epsilon_{\mu\nu\rho\sigma}\gamma^\mu\gamma^\nu\gamma^\rho\gamma^\sigma \begin{pmatrix} \mathbb{1} & 0 \\ 0 & -\mathbb{1} \end{pmatrix}. \tag{1.30}$$

The Lagrangian describing the interactions between the mass-eigenstate fermions and EW bosons after symmetry breaking is given by

$$\begin{aligned}\mathcal{L}_{\text{int}} = &- i\sum_{i,j}\frac{g_1}{\sqrt{2}}M_{ij}^{CKM}\bar{u}^i\left(\frac{1-\gamma^5}{2}\not{W}^+\right)d_j - i\sum_{i,j}\frac{g_1}{\sqrt{2}}M_{ij}^{CKM*}\bar{\mathrm{d}}^i\left(\not{W}^-\frac{1-\gamma^5}{2}\right)u_j \\ &- i\sum_i\frac{g_1}{\sqrt{2}}\bar{\nu}^i\left(\frac{1-\gamma^5}{2}\not{W}^+\right)e_i - i\sum_i\frac{g_1}{\sqrt{2}}\bar{e}^i\left(\not{W}^-\frac{1-\gamma^5}{2}\right)\nu_i \\ &- i\sum_f eq_f\bar{\psi}_f\not{A}\psi_f - i\sum_f\frac{g}{\cos\theta_W}\bar{\psi}_f\left(\left(I_f^3\frac{1-\gamma_5}{2} - q_f\sin^2\theta_W\right)\not{Z}\right)\psi_f,\end{aligned} \tag{1.31}$$

[7] In fact, the observation of neutrino oscillation hints that neutrinos are actually not massless and that the neutrino sector in SM has to be modified.

where $q_f = t_f + \frac{1}{2}Y_f$ is the electro-magnetic charge, I_3 is the weak isospin ($+\frac{1}{2}$ for $f \in \{\nu^i, u^i\}$, $-\frac{1}{2}$ else) and $e = g \sin\theta_W$ is the electro-magnetic coupling constant. The u^i, d^i, e^i, ν^i describe the different generations of up-type quarks, down-type quarks, leptons and neutrinos, respectively, while ψ_f contains all fermions.

Since it is not possible to diagonalise both the Yukawa mass-terms and the interaction with $W^\pm$-bosons at the same time, it is necessary to include M_{ij}^{CKM}, the Cabibbo-Kobayashi-Maskawa matrix[8]. In the following, we consider the top-quark as infinitely heavy, while all other quarks are considered as massless. With this degeneracy, the CKM matrix can be considered as diagonal again. For the leptons, this matrix can be diagonalized through a redefinition of neutrino fields[9]. The strong interaction is not affected by symmetry breaking and takes the same form as before for all mass states.

For simplicity, we will not discuss the interactions between the W, A, Z and H bosons after symmetry breaking in detail, since this work focusses on QCD corrections to processes where these bosons couple to quarks.

1.3 Quantisation

So far we have reviewed the definition of the SM Lagrangian only as a classical field theory. In this section, we will review the quantization of gauge theories in a path integral formulation.

The basic objects of QFTs are the quantum fields φ. In the case of a free bosonic particle, they can be described by plane waves

$$\varphi(x) = \int \mathrm{d}^3k \left(\mathrm{e}^{ik\cdot x} a_k + \mathrm{e}^{-ik\cdot} a_k^\dagger \right). \tag{1.32}$$

In the canonical quantisation procedure, bosonic fields are quantised through their commutators [79]

$$[\varphi(x), \Pi(y)] = i\delta(x-y), \tag{1.33}$$

with the conjugate momentum $\Pi = \frac{\partial \mathcal{L}}{\partial \partial_0 \varphi}$. This then leads to commutation relations between the a_i

$$[a_p, a_q^\dagger] = (2\pi)^3 \delta(\vec{p} - \vec{q}), \quad [a_p, a_q] = [a_p^\dagger, a_q^\dagger] = 0. \tag{1.34}$$

[8] This matrix contains, in fact, the only term violating a symmetry under charge-parity conjugation (CP) in the SM.

[9] With massive neutrinos, this is not possible and a similar matrix, known as the Pontecorvo-Maki-Nakagawa-Sakata-Matrix appears [77, 78].

By definition, field operators should have no effect when acting on the vacuum

$$a_p|0\rangle = 0, \text{ for all } \vec{p}. \tag{1.35}$$

Any field configuration can be created by applying operators $a_k^\dagger$ to the vacuum

$$|p\rangle = a_p^\dagger|0\rangle. \tag{1.36}$$

Therefore, these operators are also called *creation operators*, while the a_k are called *annihilation operators*. The quantum states corresponding to a field φ are denoted $|\varphi\rangle$.

Similarly, the corresponding operators for fermionic fields can be defined, which, however, have to obey anti-commutation relations in order to have a positive energy spectrum

$$\{b_p^\alpha, (b_q^\beta)^\dagger\} = (2\pi)^3\delta(\vec{p}-\vec{q})\delta^{\alpha\beta}, \quad \{b_p^\alpha, b_q^\beta\} = \{(b_p^\alpha)^\dagger, (b_q^\beta)^\dagger\} = 0, \tag{1.37}$$

where α and β are Dirac spinor indices. In gauge theories, this quantisation procedure cannot be applied directly as it also quantises the unphysical degrees of freedom which correspond to gauge transformations. This problem can conveniently be dealt with in the path integral quantisation, which we will review now.

An important object in QFT is the path integral

$$\int \mathcal{D}\phi\mathcal{D}\psi\mathcal{D}\bar{\psi}e^{-iS[\phi,\psi,\bar{\psi}]}, \tag{1.38}$$

where S is the action and

$$\mathcal{D}\phi = \prod_x \mathrm{d}\phi(x), \quad \mathcal{D}\psi = \prod_x \mathrm{d}\psi(x), \quad \mathcal{D}\bar{\psi} = \prod_x \mathrm{d}\bar{\psi}(x), \tag{1.39}$$

are integrals over all field values of bosons, Dirac fields and their respective conjugations at all points in space-time. Bosonic field values are integrated over real numbers, while the Dirac fields take values in Grassmanian (i.e. anti-commuting) numbers. Integrals over anti-commuting numbers take the simple form

$$\int d\phi = 1, \qquad \int d\phi\phi^n = 0 \ \forall n > 0. \tag{1.40}$$

By decomposing a time interval (t_0, T) into a set of smaller intervals $t_0 < t_1 < ... < t_n < T$, the path integral can be approximated by

$$\prod_{k,j}\int_x \mathrm{d}\varphi_j(\vec{x}, t_k)\left(1 - i\int_{t_k}^{t_{k+1}} \mathrm{d}t\mathcal{L}(\{\varphi_i(\vec{x}, t)\})\right)\langle\varphi_j(\vec{x}, t_{k+1})|\varphi_j(\vec{x}, t_k)\rangle + O(t_{k+1} - t_k), \tag{1.41}$$

where a complete set of states

$$\mathbb{1} = \prod_{\vec{x},j} \int \mathrm{d}\varphi_k(\vec{x}, t_k) |\varphi_j(\vec{x}, t_k)\rangle\langle\varphi_j(\vec{x}, t_k)|, \tag{1.42}$$

was inserted at every t_k. This allows to interpret the integrand as a product of transition amplitudes, which are then integrated over all possible configurations on intermediate time scales.

In gauge theories, this integral would be divergent due to the integration over physically equivalent configurations which are related by gauge transformations. However, in the path integral formulation this integral can be made explicit and split off [80].

Employing a gauge fixing term $F(\varphi)$ and a functional analogue of the δ function, the integral over the gauge orbit is made explicit

$$\int \mathcal{D}F\delta(F(\varphi)) = 1. \tag{1.43}$$

This integral can be parametrized by gauge transformation parameters ω which are independent of the field values $\varphi(x)$

$$\int \mathcal{D}\omega \det\left(\frac{\partial F}{\partial \omega}\right) \delta(F) = 1. \tag{1.44}$$

The *Fadeev-Popov determinant* $\det(\frac{\partial F}{\partial \omega})$ is the (functional equivalent to the) Jacobian of the coordinate transformation. This is now inserted into the path integral and the (unphysical) integration over gauge parameters is omitted.

It is possible to bring the path integral back into a form where it only depends on an action, employing several auxiliary fields. First, to remove the δ-function, a field Θ is employed and the gauge condition is redefined as $F(\varphi) = G(\varphi) - \Theta$. The integral is then integrated with a finite Gaussian integrand, which cancels the delta-function and moves the gauge fixing term into the exponent. Then, the Fadeev-Popov determinant can be exponentiated using two Grassmanian ghost fields [80]

$$ig \det(M) = \int \mathcal{D}\chi\mathcal{D}\bar{\chi} \exp\left(i \int \mathrm{d}^4x_1\mathrm{d}^4x_2\bar{\chi}(x_1)(gM(x_1 - x_2))\chi(x_2)\right). \tag{1.45}$$

In this form, the path integral can be defined through an exponentiated action again, where the Lagrangian is replaced by a gauge-fixed effective Lagrangian which involves the original Lagrangian, gauge fixing terms and the Fadeev-Popov ghosts.

Introducing these ghost fields and gauge-fixing terms replaces the original local gauge symmetry of the Lagrangian by the global Becchi-Rouet-Stora-Tyutin symmetry [81, 82], which allows to quantise only the physical degrees of freedom.

For QCD in 't Hooft-Feynman gauge, i.e. $G^a(A) = \partial_\mu A^{a\mu}$, this Lagrangian is then given by [81]

$$\mathcal{L} = -\frac{1}{4}G^a_{\mu\nu}G^{\mu\nu}_a - \frac{1}{2\xi}(\partial_\mu A^\mu(x))^2 + \bar{q}^i_f(i\gamma_\mu D^\mu_{ij} - m_f\delta_{ij})q^j_f + \partial_\mu\bar{\chi}_a(\partial^\mu\delta^{ab} - gf^{abc}A^\mu_c)\chi_b. \tag{1.46}$$

This gauge fixed effective action is the basis for computing correlation functions in gauge theories. In the following chapters, we will discuss how scattering amplitudes and cross-sections can be computed employing this effective action.

Chapter 2

Scattering Amplitudes & Feynman Rules

One of the most important observables in high energy physics are *scattering cross sections*, which give probabilities for finding a given set of particles in a volume element of their phase space after a collision of initial states. These cross sections are computed as phase-space integrals over squared scattering amplitudes.

In this chapter we will discuss how these amplitudes are computed in QFT, employing correlation functions which are computed from Feynman rules and the LSZ-reduction formula. Furthermore, we will review how Feynman integrals arise in the computation of amplitudes and how their ultraviolet divergences are regularised and absorbed through renormalisation.

Finally, we will briefly discuss how amplitudes are related to cross sections. In this context, we will review aspects of real radiation and infrared-save observables at fixed order in perturbation theory as well as parton distribution functions in hadronic cross-sections.

2.1 Correlation Functions

A class of important object in quantum field theory calculations are *correlation functions*, which can be obtained by inserting fields into the path integral.

The path integral (in the way it was defined in the previous chapter) contains unwanted factors, we therefore normalize it by the path integral without insertions, obtaining the correlation function

$$\langle\Omega|\varphi_{j_1}(x_1)\cdots\varphi_{j_n}(x_n)|\Omega\rangle = \frac{\int\mathcal{D}\varphi \mathrm{e}^{-iS[\phi]}\varphi_{j_1}(x_1)\cdots\varphi_{j_n}(x_n)}{\int\mathcal{D}\varphi \mathrm{e}^{-i\int \mathrm{d}^4x\mathcal{L}}}, \tag{2.1}$$

where $|\Omega\rangle$ is the ground state of the interacting theory. This quantity is computed pertur-

batively by expanding the exponentiated action in the path integral into a Dyson series[1]

$$\int \mathcal{D}\varphi \mathrm{e}^{-i\int \mathrm{d}^4x\mathcal{L}_0}\varphi_{j_1}(x_1)\cdots\varphi_{j_n}(x_n)\sum_n^\infty \frac{1}{n!}\left(-i\int \mathrm{d}^4x\mathcal{L}_{\mathrm{int}}(x)\right)^n, \tag{2.2}$$

where $\mathcal{L}_0$ contains only the kinematic terms of the Lagrangian, which are quadratic in the fields while $\mathcal{L}_{\mathrm{int}}$ contains the interactions.

Each power of $\mathcal{L}_{\mathrm{int}}$ adds additional field insertion to the correlation function, but is suppressed by a coupling constant, which are small enough to use them as expansion parameters.

The simplest case of interest is the correlation function of two scalar fields at different points in space-time to lowest order in the coupling constant, i.e. expanding the Dyson series to order 0.

$$\int \mathcal{D}\varphi \mathrm{e}^{-i\mathrm{d}^4x\left(\partial_\mu\varphi^*\partial^\mu\varphi-(m^2-i\varepsilon)|\varphi|^2\right)}\varphi(x_1)\varphi(x_2), \tag{2.3}$$

where the mass was replaced $m^2 \to m^2 - i\varepsilon$, to be considered in the limit $\varepsilon \to 0$ for reasons that will soon be apparent. Fourier transforming all φ fields, the correlation function becomes proportional to

$$\int \mathcal{D}\tilde{\varphi}\int \frac{\mathrm{d}^4k_1}{(2\pi)^4}\frac{\mathrm{d}^4k_2}{(2\pi)^4}\mathrm{e}^{-i\int \mathrm{d}^4k(k^2-m^2+i\varepsilon)|\tilde{\varphi}(k)|^2}\mathrm{e}^{-ik_1\cdot x_1-ik_2\cdot x_2}\tilde{\varphi}(k_1)\tilde{\varphi}(k_2) \tag{2.4}$$

For $k_1 \neq -k_2$, the integral over $\tilde{\varphi}(k_1)$ vanishes due to symmetry. Thus the only contribution comes from the slice $k_1 = -k_2$, where $\tilde{\varphi}(k_1)\tilde{\varphi}(-k_1) = |\tilde{\varphi}|^2(k_1)$ can then be expressed as a derivative

$$\int \frac{\mathrm{d}^4k}{(2\pi)^4} i\mathrm{e}^{-ik\cdot(x_1-x_2)}\frac{\partial}{\partial k^2}\int \mathcal{D}\tilde{\varphi}\mathrm{e}^{-i\int \mathrm{d}^4k'(k'^2-m^2+i\varepsilon)|\tilde{\varphi}(k')|^2}. \tag{2.5}$$

For $\mathrm{Im}(k'^2 - m^2 + i\varepsilon) > 0$, it is possible to evaluate the $\mathcal{D}\tilde{\varphi}$ integral as a product of Gaussian integrals (in fact, this is the reason why the $i\varepsilon$ term was included)

$$\begin{aligned}&\int \frac{\mathrm{d}^4k}{(2\pi)^4} - i\mathrm{e}^{-ik\cdot(x_1-x_2)}\frac{\partial}{\partial k^2}\prod_{k'}\sqrt{\frac{-i\pi}{m^2-k'^2-i\varepsilon}} \\ =&\int \frac{\mathrm{d}^4k}{(2\pi)^4}\frac{i\mathrm{e}^{-ik\cdot(x_1-x_2)}}{k^2-m^2+i\varepsilon}\prod_{k'}\sqrt{\frac{-i\pi}{m^2-k'^2-i\varepsilon}},\end{aligned} \tag{2.6}$$

[1]In fact, this series is divergent, because the number of terms per order grows factorially with the order of perturbation. In simpler perturbation series, which can be computed exactly, such divergences appear due to ignoring non-perturbative corrections of the form $e^{-\frac{1}{g}}$ and thus only at an order where $k \approx \frac{1}{g}$, where g is the expansion parameter while k is the perturbative order. Up to this order, the perturbation series correctly approximates the full result (see e.g. [83]). Though there is, so far, no rigorous proof on this, it is widely assumed that the same is true for quantum field theories.

where the product over the square roots is equal to the path integral and is therefore cancelled by the normalization. This results in the two-point correlation function for vanishing interaction, alias the *Feynman propagator* [84]

$$D_F(x, x_0) = \int \frac{\mathrm{d}^4k}{(2\pi)^4} \frac{i\mathrm{e}^{-ik\cdot(x-x_0)}}{k^2 - m^2 + i\varepsilon}. \tag{2.7}$$

More complicated correlation functions, such as

$$\int \mathcal{D}\varphi \mathrm{e}^{-i\int \mathrm{d}^4x\mathcal{L}_0} \varphi_{j_1}(x_1)\cdots\varphi_{j_n}(x_n)\varphi_{k_1}(y_1)\cdots\varphi_{k_n}(y_1) \tag{2.8}$$

can then be carried out by using Wick's theorem [85], i.e. pairing fields of the same type at different points in space-time in all possible ways and inserting Feynman propagators for each of the pairs. This theorem holds since every non-paired field has expectation value zero and therefore vanishes. The integrations over the space time x lead to δ functions in k, which cancel momentum space integrals and impose momentum conservation.

Typically, this expansion is carried out in momentum space, where the scalar Feynman-propagator takes the simple form

$$D_F(k) = \frac{i}{k^2 - m^2 + i\varepsilon}. \tag{2.9}$$

For fermions, on the other hand, the Feynman propagator becomes

$$D_F = \frac{\not{p} + m}{p^2 - m^2 + i\varepsilon}, \tag{2.10}$$

owing to the Dirac-equation. Moreover, additional colour- and polarisation-indices are contracted along the propagator.

2.1.1 Feynman-Rules

The method how correlation functions are carried out in practice is to employ *Feynman diagrams* [84] which correspond to certain terms in the expansion[2]. In particular, these diagrams include propagators corresponding to the contractions of two fields, and vertices that correspond to terms in $\mathcal{L}_{\text{int}}$ which appear through the expansion in eqn. (2.2).

It should be noted that, in the context of correlation functions, the diagrams cannot be interpreted as space-time diagrams showing physical particle paths, but only as terms in the expansion of a perturbation series.

The Feynman-rules relevant for this thesis, expressed in momentum space and t'Hooft-Feynman gauge (i.e. $\partial_\mu A^{a\mu} = 0$) are given in appendix A.

[2]These diagrams where first introduced by Ernst Stueckelberg, whose paper was rejected and then lost, however. They were then introduced again by Feynman in [84]

With these diagramatic building blocks and the rules to replace them by analytic expressions, Fourier transformed correlation functions are computed as follows:

1. Draw all Feynman diagrams up to a given order in the coupling constants.

2. Insert the analytic expressions and impose momentum conservation at each vertex.

3. Integrate over all momenta which are not fixed by momentum conservation [84].

This yields the Fourier transformed correlation function for a fixed polarisation and colour of the external particles. A diagram is called *connected* when every pair of two vertices in the diagram is connected via propagators and vertices and *disconnected otherwise*. The contributions of disconnected diagrams to correlation functions only have δ-function support for special values of external momenta. In the following, we are mostly concerned with connected diagrams.

Furthermore, we distinguish *tree-level* diagrams from *loop-level* diagrams, where connected tree-level diagrams become disconnected when removing any of the propagators. For connected loop-level diagrams, it is possible to remove a propagator such that the resulting diagram is still connected (see figure 2.1 for example diagrams). Similarly, we will denote amplitudes where only tree-level diagrams contribute as tree-level amplitudes.

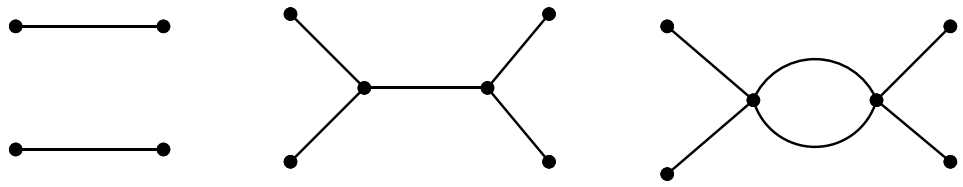

(a) A disconnected diagram

(b) A connected tree-level diagram

(c) A connected loop-level diagram

Figure 2.1: Examples for the different classes of Feynman diagrams.

2.2 Lehmann-Symanzik-Zimmermann Reduction Formula

Correlation functions are related to scattering amplitudes through the Lehman-Symanzik-Zimmermann (LSZ) reduction formula. The transition matrix elements M transform *in*-states which describe the system in a far away past to *out*-states which describe the particles long after a scattering process which is technically assumed to happen in a finite time interval.

The transition matrix element fi is closely related to the corresponding S-matrix element or amplitude

$$S_{fi} = \langle f|i\rangle\delta_{fi} + i(2\pi)^3\delta^4\left(\sum_k p_k\right)\mathcal{M}_{fi}, \tag{2.11}$$

considering all momenta as incoming. The states in this formula are Heisenberg states whose time evolution is given by the Hamiltonian of the theory. Assuming small coupling constants, the most important part of the time evolution is given by the free Hamiltonian H_0, which contains the kinetic terms and self-interactions of the field.

The time evolution of a field φ under only this Hamiltonian is described by the Klein-Gordon equation (respectively Dirac for Fermions) and gives plane-wave solutions

$$\varphi_I(\vec{x},t) = \int \frac{\mathrm{d}^3p}{(2\pi)^3}\frac{1}{\sqrt{2E_p}}\left(a_I(p)\mathrm{e}^{-ip\cdot x} + a_I(p)^\dagger\mathrm{e}^{ip\cdot x}\right). \tag{2.12}$$

This field is denoted as the *interaction picture* field. The initial and final states of an interaction are described by such fields φ_{in} and φ_{out}. The creation and annihilation operators of this field can be expressed in terms of the field

$$a_I(k) = \frac{i}{\sqrt{2E_k}}\int \mathrm{d}^3x\frac{\mathrm{e}^{ikx}}{\sqrt{2\pi}^3}\overset{\leftrightarrow}{\partial_0}\varphi_I, \tag{2.13}$$

$$a_I^\dagger(k) = \frac{i}{\sqrt{2E_k}}\int \mathrm{d}^3x\frac{\mathrm{e}^{-ikx}}{\sqrt{2\pi}^3}\overset{\leftrightarrow}{\partial_0}\varphi_I \tag{2.14}$$

where $f\overset{\leftrightarrow}{\partial_0}g = f\partial_0 g - g\partial_0 f$.

Unfortunately, it is not possible to identify the interacting Heisenberg field directly with the in and out-fields before and after the scattering process, due to self interactions of the field which are present at all times.

A weaker, but equally useful asymptotic relation developed by Lehmann, Symanzik and Zimmermann [86] is that for physical states $|\alpha\rangle, |\beta\rangle$ and a solution $f(x)$ to the Klein-Gordon equation (respectively Dirac equation for fermions), a transition from the interacting field to the in and out fields is given by

$$\lim_{t\to\pm\infty}\int \mathrm{d}^3x\langle\alpha|f(x)\overset{\leftrightarrow}{\partial_0}\varphi(x)|\beta\rangle = \sqrt{Z}\int \mathrm{d}^3x\langle\alpha|f(x)\overset{\leftrightarrow}{\partial_0}\varphi_{\text{out,in}}(x)|\beta\rangle \tag{2.15}$$

where $\sqrt{Z}$ is a renormalization constant (see section 2.4).

In the LSZ-reduction formula, these weak asymtotic relations are used to express S-matrix elements in terms of correlation functions. Assuming i initial state and f final

state particles, the transition amplitude is given by

$$\mathcal{M}_{fi} = \langle q_1 ... q_f | p_1 ... p_i \rangle = \sqrt{2\omega_{p_1}} \langle q_1 ... q_f | a^\dagger_{\text{in}}(p_1) | p_2 ... p_f \rangle. \tag{2.16}$$

To demonstrate how the fields integrate into the time ordering, we include an additional time ordered product of field operators $T[\varphi(y_1)\varphi(y_2)]$ into the bracket in the following.

Assuming that the final state particles are different from the initial state particles, we have $\langle \text{out} | a^\dagger_{\text{out}}(p) = 0$, and thus it is possible to write

$$\mathcal{M}_{fi} = \sqrt{2\omega_{p_1}} \langle q_1 \cdots q_f | T[\varphi(y_1)\varphi(y_2)] a^\dagger_{\text{in}}(p_1) - a^\dagger_{\text{out}}(p_1) T[\varphi(y_1)\varphi(y_2)] | p_2 ... p_f \rangle \tag{2.17}$$

Using eqns. (2.13, 2.14), the matrix element is written as

$$\begin{aligned} \mathcal{M}_{fi} = -i \int \mathrm{d}^3 x \frac{\mathrm{e}^{ip_1 x}}{\sqrt{2\pi}^3} \overset{\leftrightarrow}{\partial_0} \langle q_1 ... q_f | \big(T[\varphi(y_1)\varphi(y_2)] \varphi_{\text{in}}(x) \\ - \varphi_{\text{out}}(x) T[\varphi(y_1)\varphi(y_2)] \big) | p_2 ... p_f \rangle. \end{aligned} \tag{2.18}$$

Now, the weak asymptotic assumption can be inserted

$$\mathcal{M}_{fi} = -i \frac{1}{\sqrt{Z}} (\lim_{t \to -\infty} - \lim_{t \to \infty}) \int \mathrm{d}^3 x \frac{\mathrm{e}^{ip_1 x}}{\sqrt{2\pi}^3} \overset{\leftrightarrow}{\partial_0} \langle q_1 ... q_f | T[\varphi(x)\varphi(y_1)\varphi(y_2)] | p_2 ... p_f \rangle, \tag{2.19}$$

where $\varphi(x)$ can be included into the time ordering since it is ordered to the right for $t \to -\infty$ and to the left for $t \to \infty$.

The function evaluated at $t = -\infty$ and $t = \infty$ is equal to an integral over a total time derivative, hence

$$\mathcal{M}_{fi} = -i \frac{1}{\sqrt{Z}} \int \mathrm{d}^4 x \partial_0 \left(\frac{\mathrm{e}^{ip_1 x}}{\sqrt{2\pi}^3} \overset{\leftrightarrow}{\partial_0} \langle q_1 ... q_f | T[\varphi(x)\varphi(y_1) s \varphi(y_2)] | p_2 ... p_f \rangle \right). \tag{2.20}$$

Inserting the equation of motion replaces the time-derivative on e^{ikx} by spatial derivatives. Partial integration then gives

$$\mathcal{M}_{fi} = -i \frac{1}{\sqrt{Z}} \int \mathrm{d}^4 x \frac{\mathrm{e}^{ikx}}{\sqrt{2\pi}^3} (\partial_\mu \partial^\mu - m^2) \langle q_1 ... q_f | T[\varphi(x)\varphi(y_1)\varphi(y_2)] | p_2 ... p_f \rangle. \tag{2.21}$$

Following the same steps as before (now dropping the additional fields), all in- and out-fields can be pulled into the time ordered product

$$\begin{aligned} \mathcal{M}_{fi} = \int \left[\prod_i \mathrm{d}^4 x_i \frac{\mathrm{e}^{-iq_i \cdot x_i} (\partial_{x_\mu^i} \partial^{x_i^\mu} + m^2_{\text{in},i})}{\sqrt{2\pi}^3 \sqrt{Z}} \right] \left[\prod_j \mathrm{d}^4 y_j \frac{\mathrm{e}^{ip_j \cdot y_j} (\partial_{y_\mu^j} \partial^{y_j^\mu} + m^2_{\text{out},j})}{\sqrt{2\pi}^3 \sqrt{Z}} \right] \\ \times \langle 0 | T[\varphi(x_1) \cdots \varphi(x_i)\varphi(y_1) \cdots \varphi(y_f)] | 0 \rangle. \end{aligned} \tag{2.22}$$

This allows to obtain the $S-$matrix elements from correlation functions [86].

In the Fourier-transformed picture, this becomes

$$\mathcal{M}_{fi} = \left[\prod_i \frac{(p_i^2 - m_i^2)}{\sqrt{2\pi}^3\sqrt{Z}}\right]\left[\prod_j \frac{(q_j^2 - m_j^2)}{\sqrt{2\pi}^3\sqrt{Z}}\right]\Gamma(p_1, ..., p_i, q_1 ... q_f), \tag{2.23}$$

using the Fourier-transformed correlation function

$$\Gamma(p_1, ..., p_n) = \int \prod_i \mathrm{d}^4 x_i \mathrm{e}^{ip_i \cdot x_i} \langle 0|T\varphi(x_1)\cdots\varphi(x_n)|0\rangle. \tag{2.24}$$

For fermions, the procedure is similar, however, leading to factors $i\partial\!\!\!/ + m$ instead of $\partial_\mu\partial^\mu - m^2$, respectively $p\!\!\!/ - m$ instead of $p^2 - m^2$, since the fields satisfy Dirac rather than Klein-Gordon equations. Note that the factors $p_i^2 - m_j^2$ and $p\!\!\!/ - m$ are not only the inverse Feynman-propagators of the external particles, but the full inverse of two-point correlation functions (i.e. formally expanding the Dyson series in eqn. (2.2) to all orders).

The correlation function can be computed using Feynman rules, as was described in the previous section. Since the inverse propagators of external particles are set to zero in the cross section, this formula asserts that amplitudes are the residues of the correlation function on the points where the external particles are set on-shell.

This reduction formula therefore leads to a *truncation* of Feynman diagrams, i.e. the propagators (including quantum corrections) of external particles are cancelled by the pre-factors from the reduction formula. In the literature, Feynman-rules directly for amplitudes are often found, which have additional rules for external lines which are identified with polarisation vectors.

2.3 Loop-Integrals

In Feynman-rules, coupling constants appear at three- and four-point vertices. Therefore, higher orders in the coupling constant imply additional internal or external lines. Adding an internal line to a connected graph, while leaving the number of external lines constant, however implies adding a loop to the graph. Therefore, the perturbation series can be understood as a series in loops and external legs.

A different number of external legs for two diagrams does not necessarily imply that they contribute to different physical processes, since it is not possible to experimentally distinguish two states which differ by e.g. a zero energy gluon [87]. Thus a diagram with $n + k$ external legs may as well be seen as a correction to an n-point process, if for k final state particles the energy or the angular difference to another particles are too small to be experimentally distinguished. In fact, such *real radiative corrections* have to be calculated and combined with the loop amplitudes in order to cancel so called *infrared*

divergent contributions (see section 2.5.1).

In diagrams involving loops, momentum conservation does not uniquely determine the momenta in all propagators, giving rise to integrals over momentum variables. Throughout the thesis, we will refer to these *loop momenta* as ℓ^μ, while the external momenta will be referred to as k^μ. These integrals over loop-momenta are notoriously difficult to compute, especially for multi-loop diagrams.

The integrands resulting from Feynman rules are rational functions in both loop momenta and external momenta. The loop-momentum dependent denominator is given by a product of inverse propagators, which are in general given by a squared sum of momenta minus a squared mass. Thus a general L-loop *Feynman integral* is defined as

$$I = \int \frac{\mathrm{d}^D \ell_1}{i\pi^{D/2}} \cdots \frac{\mathrm{d}^D \ell_L}{i\pi^{D/2}} \frac{N(\ell_1, ..., \ell_L)}{\varrho_1 \cdots \varrho_n}, \tag{2.25}$$

where N is a polynomial in the loop momenta and using the inverse propagators

$$\varrho_j = (\alpha_j^1 \ell_1 + ... + \alpha_j^L \ell_L + \beta_j^1 k_1 + ... + \beta_j^N k_N)^2 - m_j^2, \tag{2.26}$$

where $\alpha_j^i, \beta_j^i \in \{-1, 0, 1\}$. Conventionally, all spinor, tensor and colour indices in such an integral are factored out by contracting them with indices of external states and only the remaining scalar object is called the Feynman integral.

Since rational functions have no primitive functions in general, the integration over loop momenta is highly non-trivial. Furthermore, the integration region may contain non-integrable zeroes of the denominator, which lead to infrared singularities which have to be merged with divergences in real emission contributions[3]. Moreover, for theories which are not finite, ultraviolet divergences appear and have to be regularised and absorbed into counter-terms [89], as will be discussed in the following sections.

2.3.1 Dimensional Regularisation

A peculiar property of QFT's such as the SM is that often Feynman integrals are divergent. These divergences occur due to poles in the integrand (infrared or IR divergences) as well as in the region of large momentum (ultraviolet or UV divergences). Ultraviolet divergences are cancelled through renormalisation, where coupling constants, fields and masses are redefined with infinite quantities, rendering the physical observables finite [90]. To do this in a well defined way, the integral has to be regularised first, i.e. it is necessary to define a finite integral with a new parameter whose integrand has the original integrand as a limit. The renormalisation constants are then also functions of

[3]In fact, these divergences are proven to cancel at each order in perturbation theory by the Kinoshita-Lee-Nauenberg theorem [87, 88].

these additional parameters, which are defined such that physical observables (for which infrared divergences cancel in a suitable regularisation) are finite in this limit.

Currently the most commonly used regularisation scheme for QCD-computations is *dimensional regularisation*, where the four-dimensional space-time integral is replaced by a D dimensional one. The integral is defined to be an analytic function in D and physical results are obtained by taking the limit $D \to 4$ [91, 92].

Other regularisation schemes, such as removing the integration up to infinity by introducing a cut-off [93], or imposing additional particles which cancel the UV divergences [94] exist but are seldom used in QCD calculations.

Dimensional regularisation has several advantages over other schemes: For instance, all symmetries, in particular gauge symmetries, are preserved. This implies that Ward identities [95,96] are preserved, conserving the unitarity of the S-matrix [92]. Moreover, poles in four dimensions (i.e terms proportional to $\left(\frac{1}{D-4}\right)^n$, $n > 0$) are Lorentz covariant and hence give a natural choice for counter-terms. Furthermore, for massless external particles, dimensional regularisation also regularises infrared divergences. Finally, integration-by-parts identities may contain unwanted boundary terms in other regularisation schemes, as will be discussed later on.

All integrals, integration-by-parts relations and amplitudes discussed in this thesis are defined in dimensional regularisation, therefore we will review the concept in this section. As a trivial example, consider the logarithmically divergent two-dimensional integral

$$I' = \int \mathrm{d}^2\ell \frac{1}{\ell^2 + m^2}, \tag{2.27}$$

where we define the momentum-space to be two-dimensional and Euclidean.

In dimensional regularisation, the vector-space of ℓ and also the integral is taken to be D-dimensional. Since the integrand only depends on the absolute value $|\ell| = \sqrt{\ell^2}$, the $D-1$ dimensional solid angle can be integrated out

$$I = \int \mathrm{d}^D\ell \frac{1}{\ell^2 + m^2} = \int_0^\infty \mathrm{d}|\ell| \mathrm{d}^{D-1}\Omega \; |\ell|^{D-1} \frac{1}{\ell^2 + m^2} \tag{2.28}$$

$$= \frac{S_{D-1}}{2\pi^D} \int_0^\infty d|\ell| |\ell|^{D-1} \frac{1}{\ell^2 + m^2}, \tag{2.29}$$

where

$$S_{D-1} = \frac{2\pi^{D/2}}{\Gamma(D/2)} \tag{2.30}$$

is the volume of the $(D-1)$-dimensional unit sphere, which is finite except for isolated values of D.

The remaining one-dimensional integral can be simplified by the substitution $\ell^2 = m^2 y$,

resulting in a Beta function

$$m^{D-2}\int_0^\infty \mathrm{d}y y^{\frac{D-2}{2}}\frac{1}{y+1} = m^{D-2}\mathrm{B}\left(D/2,\frac{2-D}{2}\right) = m^{D-2}\frac{\Gamma(D-1)\Gamma(\frac{2-D}{2})}{\Gamma(1)}, \tag{2.31}$$

which is finite for $D\notin\mathbb{N}_{>1}$.

For more general Feynman-integrals, the integrand only depends on scalar products of loop momenta with four-dimensional momenta or loop momenta among themselves. Thus a D dimensional L-loop Feynman integral with n (4-dimensional) external legs can be parametrized with at most $N = L\times 4 + L(L+1)/2$ parameters while the other degrees of freedom can be integrated as an $LD-N$-dimensional solid angle. In order for the action to remain dimensionless, the fermionic and bosonic fields have to have mass dimension $[\psi] = \frac{D-1}{2}$ and $[A] = \frac{D-2}{2}$, respectively. By dimensional analysis, it follows that the couplings have to be rescaled by a mass scale μ: $g\to g\mu^{2-\frac{D}{2}}$ which can be chosen arbitrarily.

Remarkably, dimensional regularisation does not only change the UV-behaviour of Feynman integrals, but also has an effect on their analytic structure which, to a large extend, is given by the residues on the leading poles of the integrand. Consider for example the integral

$$F = \int \mathrm{d}^D\ell \frac{1}{\ell^2(\ell-p_1)^2(\ell-p_1-p_2)^2(\ell+p_4)^2}. \tag{2.32}$$

In four dimensions, the leading poles of the integrand are zero-dimensional isolated points, since $\varrho_j = 0\ \forall j$ determines all components of the four-dimensional loop-momentum. In dimensional regularisation, these four equations define a continuous $(D-4)$-dimensional surface, which can be parametrised with one parameter after solid $(D-5)$-dimensional angles are integrated out. Such properties are known to influence the analytic form of the integrals.

Furthermore, one-loop integrals with five distinct propagators, can be decomposed into integrals with at most four propagators via partial fractioning in four dimensions. In D dimensions, in contrast, their leading pole is a $(D-5)$-dimensional surface and they are independent of the integrals with fewer propagators.

There are two important variants of this regularisation scheme:

- Conventional dimensional regularization (CDR) for which both loop- and external momenta are considered in D dimensions.

- The 't Hooft-Veltman scheme (HV) for which loop-momenta are taken to be D-dimensional while the external momenta remain four-dimensional. This scheme violates D-dimensional Lorentz invariance, however, it allows to treat the polarisation states or helicities of external particles in four dimensions. We therefore employ

't Hooft-Veltman scheme for all calculations.

Some difficulties in Dimensional Regularisation arise from objects which are only defined in specific dimensions, such as the fifth Dirac matrix γ_5. We detail the treatment of this object in appendix B.

2.4 Renormalisation

To illustrate the physical meaning of the renormalisation procedure, we will first consider a heuristic explanation.

Fundamental constants, such as (bare) masses or couplings, cannot be directly measured but have to be extracted from measurements of e.g. scattering processes. As an example, consider fitting a leading-order theory prediction to a process where an electron moves in an electric field to obtain the mass of the electron.

Then, the obtained mass is only valid at leading order. If one would use this bare value to compute NLO corrections, the result would match the observation worse then the leading order result, since e.g. an increase in the mass would evidently not be found in the experiment.

Therefore, even in finite theories, it is necessary to adjust the constants at each order in perturbation theory, which goes by the name of *renormalisation*. In particle physics, an additional complexity of this procedure arises from UV divergencies. As a correction to the electron mass, consider the energy density of the electric field surrounding it. The energy density goes with $|\vec{E}|^2 \propto 1/r^4$, leading to an integral $\int \mathrm{d}r \frac{1}{r^2} \to \infty$.

At NNLO, this divergence would be shielded by virtual particle-antiparticle pairs being created close to the electron. However, new divergences would occur which would be shielded at N^{3}LO and so forth. At each fixed order, the bare mass therefore has to redefined to $m_0 \to -\infty$ in a consistent way so that the visible mass remains finite.

We will discuss this procedure and the renormalisation of massless QCD in this section. Furthermore, we will briefly discuss how the renormalisation scale is chosen and how this leads to running coupling constants.

2.4.1 Renormalisation of QCD

In a renormalisable theory, the fields and constants are each multiplied with a renormalisation factor [68–70]

$$\psi_0(x) = Z_\psi^{\frac{1}{2}} \psi(x), \qquad G_0^\mu(x) = Z_G^{\frac{1}{2}} G^\mu(x), \tag{2.33}$$

$$\xi_0(c) = Z_\eta^{\frac{1}{2}} \xi(x), \qquad g_0 = Z_g g. \tag{2.34}$$

Conventionally, these renormalisation constants are split into a constant piece and a divergent *counter term* which is of higher order in the coupling constant

$$Z_i = 1 + \delta_{Z_i}. \tag{2.35}$$

By splitting off the counter terms δ_Z, the bare Lagrangian is split into a renormalised contribution and a counter-term Lagrangian

$$\mathcal{L}_0 = \mathcal{L}_{\text{renorm.}} + \mathcal{L}_{c.t.}. \tag{2.36}$$

For the Lagrangian of massless QCD, these pieces are given by

$$\mathcal{L}_0 = \sum_f \bar{\psi}_{f,0} i \not{D}_0 \psi_{f,0} - \frac{1}{4} G^a_{\mu\nu,0} G^{\mu\nu}_{a,0} \tag{2.37}$$

$$\mathcal{L}_{\text{renorm.}} = \sum_f \bar{\psi}_f i \not{D} \psi_f - \frac{1}{4} G^a_{\mu\nu} G^{\mu\nu}_a \tag{2.38}$$

$$\begin{aligned} \mathcal{L}_{\text{c.t.}} = {} & (Z_\psi - 1) \sum_f \bar{\psi}_f i \not{\partial} \psi_f + g(Z_g Z_\psi Z_G^{\frac{1}{2}} - 1) \sum_f \bar{\psi}_f i \not{G}^a T^a \psi_f \\ & - \frac{1}{4}(Z_G - 1)(\partial_\mu G^a_\nu - \partial_\nu G^a_\mu)^2 - g(Z_G^{\frac{3}{2}} Z_g - 1) \partial_\mu G^a_\nu G^b_\mu G^c_\nu f^{abc} \\ & + \frac{1}{4} g^2 (Z_G^2 Z_g^2 - 1)(f^{abc} G^\mu_b G^\nu_c)^2. \end{aligned} \tag{2.39}$$

The fact that the four-gluon, three-gluon and quark-gluon vertices can be renormalized with the same constant Z_g is guaranteed by Ward-Takahashi identities, which (in dimensional regularisation) are valid in gauge theories to all orders. To get finite results for physical observables, the constants Z_ψ and Z_G and Z_g have to be chosen such that they cancel the UV-divergencies from loop integrals. Consider the correction to the gluonic

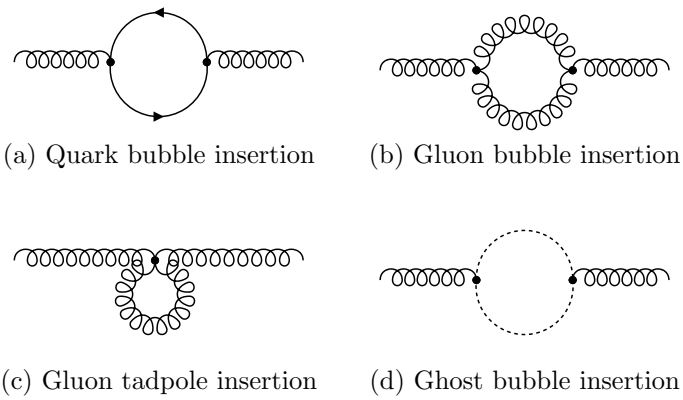

(a) Quark bubble insertion (b) Gluon bubble insertion

(c) Gluon tadpole insertion (d) Ghost bubble insertion

Figure 2.2: One-loop corrections to the gluon propagator

two-point Green's function with momentum q given by the production and anihilation

of a quark pair (see figure 2.2a)[4]. According to Feynman rules, in Feynman-gauge this diagram is given by

$$\Pi^{\mu\nu}_{ab}(q) = \frac{g^{\mu\rho}}{q^2}\delta_{ab}\,\mathrm{Tr}(T^c T^c)\mu^{4-D}\frac{g^{\nu}_{\rho}}{q^2}\Sigma_q(q), \tag{2.40}$$

with

$$-i\Sigma_q(q) = -\alpha_s \int d^D\ell \frac{\mathrm{Tr}(\not\ell\gamma_\mu(\not\ell - \not q)\gamma^\mu)}{(\ell^2+i\varepsilon)((\ell-q)^2+i\varepsilon)}, \tag{2.41}$$

where $\alpha_s = \frac{g_s^2}{4\pi}$. Using Feynman parameters, this becomes

$$\Sigma_q(q) = -4i\alpha_s \int_0^1 \mathrm{d}x \int \mathrm{d}^D\ell \frac{\mathrm{Tr}\left(\not\ell\gamma_\mu(\not\ell - \not q)\right)}{((\ell+xq)^2 - M^2)^2 + i\varepsilon}, \tag{2.42}$$

where $M^2 = -q^2x(1-x)$. In order to simplify the denominator, the integration variables are redefined $\ell \to \ell + xq$. By a Wick rotation, i.e. integrating ℓ_0 over a closed contour containing the real axis, the imaginary axis and a closure at infinity where the integrand vanishes, the integral over the real axis can be replaced by an integral over the imaginary axis which makes space-time Euclidean

$$\Sigma_q(q) = -4\alpha_s \int_0^1 \mathrm{d}x \int \mathrm{d}^D\ell_E \frac{-x(1-x)q^2}{(\ell_E^2 + M^2)^2 - i\varepsilon}, \tag{2.43}$$

where the spinor algebra has been carried out and parts linear in ℓ vanish due to symmetry. Note that the Wick rotation is only possible because we carried along the $i\varepsilon$ terms, which we can set to zero now. By using a Schwinger parameter the integrand is written as an exponential

$$\Sigma_q(q) = 4\alpha_s \int_0^1 \mathrm{d}x x(1-x)q^2 \int \mathrm{d}^D\ell_E \int_0^\infty \mathrm{d}\lambda\lambda \mathrm{e}^{-\lambda(\ell_E^2+M^2)} \tag{2.44}$$

$$= 4\alpha_s \int_0^1 \mathrm{d}x x(1-x)q^2 \int_0^\infty \mathrm{d}\lambda\lambda \mathrm{e}^{-\lambda M^2} \left(\int \mathrm{d}\ell_E^0 \mathrm{e}^{-\lambda(\ell_E^0)^2}\right)^D. \tag{2.45}$$

This is now a Gaussian integral, which can be solved before integrating over the Schwinger parameter

$$\Sigma_q(q) = 4\alpha_s\Gamma(2-\frac{D}{2})\pi^{D/2}q^2 \int_0^1 \mathrm{d}x(1-x)x(M^2(x))^{\frac{D-4}{2}}. \tag{2.46}$$

This term has to be multiplied with the number of quarks n_f running in the loop. Simi-

[4]This contribution is individually gauge invariant because by contrast to the others, it scales with the number of light fermions N_f.

larly, the other contributions to the gluon propagator can be computed [58]. The sum of these contributions gives

$$\Pi^{\mu\nu}_{ab} = \frac{1}{q^2} g^{\mu\nu}\delta_{ab} \frac{\alpha_s (4\pi^{\frac{D}{2}-2})\Gamma(2-\frac{D}{2}) q^{D-4}}{\mu^{D-4}} \frac{\Gamma(D/2)^2}{\Gamma(D)} \left(\frac{5C_A}{3} - \frac{2n_f}{3}\right), \tag{2.47}$$

which is divergent in four dimensions due to the pole of the $\Gamma(2-\frac{D}{2})$ at $D=4$. The counter terms have to cancel this divergence.

There are several schemes how to do this, with the modified minimal subtraction scheme ($\overline{\text{MS}}$) being the most frequently used in QCD calculations. In this scheme, the pole is subtracted together with a constant finite contribution coming from the pole

$$\frac{1}{\epsilon} + \log(4\pi) - \gamma_E, \tag{2.48}$$

where γ_E is the Euler-Mascheroni constant. The renormalisation constant Z_G is then chosen as

$$Z_G = 1 - \alpha_s \pi^{\frac{D}{2}-2} \Gamma\left(2-\frac{D}{2}\right)\left(\frac{5C_A}{3} - \frac{2n_f}{3}\right). \tag{2.49}$$

In a similar manner, the other renormalization constants can be computed [97]

$$Z_\psi = 1 - \alpha_s \pi^{\frac{D}{2}-2} \Gamma\left(2-\frac{D}{2}\right) C_F, \tag{2.50}$$

$$Z_g Z_\psi Z_G^{\frac{1}{2}} = 1 - \alpha_s \pi^{\frac{D}{2}-2} \Gamma\left(2-\frac{D}{2}\right)(C_F + C_A). \tag{2.51}$$

The renormalised and bare couplings are related in the following way:

$$\alpha_s^0 = \mu^{2\epsilon}\alpha_s(\mu^2)\left(1 - \frac{\alpha_s(\mu^2)}{2\pi}\frac{\beta_0}{\epsilon} + ...\right). \tag{2.52}$$

Up to two loops, this relation becomes [98]

$$\alpha_s^0/\mu^{2\epsilon} = \alpha_s(\mu^2)\left(1 - \frac{\alpha_s(\mu)}{2\pi}\frac{\beta_0}{\epsilon} + \left(\frac{\alpha_s(\mu^2)}{2\pi}\right)^2\left(\frac{\beta_0^2}{\epsilon^2} - \frac{\beta_1}{2\epsilon}\right) + O(\alpha_s^3(\mu^2))\right), \tag{2.53}$$

where

$$\beta_0 = \frac{11C_A - 2n_f}{6}, \quad \beta_1 = \frac{17C_A^2 - 5C_a n_f - 3C_F n_f}{6}. \tag{2.54}$$

It is, in fact, possible to absorb the field-renormalisations into a redefinition of fields. The renormalised amplitudes can then be computed by expressing the bare coupling in terms of the renormalized coupling, up to the total required order in α_s.

2.4.2 Choice of the Renormalisation Scale & Running Couplings

Physical observables computed exactly are independent of the renormalisation scale, since it is only an artefact of the renormalisation procedure. This is, however, not true for their perturbative expansion. Thus, varying the renormalisation scale shifts contributions between different orders in the expansion. As is given in eqn. (2.47), the μ-dependence of the one-loop vacuum polarisation is of the form

$$\left(\frac{q^2}{\mu^2}\right)^{-\epsilon}\Gamma(\epsilon)(4\pi)^{-\epsilon} = \frac{1}{\epsilon} + \log(4\pi) - \gamma_E - \log\left(\frac{q^2}{\mu^2}\right) + O(\epsilon). \tag{2.55}$$

In the $\overline{\text{MS}}$-scheme, the constant piece cancels against the counter term contribution leaving the finite piece to be $-\log\left(\frac{q^2}{\mu^2}\right)$. Such logarithms recur at all orders in perturbation theory and can be potentially large when the renormalisation scale is far from the physical scales of the process. Thus, in order for the fixed-order computation to be a good approximation, the renormalisation scale should be similar to the physical scales of the process, e.g. here the optimal scale choice is $\mu^2 = q^2$.

For simple processes such as $e^+e^- \to \mu^+\mu^-$ in QED, it can be shown that the vacuum polarisation contributions to the amplitude at all orders can be resummed into the leading order term by the choice $\mu = s$, where s is the center of mass energy [99].

Respecting such optimal choices of the renormalisation scale has an important consequence: the renormalised couplings will depend on the energy scale of the process. The bare coupling a_s^0 is a constant of the theory and hence is independent of the renormalisation scale

$$\frac{\partial \alpha_s^0}{\partial \mu^2} = 0. \tag{2.56}$$

This leads to a differential equation for the renormalised coupling

$$0 = \mu^{(2+2\epsilon)}\frac{\partial \alpha_s^0}{\partial \mu^2} = \mu^2\frac{\partial \alpha_s(\mu^2)}{\partial \mu^2}\left(1 - 2\frac{\alpha_s(\mu)}{4\pi}\frac{\beta_0}{\epsilon}\right) + \epsilon\alpha_s(\mu)\left(1 - \frac{\alpha_s(\mu)}{4\pi}\frac{\beta_0}{\epsilon}\right)O(\alpha_s^3) \tag{2.57}$$

$$\Rightarrow \frac{\partial \alpha_s(\mu)}{\partial \mu^2} = -\frac{\alpha_s^2}{4\pi}\frac{\beta_0}{\mu^2} + O(\epsilon). \tag{2.58}$$

This equation can be solved, giving

$$\alpha_s(\mu) = \frac{\alpha_s(\mu_0)}{1 + \beta_0\alpha_s(\mu_0)\log(\frac{\mu^2}{\mu_0^2})}. \tag{2.59}$$

Since $\beta_0 > 0$, this implies that at the MeV scale, we have $\alpha_s \gtrsim 1$ and the theory cannot be approximated by perturbative expansion in α_s. At higher energies, we have $\alpha_s < 1$

and hence partons behave like weakly coupled particles (asymptotic freedom) [100, 101]. For QED, however, it is found that $\frac{\partial \alpha_e}{\partial \mu} > 0$ and hence the coupling increases for large energies. At the energy scales of current and planned collider experimentsm however, the expansion parameters are small enough for the perturbation series to approximate the result.

2.5 Cross-Sections from Scattering Amplitudes

The topic of this thesis are scattering amplitudes. The physical observables measured at the LHC, however, are scattering cross sections. We will therefore briefly review how these objects are related.

Cross sections are given by phase space integrals over squared matrix elements. For $2 \to n$ elementary particle scattering with initial momenta k_1, k_2 with masses m_1, m_2 and final state momenta $k_f^1, ..., k_f^n$ with masses $m_1^f, ..., m_n^f$, the differential cross section (summed over polarisations and colours) is given by [102, 103]

$$\mathrm{d}\sigma_{i\to f} = \frac{1}{S}\frac{1}{\sqrt{(k_1k_2)^2 - (m_1)^2(m_2)^2}}\mathrm{d}\varphi_n(k_1, k_2, k_f^1, ..., k_f^n)|\mathcal{M}_{fi}|^2, \tag{2.60}$$

where S is a symmetry factor that avoids double counting of identical particles and the flux factor $\sqrt{(k_1k_2)^2 - m_1^2m_2^2}$ is a measure of the number of particles that pass each other per area and time. The phase space measure $\mathrm{d}\phi$ is given by

$$\begin{aligned}\mathrm{d}\varphi_n(k_1, k_2, k_f^1, ..., k_f^n) =&(2\pi)^4\delta^4\left(k_1 + k_2 - \sum_j k_j^f\right) \\ &\times \prod_{j_1}\frac{\mathrm{d}^4k_{j_1}^f}{(2\pi)^3}\delta\big[(k_{j_1}^f)^2 - (m_{j_1}^f)^2\big]\prod_{j_2}\frac{\mathrm{d}^4k_{j_2}}{(2\pi)^3}\delta\big[(k_{j_2})^2 - (m_{j_2})^2\big]\end{aligned} \tag{2.61}$$

accounting for the space of possible initial- and final-state momenta.

2.5.1 Final State Radiation

Cross sections for a fixed number of massless particles in the final state cannot be measured directly, because this would require, for instance, to distinguish a charged particle from the photons of the electrical field surrounding it. This, however, is not possible experimentally. As a consequence, final states where massless particles cannot be resolved are physically equivalent and have to be summed, integrating over their unresolved phase-space.

In this sense, additional particles in the final state are considered as *radiative corrections* to a process rather than as a different process. For a process with a final state f,

the physical cross section is given by

$$\sigma_{2\to f,\text{phys}} = \sum_{j=0}^{\infty} \int \mathrm{d}\Phi_{f+j} \sigma_{2\to n+j} J(\Phi_f, x_{n+1}, ..., x_{n+j}, 0, ..., 0), \tag{2.62}$$

where the variables x integrate over the regions of phase-space where the additional particles $\{1, ..., j\}$ cannot be resolved. The function J must have the limit

$$\lim_{x_i \to 0} J(\Phi_f, \{x\}) = J(\Phi_f) \tag{2.63}$$

and can be used e.g. to cluster strongly interacting particles in the final state into jets. The definition of an observable depends on the choice of J, which therefore has to be chosen consistently between theory calculations and experiments. Physical observables have to be defined as *infrared save*, i.e. such that physically indistinguishable states are summed over. For such observables, the infrared divergences in theory calculations cancel and only such observables can be measured experimentally.

2.5.2 Fixed-Order Computations

Both the cross-section and the amplitudes of a process can be expanded in terms of fundamental coupling constants. For a $2 \to n$ amplitude which is expanded in some coupling constant g, this expansion is given by

$$A_{2\to n} = F(g)\big(A^{(0)} + g^2 A^{(1)} + g^4 A^{(2)} + O(g^6)\big), \tag{2.64}$$

where $A^{(L)}$ corresponds to an $L-$loop amplitude and $F(g)$ is the coupling structure of the tree-level amplitude. Amplitudes with additional final state radiation have extra powers of the coupling constant

$$A_{2\to n+j} = F(g) g^j \big(A^{(0)} + g^2 A^{(1)} + g^4 A^{(2)} + O(g^6)\big). \tag{2.65}$$

Thus, all squared amplitudes needed to calculate the physical cross-section for $A_{2\to n}$ to order $F(g)g^4$ are

$$\begin{aligned} |A_{2\to n}|^2 = F^2(g)\Big[&|A^{(0)}_{2\to n}|^2 + g^2 A^{(0)*}_{2\to n} A^{(1)}_{2\to n} + g^2 A^{(1)*}_{2\to n} A^{(0)}_{2\to n} \\ &+ g^4 A^{(2)*}_{2\to n} A^{(0)}_{2\to n} + g^4 A^{(0)*} A^{(2)}_{2\to n} + g^4 |A^{(1)}_{2\to n}|^2 + O(g^6)\Big], \end{aligned} \tag{2.66}$$

$$|A_{2\to n+1}|^2 = F^2(g)\Big[g^2 |A^{(0)}_{2\to n+1}|^2 + g^4 A^{(0)*}_{2\to n+1} A^{(1)}_{2\to n+1} + g^4 A^{(1)*}_{2\to n+1} A^{(0)}_{2\to n+1} + O(g^6)\Big], \tag{2.67}$$

$$|A_{2\to n+2}|^2 = F^2(g)\Big[g^4 |A^{(0)}_{2\to n+2}|^2 + O(g^6)\Big]. \tag{2.68}$$

Inserting this into eqn. (2.60) and performing the summation of eqn. (2.62) we find for the infrared save observable

$$\begin{aligned}\sigma_{2\to n,\text{phys}} =& \frac{F(g)^2}{\sqrt{(k_1k_2)^2-(m_1^i)^2(m_2^i)^2}}\Bigg[\int \mathrm{d}\Phi_n |A^{(0)}_{2\to n}|^2 J \\ &+ g^2\left[\left(\int \mathrm{d}\Phi_n A^{(0)*}_{2\to n}A^{(1)}_{2\to n}J + A^{(1)*}_{2\to n}A^{(0)}_{2\to n}J\right) + \left(\int \mathrm{d}\Phi_{n+1}|A^{(0)}_{2\to n+1}|^2 J\right)\right] \\ &+ g^4\Bigg[\int \mathrm{d}\Phi_n A^{(2)*}_{2\to n}A^{(0)}_{2\to n} + A^{(0)*}A^{(2)}_{2\to n}J + |A^{(1)}_{2\to n}|^2 J \\ &+\Big(\int \mathrm{d}\Phi_{n+1}A^{(0)*}_{2\to n+1}A^{(1)}_{2\to n+1}J + A^{(1)*}_{2\to n+1}A^{(0)}_{2\to n+1}J\Big) + \int \mathrm{d}\Phi_{n+2}|A^{(0)}_{2\to n+2}|^2 J\Bigg] + O(g^6)\Bigg],\end{aligned} \tag{2.69}$$

where we dropped the arguments of J. The amplitudes $A^{(n)}$ each contain infrared divergences for $n > 0$, i.e. they can only be defined as the (singular) limits of their regularised versions (see section 2.3.1). The same is true for the phase space integrals which become singular when the unresolved particles have zero energy (*soft* divergence) or are parallel to the final state particles (*collinear* divergence). It turns out, however, that these divergences cancel against each other at each order in perturbation theory, which is proven by the Kinoshita-Lee-Nauenberg theorem [87,104]. Thus, the complete terms proportional to $F(g)g^2$ and $F(g)g^4$ are finite[5]. Since the integrations over the phase-spaces are typically carried out numerically, making these cancellaions explicit is a highly non-trivial problem which is actively being investigated (see e.g. [27,105–113]). This applies, in particular, for processes whose final states contain several light partons. Recently, such a cross-section computation was carried out at NNLO for three strongly interacting particles in the final state for the first time [27]. In this work, however, we focus on another bottleneck of the computation: the two-loop amplitudes $A^{(2)}_{2\to n}$.

2.5.3 Parton Model

At the LHC protons are collided instead of elementary particles. At sufficiently high energies, however, the strong coupling constant becomes small (see section 2.4), so that the process can be modelled as the constituents colliding as free particles [114,115] . The constituents, however, will only carry a fraction of the protons momentum.

To obtain predictions for a proton-proton collision the partonic cross-section therefore has to be equipped with the parton distribution functions (PDFs) $f_{P,p}(x,\mu_F)$, describing the probability that the proton P contains a parton p carrying the momentum fraction x. These functions depend on the energy scale μ_F at which the protons scatter.

[5]Assuming that the ultraviolet divergences are removed through renormalisation (see section 2.4)

The differential cross-section is then given by

$$\mathrm{d}\sigma_{PP\to f}(k_1,k_2,\{k_f\}) = \mathrm{d}x_1\mathrm{d}x_2 \sum_{p_1,p_2} f_{P,p_1}(x_1,\mu_F) f_{P,p_2}(x_2,\mu_F) \frac{\mathrm{d}\sigma_{p_1,p_2\to f}(x_1k_1,x_2k_2,\{k_f\})}{\mathrm{d}x_1\mathrm{d}x_2}. \tag{2.70}$$

These PDF's cannot be computed in perturbation theory, since QCD is non-perturbative at the binding energy of the proton. Instead, they are typically extracted from measurements[6]. The dependence of the PDFs on the scale μ_F can however be computed perturbatively by Dokshitzer-Gribow-Lipatow-Altarelli-Parisi evolution equations [118–120] (DGLAP). It is therefore possible to measure the PDFs at one energy scale and extrapolate to another, or combine data from different scales to fit PDFs. In addition to the PDFs, strongly interacting final states will radiate additional strongly interacting particles due to the strength of their interaction and eventually form hadrons. Therefore, in a particle detector multi-particle jets are observed instead of elementary quarks and gluons. This multi-particle creation from a single parton is modelled in *parton showers* (see e.g. [121]) and *hadronisation models* (see e.g. [122–124]). These have to be multiplied to the partonic cross-section and merged carefully with real radiation corrections, avoiding double counting. Since this work focusses on amplitudes, however, we will not go into details of PDF evolution, parton showers or hadronisation here.

[6] An alternative could be to use lattice QCD for PDF determination (see e.g. [116, 117] for recent reviews), which however is not competitive to this day.

Chapter 3

Multi-Loop Feynman-Integrals

So far, we have reviewed the definition of scattering amplitudes and how they can be computed using Feynman rules. In this approach, however, a number of challenges appear for increasing the number of loops and/or external legs: First, drawing all diagrams and applying Feynman rules can be algebraically very complicated due to the factorial growth of diagrams with loops and external legs. Second, reducing Feynman diagrams to a basis of master integrals via integration-by-parts reduction leads to enormous equation systems. Finally, the remaining multi-dimensional master integrals are difficult to integrate.

In this chapter, we will review integral reduction and the powerful approach of differential equations used for the computation of master integrals.

3.1 Integral Reduction

In this thesis we are concerned with Feynman integrals defined in dimensional regularisation which have at most two loops and whose propagators are massless. Therefore, their most general form is

$$I = \int \frac{\mathrm{d}^D \ell_1}{i\pi^{D/2}} \frac{\mathrm{d}^D \ell_2}{i\pi^{D/2}} \frac{N(\ell_1, \ell_2)}{\varrho_1^{e_1} \cdots \varrho_n^{e_n}}, \tag{3.1}$$

where

$$\varrho_j = (\alpha_1^j \ell_1 + \alpha_2^j \ell_2 + \beta_1^j k_1 + ... + \beta_n^j k_n)^2$$

are the inverse propagators with $\alpha_i^j, \beta_i^j \in \{-1, 0, 1\}$. N is a polynomial in loop momenta and the exponents $e_j \in \mathbb{N}_{>0}$.

Note that in this context, propagators involving only external momenta are factored from the integral and only the loop-momentum dependent denominators are considered the denominator of the integrand. In the following, the term *inverse propagator* will refer to loop-momentum dependent inverse propagators unless explicitly stated otherwise.

Conventionally, Feynman integrals sharing the same set of inverse propagators are

defined to belong to the same *integral topology*. Such topologies are denoted according to the number of propagators involving ℓ_1, respectively ℓ_2. Integrals involving n internal propagators that depend on ℓ_1 and k propagators depending on ℓ_2 are called a $n-k$-gon integral. If these propagators involving ℓ_1, respectively ℓ_2 do not overlap, the integrals over the loop momenta factorise, and hence such a topology is called *factorising*. If there is exactly one propagator involving both ℓ_1 and ℓ_2, the topology is called *planar* and diagrams which are neither factorizing nor planar are called *non-planar*. It is conventional to denote mono-, di-, tri- and tetragons as tadpoles, bubbles, triangles and boxes, respectively. Two-loop diagrams have one or two *nodes*, i.e. vertices which are attached to propagators containing only ℓ_1 as well as propagators involving only ℓ_2.

We denote topologies as *simple* if no external lines are attached to the nodes, *generic* if external lines are attached to all nodes and *semi-simple* else (see figure 3.1 for example topologies).

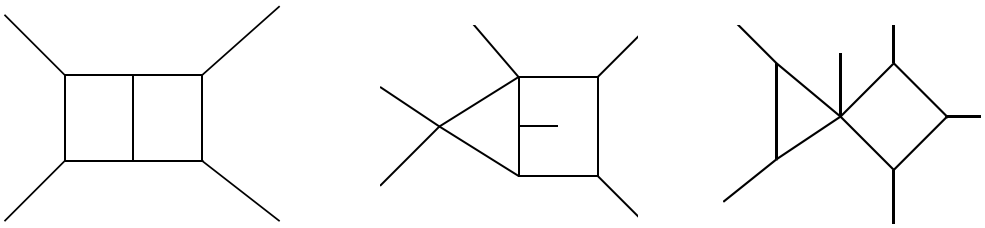

(a) Simple planar BoxBox

(b) Semi-simple non-planar BoxPentagon

(c) Generic factorizing TriangleBox

Figure 3.1: Examples of our naming convention for topologies.

There are some graph-theoretic symmetries between the diagrams; e.g. a $n-k$-gon and a $k-n$-gon can be transformed into each other by exchanging ℓ_1 and ℓ_2. Similarly, non-planar $n-$triangles are related to planar $(n-1)$-triangles by substituting $\ell_2 \to -\ell_2 - \ell_1$. We consider topolgies only modulo these symmetries.

Some diagrams are related in a more subtle way. In particular, a semi-simple $n-$bubble with momentum p_1 attached to one of the nodes and $p_2, ..., p_{n-1}$ on the loop is equal to a (graph-theoretically) different $n-$bubble with p_n attached to the node (see figure 3.2 for an example 3.2). For technical reasons, these topologies are considered as different.

After Feynman integrals and their possible numerators are defined, the first step is to find as many relations between these integrals as possible, leaving a minimal independent basis of integrals to be computed.

This is done both at integrand and integral level. In this section we will review the concepts of integrand level reduction, in particular the decomposition of scalar insertions into inverse propagators and irreducible scalar products. Moreover, the reduction at integral level through *integration-by-partsrelations* (IBPs) will be discussed.

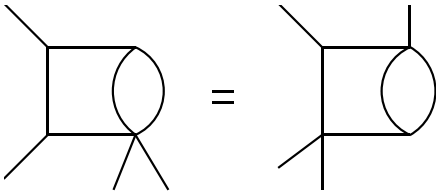

Figure 3.2: Two seemingly different integral topolgies which turn out to be equivalent.

3.1.1 Passarino-Veltmann Reduction

At first we will review relations between different integrands following the discussion of Passarino and Veltman [125].

The numerators $N(\ell_1, \ell_2)$ of the integrand are a polynomial in the loop-momenta ℓ and can be expressed in a basis of scalar products $\ell_i \cdot \ell_j$, $\ell_i \cdot k_j$, where k_j are external momenta and $\ell_j \cdot n_j$, where the n_j describe the D-dimensional vectors transverse to the *scattering plane*, i.e. the space spanned by the k_i. The n_j are conveniently normalised to $n_i \cdot n_j = \delta_{ij}$. Many of these scalar products are linear combinations of inverse propagators, hence the coordinate set which is used to describe numerators is chosen as $\{\varrho_1, ..., \varrho_n, \alpha_1, ..., \alpha_a, \beta_1, ..., \beta_b, n_j \cdot \ell_i\}$ [126]. The products of loop momenta with the transverse vectors $\ell_i \cdot n_j$ are denoted *transverse irreducible scalar products* (transverse ISPs) while the non-transverse ISPs α_j, β_j are a basis of scalar products of loop-momenta with external momenta which cannot be reduced to a linear combination of inverse propagators. In terms of these coordinates, the numerator can then be expressed as

$$N = \Delta(\{\alpha\}, \{\beta\}, \{\ell_i \cdot n_j\}) + \sum_j f_j(\ell_1, \ell_2)\varrho_j, \tag{3.2}$$

where both Δ and f_j are polynomials. All terms proportional to an inverse propagator ϱ_j cancel with the denominator and hence correspond to Feynman integrals in topologies with fewer propagators, conventionally called *descendant* topologies. Conversely, a topology is called an *ancestor* topology of another topology if the latter is a descendant of the first[1].

In Passarino-Veltman reduction these terms are split off and merged with the integrands of descendant topologies, such that the remainder Δ only depends on transverse and non-transverse ISPs. Equivalently, instead of ISPs it is possible to use quadratic terms, e.g. instead of $\ell_1 \cdot k_4$ one can use $(\ell_1 + k_4)^2$ if ℓ_1^2 is an inverse propagator, providing a more uniform treatment of propagators and ISPs.

To illustrate the treatment of the terms involving transverse ISPs $n \cdot \ell$, we consider the one-loop box diagram in D dimensions where the four inverse propagators are given

[1] In the literature ancestor and descendant topologies are sometimes also denoted *parent* and *daughter* topologies.

by

$$\varrho_1 = \ell^2 - m_1^2, \qquad \varrho_2 = (\ell - k_1)^2 - m_2^2, \tag{3.3}$$

$$\varrho_3 = (\ell - k_1 - k_2)^2 - m_3^2, \quad \varrho_4 = (\ell - k_1 - k_2 - k_3)^2 - m_4^2. \tag{3.4}$$

In this example, all scalar products of loop and external momenta as well as ℓ^2 can be expressed through inverse propagators

$$\ell^2 = m_1^2 + \varrho_1, \tag{3.5}$$

$$\ell \cdot k_1 = \frac{1}{2}\left(-\varrho_2 + \varrho_1 - m_2^2 + k_1^2\right), \tag{3.6}$$

$$\ell \cdot k_2 = \frac{1}{2}\left(-\varrho_3 + \varrho_2 - m_3^2 + m_2^2 + 2k_1 \cdot k_2 + k_1^2 + k_2^2\right), \tag{3.7}$$

$$\ell \cdot k_3 = \frac{1}{2}\left(-\varrho_4 + \varrho_3 - m_4^2 + m_3^2 + 2k_1 \cdot k_3 + 2k_2 \cdot k_3 + k_3 \cdot k_3\right), \tag{3.8}$$

$$k_4 \cdot \ell_1 = -\left(k_1 + k_2 + k_3\right) \cdot \ell, \tag{3.9}$$

hence the remaining numerator Δ only depends on transverse ISPs $n_i \cdot \ell$.

These vectors can be split into a four-dimensional vector n_4 and vectors n_ϵ^i which are transverse to the four-dimensional plane. The $(D-4)$-dimensional parts of ℓ can only enter into the numerator through squaring of the loop momentum, hence the scalar products $n_\epsilon^i \cdot \ell$ appear exclusively as the $(D-4)$-dimensional modulus

$$\mu^2 = \sum_i (n_\epsilon^i \cdot \ell)^2. \tag{3.10}$$

Expanding the loop momentum in terms of the external momenta and n_j

$$\ell = \sum_{j=1}^{3} k_j + a_4 n_4 + \sum_i a_\epsilon^i n_\epsilon^i, \tag{3.11}$$

gives coefficients $a_i = G_{ij}^{-1} \ell \cdot p_j$, where $p_{1,2,3} = k_{1,2,3}$ and $p_{4,5,6,\ldots} = n_4, n_\epsilon^{1,2,\cdots}$ while $G = \{p_i \cdot p_j\}$ is the Gram matrix of the external momenta and the ${n_j}^2$.

Inserting this expansion into the first inverse propagator gives

$$\ell^2 = (n_4 \cdot \ell)^2 + \sum_i (n_\epsilon^i \cdot \ell)^2 + \sum_{i,j} G_{ij}^{-1} (k_i \cdot \ell)(k_j \cdot \ell), \tag{3.12}$$

$$\Rightarrow (n_4 \cdot \ell)^2 + \mu^2 = \text{constant+inv. propagators}. \tag{3.13}$$

Hence all insertions in μ^2 can be reduced to insertions in the transverse momentum $n_4 \cdot \ell$,

[2]For $i > 3$ or $j > 3$, this matrix becomes δ_{ij} such that inversion is possible despite it being formally infinite dimensional.

the constant numerator and descendant integrals. In the multi-loop case, the number of propagators and the number of external legs do not coincide, hence some of the non-transverse scalar products $k_i \cdot \ell_j$ are ISPs themselves. Thus, the relevant variables are transverse and non-transverse ISPs. A basis of numerators is given by all monomials in these ISPs up to some maximal degree.

3.1.2 Integral-Level Reduction

Passarino-Veltman reduction allowed to e.g. reduce the integrand basis for the one-loop box diagram to be evaluated from 126 to five (not counting descendant topologies), namely the numerators $(\ell \cdot n_4)^n$, $n \in \{0, 1, 2, 3, 4\}$. Although this is a great simplification, the computation of the remaining integrals is still difficult, especially at multi-loop level. In this section we will review how further reduction is possible employing traceless completions following from Lorentz invariance and (more generally) integration-by-parts relations.

Traceless Completions

Integrals which are different at integrand level can still be related in their integrated form. As an example for such an identity consider the integrals

$$I_1 = \int \mathrm{d}^D\ell_1 \mathrm{d}^D\ell_2 \frac{(\ell_1 \cdot k)^2}{\ell_1^2 \ell_2^2}, \quad I_2 = \int \mathrm{d}^D\ell_1 \mathrm{d}^D\ell_2 \frac{(\ell_2 \cdot k)^2}{\ell_1^2 \ell_2^2}. \tag{3.14}$$

Evidently $I_1 = I_2$, although $\ell_1 \cdot k \neq \ell_2 \cdot k$ and the denominator does not permit a further reduction. For the computation of scattering amplitudes it is extremely useful to find and apply such relations in order to reduce the computational effort.

As an example, we consider again the one-loop box, whose integrand basis in YM-theories is given by

$$\{1, n_4 \cdot \ell, (n_4 \cdot \ell)^2, (n_4 \cdot \ell)^3, (n_4 \cdot \ell)^4\}. \tag{3.15}$$

Odd powers of $n_4 \cdot \ell$ are antisymmetric in the component of ℓ parallel to n_4. Propagators, on the other hand, are quadratic in these components, hence the integrand is anti-symmetric and therefore vanishes upon integration. Another integral-level identity allows the complete reduction of even powers. If the integrand does not explicitly depend on transverse vectors, the rotational symmetry between transverse vectors prohibits that the integral depends on them and thus it can be parametrised with the metric and external momenta only

$$\int \frac{\mathrm{d}^D\ell_1}{i\pi^{D/2}} \frac{\mathrm{d}^D\ell_2}{i\pi^{D/2}} \frac{N(\ell_1, \ell_2, \{k\})\ell_a^\mu \ell_a^\nu}{\varrho_1^{e_1} \cdots \varrho_n^{e_n}} = c_0 g^{\mu\nu} + \sum_{i,j} c_{i,j} k_i^\mu k_j^\nu. \tag{3.16}$$

Contracting both sides with $n_j^\mu n_j^\nu - \frac{g^{\mu\nu}_{[D-4]}}{D-4}$ (without summation over j), where

$$g^{\mu\nu}_{[D-4]} = g^{\mu\nu} \quad \text{for} \quad \mu,\nu > 3, \quad 0 \quad \text{else} \tag{3.17}$$

gives [127]

$$\int \frac{\mathrm{d}^D\ell_1}{i\pi^{D/2}} \frac{\mathrm{d}^D\ell_2}{i\pi^{D/2}} \frac{N(\ell_1,\ell_2,\{k\})\left((\ell_a\cdot n_j)^2 - \frac{\mu_{aa}}{D-4}\right)}{\varrho_1^{e_1}\cdots\varrho_n^{e_n}} = 0. \tag{3.18}$$

Similarly, relations for any even power of $\ell_i \cdot n_j$ can be created by contracting products of loop-momenta $\prod_j \ell_{k_j}^{\mu_j}$ with the tensors

$$n_j^{\mu_1}\cdots n_j^{\mu_n} - \frac{1}{n}\frac{1}{D-4} \sum_{\sigma\in\text{perm. of}(1,\ldots,n)} g^{\mu_{\sigma(1)}\mu_{\sigma(2)}}_{[D-4]} n_j^{\mu_{\sigma(3)}}\cdots n_j^{\mu_{\sigma(n)}}. \tag{3.19}$$

These tensors vanish when contracted with $g^{\mu_i\mu_j}$, hence the name *traceless*. The resulting relations, called *traceless completions*, allow to reduce the dependence on transverse ISPs for all integrals. For example, this allows to completely reduce the box-integral to the scalar numerator 1.

Integration-by-Parts Reduction

There are additional relations between integrals depending on non-transverse ISPs. Such relations were first constructed and applied by Chetrykin and Tkachov [128] by applying derivatives to the integrand:

$$\int \frac{\mathrm{d}^D\ell_1}{i\pi^{D/2}}\cdots\frac{\mathrm{d}^D\ell_L}{i\pi^{D/2}} \frac{\partial}{\partial\ell_a^\mu} \frac{N}{\varrho_1\cdots\varrho_N}. \tag{3.20}$$

By Stokes theorem such integrals give boundary terms

$$\int \frac{\mathrm{d}^D\ell_1}{i\pi^{D/2}}\cdots\frac{\mathrm{d}^{D-1}\ell_a}{i\pi^{D/2}}\cdots\frac{\mathrm{d}^D\ell_L}{i\pi^{D/2}} \frac{N}{\varrho_1\cdots\varrho_N}\Big|^{\ell_a^\mu = \infty}_{\ell_a^\mu = -\infty}. \tag{3.21}$$

In dimensional regularisation, these boundary terms are treated to be zero since for each integral there is a dimensional parameter $D' \in \mathbb{R}$ such that for $\mathrm{Re}(D) < D'$ these surface terms are zero. Analytically continuing in D, starting from this region, the boundary terms vanish in all dimensions [129]. Since Feynman integrals have no branch cuts in D, the analytical continuation is independent from the starting point.

When applying such derivatives to integrals with fixed dimension in a finite theory, or a four-dimensional regularisation involving e.g. a cut-off, non-vanishing boundary terms have to be taken into account [130]. Since Stokes theorem is only valid for finite integrals, it is furthermore necessary to regularise IR divergences formally before applying

derivatives. While this requires some care in other regularisation schemes, IR divergences are automatically regularised in dimensional regularisation (see section 2.3.1). Taking eqn. (3.20) and expanding the derivative gives a vanishing sum of integrands, i.e. a linear dependence. Such relations are known as integration-by-parts (IBP) relations [128]. The standard procedure to reduce integrals via such relations is Laporta's alorithm. The idea is to apply all derivatives $k_\mu \cdot \frac{\partial}{\partial \ell_\mu^a}, \ell_\mu^b \cdot \frac{\partial}{\partial \ell_\mu^a}$ to a set of monomials and reduce the resulting linear system [131].

This allows, for example, to reduce one-loop integrals with arbitrary propagator powers to integrals where all propagators have power one, e.g. for the massless one-loop box [132]

$$\int \frac{\mathrm{d}^D \ell}{i\pi^{D/2}} \frac{1}{\varrho_1^2 \varrho_2 \varrho_3 \varrho_4} = \frac{D-5}{s} \int \frac{\mathrm{d}^D \ell}{i\pi^{D/2}} \frac{1}{\varrho_1 \varrho_2 \varrho_3 \varrho_4} - \frac{4(D-5)(D-3)}{(D-6)st^2} \int \frac{\mathrm{d}^D \ell}{i\pi^{D/2}} \frac{1}{\varrho_2 \varrho_4}, \quad (3.22)$$

where $s = (k_1 + k_2)^2$, $t = (k_1 - k_3)^2$ and ϱ are the inverse propagators from eqn. (3.3) with $m_j = 0$. IBP-reduction furthermore allows to reduce triangles with two massless legs to bubbles [132]

$$\int \frac{\mathrm{d}^D \ell}{i\pi^{D/2}} \frac{1}{\varrho_1 \varrho_2 \varrho_4} = \frac{2(D-3)}{(D-4)t} \int \frac{\mathrm{d}^D \ell}{i\pi^{D/2}} \frac{1}{\varrho_2 \varrho_4}, \quad (3.23)$$

with the inverse propagators defined in eqn. (3.3). In the multi-loop case, IBPs reduce all possible numerators down to a small number of irreducible integrals. These remaining integrals are then called *master* integrals.

For two-loop processes with five external momenta, typically $O(100)$ different monomials per topology contribute to the amplitude, while most topologies have zero to two master integrals, with a few exceptions where up to nine masters have to be computed.

In principle, IBP-relations between different topologies on the same level are possible. For example, this can occur when a derivative applied to an integral gives only terms which are integrals in the descendant topologies. This could lead to cases where the master integrals of two topologies which are only related by common ancestors are dependent [133]. We find it convenient, however, to consider the topologies one by one, reducing each topology to its own masters and descendants and therefore not considering such relations.

Solving the linear systems obtained by such generic derivatives is challenging in general, since the relations span a huge function space. In fact, the reduction to master integrals is a bottleneck in the computation of multi-loop amplitudes. There are many publicly available programs which automate this procedure, such as Fire [134], Reduze [135], LiteRed [136] or Kira [137]. However, for two-loop integral topologies with more than four kinematic invariants these programs are computationally intense.

We therefore use an alternative approach: unitarity compatible IBP-relations (see

chapter 4) combined with numerical unitarity (see section 5.5).

3.2 The Differential Equation Approach to Master Integrals

Integration-by-parts reduction allows to reduce the large amount of Feynman-Integral numerators to a relatively small number of master integrals. These master integrals can be computed via direct integration (see e.g. [138–143]), or with the method of differential equations [29, 30, 144–146].

Multi-loop amplitude computation consists of computing sets of master integrals and expressing amplitudes through them. This work focusses on the latter part, i.e. expressing amplitudes in terms of master integrals. Nevertheless, since we will exploit some properties of the master integral basis chosen and since the master integrals themselves are an important ingredient in the computation, we will briefly review how they have been computed for the processes that we consider. Specifically, we will review the approach of differential equations in their canonical form [31] which has demonstrated great success in the computation of multi-loop master-integrals.

In the previous section, derivatives with respect to loop momenta have been a applied to Feynman integrands. Similarly, the integrals (or equivalently the integrands) can be differentiated with respect to an external momentum

$$\begin{aligned} I &= k_i^\mu \frac{\partial}{\partial k_j^\mu} \int \frac{\mathrm{d}^D \ell_1}{i\pi^{D/2}} \frac{\mathrm{d}^D \ell_2}{i\pi^{D/2}} \frac{N(\ell_1, \ell_2)}{\varrho_1 \cdots \varrho_n} \\ &= \int \frac{\mathrm{d}^D \ell_1}{i\pi^{D/2}} \frac{\mathrm{d}^D \ell_2}{i\pi^{D/2}} \left(\frac{k_i^\mu \frac{\partial}{\partial k_j^\mu} N(\ell_1, \ell_2)}{\varrho_1 \cdots \varrho_n} - \sum_i \frac{N(\ell_1, \ell_2) k_i^\mu \frac{\partial}{\partial k_j^\mu} \varrho_i}{\varrho_1 \cdots \varrho_i^2 \cdots \varrho_n} \right), \end{aligned} \tag{3.24}$$

where the objects on the right hand side are again Feynmn integrals, in the same topology or its descendants. Typically, the derivatives are not taken w.r.t. external momenta but kinematic invariants $\frac{\partial}{\partial s_{ij}} = (\frac{\partial s_{oj}}{\partial k_n^\mu})^{-1} \frac{\partial}{\partial k_n^\mu}$. As was discussed in the previous section, all integrals in a topology and its descendants can be reduced to a basis of a few master integrals.

Differentiating such a basis $\vec{f}(\{s_{ij}, D)$ w.r.t. kinematic invariants and reducing the r.h.s. back to the basis therefore gives a linear partial differential equation of first order [29, 30, 144–146]

$$\partial_{s_{ij}} \vec{f}(\{s_{ij}\}, D) = A_{s_{ij}}(\{s_{ij}\}, D) \vec{f}(\{s_{ij}\}, D). \tag{3.25}$$

For example, for the massless one-loop box with the master integral basis

$$\vec{f}(s,t,D) = \left(\int \frac{\mathrm{d}^D\ell}{i\pi^{D/2}} \frac{1}{\varrho_2\varrho_4}, \quad \int \frac{\mathrm{d}^D\ell}{i\pi^{D/2}} \frac{1}{\varrho_1\varrho_3}, \quad \int \frac{\mathrm{d}^D\ell}{i\pi^{D/2}} \frac{1}{\varrho_1\varrho_2\varrho_3\varrho_4}\right)^T, \tag{3.26}$$

the differential equations are given by

$$\partial_s \vec{f}(s,t,D) = \begin{pmatrix} 0 & 0 & 0 \\ 0 & \frac{D-4}{2s} & 0 \\ \frac{-2(D-3)}{st(s+t)} & \frac{2(D-3)}{s^2(s+t)} & \frac{-2s+t(D-6)}{2s(s+t)} \end{pmatrix} \vec{f}(s,t,D), \tag{3.27}$$

$$\partial_t \vec{f}(s,t,D) = \begin{pmatrix} \frac{D-4}{2t} & 0 & 0 \\ 0 & 0 & 0 \\ \frac{-2(D-3)}{t^2(s+t)} & \frac{-2(D-3)}{st(s+t)} & \frac{-2t+s(D-6)}{2t(s+t)} \end{pmatrix} \vec{f}(s,t,D). \tag{3.28}$$

Instead of directly integrating the Feynman integrals in loop-momentum space, their solution can be obtained by solving this differential equations and fixing boundary conditions.

3.2.1 Differential Equations in Canonical Form

During IBP-reduction a choice has to be made as to which integrals are considered as master integrals. Moreover, it is always possible to multiply master integrals with functions in the kinematic invariants and D, since such functions factorise from the IBP-reduction. It is desirable to exploit this non-uniqueness of master-integrals in order to find a basis for which the differential equation is particularly simple.

From the structure of Feynman integrals it is natural to expect that near a singular variety described by a polynomial $W(\{s_{ij}\}) = 0$, the integral behaves like $W(\{s_{ij}\})^{-n}$ for some $n \in \mathbb{Z}$, i.e. that the system of differential equations is Fuchsian.

If this is the case, there is always a linear transformation $\vec{g} = A(\{s_{ij}\}, D)\vec{f}$ such that the differential equation for an arbitrary combination of kinematic invariants x becomes

$$\partial_x \vec{g} = \left(\frac{1}{W(\{s_{ij}\})} A(D) + O(W^0)\right) \vec{g}, \tag{3.29}$$

where $A(D)$ is a matrix depending only on the dimension D. It turns out that this can be done for all singularities at the same time, reducing the differential equation to the sum[3]

$$\partial_x \vec{g}(\{s_{ij}\}, D) = \left(\sum_i \frac{\partial_x W_i}{W_i} A_i(D) + p(s_{ij}, D)\right) \vec{g}(\{s_{ij}\}, D), \tag{3.30}$$

where p is a polynomial in the kinematic invariants. This polynomial can be removed by introducing additional (rational) W_i.

[3]The objects $\frac{\partial W_i}{W_i} = \partial_x \log(W_i)$ are often referred to as dlog forms.

In most cases, in particular in phenomenological applications, master integrals are studied close to four dimensions, i.e. they are expressed in terms of $\epsilon = \frac{4-D}{2}$ and expanded for small ϵ. Therefore, a particularly convenient form of the differential equation is to have the epsilon-dependence factorised from the integral, such that the derivatives are of higher order in ϵ than the integral itself. If this is the case and, at the same time, the integral can be written in the form of eqn. (3.30) [147], the basis is called pure and the differential equation in its *canonical form* is given by [31]

$$\frac{d}{dx}\vec{g}(\{s_{ij}\}),\epsilon) = \epsilon \sum_i \frac{\partial_x W_i}{W_i} A_i \vec{g}(\{s_{ij}\},\epsilon), \tag{3.31}$$

where the A_i are constant matrices, i.e. they contain only rational numbers. The W_i in such a basis are called *letters of the symbol alphabet*. In the one-loop massless box example discussed above, such a basis is given by

$$g_1 = \epsilon \mathrm{e}^{\epsilon\gamma_E}(-s)^\epsilon t \int \frac{\mathrm{d}^D\ell}{i\pi^{D/2}} \frac{1}{\varrho_2\varrho_4^2}, \tag{3.32}$$

$$g_2 = \epsilon \mathrm{e}^{\epsilon\gamma_E}(-s)^\epsilon s \int \frac{\mathrm{d}^D\ell}{i\pi^{D/2}} \frac{1}{\varrho_1\varrho_3^2}, \tag{3.33}$$

$$g_3 = \epsilon^2 \mathrm{e}^{\epsilon\gamma_E}(-s)^\epsilon st \int \frac{\mathrm{d}^D\ell}{i\pi^{D/2}} \frac{1}{\varrho_1\varrho_2\varrho_3\varrho_4}, \tag{3.34}$$

which fulfils the (canonical) differential equation

$$\partial_x \vec{g} = \epsilon \left(\frac{\partial_x W_1}{W_1} \begin{pmatrix} -1 & 0 & 0 \\ 0 & 0 & 0 \\ -2 & 0 & 1 \end{pmatrix} - \frac{\partial_x W_2}{W_2} \begin{pmatrix} -1 & 0 & 0 \\ 0 & 0 & 0 \\ -2 & 0 & 1 \end{pmatrix} - b\frac{\partial_x W_3}{W_3} \begin{pmatrix} 0 & 0 & 0 \\ 0 & 0 & 0 \\ 2 & 2 & 1 \end{pmatrix} \right) \vec{g}, \tag{3.35}$$

with the three letters $W_1 = s, W_2 = t, W_3 = \frac{t}{s+t}$. The advantage of such a differential equation with factorized ϵ is that the pieces of the ϵ expansion can be computed recursively. With

$$\vec{g} = \sum_i \vec{g}_i \epsilon^i, \tag{3.36}$$

the individual terms are given by

$$\vec{g}_{n+1}(s_{ij}) = \vec{g}_{n+1}(s_{ij}^0) + \int_{s_{ij}^0}^{s_{ij}} \left(\sum_j \frac{\partial_{s'_{ij}} W_j}{W_j} \vec{g}_n(s'_{ij}) \right) \mathrm{d}s'_{ij}. \tag{3.37}$$

The boundary conditions $\vec{g}_n(s_{ij}^0)$ can be found either by limits in which the integrals are known (e.g. when external momenta become zero and thus the $n-$point integral becomes

an $n-1-$point integral) or by demanding certain properties of Feynman integrals such as the absence of spurious logarithms [34].

The integration can then be done either numerically along a path [34,38–40], through iterated integral methods in the form of so called *pentagon functions* [41–43] or analytically in terms of multiple poly-logarithms [33,36].

There are known cases, in particular elliptic integrals, where no canonical form of the differential equation exists. Nevertheless, great progress on elliptic integrals has been made in recent years, partially employing the method of differential equations (see e.g. [148–166]). For the processes considered in this thesis, however, such bases have been found in [167] and [42], respectively.

Another advantage of using a pure basis is that the coefficients of integral reduction in this basis are particularly simple (see section 5.6). In particular, it has been observed that for pure basis the ϵ-dependence factorises from master-integral coefficients and the kinematically dependent numerators factor into symbol letters [57].

Chapter 4

Integral Reduction via Generating Vectors

In the previous chapter we have reviewed integration-by-parts identities. In general, the function space spanned by these IBP-relations generated by generic derivatives is unnecessarily larger than the space of functions needed for the integral reduction, making a direct application of Laporta's algorithm computationally intense. In this chapter, we will discuss how integral relations within defined function spaces can be generated by applying derivatives in special directions described by polynomial vector-fields called *IBP-generating vectors* [47]. Besides the smaller function space, another advantage of this representation is that the relations can be expressed in terms of vector components which cache the complicated functional dependencies and hence reduce the file-size and numerical-evaluation time of the sets of relations. We will describe how we compute these vectors and discuss some observed properties.

4.1 Integration-by-Parts Generating Vectors

Depending on the coordinates employed for the construction of IBP's, the problem of a reduced function-space takes different forms. In this section, we will review different formulations and their respective defining equations for IBP-vectors. In particular, we will discuss the formulations in loop-momentum space, Baikov-coordinates and a projective embedding space of the loop momenta.

4.1.1 Fixed Propagator Powers

A general (Lorentz-invariant) IBP-relation is obtained as a divergence

$$0 = \int \frac{\mathrm{d}^D \ell_1}{(i\pi)^{D/2}} \cdots \frac{\mathrm{d}^D \ell_L}{(i\pi)^{D/2}} \frac{\partial}{\partial \ell_a^\mu} \frac{v_a^\mu N}{\varrho_1^{a_1} \cdots \varrho_N^{a_n}}, \tag{4.1}$$

where $\varrho_i^{a_i}$ are the inverse propagators raised to some power a_i, while N and v_a^μ are polynomials in the loop-momenta. Applying such derivatives with respect to loop momenta to Feynman-integrals in general leads to raised propagator powers, since

$$\frac{\partial}{\partial \ell_a^\mu}\frac{1}{\varrho_i^{a_i}} = -a_i \frac{1}{\varrho_i^{a_i+1}}\frac{\partial \varrho_i}{\partial \ell_a^\mu}. \tag{4.2}$$

Feynman rules, however, typically give integrals with propagator powers less or equal to one[1]. Therefore, for integral reduction the space of functions can be greatly reduced by avoiding raised propagator powers. Such IBP-relations without doubled propagators are in fact also necessary for generalised unitarity (see section 5.5). Therefore, such relations are denoted as *unitarity compatible* IBPs [46].

IBP-relations with this property can be obtained by imposing conditions on the vector fields $v_a^\mu(\ell_b)$, in particular

$$v_a^\mu(\ell_b)\frac{\partial \varrho_i}{\partial \ell_a^\mu} = P_i(\ell_b)\varrho_i \quad \forall i, \tag{4.3}$$

where the P_i and the vector components v_i^μ are polynomials in the loop momenta [46,47]. Such IBP-generating vectors lead to the relations

$$0 = \int \frac{\mathrm{d}^D \ell_1}{(i\pi)^{D/2}} \cdots \frac{\mathrm{d}^D \ell_L}{(i\pi)^{D/2}} \frac{\partial}{\partial_{\ell_a^\mu}} \frac{v_a^\mu N}{\varrho_1^{a_1}\cdots\varrho_N^{a_n}} \tag{4.4}$$

$$= \int \frac{\mathrm{d}^D \ell_1}{(i\pi)^{D/2}} \cdots \frac{\mathrm{d}^D \ell_L}{(i\pi)^{D/2}} \frac{v_a^\mu \left(\frac{\partial N}{\partial \ell_a^\mu}\right) + N\left(\frac{\partial v_a^\mu}{\partial \ell_a^\mu} - \sum_i a_i P_i\right)}{\varrho_1^{a_1}\cdots\varrho_N^{a_n}}. \tag{4.5}$$

One-Loop Example: Massless Box

To exemplify the reduction with unitarity compatible IBP-relations, we consider again the one-loop box integral

$$I = \int \frac{\mathrm{d}^D \ell}{i\pi^{D/2}} \frac{N}{\varrho_1 \cdots \varrho_4}. \tag{4.6}$$

An IBP-generating vector satisfying eqn. (4.3) can be constructed constructed by taking n_4 and components of ℓ which are transverse to the scattering plane and antisymmetrising over them

$$v^\mu = \mu^2 n_4^\mu - (n_4 \cdot \ell)\left[\ell^\mu - G_{ij}^{-1}(\ell \cdot k_i)k_j^\mu - (n_4 \cdot \ell)n_4^\mu\right], \tag{4.7}$$

where μ^2 is the $(D-4)$ dimensional part of the loop-momentum squared (see eqn. (3.10)) and n_4 is a vector transverse to the scattering plane with $n_4^2 = 1$. The term proportional

[1]Exceptions are topologies where two propagators attached to a sub-loop bubble are the same.

to $n_4 \cdot \ell$ projects ℓ onto the $D-4$ dimensional subspace, thereby

$$v^\mu \ell_\mu = \mu^2 (n_4 \cdot \ell) - (n_4 \cdot \ell)\mu^2 = 0, \qquad v^\mu k_\mu^j = 0 \;\; \forall j \tag{4.8}$$

$$\Rightarrow \;\; v^\mu \frac{\partial}{\partial \ell^\mu} \varrho_i = 0 \;\; \forall i. \tag{4.9}$$

Applying this vector to the integrand with numerator $N = n_4 \cdot \ell$ gives

$$0 = \int \frac{\mathrm{d}^D \ell}{i\pi^{D/2}} \frac{\partial}{\partial \ell^\mu} \frac{(n_4 \cdot \ell) v^\mu}{\varrho_1 \cdots \varrho_4} = \int \frac{\mathrm{d}^D \ell}{i\pi^{D/2}} \frac{1}{\varrho_1 \cdots \varrho_4} \Big[(n_4 \cdot \ell) \Big(n_4^\mu \frac{\partial \mu^2}{\partial \ell^\mu} - 2 n_4^\mu \left[\ell_\mu - (n_4 \cdot \ell) n_{4,\mu} \right] \tag{4.10}$$

$$- (n_4 \cdot \ell) \left[\frac{\partial \ell^\mu}{\partial \ell^\mu} - G_{ij}^{-1} G_{ij} - n_4^2 \right] \Big) + \mu^2 n_4^2 \Big]$$

$$= \int \frac{\mathrm{d}^D \ell}{i\pi^{D/2}} \frac{1}{\varrho_1 \cdots \varrho_4} \left((4-D)(n_4 \cdot \ell)^2 + \mu^2 \right). \tag{4.11}$$

This reproduces the traceless completion from eqn. (3.18). We will now consider an example where ISP's without transverse vectors n_i^μ are present.

Two-Loop Example: The Sunrise

Consider the two-loop sunrise integral with massive external legs with momentum p and massless internal propagators

$$\varrho_1 = \ell_1^2, \qquad \varrho_2 = (\ell_2 - p)^2, \qquad \varrho_3 = (\ell_1 - \ell_2)^2. \tag{4.12}$$

This integral topology has eight ISPs

$$\nu_1 = \ell_1 \cdot n_2, \quad \nu_2 = \ell_1 \cdot n_3, \quad \nu_3 = \ell_1 \cdot n_3, \tag{4.13}$$

$$\nu_4 = \ell_2 \cdot n_2, \quad \nu_5 = \ell_2 \cdot n_3, \quad \nu_6 = \ell_2 \cdot n_3, \tag{4.14}$$

$$\alpha_1 = \ell_1 \cdot p, \quad \beta_1 = \ell_2^2, \tag{4.15}$$

where $n_{1,2,3}$ are chosen such that $n_i \cdot n_j = \delta_{ij}$ and $n_i \cdot p = 0$. Since the reduction of transverse ISPs can be achieved through transverse completions, we only consider non-transvwerse ISPs and IBP-vectors within the space spanned by ℓ_1, ℓ_2, p

$$v_a^\mu = b_a^1 \ell_1^\mu + b_a^2 \ell_2^\mu + b_a^3 p^\mu. \tag{4.16}$$

The condition that propagator powers are not raised (eqn. (4.3)) is thus expressed as

$$b_1^1\ell_1^2 + b_1^2\ell_2\cdot\ell_1 + b_1^3 p\cdot\ell_1 = P_1\ell_1^2, \tag{4.17}$$

$$b_2^1\ell_1\cdot(\ell_2+p) + b_1^2\ell_2\cdot(\ell_2+p) + b_2^3 p\cdot(\ell_2+p) = P_2(\ell_2+p)^2, \tag{4.18}$$

$$\begin{aligned} &b_1^1\ell_1\cdot(\ell_1-\ell_2) + b_1^2\ell_2\cdot(\ell_2-\ell_2) + b_1^3 p\cdot(\ell_1-\ell_2) \\ &+b_2^1\ell_1\cdot(\ell_1-\ell_2) + b_1^2\ell_2\cdot(\ell_1-\ell_2) + b_2^3 p\cdot(\ell_1-\ell_2) = P_3(\ell_1-\ell_2)^2. \end{aligned} \tag{4.19}$$

One of the solutions to this system of equations is given by

$$v_1^\mu = \ell_1^\mu(\ell_1\cdot\ell_2 + \ell_2\cdot p), \tag{4.20}$$

$$v_2^\mu = \ell_1^\mu(\ell_2\cdot p + p^2) + \ell_2^\mu(\ell_1\cdot\ell_2 + \ell_1\cdot p). \tag{4.21}$$

Applying this vector to a generic numerator gives the IBP

$$0 = \int \mathrm{d}^D\ell_1\mathrm{d}^D\ell_2 \frac{\partial}{\partial\ell_a^\mu}\frac{v_a^\mu \alpha_1^{e_1}\beta_1^{e_2}}{\varrho_1\varrho_2\varrho_3} \tag{4.22}$$

$$\begin{aligned} &= \int \mathrm{d}^D\ell_1\mathrm{d}^D\ell_2 \frac{1}{\varrho_1\varrho_2\varrho_3} \\ &\times\Big(3e_1 s\alpha^{e_1}\beta^{e_2+1} + 3e_2p^2\alpha^{e_1}\beta^{e_2+1} - 6p^2\alpha^{e_1}\beta^{e_2+1} + 2e_1\alpha^{e_1}\beta^{e_2+2} + 3e_2\alpha^{e_1}\beta^{e_2+2} \\ &- 6\alpha^{e_1}\beta^{e_2+2} + 2e_1\alpha^{e_1+1}\beta^{e_2+1} + 4e_2\alpha^{e_1+1}\beta^{e_2+1} - 8\alpha^{e_1+1}\beta^{e_2+1}\Big) + O(\varrho), \end{aligned} \tag{4.23}$$

where we omitted terms proportional to inverse propagators, because they correspond to massless tadpole integrals which vanish in dimensional regularisation. It can be shown that these IBPs, together with the relations generated by a second vector, allow to reduce all powers of α_1 and β_1 to the scalar integral (i.e. $e_1 = e_2 = 0$) [168].

The defining equations of IBP-generating vectors (eqns. (4.3,4.17)) are linear equations defined over the ring of polynomials in ℓ. In the context of algebraic geometry, the solutions to such equations are called *syzygies*[2]. We will discuss how these syzygies are found using *Gröbner basis* methods in section 4.2.2. Before, however, we will discuss two other formulations of the syzygy problem, which we find useful for the practical computation but also for the analysis of IBP-vectors.

4.1.2 Fixed Dimension in Baikov Coordinates

A different approach to the syzygy-problem uses *Baikov coordinates* [169,170] which trivialise the constraint of doubled propagators. The idea of Baikov coordinates is to use the inverse propagators and ISPs directly as variables.

For this purpose, first the $D-4$ dimensional loop momentum dependence is trans-

[2]from ancient Greek $\sigma\upsilon\zeta\upsilon\gamma\iota\alpha$, conjunction, yoked together.

formed to μ's

$$I = \int \mathrm{d}^D\ell_1 \cdots \mathrm{d}^D\ell_L \frac{N(\ell)}{\varrho_1(\ell)\cdots\varrho_N(\ell)} \tag{4.24}$$

$$= F(D) \int \mathrm{d}^4\ell_1 \cdots \mathrm{d}^4\ell_L \left(\det \begin{pmatrix} \mu_{11} & \dots & \mu_{1L} \\ \vdots & \ddots & \vdots \\ \mu_{1L} & \dots & \mu_{LL} \end{pmatrix}\right)^{(D-5-L)/2} \prod_{1\le i\le j\le L} \mathrm{d}\mu_{ij} \frac{N(\ell)}{\varrho_1(\ell)\cdots\varrho_N(\ell)}, \tag{4.25}$$

where $F(D)$ is a function that arises from the integration $D-n$ dimensional unit spheres for some integers n. Since it factorises from the integral, we will omit it in the following.

The desired integration variables are inverse propagators and ISPs. In order to achieve this, we first use a linear transformation to the inverse propagators and ISPs to a set of variables $\{\ell_a \cdot \ell_b\}$, $\{\ell_a \cdot p_i\}$, where p_i contains the external momenta p_i but also the transverse vectors in four dimensions n_i. We then have

$$\frac{\partial \mu_{ab}}{\partial(\ell_a \cdot p_j)} = 2G^{-1}_{ij} p_i \cdot \ell_b, \qquad \frac{\partial \mu_{ab}}{\partial(\ell_c \cdot \ell_d)} = \delta_{ac}\delta_{bd} + \delta_{ad}\delta_{bc}, \tag{4.26}$$

$$\frac{\partial \ell_b^{\mu=0,\dots,3}}{\partial(\ell_a \cdot p_i)} = \text{const.}, \qquad \frac{\partial \ell_b^{\mu=0,\dots,3}}{\partial(\ell_a \cdot \ell_b)} = 0, \tag{4.27}$$

where G is the Gram matrix of external momenta and n. The last equation is valid since the p_i span the four-dimensional space. The transformation matrix thus can be written as block-triangular, with the loop-momentum dependent pieces in the off-diagonal block. Therefore, the total Jacobian is constant.

The linear transformation from the $\{\ell_a \cdot \ell_b\}$, $\{\ell_a \cdot p_i\}$ back to inverse propagators and ISPs evidently also has a constant Jacobian, hence the integral in Baikov coordinates is given by

$$I = C \int \mathrm{d}\alpha_1 \cdots \mathrm{d}\alpha_m \mathrm{d}\varrho_1 \cdots \mathrm{d}\varrho_N B(\alpha_j, \varrho_j)^{(D-5-L)/2} \frac{N(\{\alpha, \varrho\})}{\varrho_1 \cdots \varrho_N}, \tag{4.28}$$

where the *Baikov Polynomial* $B(\alpha_j, \varrho_j)$ is the $D-4$ dimensional determinant of $\{\mu_{ij}\}$ expressed in terms of the ISPs and inverse propagators. The integration region in μ's is defined such that the moduli of $(D-4)$-dimensional parts of loop momenta are positive, i.e. That all eigenvalues of $\{\mu_{ij}\}$ are positive. In Baikov coordinates, this defines one component of the space where $B > 0$. In these coordinates IBP-relations are generated by vectors

$$v_{\alpha_i} \frac{\partial}{\partial_{\alpha_i}} + v_{\varrho_i} \frac{\partial}{\partial_{\varrho_i}}. \tag{4.29}$$

In contrast to loop-momentum coordinates, the integration domain now has boundaries

within the finite region. However, since all integrands are proportional to some power of the Baikov B^{D-N} and $B = 0$ at the boundary of the integration domain, these boundary terms are zero for D large enough. By analytical continuation, it follows that the boundary terms can be ignored for all D.

The constraint that propagator powers should not be raised takes the simple form

$$\left(v_{\alpha_j}\frac{\partial}{\partial\alpha_j} + v_{\varrho_k}\frac{\partial}{\partial\varrho_k}\right)\varrho_i = P_i\varrho_i \quad \forall i, \tag{4.30}$$

$$\Rightarrow \quad v_{\varrho_i} = P_i\varrho_i, \tag{4.31}$$

rendering the propagator doubling condition (eqn. (4.3)) trivial. However, the space of integral relations is enlarged in a different way, since the derivatives also act on the Baikov-polynomial

$$\frac{\partial}{\partial\alpha_i}B(\alpha_j,\varrho_k)^{(D-5-L)/2} = \frac{(D-5-L)}{2}B(\alpha_j,\varrho_k)^{((D-2)-5-L)/2}\frac{\partial B(\alpha_j,\varrho_k)}{\partial\alpha_i}, \tag{4.32}$$

which corresponds to an integral of the same topology in a lower dimension. Similar dimension shifts can be obtained by taking derivatives with respect to propagators. This displacement in the dimension can, in fact, be translated to raised propagator powers using Tarasov shifts [171]. In order to construct integration-by-parts relations within the same dimension, one therefore needs to impose the condition

$$\sum_j v_{\alpha_j}\frac{\partial B}{\partial\alpha_1} + \sum_i \varrho_i\frac{\partial B}{\partial\varrho_i} = P(\alpha,\varrho)B. \tag{4.33}$$

The parametrisation in Baikov coordinates has certain advantages, in particular, only one syzygy equation has to be considered instead of a set. This equation, however, is of higher polynomial degree than the equation in loop-momentum space. We therefore use these coordinates for formal discussions and for the application of IBP-vectors. For their explicit construction, however, we find it useful to split the problem into several equations which can be solved sequentially.

4.1.3 Embedding-Space Formulation

Planar Feynman integrals with massless propagators can be written in region-space coordinates $\{x_i, y_a\}$ such that all inverse propagators are written as either $(y_a - x_j)^2$ or $(y_a - y_b)^2$, for $a \neq b$ [172]. For an $n-$point process, region space momenta are implicitly defined as

$$k_{j<n} = x_{j+1} - x_j, \qquad k_n = x_1 - x_n, \qquad \ell_k = y_k - x_1. \tag{4.34}$$

The points x_j and y_a are denoted as external and internal points, respectively.

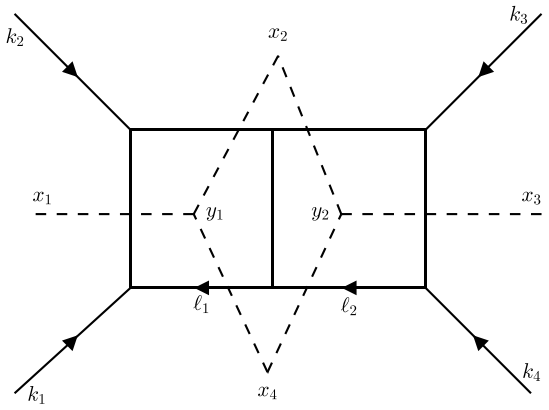

Figure 4.1: The planar double-box with momentum space coordinates and region-space coordinates.

These variables are defined in an affine space with Poincaré-symmetry, automatically imposing momentum conservation. As an example, consider the two-loop planar double box integral (see figure 4.1)

$$I = \int \mathrm{d}^D\ell_1 \mathrm{d}^D\ell_2 \frac{N(\ell_a}{\ell_1^2(\ell_1-k_1)^2(\ell_1-k_1-k_2)^2\ell_2^2(\ell_2+k_4)^2(\ell_2+k_3+k_4)^2(\ell_1-\ell_2)^2}. \quad (4.35)$$

The dual points are defined as

$$\begin{aligned} &k_1 = x_2 - x_1, \quad k_2 = x_3 - x_2, \quad k_3 = x_4 - x_3, \quad k_4 = x_1 - x_4, \\ &\ell_1 = y_1 - x_1, \quad \ell_2 = y_2 - x_1. \end{aligned} \quad (4.36)$$

In these coordinates the integral is expressed as

$$I = \int \mathrm{d}^D y_1 \mathrm{d}^D y_2 \frac{N(y)}{(y_1-x_1)^2(y_1-x_2)^2(y_1-x_3)^2(y_2-x_2)^2(y_2-x_3)^2(y_2-x_4)^2(y_1-y_2)^2}. \quad (4.37)$$

In the non-planar case it is not possible to write all inverse propagators as $(y_a - x_j)^2$ or $(y_a - y_b)^2$. However, all inverse propagators can be expressed as sums over such binomial squares. For a suitable ordering of external momenta all inverse propagators are squared sums of loop momenta plus sums of consecutive external momenta and can therefore be

expressed as

$$(\ell_1 - k_0 - ... + -_{n_1})^2 = (y_1 - x_{n_1})^2, \tag{4.38}$$
$$(\ell_2 - k_m - ... + -_{n_2})^2 = (y_2 - x_{n_2})^2, \tag{4.39}$$
$$\begin{aligned}&(\ell_1 - \ell_2 - k_I - ... + -_F)^2 = (y_1 - y_2 + x_i - x_f)^2 \\ =&(y_1 - y_2)^2 + (x_i - x_f)^2 + (y_1 - x_i)^2 + (y_2 - x_f)^2 - (y_1 - x_f)^2 - (y_2 - x_i)^2.\end{aligned} \tag{4.40}$$

Starting from these region-space coordinates most of the quadratic terms can be removed from the polynomial equations by embedding the momenta into a $(D+1)$-dimensional projective embedding space [173]. The embedding maps each dual point z to a $(D+2)$-component object

$$z^\mu \to Z^A = \begin{pmatrix} Z^\mu \\ Z^- \\ Z^+ \end{pmatrix} = \begin{pmatrix} z^\mu \\ -\hat{z}^2 \\ 1 \end{pmatrix}. \tag{4.41}$$

For now, we consider $\hat{z}^2$ as an independent variable which can differ from $z_\mu z^\mu$. As this space is projective, the vectors are defined modulo a $GL(1)$ transformation, i.e. $Z \to \alpha Z$, with $\alpha \neq 0$. The vector $(0,0,0)$ is not part of the projective space; the vector $x^\mu = 0, \hat{x}^2 = 0$ translates to $(0,0,1)$. A scalar product on this space is defined with the (SO$(D,2)$-invariant) inner product

$$(XY) = X^A Y_A = 2X^\mu Y_\mu + X^+ Y^- + X^- Y^+. \tag{4.42}$$

This product is not scaling invariant but is bilinear in the scalings of X and Y. The physical points are identified with embedding-space points for which $\hat{z}^2 = z^\mu z_\mu$. The *physical space* can hence be defined using quadratic surfaces $(ZZ) = 0$. Derivatives with respect to projective vectors are given by

$$\frac{\partial}{\partial Y^A}(XY) = X^A. \tag{4.43}$$

Additionally, the point at infinity

$$I = \begin{pmatrix} 0 \\ 1 \\ 0 \end{pmatrix} \tag{4.44}$$

is introduced which can be interpreted as a non-light-like vector x^μ taken to infinity modulo scaling. Allowing this point for the parametrisation of loop-momenta compactifies the momentum space [174]. The scaling freedom of this point is removed by the gauge

choice $I^- = 1$, such that it can be used to remove the scaling dependence of all other scalar products

$$(Z_i Z_j) \to \frac{(Z_i Z_j)}{(Z_i I)(Z_j I)}. \tag{4.45}$$

This allows to write inverse propagators as scalar products with a normalisation

$$(y_a - x_j)^2 = -\frac{(X_j Y_a)}{(IX_j)(IY_a)}, \quad (y_1 - y_2)^2 = -\frac{(Y_1 Y_2)}{(IY_1)(IY_2)}. \tag{4.46}$$

It is also possible to define massive propagators in embedding space, either by changing the products to sums $(XY) \to (XY) + m^2(IY)$ or, more elegantly, by including the mass terms to the external points [174]

$$X_j = \begin{pmatrix} x_j^\mu \\ -x_j^2 + m^2 \\ 1 \end{pmatrix} \tag{4.47}$$

and thus changing the propagator equations to

$$(x_j - y_a)^2 - m_j^2 = -\frac{(Y_a X_j)}{(Y_a I)}. \tag{4.48}$$

This changes the on-shell condition for X to $(XX) = 2m^2$. At one-loop level, this allows general masses for propagators. At two-loop level, on the other hand, this way of adding masses requires some degeneracy among the propagator masses. Within this thesis, however, we are only concerned with massless propagators.

Since the external points are considered as parameters rather than variables, it is possible to remove their scaling degree of freedom by imposing $(XI) = 1$. Feynman integrals in these coordinates are defined as scaling invariant and on the physical spaces i.e.

$$I = \int \left[\prod_{a=1}^{L} \frac{1}{\mathrm{Vol}(\mathrm{GL}(1))} \mathrm{d}^{(D+2)} Y_a \delta[(Y_a Y_a)] (IY_a)^{-D} \right] \frac{N}{\varrho_1 \cdots \varrho_n}, \tag{4.49}$$

where the numerator N and the inverse propagators ϱ are polynomial expressions in $(Y_a X_i)$ and $(Y_a Y_b)$, that are invariant under rescalings of Y_a (i.e. divided by the corresponding powers of IY_a). Moreover, since the integral also goes over the rescaling-orbit for each internal point Y, the volume of the rescaling group is formally divided out. In the following, we specialise on the case $L = 2$.

For inverse propagators in the form[3] $(YX_i)/(IY)$ or $(Y_1 Y_2)/\big((IY_1)(IY_2)\big)$, the condition

[3]For planar diagrams, all propagators can be written in this form.

that propagator powers are not raised in the IBP-relation translates to

$$\sum_{a,A} V_a^A \frac{\partial}{\partial Y_a^A}(X_i Y) = P_i(Y_b)\ (X_i Y) \tag{4.50}$$

$$\sum_{a,A} V_a^A \frac{\partial}{\partial Y_a^A}(Y_1 Y_2) = P(Y_b)\ (Y_1 Y_2 .) \tag{4.51}$$

Since the Feynman integrands are defined to be scaling invariant, components of V_a in the direction of Y_a map any integrand to zero as

$$Y_a \frac{\partial}{\partial Y_a} \frac{(ZY_a)^n}{(IY_a)^n} = n\frac{(ZY_a)^n}{(IY_a)^n} - n\frac{(ZY_a)^n}{(IY_a)^n} = 0. \tag{4.52}$$

An IBP-generating vector can therefore be parametrised by

$$V_i^a = v_1 X_1 + ... + v_n X_n + v_i I + \sum_{a \neq b} v_{y_b} Y_b. \tag{4.53}$$

where the redundant directions $Y_a \frac{\partial}{\partial Y_a}$ have been removed. The components v_α are polynomials in the Y variables chosen such that $V_i^a \partial_{Y_a}$ is scaling invariant. The syzygy equation described in eqn. (4.51) then becomes

$$\sum_i {c_1'}^i (X_i X_p) + c_1^I + d_1^2 (Y_2 X_P) = P(Y_a)\ (Y_1 X_P),$$

for the original inverse propagator $(Y_1 X_p)/(Y_1 I)$. Note that this equation contains only two linear terms with the rest being constant. In contrast, for loop-momentum coordinates the equations are quadratic. For inverse propagators $(Y_1 Y_2)/\left((IY_1)(IY_2)\right)$ the equation is also linear in embedding space formulation.

In addition to the requirement that the IBP-vectors should not raise propagator powers, they also should not change δ-functions in the integrand (eqn. (4.49)), which is achieved by imposing[4]

$$V_a \frac{\partial}{\partial Y_a} \delta[(Y_a Y_a)] = 0 \tag{4.54}$$

$$\Leftrightarrow\ V_a \frac{\partial}{\partial Y_a}(Y_a Y_a) = 0. \tag{4.55}$$

This gives two additional conditions whose terms are proportional to inverse propagators and ISP's. However, especially for planar topologies, the advantages of the constant terms outweigh the complexity of these additional equations. In the following, we set $(Y_a Y_a)$ to

[4]Since $\int \mathrm{d}x \delta'(x) x F(x) = -F(0)$, one might argue that it is possible to replace $x\delta'(x) \to -\delta(x)$ and thus it would be sufficient to have $V\partial_{Y_a}(Y_a Y_a) \propto (Y_a Y_a)$. However, this replacement in fact involves integration-by-parts and hence the resulting surface-terms are trivially zero.

zero, since terms proportional to it vanish due to the $\delta-$function. For a general planar two-loop N-point topology the conditions can be expressed in matrix form. To this end, we introduce the matrix corresponding to the l.h.s. of eqns. (4.54,4.55)

$$C = \begin{pmatrix} (X_1X_1) & ... & (X_1X_N) & 1 & (X_1Y_2) & & & & & \\ \vdots & \ddots & \vdots & \vdots & \vdots & & & & & \\ (X_KX_1) & ... & (X_KX_N) & 1 & (X_KY_2) & & & & & \\ 2(X_1Y_1) & ... & 2(X_NY_1) & 2(IY_1) & 2(Y_2Y_1) & & & & & \\ & & & & & (X_1X_1) & \cdots & (X_1X_N) & 1 & (X_1Y_1) \\ & & & & & (X_KX_1) & \cdots & (X_KX_N) & 1 & (X_KY_1) \\ & & & & & (X_{K+1}X_1) & \cdots & (X_{K+1}X_N) & 1 & (X_{K+1}Y_1) \\ & & & & & \vdots & \ddots & \vdots & \vdots & \vdots \\ & & & & & (X_NX_1) & \cdots & (X_NX_N) & 1 & (X_NY_1) \\ & & & & & 2(X_1Y_2) & ... & 2(X_NY_2) & 2(IY_2) & 2(Y_1Y_2) \\ (X_1Y_2) & ... & (X_NY_2) & (IY_2) & 0 & (X_1Y_1) & ... & (X_NY_1) & (IY_1) & 0 \end{pmatrix} \tag{4.56}$$

and a matrix corresponding to their r.h.s

$$W = \begin{pmatrix} \text{diag}\left((X_1Y_1), ..., (X_KY_1)\right) & & & \\ 0 & & 0 & \\ & & \text{diag}\left((X_1Y_2), (X_KY_2), (X_{K+1}Y_2), ..., (X_NY_2)\right) & \\ & & 0 & 0 \\ & & & (Y_1Y_2) \end{pmatrix}. \tag{4.57}$$

The grey lines are present for simple diagrams (i.e. no external legs are attached to the nodes) while one or two of them should be omitted for semi-simple and generic diagrams, respectively. For an IBP-vector $V_a^A = \sum_j v_a^j X_j^A + v_a^I I^A + v_a^y Y_{b\neq a}^A$, the defining equations are

$$C \cdot (v_1^1, ..., v_1^y, v_2^1, ..., v_2^y)^T = W \cdot (\mathcal{W}_1^1, ..., \mathcal{W}_1^K, \mathcal{W}_2^1, ..., W_2^M, W_{12})^T, \tag{4.58}$$

where v and $\mathcal{W}$ are polynomials. For non-planar diagrams the scaling factors (IY) do not factor for all propagators. The defining equation for IBP-vectors that do not raise the power of an inverse propagator $(y_1 - y_2 - x_i + x_f)$ is thus

$$\begin{aligned} V^a \frac{\partial}{\partial Y_a} &\left[(Y_1Y_2) + (IY_2)\left[(X_1Y_1) - (X_fY_1)\right] + (IY_1)\left[(X_fY_2) - (X_iY_2)\right] - (X_iX_f)(Y_1I)(Y_2I)\right] \\ &\propto \left[(Y_1Y_2) + (IY_2)\left[(X_1Y_1) - (X_fY_1)\right] + (IY_1)\left[(X_fY_2) - (X_iY_2)\right] - (X_iX_f)(Y_1I)(Y_2I)\right], \end{aligned} \tag{4.59}$$

adding a further equation which is bilinear in Y_1 and Y_2.

We find the low-polynomial degree of the conditions in embedding space useful for the practical computation of syzygies. Therefore, we will mostly construct IBP-vectors in embedding space and then translate them to Baikov-coordinates where we apply them to generic numerators.

4.2 Constructing IBP-Vectors

In the previous section we have reviewed the defining equations for IBP-generating vectors in loop-momentum Baikov and embedding space coordinates. In this section, we will present methods to solve these equations in order to construct IBP-generating vectors.

4.2.1 Generic IBP-Vectors from Cramer's Rule

The defining equation for IBP-vectors in embedding space is

$$\big(C, -W\big) \cdot (v_1^1, ..., v_1^y, v_2^1, ..., v_2^y, \mathcal{W}_1^1, ..., \mathcal{W}_1^K, \mathcal{W}_2^1, ..., W_2^M, W_{12})^T = 0, \tag{4.60}$$

with the matrices C and W defined in eqn. (4.57). Any solution to this problem is at the same time a solution to the linear-algebra problem where the v and $\mathcal{W}$ are defined as rational functions. Conversely, every solution to the linear algebra problem can be turned into a syzygy by multiplying it with common denominators. For an $n \times m$ matrix, a straightforward way to obtain such syzygies (which we will call trivial syzygies) is to pick square sub-matrices $C_i, ..., C_{i+m}$ and compute their null-space via Cramer's rule[5] [48]

$$v_j = (-1)^i \det(C_i, ..., C_{j-1}, C_{j+1}, ..., C_m). \tag{4.61}$$

An improvement of this method is to set inverse propagators in the equation to zero, solving the equations and compute the coefficients $\mathcal{W}$ at the end. This gives, in general, vectors with comparably high polynomial degree. When considering the syzygies as a vector space, rather than a module, the on-shell parts of non-trivial IBP-vectors are linearly dependent on the trivial ones. This implies that non-trivial vectors can always be written as a linear combination of trivial IBP-vectors with a polynomial factored out. In general, these sets of trivial vectors do not generate all IBP-relations. Therefore, they are only used in combination with other vectors.

Crossing of Simpler Vectors

The method described above can be used to solve all syzygy equations. However, it is also possible to single out the equation of one propagator which is solved by antisymmetrisa-

[5]The columns of W are not included here, as the resulting vectors would vanish on-shell.

tion, while the other equations are solved before through other means. Let $(C, -W)$ be the matrix defining the syzygy-problem for a descendant topology for which we obtain a set of solutions $\{v_i\}$

$$C \cdot v_i = \{W_1 \varrho_1, ..., W_n \varrho_n\}. \tag{4.62}$$

The additional syzygy equation that vectors of a topology with one more propagator have to fulfil can be expressed by some vector f. Then, all pairs of vectors are taken and combined to IBP-vectors for the parent topology via anti-symmetrisation.

$$v_{ij} = (v_i \cdot f)v_j - (v_j \cdot f)v_i. \tag{4.63}$$

Again, the inverse propagator ϱ_n can be set to zero, leading to a non-zero coefficient $\mathcal{W}_n$. This technique is called *crossing over* ϱ_n [175]. In ref. [175], this technique was applied to planar diagrams, computing one-loop sub-vectors and crossing over the propagator containing both loop momenta.

We also find this method very useful for non-planar diagrams where we cross over the inverse propagators (Y_1Y_2) or $(Y_1Y_2) + (Y_1X_i)(IY_2) + ...$. We also find it beneficial to not only cross over one propagator, but apply it to several propagators and combine the results. We find that this method is often sufficient to reduce complicated integral-topologies. In other cases, these vectors can be added to vectors obtained through other means to obtain all necessary integral relations. It is, however, necessary to compute the syzygies of the simplified problem (i.e. the equations for the propagators which are not crossed over). In the following we will discuss how this is done using methods from algebraic geometry.

4.2.2 Gröbner Basis and Syzygies

Unitarity-compatible IBP-vectors are defined by solutions to syzygy equations, which are thoroughly studied in the context of algebraic geometry. Therefore, we will review some definitions and theorems from algebraic geometry and a general algorithm which finds the solutions to syzygy equations.

A central object in algebraic geometry is the polynomial ring $\mathbb{F}[z_1, ..., z_n]$, i.e. all polynomials in variables $z_1, ..., z_n$ with coefficients in the field $\mathbb{F}$. In this thesis, the field will usually be the complex numbers $\mathbb{C}$ or a finite field. The polynomials can be expressed in a basis of monomials $m_i = z^{\vec{\alpha}} := z_1^{\alpha_1} \cdots z_n^{\alpha_n}$.

Definition 1 *For two monomials* $m_1 = z^{\vec{\alpha}_1}, m_2 = z^{\vec{\alpha}_2}$, m_1 *divides* m_2 *iff* $\alpha_{1j} < \alpha_{2j}\ \forall j$.

Any polynomial can be written as $c_i m_i$, where the c_i are numbers in the field. On the ring of polynomials, sub-rings which are called ideals are defined.

Definition 2 *Given a polynomial ring* $R = \mathbb{F}[z_1, ..., z_n]$ *, an ideal* $I \in R$ *is a subset of* R *such that*

- $0 \in I$,
- $f \in I \;\Rightarrow\; -f \in I$,
- $f_1, f_2 \in I \;\Rightarrow\; f_1 + f_2 \in I$,
- $f \in I, h \in R \;\Rightarrow\; fh \in I$,

A *generating set* for an ideal is given by polynomials $f_1, ..., f_n$ such that for every $g \in I$

$$g = h_1 f_1 + ... + h_n f_n, \qquad h_1, ..., h_n \in \mathbb{F}(z_1, ..., z_m). \tag{4.64}$$

Usually, ideals are introduced through a defining generating set $I = \langle f_1, ..., f_n \rangle$. Ideal membership can be verified by polynomial division (see algorithm 1), where the polynomials are ordered by the leading term $\mathrm{LT}(g)$ which, in the univariate case, is given by the monomial in g with the highest degree.

Algorithm 1 Polynomial division

Input: $g, f_1, ..., f_n$

$h_i = 0 \;\forall i$, $r = 0$
while $g \neq 0$ **do**
  divisible=**false**
  for $i = 1$ to n **do**
    if $\mathrm{LT}(f_i)$ divides $\mathrm{LT}(g)$ **then**
      $h_i := h_i + \frac{\mathrm{LT}(g)}{\mathrm{LT}(f_i)}$
      $g := g - \frac{\mathrm{LT}(g)}{\mathrm{LT}(f_i)} f_i$
      divisible=**true**
      break
    end if
  end for
  if *divisible*=**false then**
    $r := r + \mathrm{LT}(g)$
    $g = g - \mathrm{LT}(g)$
  end if
end while
return $h_1, ..., h_k, r$

If this algorithm returns $r = 0$, then $g \in \langle f_1, ..., f_n \rangle$. In order to define polynomial division for multivariate polynomials, an ordering of the monomials has to be defined, as a simple ordering by degree is not unique.

Definition 3 *Given a polynomial ring $R = \mathbb{F}[z_1, ..., z_n]$ and all monomials with coefficient one $M = \{z_1^{k_1} \cdots z_n^{k_n} | k_1, ..., k_n \in \mathbb{N}_0\}$, a monomial ordering $\prec$ is an ordering on R such that*

1. *For $m_1 \neq m_2 \in M$, either $m_1 \prec m_2$ or $m_2 \prec m_1$*
2. *For $m_1 \prec m_2$ and $m_3 \in M$, $m_1 m_3 \prec m_2 m_3$.*
3. *For all $m \in M$, $m \neq 1$, $1 \prec m$.*

Such an ordering always involves an ordering of variables. Without loss of generality, we will order them as $z_1 \prec ... \prec z_n$. For two monomials $g_1 = z_1^{a_1} \cdots z_n^{a_n}$ and $g_2 = z_1^{b_1} \cdots z_n^{b_n}$ examples for monomial orderings are

- Lexicographic order. If $a_1 < b_1$, $g_1 \prec g_2$. If $a_i = b_i \; \forall i < k$, if $a_k < b_k$, $g_1 \prec g_2$.
- Reverse lexicographic order. If $a_n < b_n$, $g_1 \prec g_2$. If $a_i = b_i \; \forall i > k$, if $a_k < b_k$ $g_1 \prec g_2$.
- Degree reverse lexicographic order (grevlex). If $\sum_j a_j < \sum_j b_j$, then $g_1 \prec g_2$. If $\sum_j a_j = \sum_j b_j$ order g_1 and g_2 by reverse lexicographic order.

E.g. the set of all degree three polynomials in xyz in lexicographic or reverse lexicoraphic ordering is given by

- Lexicographic $x^3, x^2y, x^2z, xy^2, xyz, xz^2, y^3, y^2z, yz^2, z^3$
- Reverse Lexicographic $x^3, x^2y, xy^2, y^3, x^2z, xyz, y^2z, xz^2, yz^2, z^3$.

For the application in the context of IBP-vectors, ordering unwanted variables to the end turns out to be beneficial, hence the most efficient ordering appears to be degree reverse lexicographic ordering. Another important ordering is *weighted reverse lexicographic ordering* with weights $w_1, ..., w_n$ which orders the monomials $z_1^{a_1} \cdots z_n^{a_n}$ first by $\sum_i a_i w_i$ and then by reversed lexicographic ordering.

The definition of a monomial ordering allows to define the leading term of multivariate polynomials. For $f = c_1 m_1 + ... + c_n m_n$, where $c_j \neq 0$ are constants, $\mathrm{LT}(f) = c_j m_j$ such that $m_i \prec m_j$, for all $i \neq j$. This definition allows to apply algorithm 1 to multivariate polynomials, providing a way to verify (not falsify, however) ideal membership in the multivariate case.

The generating set of an ideal is ambiguous. As a simple example, consider

$$f_1 = x^3 + 4x^2 + 4x + 1, \quad f_2 = x^2 + 2x + 1, \quad f_3 = x + 1, \tag{4.65}$$

$$I = \langle f_1, f_2 \rangle = \langle f_3 \rangle. \tag{4.66}$$

Both generating sets can be expressed through each other, since $f_2(x+2) - f_1 = f_3$ and $f_2 = f_1^2$. However, there is no polynomial h such that $f_3 = hf_2$, hence given the first basis it is not obvious that the ideal can be generated by just one polynomial. This simple example also demonstrates that polynomial division does not provide a necessary criterion for ideal membership, since $\mathrm{LT}(f_3) = x$ is neither divided by x^3 nor x^2 and therefore f_3 is not decomposed to f_1, f_2 by the polynomial division algorithm.

In this example, the basis $\{x+1\}$ has the peculiar property that polynomial division does not only provide a sufficient criterion for ideal membership, but a necessary one. Generating systems with this property are called *Gröbner bases.*

Definition 4 *For an ideal I over the ring R and a given monomial order $\prec$, a Gröbner basis is a generating system $G(I) = \{g_1, ...g_n\}$ such that for every $f \in I$, there exists a $g_i \in G(I)$ such that*

$$LT(g_i) \text{ divides } LT(f). \tag{4.67}$$

For any polynomial $p \in I$ with leading term $\mathrm{LT}(f)$, this means that line 5 of algorithm 1 applies for some i. The remaining polynomial $p' = p - \frac{\mathrm{LT}(p)}{\mathrm{LT}(g_i)g_i}$ is again a member of the ideal with $\mathrm{LT}(p') \prec \mathrm{LT}(p)$. Repeatedly applying this argument, the leading term of the remaining polynomial is strictly monotonously decreasing w.r.t. the monomial ordering until (after finitely many steps) the remainder is 0. Thus indeed any polynomial in I can be expressed through the Gröbner basis.

The Gröbner basis depends on the choice of the monomial ordering through the definition of leading terms. For example $\{x + y^2, x^2\}$ is the Gröbner basis of the corresponding ideal in grevlex, while in lexicographic ordering the Gröbner basis is $\{x + y^2, y^4\}$.

Buchberger's Algorithm

We will now review how Gröbner bases can be computed via Buchberger's algorithm, thereby proving their existence. Moreover, we will review how all solutions to syzygy-equations can be found using Gröbner bases.

For each two polynomials f, g from the generating set of an ideal I, the S-polynomial $S \in I$ is defined as

$$S(f,g) = \frac{\mathrm{LCM}\left(\mathrm{LT}(f), \mathrm{LT}(g)\right)}{\mathrm{LT}(f)} f - \frac{\mathrm{LCM}\left(\mathrm{LT}(f), \mathrm{LT}(g)\right)}{\mathrm{LT}(g)} g, \tag{4.68}$$

where $\mathrm{LCM}(a,b)$ is the least common multiple of a and b. The leading terms of S cancel out so neither f, g divide S. This property of S polynomials is used in *Buchberger's algorithm* (algorithm 2) [176], which, given a monomial ordering and a generating set $\{f_1, ..., f_n\}$ returns the Gröbner basis of $I = \langle f_1, ..., f_n \rangle$.

Algorithm 2 Buchberger's algorithm

Input: monomial order $\prec$ and $f_1, ..., f_n$

1: B:=$\{f_1, ..., f_n\}$
2: *pairs*:= all pairs $\{f_i, f_j\}$
3: **while** *pairs*$\neq \emptyset$ **do**
4: $\{f, g\}$:=$pairs_1$
5: Apply polynomial division (algorithm 1) to $S(f, g)$, over all polynomials in B. (gives, $q_1, ..., q_n, r$)
6: **if** $r \neq 0$ **then**
7: $B := B \cup r$
8: *pairs*:=*pairs*$\cup \{\{B_1, r\}, ..., \{(B_N), r\}\}$
9: **end if**
10: **delete** $pairs_1$
11: **end while**
12: **for** i=1 to Length(B) **do**
13: Apply polynomial division to B_i over all other elements of B (gives $q_1, ..., q_n, r$)
14: **if** $r = 0$ **then**
15: **delete** B_i from B
16: **end if**
17: **end for**
18: **return** B

Theorem 1 *This algorithm terminates [176].*

Proof: For every remainder r that is added to B in line 7, LT(r) cannot be divided by the leading terms of B by the definition of polynomial division. Thus, the monomial ideal given by $\{\text{LT}(b)|b \in B\}$ is strictly monotonously increasing.

It can be shown by induction, however, that this increase has to terminate after finitely many iterations. In the univariate case, where the generating system contains a leading term x^a, it is clear that only functions with leading term x^b, $b < a$ can be added to the basis, thus the computation terminates after at most a steps. In the bivariate case with leading term $x_1^{a_1} x_2^{a_2}$ in the generating system, there are two possibilities for the leading term of a new function

- $x_1^{a_1 - j_1} x_2^{a_2 + m_{j_1}}$ where $0 < j_1 < a_1$ and $m_{j,1} \in \mathbb{Z}$,
- $x_1^{a_1 + m_{j_2}} x_2^{a_2 - j_2}$ where $0 < j_2 < a_2$ and $m_{j,2} \in \mathbb{Z}$.

In the first case, for every j_1 the first occurence of such a term fixes the maximum of m_{j_1} and only a finite number of monomials $x_1^{a_1 - j_1} x_2^{a_2 + m'_{j_1}}$, with $m'_{j_1} < m_{j_1}$ can be added to the

monomial ideal. Vice versa, for every j_2 the number of terms is also finite. Since there is only a finite number of choices for j_1, j_2 the monomial ideal can only increase in a finite number of steps.

The induction hypothesis is that for $n-1$ variables this is true. For n variables, where the generating system contains a leading term $x_1^{a_1} \cdots x_n^{a_n}$ a new monomial takes the form

$$x_1^{a_1+m_{j_i,1}} \cdots x_{i-1}^{a_{i-1}+m_{j_i,i-1}} x_i^{a_i-j_i} x_{i+1}^{a_{i+1}+m_{j_i,i+1}} \cdots x_n^{a_n+m_{j_i,n}}. \tag{4.69}$$

By the induction hypothesis, for each j_i, the monomial ideal is only increased a finite number of times and thereby it is only increased a finite number of times in total [177]. This proves that after a finite number of iterations, the remainder of every polynomial division in line five of algorithm 2 is 0 and the algorithm terminates.

Theorem 2 *The resulting generating system is a Gröbner basis [176].*

Proof: As provided by the terminating condition for $f, g \in B$, $S(f,g)$ is divided by the basis B. Suppose a function $f \in I$ which cannot be divided by B. After applying polynomial division the remainder g cannot be divided by the leading terms of B. Since g is in the ideal, it can be expanded into

$$g = h_1 b_1 + ... + h_n b_n. \tag{4.70}$$

The maximal term of this decomposition is given by $M = \max\{\mathrm{LT}(h_1 b_1), ...,\mathrm{LT}(h_n b_n)\}$, where the maximum is given by $\mathrm{LT}(h_i b_i)$ such that for all j either $\mathrm{LT}(h_j b_j) \prec \mathrm{LT}(h_i b_i)$ or $\mathrm{LT}(h_i b_i) = \mathrm{LT}(h_j b_j)$. The sum can then be decomposed into terms which contribute to M and terms that do not

$$g = \sum_{\mathrm{LT}(h_j)\mathrm{LT}(b_j)=c_j M} h_j b_j \quad + \sum_{\mathrm{LT}(h_j)\mathrm{LT}(b_j)\prec M} h_j b_j \tag{4.71}$$

$$= \sum_{\mathrm{LT}(h_j)\mathrm{LT}(b_j)=c_j M} \mathrm{LT}(h_j) b_j \quad + \sum_{\mathrm{LT}(h_j)\mathrm{LT}(b_j)=c_j M} (h_j - \mathrm{LT}(h_j))\, b_j \quad + \sum_{\mathrm{LT}(h_j)\mathrm{LT}(b_j)\prec M} h_j b_j. \tag{4.72}$$

By assumption, $\mathrm{LT}(g) \prec M$, since M can clearly be divided by the leading terms of B. This implies that the leading term of the first sum is $\prec M$. The leading terms of h_j can be expressed as $c_j x_j^{\alpha_j}$, where for $\alpha = \{a_1, ..., a_n\}$, $x^\alpha = x_1^{a_1} \cdots x_n^{a_n}$. The first sum in eqn. (4.72) can then be written as a telescope sum

$$\begin{aligned}\sum c_j x^{\alpha_j} b_j =& c_1(x^{\alpha_1} b_1 - b^{\alpha_2} b_2) + (c_1 + c_2)(x^{\alpha_2} b_2 - x^{\alpha_3} b_3) + ... + \\ & (c_1 + ... + c_{k-1})(x^{\alpha_{k-1}} b_{k-1} - x^{\alpha_k} b_k) + (c_1 + ... + c_k) x^{\alpha_k} b_k.\end{aligned} \tag{4.73}$$

All coefficients $c_1, ..., c_k$ contribute to M, therefore $c_1 + ... + c_n = 0$. For the remaining terms, the S-polynomials are given by

$$S(x^{\alpha_i} b_i, x^{\alpha_j} b_j) = \frac{M}{M} x^{\alpha_i} b_i - \frac{M}{M} x^{a_j} b_j = x^{\alpha_i} b_i - x^{\alpha_j} b_j, \tag{4.74}$$

since we only considered terms which contribute to M. On the other hand

$$S(x^{a_i} b_i, x^{\alpha_j} b_j) = \frac{M}{x^{\alpha_i} \mathrm{LT}(b_i)} x^{\alpha_i} b_i - \frac{M}{x^{\alpha_j} \mathrm{LT}(b_j)} x^{\alpha_j} b_j \propto S(b_i, b_j). \tag{4.75}$$

All terms $x^{\alpha_j} b_j - x^{\alpha_k} b_k$ can therefore be decomposed into S-polynomials of the generating system which by assumption can be decomposed into the basis elements b_i by polynomial division,

$$\sum_{\mathrm{LT}(h_j)\mathrm{LT}(b_j)=M} \mathrm{LT}(h_j) b_j = \sum_i d_i b_i, \quad \text{with } \max\{\mathrm{LT}(d_i)\mathrm{LT}(b_i)\} \prec M. \tag{4.76}$$

Therefore, for every $\{h_1, ..., h_n\}$ such that $g = \sum_j h_j b_j$ with maximal term M it is possible to find $h'_j = h_j - \mathrm{LT}(h_j) + d_j$ such that $g = h'_j b_j$ with maximal term $M' \prec M$. Since this cannot be true for $M = 1$, a $g \in I$ that is not divisible by B does not exist and hence the generating set is indeed a Gröbner basis [176].

Corollary 1 *For every ideal defined by a generating set $I = \langle f_1, ..., f_n \rangle$ a Gröbner basis exists, since Buchbergers algorithm terminates after finitely many steps and gives a Gröbner basis.*

In this thesis, we use a public implementation SINGULAR [178], which uses Faugère's F4 algorithm. This algorithm is based on the same mathematical principles as Buchberger's algorithm, but uses fast row-reduction to reduce the S-polynomials of all pairs at the same time [179], which, in general, leads to a great reduction in computing time compared to Buchbergers algorithm.

Gröbner-Bases for Modules

In the computation of IBP-vectors, one is not only interested in solving just one syzygy, but several of them at the same time. This requires to extend the definitions made above to modules.

Definition 5 *A module M over a ring R is an abelian group with group operation $(+)$ and a map $\cdot : R \times M \to M$ such that*

1. $r \cdot (m_1 + m_2), = r \cdot m_1 + r \cdot m_2$,
2. $(r_1 + r_2) \cdot m = r_1 \cdot m + r_2 \cdot m$,

3. $r_1 r_2 \cdot m = r_1 \cdot (r_2 \cdot m)$,

4. $1 \cdot m = m$

for all $m, m_1, m_2 \in M$ *and* $r_1, r_2, r \in R$.

In the context of IBP-vectors sub-modules of F^m appear where each element is a set of polynomials $m = (f_1, ..., f_n) = \sum_j f_j \mathbf{e}_j$. A monomial in a module is defined as $\mathbf{e_j} x^{\vec{\alpha}}$, where $x^{\vec{\alpha}}$ is a monomial over the field. Monomial division of module elements is defined such that a monomial $\mathbf{e}_i x^{\vec{\beta}}$ *divides* a monomial $\mathbf{e}_i x^{\vec{\alpha}}$ if and only if $i = j$ and $x^{\vec{\beta}}$ divides $x^{\vec{\alpha}}$. The quotient of the two monomials is then $x^{\vec{\alpha}}/x^{\vec{\beta}}$. Given a monomial ordering, the leading term of a module element $m = (f_1, ..., f_n)$ is defined as $\mathrm{LT}(m) = \mathbf{e_j}\mathrm{LT}(f_j)$ such that $\mathrm{LT}(f_j) = \max\{\mathrm{LT}(f_1), ...,\mathrm{LT}(f_n)\}$, where LT on the r.h.s. is the leading term defined for polynomials and the maximum is defined with respect to the monomial ordering. If there are more than one components with the same leading term, the term with smallest j is chosen as the leading term. With these definitions, the algorithm for polynomial division (algorithm 1) can also be applied in the module case.

The missing ingredient for Gröbner basis compuation is the least common multiple of two monomials in M, defined as $\mathrm{LCM}(\vec{x}^{\alpha}\mathbf{e}_j, \vec{x}^{\beta}\mathbf{e}_i) = \delta_{ij}\mathrm{LCM}(\vec{x}^{\alpha}, \vec{x}^{\beta})$. This allows to define the S-vector of two module elements $m_1 = \{f_1, ..., f_n\}$, $m_2 = \{g_1, ..., g_n\}$ as

$$S(m_1, m_2) = \frac{\mathrm{LCM}\left(\mathrm{LT}(m_1), \mathrm{LT}(m_2)\right)}{|\mathrm{LT}(m_1)|} m_1 - \frac{\mathrm{LCM}\left(\mathrm{LT}(m_1), \mathrm{LT}(m_2)\right)}{|\mathrm{LT}(m_2)|} m_2, \tag{4.77}$$

where $|e_j x^{\vec{\alpha}}| = x^{\vec{\alpha}}$. With these definitions, Buchberger's algorithm (algorithm 2) also extends to the module case. In particular, the proof that Buchbergers algorithm produces a Gröbner basis also remains valid, since eqns. (4.73-4.75) are valid for modules.

Syzygy Computation

In the context of IBP-reduction, we are particularly interested in *syzygy*-modules.

Definition 6 *Given a polynomial ring R and a module M with elements $m_1, ..., m_k \in M$, the syzygy module $syz(m_1, ..., m_k)$ is a sub-module of R^k which consists of all elements $(a_1, ..., a_k)$ such that*

$$a_1 \cdot m_1 + ... + a_k \cdot m_k = 0. \tag{4.78}$$

The fact that syzygies form a module also implies that IBP-vectors also form a module, i.e. any linear combination of IBP-vectors with polynomial coefficients is again an IBP-vector.

The syzygy module is trivial to compute for a set of monomials $\{M_1, ..., M_n\}$. With M_{ij} the greatest common divisor of M_i and M_j, the generators of the syzygy module are

$$\{0, ..., 0, M_i/M_{ij}, 0, ..., 0, -M_j/M_{ij}, 0, ..., 0\}. \tag{4.79}$$

For more general polynomials, syzygies can be found by Gröbner basis computation. Taking the S-polynomial $S(g_i, g_j) = a_i g_i + a_j g_j$, a syzygy is given by the *reduction of an S-polynomial*

$$0 = a_i g_i + a_j g_j + \sum_k q_k g_k = (a_i + q_i) g_i + (a_j + q_j) g_j + \sum_{k \neq i,j} q_k g_k, \tag{4.80}$$

where $q_1, ..., q_k$ is the output of the polynomial division algorithm. Since the leading term of $S(g_i, g_j)$ cannot be divided by the leading terms of g_i, g_j, the set

$$\{q_1, ..., (a_i + q_i), ..., (a_j + q_j), ..., q_n\} \tag{4.81}$$

is a non-trivial member of the syzygy module of $g_i, ..., g_n$.

According to Schreyer's theorem [180], reductions of S-polynomials generate the syzygy module for any ideal in Gröbner basis form. The proof of this theorem is similar to the proof that the output of Buchbergers algorithm is a Gröbner basis:

The Gröbner basis of the syzygies of the monomial ideal $\langle \mathrm{LT}(g_i) \rangle$ is generated by the leading terms of reduced $S-$polynomials, as follows from the syzygy module of a monomial list (see eqn. (4.79)). Therefore, the leading terms of a general element of the syzygy module $(f_1, ..., f_n) \in \mathrm{syz}(g_1, ..., g_n)$ can be reduced to leading terms in reduced $S-$polynomials. This allows to rewrite $(f_1, ..., f_n)$ as a part generated by reduced S-polynomials and a remainder $(f'_1, ..., f'_n)$ which is smaller than $(f_1, ..., f_n)$ in the chosen module ordering. Repeating this a finite number of times expresses $f_1, ..., f_n$ in terms of reductions of S-polynomials with remainder zero.

For generic polynomials $f_1, ..., f_k$ the syzygy module is computed by transforming to a Gröbner basis $g_1, ..., g_m$ with $f_i = a_i^j g_j$ and transforming back the reductions of S-polynmomials via $a_j^i \mathbf{e_i}$. In fact, the Gröbner basis algorithms already produce the reduced S-polynomials and the transformation matrix, since the fifth line in algorithm 2 in the case of vanishing remainder is the reduction of S-polynomials, while the transformation matrix is computed in line thirteen. With the definition of leading terms and S-vectors, the proof of this theorem carries over to syzygy modules of modules, which we will use to construct IBP-generating vectors.

A useful modification of the Gröbner basis algorithms implemented in Singular, is to drop all S-vectors with total degree $d > d_{\max}$, for some choice of the maximal degree $d_{\max}$. This limit will greatly speed up syzygy computations which otherwise would not

be feasible. In general, however, the algorithm will then not exactly produce Gröbner bases and therefore the reduced S-polynomials will not generate the full syzygy module (Schreyer's theorem only applies to Gröbner bases). If the degree bound is set too low, the syzygies should be extended by solutions computed with linear algebra methods. Moreover, when considering kinematic invariants as variables, a degree bound can also be used to limit the complexity IBP-relations as functions of external kinematics.

Gröbner basis algorithms give the complete set of IBP-vectors. However, for many complicated topologies these algorithms do not terminate within reasonable time or need an excessive amount of memory when the degree bound is set sufficiently high. In such cases, we typically solve a simpler syzygy problem with Gröbner basis methods and use its solutions to construct solutions to the full problem via linear algebra.

4.2.3 Syzygies from Linear Algebra

Polynomials form an (infinite dimensional) vector-space over their defining field which has the set of all monomials as a basis. Truncating the polynomials at some maximal $d_{\max}$, this vector space becomes finite-dimensional [181]. The solutions to the syzygy problem within this finite space can be found by considering the problem up to degree $d_{\max}+1$ as a linear equation system. For example, for the syzygy problem

$$p_1(x,y)x + p_2(x,y)y = 0 \tag{4.82}$$

and a maximal degree of 2, one can use the ansatz

$$p_j = c_j^0 + c_j^{10}x + c_j^{01}y + c_j^{20}x^2 + c_j^{11}xy + c_j^{02}y^2 \tag{4.83}$$

to obtain the linear equation system

$$\begin{pmatrix}
0 & & & & & ... & & & & & & 0 \\
1 & 0 & & & & & ... & & & & & 0 \\
0 & & & ... & & 0 & 1 & 0 & & ... & & 0 \\
0 & 1 & 0 & & & & ... & & & & & 0 \\
0 & 0 & 1 & 0 & 0 & 0 & 0 & 1 & 0 & ... & & 0 \\
0 & & & & ... & & & 0 & 1 & 0 & 0 & 0 \\
0 & 0 & 0 & 1 & & & & ... & & & & 0 \\
0 & 0 & 0 & 0 & 1 & 0 & 0 & 0 & 0 & 1 & 0 & 0 \\
0 & & ... & & 0 & 1 & 0 & 0 & 0 & 0 & 1 & 0 \\
0 & & & & & ... & & & & & 0 & 1
\end{pmatrix}
\begin{pmatrix}
c_1^0 \\ c_1^{10} \\ c_1^{01} \\ c_1^{20} \\ c_1^{11} \\ c_1^{02} \\ c_2^0 \\ c_2^{10} \\ c_2^{01} \\ c_2^{20} \\ c_2^{11} \\ c_2^{02}
\end{pmatrix} = 0. \tag{4.84}$$

Here, $c_1^0, ..., c_2^{02}$ are constants and thus the syzygy-problem is reduced to linear algebra. A clear advantage of this method compared to Gröbner basis methods with degree bound is that it is guaranteed to find all syzygies up to the specified degree. In realistic cases, however, these computations are challenging due to the large function spaces. For complicated topologies the solution of such large linear systems even remains challenging when using numeric values for the kinematic invariants.

In suitable coordinates, such as the embedding space formulation, we can remedy this situation, however, by splitting the matrix in the defining equation for IBP-vectors into a constant and a linear part

$$C = C_0 + C_1. \tag{4.85}$$

We have $C \cdot V = 0$, thus in particular for all monomials with degree $d_{\max} + 1$

$$C_1 V_m = 0, \tag{4.86}$$

where V_m is the piece of V with maximal degree $d_{\max}$. This defines a simpler syzygy problem, which can be solved with Gröbner basis methods. The obtained vectors v_m^i of degree $d_{\max}$ are combined in an Ansatz together with all monomials up to degree $d_{\max} - 1$, which then has to be constrained up to degree $d_{\max}$ (at degree $d_{\max} + 1$, the equations are trivially solved since the v_m are in the syzygy-module of C_1)

$$v = c_0 + c_{10...0}\alpha_1 + ... + c_{0,...,d_{\max}-1}\varrho_n^{d_{\max}-1} + \sum_i c_v^i v_m^i \tag{4.87}$$

In realistic cases, in embedding space coordinates, the necessary degrees of vectors are typically ≤ 4, while there are > 10 variables. Hence removing the highest degree term reduces the size of the system by a factor $\gtrsim 10$. We find this way of solving the syzygy equation particularly fruitful in approaches where the equations are solved numerically, as we will discuss now.

4.2.4 Semi-Numeric IBP-Vectors

Presently, two-loop ampliudes are often computed in finite fields and these evaluations are then used to functionally reconstruct their analytic form [50]. For such approaches it is in fact not necessary to compute analytic IBP-relations. Instead, it is sufficient to provide a (fast enough) way to generate them for numerical values of the kinematic invariants.

We achieve this with the following method:

- For a syzygy defining matrix C, set s_{ij} to numeric values and solve the problem to obtain the numeric IBP-vectors v_n.

- Replace each non-zero number in v_n by a coefficient c_i to construct an ansatz v_a for the vector.
- Insert the ansatz back into the syzygy equation $0 = C \cdot v_a$. This gives a linear equation system L.
- Find all linear dependencies of the columns of L. Reduce the number of coefficients c_i in v_a by inserting these dependencies. Remove dependent rows.
- If the system does not have full rank, generate all $n \times (n+1)$ minors of the system.

This results in small linear system L' and an IBP-vector with coefficients c_i' which, at a (generic) numerical point, are given by the (unique) solution to L' on this point. In practice, we use numbers in a finite field (see appendix C) rather than floating point or rational numbers, since this gives fast and stable results.

We find that this method works particularly well together with the method of reducing the syzygy-problem to linear algebra (see section 4.2.3), since there the linear equation system becomes a purely numeric system which can be solved efficiently. E.g. for the massless non-planar double-pentagon, the resulting systems are of the size 2000×2000 and 20 vectors are necessary to span the complete space of IBP-relations.

The linear systems can be further improved by finding linear relations of the solutions via numeric sampling, which allows to even further reduce the linear system.

4.2.5 Semi-Numeric Power Reduction

For the reduction of amplitudes using surface terms and numerical unitarity, it is usually required to have a set of surface terms which together with the master integrals span the space of all monomials in ISPs up to some maximal power. In the SM, loop momenta in the numerator appear either at vertices of bosons or through the numerators of fermion propagators. An upper bound for the degree of the numerator in Yang-Mills theories is therefore given by the number of vertices. For planar diagrams, it is possible to additionally constrain the degrees of the individual loop momenta, since propagators and ISP's involving ℓ_1 and ℓ_2 can only appear at propagators that include this momentum. This is, however, not true in the non-planar case, since for inverse propagators $\varrho_1 = \ell_1^2$, $\varrho_2 = \ell_2^2$, $\varrho_3 = (\ell_1 - \ell_2)^2$ and $\varrho_4 = (\ell_1 - \ell_2 - p)^2$ we have

$$(\ell_1 - p)^2 = \rho_4 - \rho_3 + \rho_1 + \rho_2 + p^2 - (\ell_2 + p)^2 \tag{4.88}$$

and hence both inverse propagators and ISPs including only ℓ_2 can appear at vertices in the first sub-loop. Total power-counting nevertheless remains valid.

After having computed a set of IBP-vectors for a topology, we often find that the relations within power-counting generated by them do not span the space completely.

Instead, it is necessary to include linear combinations of IBP-relations that go beyond the power-counting. As a simple example consider a case where the space of monomials that should be spanned is given by $\{1, x, y, xy\}$ with one IBP-vector

$$v = (x + y, x + y), \tag{4.89}$$

which gives the following surface-term when applied to a monomial m

$$r(v, m) = \frac{\partial}{\partial x}(v_1 m) + \frac{\partial}{\partial y}(v_2 m). \tag{4.90}$$

Applying this vector to $\{1, x, y, x^2, xy, y^2\}$ gives

$$\{r_i\}_{i=1,...,6} = \{2, 3x + y, x + 3y, 4x^2 + 2xy, x^2 + 4xy + y^2, 2xy + 4y^2\}. \tag{4.91}$$

Evidently, there is no subset of these functions that spans the desired space of monomials while being contained in it. Such a set can be obtained, however, by combining relations that go beyond power-counting

$$\{r'_i\}_{i=1,...,4} = \{r_1, r_2, r_3, r_4 + r_6 - 4r_5\}. \tag{4.92}$$

Due to such effects at the boundary of the space of relations, it is necessary to compute IBP-relations whose degrees exceed the power-counting and combine them in such a way that the pieces beyond power-counting cancel.

In realistic cases, this reduction is far less straightforward than in the example above, since the coefficients of the monomials are functions of kinematic invariants rather than constants and the space of functions required is considerably larger. Therefore, analytic solutions to the linear system are often not feasible. As a work-around for this obstacle we employ a procedure similar to the computation of semi-numerical IBP-vectors:

- Compute all IBP-relations up to power-counting degree plus one.
- Take the relations r_i that go beyond power-counting and split them into parts within and beyond power counting r_i^w, r_i^b.
- Fix numerical values for the s_{ij}. Solve the system $r_1^b, ..., r_1^b$ as a syzygy with the dimension D as variable.
- Pick solutions that span the desired space of IBP-relations together with the relations within. We denote their maximal degree in D by d.
- For each non-vanishing coefficient in the picked solution, make an ansatz by replacing each number by coefficients $c_i^0, c_i^1 D, ..., c_i^d D^d$.

- Build the linear system

$$0 = \sum_i \sum_{k=0}^{d} c_i^k D^k r_b^i, \tag{4.93}$$

  remove linearly dependent rows and remove dependent columns by inserting dependencies of coefficients into the ansatz.

As in the previous section, we compute in a finite field to get fast and stable results. The resulting equation system typically has sizes $\lesssim 1500 \times 1500$.

There are two useful improvements to this method: First, the complexity of the reduction greatly depends on the space of functions that needs to be spanned by master integrands and surface terms. Therefore, the reduction often becomes feasible by increasing the function space. In the trivial example discussed above (eqn. (4.91)), the reduction becomes trivial when increasing the function space to $1, x, y, x^2, xy, y^2$. This will, in general, slow down the computation of the amplitude however.

Secondly, it can be helpful to allow relations that go beyond power-counting but are contained in it on-shell. For most amplitudes, the numerator insertions on top-level topologies do not span the full space expected by naïve Yang-Mills power-counting; thus it is possible to compute their surface-terms only to a reduced power-counting. Since the power-counting of descendant topologies needs to be higher anyway, it is not necessary to solve the power-counting equations for the top-level topologies fully off-shell. Moreover, if descendant integrals are considerably simpler (e.g. factorizing topologies or planar descendants of non-planar topologies), the additional cost of increasing their power-counting is often tolerable.

For non-planar topologies, we have to employ all of these methods: We increase power-counting such that it is possible to numerically solve the power-counting equations with all planar descendants set to zero. We then use these numeric solutions to generate linear systems that can be solved at every phase-space point during reconstruction. The power-counting of the planar topologies is then adjusted accordingly.

4.3 Properties of IBP-Vectors

IBP-vectors are not only a useful technical tool for integral reduction but also have some interesting properties which can be related to the geometry of the cut-surface. In this section, we will discuss some of these observed properties.

4.3.1 IBP-Vectors as Polynomial Tangent Vector Fields

While the algebraic aspects of algebraic geometry are very useful for practical computations, it also contains geometric aspects which permit a deeper understanding of IBP-reduction. For each ideal I, the *algebraic set* $\mathcal{Z}(I)$ is defined as the set of points z_i such that $f(z_i) = 0$ for all $f \in I$. Ideals and algebraic sets are related via Hilbert's Nullstellensatz [182]:
For any ideal I with algebraic set $\mathcal{Z}(I)$, and any function f such that

$$\begin{aligned} f(p) = 0 \ \forall p \in \mathcal{Z}(I), \\ \exists k \in \mathbb{N} \text{ such that } f^k \in I. \end{aligned} \tag{4.94}$$

An ideal is defined to be *prime* if

$$f^k \in I \Rightarrow f \in I. \tag{4.95}$$

For such prime ideals, there is a one-to-one correspondence between the algebraic set of an ideal and the ideal itself. In the context of Feynman integrals the algebraic set whose ideal is generated by the inverse propagators ϱ_i is called the *maximal cut-surface*. Modules, in this geometric interpretation, provide a vector space on every point of such a variety. In particular, the IBP-vectors are tangent vector fields to the cut-surface [183]. The latter are defined by

$$v_i \frac{\partial \varrho_j}{\partial z_i} \mid_{\varrho_j = 0} = 0 \quad \forall_i. \tag{4.96}$$

for the surface $\mathcal{Z}(\langle \varrho_1, ..., \varrho_n \rangle)$. The generators $v_i \frac{\partial}{\partial z_i}$ hence form a set of Lie-derivatives from $R/\langle \varrho_1, ..., \varrho_n \rangle$ to $R/\langle \varrho_1, ..., \varrho_n \rangle$, since in a parametrisation of the surface $\varrho_i = 0 \forall i$ these are directional derivatives $v_i \frac{\partial}{\partial z_i}$ in R.

Therefore, unitarity-compatible IBP-vectors lie in the vector bundle of the maximal cut surface. Feynman integrals restricted to the cut are volume forms on this manifolds (and therefore closed forms). Applying an IBP-generator to a Feynman integrand gives a form which can be written as a derivative. Hence IBP-relations define exact forms on the cut-surface. The complete tangent space of the cut-surface is given by the vectors

$$v_i^\mu \frac{\partial}{\partial \ell_i^\mu} \varrho_j = \sum_k c_k \rho_k. \tag{4.97}$$

The IBP-vectors satisfy this equation but, in addition, they are also tangent to each individual surface $\varrho_i = 0$, i.e. they do not include vectors which lead to terms ϱ_i/ϱ_j^2. In fact, however, for all known cases the IBP-vectors do span the full tangent space,

since terms with doubled propagators apparently can always be reduced to integrals with propagators of power one. Since the generators are related to the tangent space of the surface, one expects them to fulfil a Lie-algebra

$$\left[(v_a)_i^\mu \frac{\partial}{\partial \ell_i^\mu}, (v_b)_j^\nu \cdot \frac{\partial}{\partial \ell_j^\nu}\right] = f_{abc} \cdot (v_c)_k^\sigma \frac{\partial}{\partial \ell_k^\sigma}, \tag{4.98}$$

where the f^{abc} are polynomial structure constants. We find that this is indeed the case, since the left hand side gives

$$\left((v_a)_i^\mu \frac{\partial (v_b)_k^\sigma}{\partial \ell_i^\mu} - (v_b)_j^\nu \frac{\partial (v_a)_k^\sigma}{\partial \ell_j^\nu}\right) \frac{\partial}{\partial \ell_k^\sigma}. \tag{4.99}$$

Since the IBP-vectors form a module (see section 4.2.2), the expression in the bracket is clearly an IBP-vector. The Lie-derivatives along the tangent space span the space of exact forms on the cut-surface. Master integrals are therefore all closed forms modulo exact forms on the cut-surface, which defines the De-Rham cohomology group of this surface [184]. Due to Poincaré-duality, the master integrals can be related to the incontractible cycles on the cut-surface, i.e. the singular homology group [185]. This property can be used e.g. to count the number of master-integrals as a check of completeness for IBP-systems.

It is natural to study the geometry of this surface in Baikov coordinates, where the conditions that $\varrho_j = 0 \forall_j$ define a hyperplane. The geometry of the integration region in these coordinates is defined by the Baikov polynomial B (see section 4.1.2). For all of the topologies relevant for this thesis, the number of incontractible cycles is given by the number of extrema of the Baikov polynomial on the hyperplane that are not singularities, i.e.

$$\frac{\partial B(\{\hat{\alpha}_i\}, \{\hat{\varrho}_j\})}{\partial \alpha_k} = 0 \quad \forall k, \tag{4.100}$$

$$\hat{\varrho}_i = 0 \quad \forall i, \tag{4.101}$$

$$B(\{\hat{\alpha}_i\}, \{\hat{\varrho}_j\}) \neq 0. \tag{4.102}$$

This is plausible since within the area described by a non-contractible cycle of the surface $B = 0$, we have either $B > 0$ or $B < 0$ and therefore there has to be a local minimum or maximum. There are, however certain caveats of this argument (see e.g. [185]).

Complementary to the approaches discussed in this thesis, there are efforts to exploit the duality between the cycles and master integrals by integrating Feynman integrands over such cycles in order to obtain their master integral coefficients (see e.g. [186–191]).

While in general the number of incontractible cycles is only a lower bound for the number of master integrals due to the vectors possibly not spanning the full tangent space, these numbers are the same for all topologies discussed in this thesis.

4.3.2 IBP-Vectors at Extrema & Singularities of the Baikov Polynomial

One of the challenges in IBP-reduction is to find a sufficient set of generators. In this section, we provide a geometric criterion that such a set has to fulfil in order to generate all surface-terms.

Recall the formulation of the syzygy problem in Baikov coordinates [192].

$$\sum_i c_i \frac{\partial}{\partial \alpha_i} B(\{\alpha_i, \varrho_i\}) + \sum_j d_j \varrho_j \frac{\partial}{\partial \varrho_j} B(\{\alpha_i, \varrho_i\}) = f(\{\alpha_i, \varrho_i\}) B. \tag{4.103}$$

We are interested in the solutions to this problem around the extrema and singularities of the Baikov polynomial which are respectively defined by

$$\frac{\partial}{\partial \alpha_i} B = 0 \quad \forall i, \quad B \neq 0 \quad \varrho_k = 0 \quad \forall k, \tag{4.104}$$

$$\frac{\partial}{\partial \alpha_i} B = 0 \quad \forall i, \quad B = 0 \quad \varrho_k = 0 \quad \forall k. \tag{4.105}$$

For most topologies, in particular for those which are challenging to reduce, the singularities are given by isolated points[6]. Close to these points, the Baikov polynomial can be expanded in some local coordinates z, such that

$$B = b_0 + z_i C_{ij} z_j + O(z^3), \tag{4.106}$$

where C_{ij} is as symmetric matrix with full rank. A global solution to the syzygy problem must also be a local solution. The local IBP-problem is given by

$$v_i (2C_{ij}) z_j = P(z)(b_0 + z_i C_{ij} z_j) + O(z^2). \tag{4.107}$$

There are three types of vectors that fulfil this equation

(a) Rotation vectors: Choose two components j_1, j_2. The IBP-vector is then given by

$$v_{j_1} = \sum_i C_{j_2,i} z_i + O(z^2), \tag{4.108}$$

$$v_{j_2} = -\sum_i C_{j_1,i} z_i + O(z^2), \tag{4.109}$$

$$v_k = O(z^2) \quad \forall k \neq j_1, j_2, \tag{4.110}$$

$$P = O(z^2). \tag{4.111}$$

[6] In cases where the singularities are not point-like, higher derivatives of the Baikov polynomial can be set to zero until the surface is zero dimensional.

(b) Generic vectors: Choose a component j. The vector is given by

$$v_j = B + O(z^2), \tag{4.112}$$
$$v_k = 0 + O(z^2) \quad \forall k \neq j, \tag{4.113}$$
$$P = C_{jk} z_k + O(z^2). \tag{4.114}$$

(c) At singularities $b_0 = 0$, we additionally have scaling vectors:

$$v_i = z_i + O(z^2) \forall i, \tag{4.115}$$
$$P = 1 + O(z^2). \tag{4.116}$$

Locally, all IBP-generating vectors can be written as a linear combination of such vectors or are of higher order in z. It is noteworthy that the vector components vanish on the singularities, which implies that all IBP-vectors vanish on all singularities. In fact, this property can be used to find the ideal whose algebraic set is given by the singularities analytically. In particular, the vector-components are a generating set of this ideal. Moreover, vectors that can locally be described as rotation vectors (case (a)) also vanish on the extrema, while generic vectors become constant there. the proportionality constants P, however, do vanish at the extrema for all vectors. This means that IBP-vectors can also be used to find the extrema, which for instance allows to determine the number of master integrals. Vectors which are constructed via anti-symmetrisation globally, i.e.

$$v = \{0, ..., \frac{\partial}{\partial \alpha_j} B, ..., -\frac{\partial}{\partial \alpha_i} B, .., 0\}, \tag{4.117}$$
$$v = \{0, ..., B, 0, ..., 0\} \tag{4.118}$$

are rotation, respectively generic vectors also on the singularities and extrema. Therefore, vectors which are scaling vectors on a sub-set of the singularities are not within the module spanned by these trivial vectors.

The IBP-relations corresponding to the vectors applied to some polynomial $f(z_i)$ are locally given by

(a) Rotation vectors

$$\sum_i C_{j_2,i} z_i \frac{\partial}{\partial z_{j_1}} f - C_{j_1,i} z_i \frac{\partial}{\partial z_{j_2}} f + O(z^2). \tag{4.119}$$

(b) Generic vectors

$$B \frac{\partial}{\partial z_j} f + (D - n) f \frac{\partial}{\partial z_j} B + O(z^2), \tag{4.120}$$

where n is an integer depending on the dimension of the scattering plane associated to the Feynman diagram.

(c) Scaling vectors

$$(D-n)f + \sum_i z_i \frac{\partial}{\partial z_i} f + O(z^2). \tag{4.121}$$

By inspection, we find that the IBP-relations generated by rotation vectors vanish both on singularities and extrema. The relations generated by generic vectors vanish at singularities while they are proportional to the Baikov polynomial near an extremum. Thus locally, the space of IBP-relations generated via generic and rotation vectors lies within the ideal generated by the Baikov-polynomial and its derivatives. The relations generated by scaling vectors, on the other hand, can be non-zero on the singularity.

This implies that, for generic D, at a singularity, at least one relation generated by a scaling vector is linearly independent from the relations generated by rotation and generic vectors. Hence in order to obtain all IBP-relations, for each singularity the set of vectors has to contain at least one vector which locally is a scaling vector at the singularity. We find this a useful criterion to decide whether a set of vectors could be sufficient before computing all IBP-relations.

4.3.3 Gauge-Transformations of IBPs

Applying IBP-generating vectors to polynomials gives surface terms. The inverse map from surface-terms to IBP-generators is however not unique. For instance, in Baikov formulation it is possible to obtain vectors which produce vanishing IBP-relations by applying the vector

$$\{0, ..., 0, \left(\frac{\partial(Bf)}{\partial\alpha_j}\right), 0, ..., 0, \left(\frac{\partial(Bf)}{\partial\alpha_i}\right), 0, ..., 0\}, \tag{4.122}$$

where B is the Baikov polynomial and f is an arbitrary polynomial to functions g that depend neither on α_i nor α_j, which gives

$$\frac{\partial}{\partial\alpha_i}\left(\frac{\partial(Bf)}{\partial\alpha_j}\right) g - \frac{\partial}{\partial\alpha_j}\left(\frac{\partial(Bf)}{\partial\alpha_i}\right) g = 0. \tag{4.123}$$

We denote such generators as *gauge*-transformations of IBP-generators[7]. The existence of such gauge generators has two important consequences: First, it is not necessary to have a complete basis for the module of IBP-vectors in order to achieve the full IBP-

[7]In this language we absorb the numerator polynomial into the vector, thereby giving up the module structure of IBP-generators.

reduction. Second, when applying IBP-vectors to monomials in order to construct a set of IBP-relations, it is possible to work modulo gauge generators from the start.

4.4 Implementation & Validation

The methods described in this chapter are implemented in a `Mathematica`-package, using interfaces to SINGULAR and RUST. We automatically compute the propagators and ISP's, their representation in embedding space and the definition of the syzygy problem in `Mathematica`. We then use SINGULAR for Gröbner basis methods, or a finite-field linear solver implemented in RUST for linear-algebra based approaches.

We then use `Mathematica` to translate these vectors to Baikov coordinates and apply them to all monomials. Afterwards we identify an independent set and construct the linear equation defining the power-counting reduction, which is then solved with the RUST solver. As a cross-check we fix numerical values for the kinematic invariants and the dimension D and reduce the surface-terms with FIRE5 [193]. Finally, we convert the surface-terms and linear systems to files readable by the C++-framework Caravel by using MATHEMATICA's build-in package SYMBOLICC.

Chapter 5

Multi-Loop Amplitude Computation

In the previous chapters we have reviewed how amplitudes are defined in particle physics and how they relate to scattering cross-sections. This included the discussion how multi-loop integrals arise, how they can be reduced to master integrals and how these master integrals can be computed employing differential equations. Furthermore, we have discussed how unitarity-compatible IBP-relations can be obtained from IBP-vectors which are defined through syzygy computations.

In this section, we will discuss how these relations are used in the numerical unitarity method and how analytic two-loop amplitudes are obtained with functional reconstruction. We will first review some technical tools for the computation of tree-level amplitudes, discussing colour decomposition and recursion relations. We will furthermore review some useful approximations, such as the leading-colour approximation and the heavy-top-loop approximation. Furthermore, we will discuss the definition of finite remainders which we will eventually compute. Next, we will review the method of numerical unitarity. Finally, we will explain the methods of functional reconstruction which used to obtain analytic results.

5.1 Colour-Ordering & Recursion Relations

Explicit computations with Feynman diagrams are often cumbersome, e.g. a six gluon amplitude at tree level has 220 contributing Feynman-diagrams, while the 10 gluon amplitude already has more than a million contributing diagrams. Since the Feynman rules for the gluon-self-interaction vertices moreover involve six terms each, each of these diagrams contributes hundreds of thousands of terms.

A first step towards a simplification is to organise the computation through colour decomposition. Each external gluon carries a colour matrix T_a^{ij} while quarks carry a single colour index i. The algebra of these colour operators is independent of the kinematics,

hence it is possible to organise the computation by it. Employing the identities

$$if^{abc} = \mathrm{Tr}(T^a T^b T^c) - \mathrm{Tr}(T^b T^a T^c), \tag{5.1}$$

$$T^a_{ij} T^{kl}_a = \delta_{il}\delta_{kj} - \frac{1}{N_c}\delta_{ij}\delta_{kl}, \tag{5.2}$$

the colour dependence of the amplitude can be expressed in terms of traces over a product of matrices T^{ij}_a. In the case of an n-gluon amplitude, this leads to the *colour-trace decomposition* [194]

$$\mathcal{A} = \frac{1}{n!} \sum_{\sigma \in S_n(\{1,\ldots,n\})} \mathrm{Tr}(T^{a_1} T^{a_{\sigma(2)}}, \ldots, T^{a_{\sigma(n)}}) A\left(\sigma(1), \ldots, \sigma(n)\right), \tag{5.3}$$

where S_n is the group of permutations of n elements. The colour ordered amplitudes A have cyclically ordered external particles[1] and their gluonic Feynman rules simplify to

- 3-gluon vertex $V^{\{\mu_1\mu_2\mu_3\}}(p_1, p_2, p_3) = -\sqrt{2}(g^{\mu_1\mu_2} p_1^{\mu_3} + g^{\mu_2\mu_3} p_1^{\mu_1} + g^{\mu_3\mu_1} p_1^{\mu_2})$,
- 4-gluon vertex $V^{\{mu_1\mu_2\mu_3\mu_4\}}(p_1, p_2, p_3, p_4) = g^{\mu_1\mu_3} g^{\mu_2\mu_4}$.

In practice, such a decompositions is employed and Feynman rules for colour-ordered amplitudes are used. These are then summed according to eqn. (5.3).

Additional simplification can be achieved by employing recursion relations. To make this visible, the last gluon in an amplitude is set off-shell and its polarisation vector is omitted defining the current

$$J^\mu(k_1^{\lambda_1}, \ldots, k_n^{\lambda_n}) \epsilon^\pm_\mu \,|_{(\sum_{i=1}^n p_i)^2 = 0} = A(k_1^{\lambda_1}, \ldots, k_n^{\lambda_n}, k^\pm_{n+1}). \tag{5.4}$$

These currents can be computed recursively. Consider a colour ordered $(n+1)$-gluon current. Following the $(n+1)$th gluon, after the first vertex, any graph splits into 2 or 3 sub-graphs with $i, n-i$, respectively $i, j-i, n-j$ external gluons (see figure 5.1). From the construction using Feynman rules, it is evident that, in the sum over all possible diagrams, in any split, all possible sub-graphs are summed over. This sum is then again a current. Therefore, the following recursion relation is valid

$$\begin{aligned} J^\mu(k_1^{\lambda_1}, \ldots, k_n^{\lambda_n}) = & \sum_{i=1}^{n-1} V_3^{\mu\nu\rho} \frac{1}{(\sum_{j=1}^i p_j)^2 (\sum_{k=i+1}^n p_k)^2} J_\nu(k_1^{\lambda_1}, \ldots, k_i^{\lambda_i}) J_\rho(k_1^{\lambda_i+1}, \ldots, k_i^{\lambda_n}) \\ & + \sum_{0<i<j<n} V_4^{\mu\nu\rho\sigma} \frac{1}{(\sum_{k_1=1}^i p_{k_1})^2 (\sum_{k_2=i+1}^j p_{k_2})^2 (\sum_{k_3=j+1}^n p_{k_3})^2} \\ & \times J_\nu(k_1^{\lambda_1}, \ldots, k_i^{\lambda_i}) J_\rho(k_1^{\lambda_i+1}, \ldots, k_i^{\lambda_j}) J_\sigma(k_1^{\lambda_j+1}, \ldots, k_i^{\lambda_n}), \end{aligned} \tag{5.5}$$

[1] Not that the cyclic ordering is only respected for coloured particles.

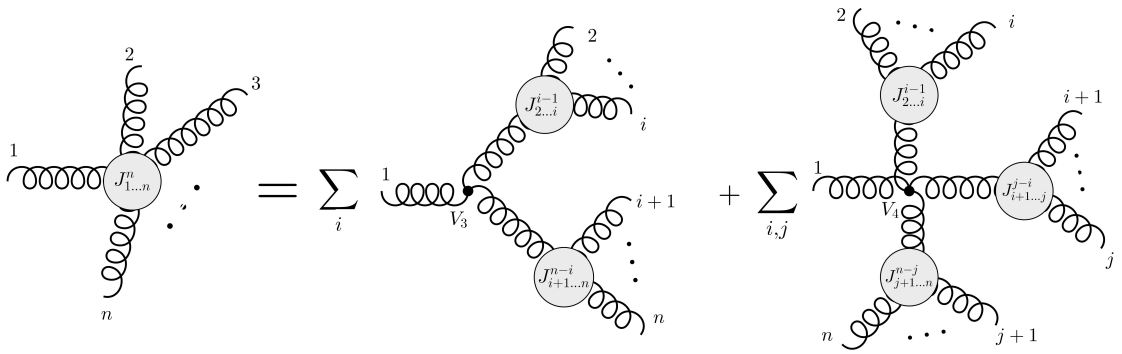

Figure 5.1: Visualization of the Berends-Giele recursion [195].

where the prefactors of V_3 and V_4 are the vertices in the colour trace decomposition and the factors $1/\sum p$ are the propagators of the off-intermediate gluons. The simplest one-particle currents are given by polarisation vectors

$$J^\mu(k^\lambda) = \epsilon^{\lambda\mu}(k). \tag{5.6}$$

Setting the $(n+1)$th gluon on-shell and contracting with a polarisation vector, this allows to compute tree-level amplitudes with many gluons recursively from currents with less gluons. Similar recursion formulae exist also for $q\bar{q}$+n-gluon and $q\bar{q}V$+n-gluon, where $q\bar{q}$ is quark line and V is a massive or massless vector boson [195]. We employ these recurrence relations whenever we compute tree-amplitudes, making their evaluation straightforward.

5.1.1 Unitarity and Factorisation

Recursion relations are related to the unitarity of the S-matrix defined in eqn. (2.11)

$$S^\dagger S = \mathbb{1}. \tag{5.7}$$

For the transition matrix $T = -i(S - \mathbb{1})$ unitarity implies that

$$i(T^\dagger - T) = T^\dagger T. \tag{5.8}$$

inserting a complete set of (multi-particle) states $T^\dagger \mathbb{1} T = \sum_x T^\dagger |x\rangle\langle x| T$ and considering initial and final states f and i gives a similar relation between amplitudes

$$i\left((A_{i\to f}(\mathbf{s}) - A^*_{f\to i}(\mathbf{s})\right)\delta_{p_f - p_i} = \sum_x \delta_{p_x - p_i}\delta_{p_f - p_x} A_{i\to x}(\mathbf{s}) A^*_{f\to x}(\mathbf{s}), \tag{5.9}$$

since $\langle x|T^\dagger|f\rangle = \langle f|T|x\rangle^* = A^*_{f\to x}\delta_{p_x - p_f}(\mathbf{s})$. The parameters $\mathbf{s}$ describe the momenta and helicities of the external particles. Since both sides only have δ-function support for $p_i - p_f = 0$, we can drop each one $\delta-$function. By crossing symmetry, this gives the

relation [196]

$$A_{i\to f}(\mathbf{s}) - A_{i\to f}(\mathbf{s}^*) = \sum_x \delta_{p_i - p_x} A_{i\to x}(\mathbf{s}) A_{x\to f}(\mathbf{s}^*). \tag{5.10}$$

Recall that in order for propagators to be causal, squared momenta were replaced as $k^2 \to k^2 - i\varepsilon$ in section 2.2. Thus, the l.h.s. of eqn. (5.10) is only non-zero when such a propagator is set on-shell. In the case of one-particle intermediate states at leading order, the equation gives the residue of the amplitude on an intermediate propagator. Summing over all possible residues of a tree amplitude, this allows to express a tree amplitude in terms of products of simpler tree amplitudes, similar to eqn. (5.5) [197].

For multi-particle intermediate states, comparison of the order of coupling constants shows that this formula relates discontinuities of loop-level amplitudes to products of amplitudes with less loops. Techniques based on *generalised unitarity* employ these factorisation formulae to express the integrands of higher order amplitudes in terms of tree-level amplitudes (see section 5.5).

5.2 Heavy-Top-Loop Approximation

A particularly interesting part of the SM is the Higgs-sector, whose coupling to light particles is dominated by top-quark loops. Including these loops into multi-loop computations, however, is notoriously difficult since Feynman-integrals with massive propagators often have a complicated analytical structure leading to elliptic (or even more complicated) integrals. To circumvent this problem and calculate amplitudes to higher orders in the coupling, the full theory can be approximated by a simpler effective theory. We will briefly review this theory and its effective operator.

In the heavy-top-loop approximation (HTL) the top quark mass is considered the largest scale in the compuation. This allows to integrate out top-loops, resulting in an effective operator [8]

$$\alpha_{ggH} G_a^{\mu\nu} G^a_{\mu\nu} H. \tag{5.11}$$

The coupling constant of this operator at leading order is obtained from computing the amplitude of two on-shell gluons with momenta k_1 and k_2 producing an on-shell Higgs via a top loop. After computing the colour trace, this amplitude is given by the integral

$$\begin{aligned} I = &- i g_s^2 \delta^{ab} \frac{m_t}{v} \int \frac{\mathrm{d}^D \ell}{(2\pi)^D} \times \\ &\frac{8 m_t \left[k_1^\mu k_2^\nu - k_1^\nu k_2^\mu + 2 k_2^\mu \ell^\nu - 2 k_1^\nu \ell^\mu + 4 \ell^\mu \ell^\nu - g^{\mu\nu} k_1 \cdot k_2 - g^{\mu\nu} \ell^2 + g^{\mu\nu} m_t^2\right]}{\left(\ell_1^2 - m_t^2\right)\left((\ell - k_1)^2 - m_2^2\right)\left((\ell + k_2)^2 - m_t 2\right)}. \end{aligned} \tag{5.12}$$

Since k_1^2 and k_2^2 are zero, the solution can only depend on the Higgs mass. The result of this integral is well known [198]:

$$I = \delta^{ab}\frac{-ig_s^2}{2\pi v}\left(1-\left(1-\frac{4m_t^2}{m_H^2}\right)\arcsin^2\left(\frac{m_H}{2m_t}\right)\right). \tag{5.13}$$

This determines the coefficient of the GGH operator which has to be equal to this in the $m_t \to \infty$ limit. This SU(3) gauge invariant operator leads to vertices with two, three and four gluons plus a Higgs. The Lagrangian of the effective theory is therefore given by omitting all terms containing top quarks and adding the additional piece[2]

$$\mathcal{L}_{ggH} = \frac{g_s^2}{2\pi v}\left(1-\left(1-\frac{4m_t^2}{m_H^2}\right)\arcsin^2\left(\frac{m_H}{2m_t}\right)\right)G_a^{\mu\nu}G^a_{\mu\nu}H. \tag{5.14}$$

For scattering energies which are too small to produce two top-quarks close to their mass-shells $s \ll 2m_t$ this effective theory gives a good approximation to the SM.

In general, the renormalisation of effective theories cannot be carried out in the way described in section 2.4, since a redefinition of the existing couplings does not remove all UV divergences and therefore, additional operators such as $\alpha_{ggHH}G^a_{\mu\nu}G_a^{\mu\nu}HH$ have tu be introduced. However, no such operators are necessary for QCD corrections to single Higgs-production in association with jets and hence it is sufficient to renormalise the coupling α_{ggH}. Up to order α_s^2, this renormalisation is given by [199]

$$\alpha^0_{ggH}/\mu^{2\epsilon} = \alpha_{ggH}(\mu^2)\left(1-\frac{\alpha_s(\mu)}{2\pi}\frac{\beta_0}{\epsilon}+\left(\frac{\alpha_s(\mu^2)}{2\pi}\right)^2\left(\frac{\beta_0^2}{\epsilon^2}-\frac{\beta_1}{\epsilon}\right)+O(\alpha_s^3(\mu^2))\right), \tag{5.15}$$

with β_0 and β_1 as defined in eqn. (2.54).

5.3 Leading-Colour Approximation

It is possible to split the amplitude into gauge invariant contributions which scale differently with the number of colours N_c. Due to the size of the strong coupling constant $\alpha_s \sim 0.1$, it is possible to use the leading colour contribution as an approximation, which often greatly simplifies the calculation. We will review this approximation and its effect on the diagrams.

Approximating $\frac{1}{N_c} \ll 1$, the colour indices of gluons can be replaced by two quark colour indices using $T^a_{ij}T^a_{kl} = \frac{1}{2}\delta_{il}\delta_{jk} + O(\frac{1}{Nc})$ and omitting the $\frac{1}{N_c}$ part (see figure 5.2). This approximation allows a very simple treatment of the colour algebra which is then reduced to the possible colour lines (see figure 5.2) [200].

[2]We ignore additional operators that do not contribute to single Higgs-production from QCD processes.

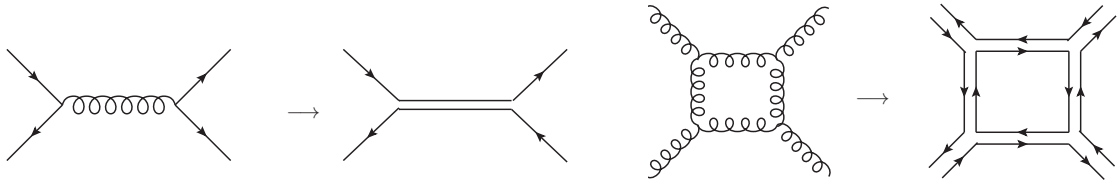

(a) Leading-colour approximation for a simple gluon propagator: The colour flow is described by $\delta_{ik}\delta_{jl}$, omitting the factor $\frac{1}{N_c}\delta_{ij}\delta_{kl}$.

(b) Leading-colour approximation for the one-loop gluonic box diagram.

Figure 5.2: Approximation of a gluon using two quark colour indices: the gluon colour transport $T^a_{ij}\delta_{ab}T^b_{kl}$ is replaced by $\delta_{ik}\delta_{kl}$ using the Fierz identity, omitting subleading terms

In this approximation colour non-planar diagrams are suppressed, where planar denotes the property that the colour flow lines can be drawn to infinity without crossing internal lines in the diagrammatic representation. For colour planar diagrams, each loop contains a closed colour flow line, which results in a factor of N_c (see figure 5.3).

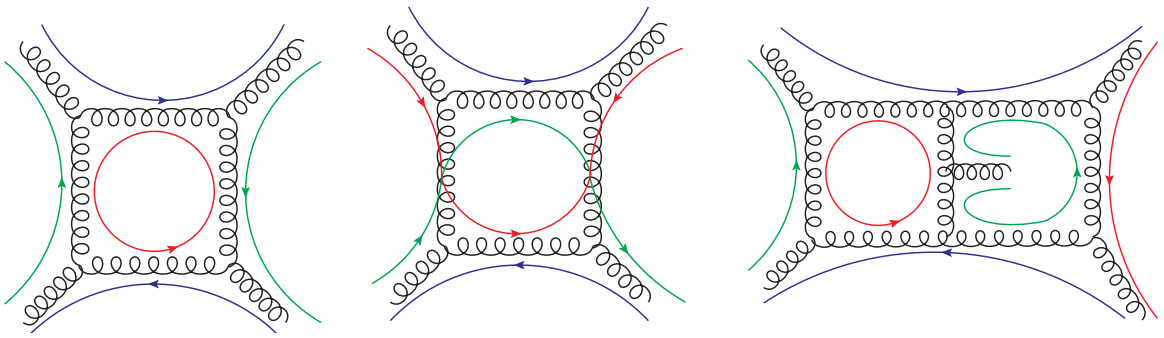

(a) A colour planar one-loop box diagram. Every internal and extermal colout line yields a sum over fundamental colour indices.

(b) A colour non-planar diagram. Only external colour lines yield a sum over fundamental colour indices, because no closed colour line is present. Therefore, the diagram is supressed by $1/N_c$ compared to (a).

(c) A kinematically non-planar two-loop diagram. There is no colour configuration such that two closed colour lines appear, hence the diagram is automatically subleading in colour.

Figure 5.3: Planar and non-planar gluonic diagrams with colour-flow lines. Each coloured line is summed over all quark colours in an amplitude.

For colour non-planar diagrams there are less of these traces and hence their contribution to pure QCD amplitudes is suppressed by at least a factor of $1/N_c$. For pure Yang-Mills amplitudes, the diagrams contributing to non-planar integral topologies are automatically also colour non-planar, since the colour flow line of at least one loop has to be interrupted at external particles attached to the central rung. This allows to compute the leading colour approximation of amplitudes without taking non-planar integral

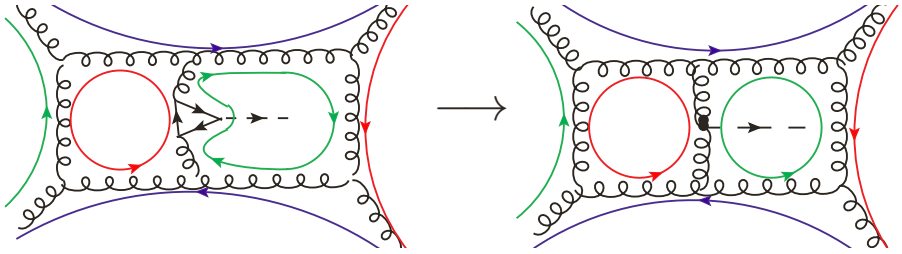

Figure 5.4: A kinematically non-planar diagram contributing to Higgs production via gluon fusion at leading colour.

topologies into account.

The suppression of (kinematically) non-planar diagrams by $1/N_c$ is, in general, not valid for amplitudes containing Yukawa- or electro-weak couplings. For instance, using the high top-mass approximation discussed in section 5.2 for Higgs production via gluon fusion, the two-gluon-Higgs vertex imposes colour conservation among the gluons. Therefore, some non-planar diagrams contribute e.g. to Higgs-plus-two-jet production from gluon fusion at leading colour (see figure 5.4).

Another type of processes where non-planar pieces might matter are processes where electro-weak bosons couple to closed fermion loops. While these processes are usually colour suppressed compared to processes with gluon loops, they are enhanced by the number of fermions circulating in the loop and therefore may lead to sizeable corrections.

5.4 Finite Remainders

As described in section 2.4, the renormalized amplitudes in $\overline{\text{MS}}$ scheme can be obtained by replacing bare couplings α_κ^0 by renormalised couplings by renormalized coupling $\alpha_\kappa(\mu)$. e.g. for α_s

$$\alpha_s^0(\mu) = \alpha_s(\mu)\left(1 - \frac{\beta_0}{\epsilon}\frac{\alpha_s(\mu)}{2\pi} + \left(\frac{\beta_0^2}{\epsilon^2} - \frac{\beta_1}{2\epsilon}\right)\left(\frac{\alpha_s(\mu)}{2\pi}\right)^2 + \mathcal{O}\left(\alpha_s^3(\mu)\right)\right). \tag{5.16}$$

The coefficients β_0 and β_1 defined as in eqn. (2.54). Replacing bare couplings by renormalised couplings gives renormalised amplitudes. For example, for an amplitude where $\mathcal{A}_\kappa^{(0)} \propto \alpha_s^q$, the renormalised amplitudes $\mathcal{A}_{\kappa,R}^{(L)}$ relate to the bare amplitudes $\mathcal{A}_\kappa^{(L)}$ via

$$\begin{aligned}
\mathcal{A}_{\kappa,R}^{(0)} &= \mathcal{A}_\kappa^{(0)}, \\
\mathcal{A}_{\kappa,R}^{(1)} &= \mathcal{A}_\kappa^{(1)} - q\frac{2\beta_0}{\epsilon N_c}\mathcal{A}_\kappa^{(0)}, \\
\mathcal{A}_{\kappa,R}^{(2)} &= \mathcal{A}_\kappa^{(2)} - (q+1)\frac{2\beta_0}{\epsilon N_c}\mathcal{A}_\kappa^{(1)} + \left((q+1)\frac{2\beta_0^2}{\epsilon^2 N_c^2} - q\frac{2\beta_1}{\epsilon N_c^2}\right)\mathcal{A}_\kappa^{(0)}.
\end{aligned} \tag{5.17}$$

Infrared divergences of multi-loop QCD-integrals occur when a gluon that is exchanged between two external legs becomes soft or collinear to one of the legs. In fact, these divergencies appear as universal factors which can be subtracted to obtain the *finite remainder* [201–203]

$$\mathcal{R}_\kappa = \mathcal{R}_\kappa^{(0)} + \frac{\alpha_s}{2\pi}\mathcal{R}_\kappa^{(1)} + \left(\frac{\alpha_s}{2\pi}\right)^2 \mathcal{R}_\kappa^{(2)} + \mathcal{O}(\alpha_s^3)\,, \tag{5.18}$$

with the $\mathcal{R}_\kappa^{(i)}$ defined as

$$\begin{aligned} \mathcal{R}_\kappa^{(0)} &= \mathcal{A}_{\kappa,R}^{(0)}, \\ \mathcal{R}_\kappa^{(1)} &= \mathcal{A}_{\kappa,R}^{(1)} - \mathbf{I}_\kappa^{(1)}\mathcal{A}_{\kappa,R}^{(0)} \ + \mathcal{O}(\epsilon), \\ \mathcal{R}_\kappa^{(2)} &= \mathcal{A}_{\kappa,R}^{(2)} - \mathbf{I}_\kappa^{(1)}\mathcal{A}_{\kappa,R}^{(1)} - \mathbf{I}_\kappa^{(2)}\mathcal{A}_{\kappa,R}^{(0)} \ + \mathcal{O}(\epsilon). \end{aligned} \tag{5.19}$$

For colour-ordered $N-$point amplitudes, the operator $\mathbf{I}_\kappa^{(1)}$ is given by [201]

$$\mathbf{I}_\kappa^{(1)}(\epsilon) = -\frac{e^{\gamma_E \epsilon}}{\Gamma(1-\epsilon)} \sum_{i=1}^{N} (s_{i,i+1})^{-\epsilon} \gamma_{t_i,t_{i+1}}, \tag{5.20}$$

where s_{ij} are the Mandelstam variables, t_i denotes the particle type of the ith external particle and the *anomalous dimension* γ depends on the particles

$$\gamma_{gg} = \left(\frac{1}{\epsilon^2} + \frac{1}{\epsilon}\frac{\beta_0}{N_c}\right), \qquad \gamma_{q_1 \neq q_2} = \left(\frac{1}{\epsilon^2} + \frac{3}{2\epsilon}\right), \tag{5.21}$$

$$\gamma_{qg} = \left(\frac{1}{\epsilon^2} + \frac{1}{\epsilon}\frac{\beta_0}{2N_c} + \frac{3}{4\epsilon}\right). \tag{5.22}$$

The operator $\mathbf{I}_\kappa^{(2)}$ is given by [201]

$$\begin{aligned} \mathbf{I}_\kappa^{(2)}(\epsilon) = &-\frac{1}{2}\mathbf{I}_\kappa^{(1)}(\epsilon)\mathbf{I}_\kappa^{(1)}(\epsilon) - \frac{2\beta_0}{N_c\epsilon}\mathbf{I}_\kappa^{(1)}(\epsilon) + \frac{e^{-\gamma_E\epsilon}\Gamma(1-2\epsilon)}{\Gamma(1-\epsilon)}\left(\frac{2\beta_0}{N_c\epsilon} + K\right)\mathbf{I}_\kappa^{(1)}(2\epsilon) \\ &+ \frac{e^{\gamma_E\epsilon}}{\epsilon\Gamma(1-\epsilon)}\mathbf{H}_\kappa\,, \end{aligned} \tag{5.23}$$

where

$$K = \frac{67}{9} - \frac{\pi^2}{3} - \frac{10}{9}\frac{N_f}{N_c}\,. \tag{5.24}$$

The operator $\mathbf{H}_\kappa$ is given by $\mathbf{H}_\kappa = \sum_i H_{t_i}$, where

$$\begin{aligned} H_{\mathrm{g}} &= \left(\frac{\zeta_3}{2} + \frac{5}{12} + \frac{11\pi^2}{144}\right) - \left(\frac{\pi^2}{72} + \frac{89}{108}\right)\frac{N_f}{N_c} + \frac{5}{27}\left(\frac{N_f}{N_c}\right)^2, \\ H_q &= \left(\frac{7\zeta_3}{4} + \frac{409}{864} - \frac{11\pi^2}{96}\right) + \left(\frac{\pi^2}{48} - \frac{25}{216}\right)\frac{N_f}{N_c}\,. \end{aligned} \tag{5.25}$$

The representation in terms of finite remainders is independent of the renormalisation and regularisation schemes (see e.g. [204]) and can be used for physical applications (see e.g. [205]). Moreover, it often takes a simpler form than the full amplitude by subtracting contributions from the ϵ^0 terms of the amplitudes.

Note that, however, the cancellation of poles in ϵ only becomes explicit when the one- and two-loop amplitudes are expressed in the same set of linearly independent and ϵ-free functions. Such a basis can be obtained by expanding the master integrals order by order in the dimensional regulator ϵ. In such an expansion the master integrals can often be expressed in terms of multiple polylogarithms (MPLs), whose linear relations are well understood [206–208] or iterated integrals satisfying a shuffle-algebra. This allows to construct a basis of linearly independent *pentagon functions*, which are available for all amplitudes and remainders discussed in this thesis [41–43].

A useful strategy for the computation of the loop amplitudes is to directly reconstruct the finite remainders defined in eqn. (5.19) from numerical evaluations of the amplitude. This is achieved by first numerically reducing the amplitude to a basis of master integrals, which are themselves expanded in terms of a basis of pentagon functions. We can then subtract the known divergences and obtain a numerical decomposition of the remainders in terms of pentagon functions.

In the following, we will discuss how we obtain the numeric decomposition of amplitudes to master-integral coefficients. The maps from these master-integral coefficients to pentagon-function coefficients are given in the ancillary files of [41–43].

5.5 Two-Loop Numerical Unitarity

In order to obtain a decomposition of amplitudes in terms of master integrals, we use the framework of two-loop numerical unitarity [48, 55–57, 167, 209], which we will review in this section.

We begin by parametrizing the integrand of the colour-ordered amplitude $\mathcal{A}_\kappa^{(2)[j]}(\ell_l)$ in terms of surface terms (a.k.a. unitarity compatible IBP-relations) and master integrands [48]. The latter become the master integrals when integrated while the surface terms integrate to zero. We organize this decomposition by the topologies, i.e. the propagator structures of Feynman integrals contributing to the process

$$\mathcal{A}_\kappa^{(2)[j]}(\ell_l) = \sum_{\Gamma\in\Delta} \sum_{i\in M_\Gamma\cup S_\Gamma} c_{\Gamma,i} \frac{m_{\Gamma,i}(\ell_l)}{\prod_{j\in P_\Gamma} \varrho_j}\,, \tag{5.26}$$

where Δ is the set of propagator structures Γ, and P_Γ are the multisets of inverse propagators and M_Γ, S_Γ denote the sets of master integrands and surface terms $m_{\Gamma,i}(\ell_l)$, respectively. The $c_{\Gamma,i}$ are the coefficients of the ansatz. The l.h.s. of eqn. (5.26) could,

in principle, be obtained as the sum of all possible Feynman diagrams. However, we use a different approach based on unitarity. The sets of surface terms are constructed with the methods described in chapter 4. Since this ansatz will be fitted only numerically, we can either use fully analytic surface terms, or we can employ files which generate numeric surface terms sufficiently fast for every phase-space point (see sections 4.2.5, 4.2.4).

The master-integral bases for the processes under consideration have been computed in [42, 167]. These master integrals are often not in a form compatible with eqn. (5.26), since they include doubled propagators or integrals which are linearly dependent on-shell and only differ by descendant topologies. Reducing these integrals to a unitarity compatible basis could be done with the methods discussed in chapter 4. However, since they typically have low degree in the loop momenta, while IBP-relations generated from IBP-vectors have high degrees, it turns out that Laporta's algorithm, in combination with functional reconstruction (see section 5.6), is more efficient. For this purpose, a public implementation of this method in `LiteRed` [136] has been used to obtain unitarity compatible master integrals.

Constraining this ansatz via numeric sampling of the l.h.s. directly would lead to enormous linear systems whose solution would be very time-consuming even when choosing external momenta numerically. We therefore employ *numerical unitarity*, a cut-based method which naturally block-triangularises these systems. The principle of methods based on generalised unitarity is to rely on factorization properties of the integrand. In particular, when taking the integrand $\mathcal{A}_\kappa^{(2)[j]}(\ell_l)$ to loop-momentum configurations ℓ_l^Γ where a set of propagators are on-shell, that is $\varrho_j(\ell_l^\Gamma) = 0$ iff $j \in P_\Gamma$, the residue of the ansatz in eqn. (5.26) is equal to a product of tree-level amplitudes

$$\sum_{\text{states}} \prod_{i \in T_\Gamma} \mathcal{A}_i^{(0)}(\ell_l^\Gamma) = \sum_{\Gamma' \geq \Gamma, i \in M_{\Gamma'} \cup S_{\Gamma'}} \frac{c_{\Gamma',i} m_{\Gamma',i}(\ell_l^\Gamma)}{\prod_{j \in (P_{\Gamma'} \setminus P_\Gamma)} \rho_j(\ell_l^\Gamma)} \,. \tag{5.27}$$

On the left-hand side of this equation we denote by T_Γ the set of tree-level amplitudes associated with the vertices in the diagram corresponding to Γ and the sum is over the states propagating through the internal lines of Γ. On the right-hand side, we sum over the propagator structures which contribute to the limit, denoted Γ', for which $P_\Gamma \subseteq P_{\Gamma'}$.

The fact that the factorization on the l.h.s. holds can be seen from the construction via Feynman rules: The amplitude is defined as the sum over all possible graphs with a given set of external particles. The residue can be constructed from Feynman-rules by drawing these propagators with all possible particles, and connect the propagators and external particles in all ways allowed by Feynman rules. These connections in all possible ways are in fact all possible ways to draw diagrams which have the particles in the propagators as external states and are thus tree-level amplitudes [210–214]. When taking only physical polarisation states into account for internal gluons, it is in fact

possible to omit the contributions of ghost fields, which otherwise would be necessary to cancel the longitudinal polarisation states of gluons.

Alternatively, one could obtain such factorization formulae from the unitarity of the S-matrix as we discussed in section 5.1.1 (hence the name *generalised unitarity*).

In numerical unitarity the coefficients $c_{\Gamma,i}$ are determined numerically by sampling eqn. (5.27) over a sufficient number of values of ℓ_l^Γ. This allows to constrain the ansatz topology by topology, where ancestor integrals with their coefficients have to be subtracted from the amplitudes when constraining the coefficients of descendants. For eqn. (5.27) to be valid for colour-stripped amplitudes, a special unitarity-based colour decomposition approach introduced in refs. [215, 216] has to be used.

5.5.1 Dimensions of Internal States

The tree-level amplitudes in eqn. (5.27) are defined in D-dimensions, giving rise to D-dependence on the left-hand side of the ansatz due to sums over the polarisation states. In order to compute these D-dimensional tree-level amplitudes, the D-dependence of master integrals and surface terms is differentiated from the dimension of internal states D_s. The D_s dependence arises only from sums over polarizations of the tree amplitudes. Their $(D_s - 4)$ dimensional spinor- and vector-indices have to be contracted either along one of the loops, or with one of the external particles, where they vanish. Therefore, the residue can depend on D_s at most quadratically in the two-loop case.

For even integer values of D_s, spinor representations with $2^{D_s/2}$ dimensions exist (see e.g. [127]). It is therefore possible to constrain the ansatz by evaluating the tree-level amplitudes with explicit representations of the D_s-dimensional Clifford algebra in $D_s = \{6, 8, 10\}$ dimensions and reconstruct the analytic D_s dependence from there [127, 217, 218]. Afterwards, the dimensions are considered in 't Hooft-Veltmann scheme again, i.e. $D_s \to D$. The tree-level amplitudes are evaluated through Berends-Giele recursion [195], which seamlessly carries over to the D_s dimensional case.

In this way a constraining system of equations for the $c_{\Gamma,i}$ can be built which allows to determine the numeric master integral coefficients. By performing all these calculations using finite-field arithmetic (see appendix C) fast computations without any loss of precision are possible. This however requires a rational parametrization of the phase space, which can be obtained using momentum twistors (see e.g. [219]). By solving these systems and discarding the surface-term coefficients, we arrive at a decomposition of the amplitude in terms of master integrals.

As a final remark, we emphasize that after the computation of the amplitude on one (sufficiently generic) phase-space point, it is possible to analyse which of the coefficients of master integrals and surface terms vanish. When repeating the computation on different phase-space points, these master integrals and surface terms are excluded from the ansatz

which reduces the number of sampling points and thereby leads to a significant efficiency gain.

5.5.2 Remainders and Pentagon Functions

Having evaluated the coefficients $c_{\Gamma,i}$ as described above, we insert expressions for the master integrals in terms of pentagon functions, thereby obtaining a decomposition of the amplitude in terms of pentagon functions

$$\mathcal{A}_\kappa^{(2)[j]} = \sum_{i\in B} \sum_{k=-4}^{0} \epsilon^k d_{k,i} h_i + \mathcal{O}(\epsilon)\,, \tag{5.28}$$

with pentagon function monomials $\{h_i\}_{i\in B}$, and the the associated set of labels B. Employing the same procedure for one-loop amplitudes, we obtain

$$\mathcal{R}_\kappa^{(2)[j]} = \sum_{i\in B} r_i h_i\,, \tag{5.29}$$

where the r_i are rational functions of the external kinematics.

We employ a twistor parametrisation of the phase space to get rational results and obtain the pentagon-function decomposition in finite field arithmetic.

5.6 Analytic Reconstruction

In the previous sections we have described how master integral coefficients of amplitudes, respectively the pentagon function coefficients of finite remainders are computed numerically within the framework of two-loop numerical unitarity.

In this section, we will discuss how the analytic coefficients can be obtained from the numeric evaluations and functional reconstruction. Compared to generic functional reconstruction algorithms we use several improvements based on the physical properties of amplitudes: First, in ref. [57] it has been conjectured that the denominators of pentagon function coefficients can be extracted from the coefficients reconstructed on a univariate slice and knowledge of the symbol alphabet describing the branch-cut structure of the pentagon functions.[3]

Second, in ref. [40] it was noticed that the analytic form of the coefficients can be simplified by univariate partial fractioning which can be performed before the full functional reconstruction.

Finally, in ref. [51], an advantageous choice of sampling points was used to reconstruct

[3]Related methods have since been put forward [220].

polynomials from structured linear systems which can be efficiently solved. Complementary to this approach, we also review a reconstruction method based on spinor brackets.

5.6.1 Parametrisation in Terms of Mandelstam Invariants

A natural choice of variables to perform the analytic reconstruction is given by the Mandelstam variables, as they are Lorentz-invariant and resemble physical configurations, e.g. propagators of tree-level amplitudes. In general, helicity-amplitudes have a spinor-weight (see appendix E), due to the contraction with fermion polarisation vectors. We therefore normalise loop-amplitudes by a spinor weight factor, leaving a function which can be expressed through only Mandelstam Invariants. The pentagon function coefficients in normalised finite remainders with up to five external particles are then rational functions of the Mandelstam invariants and $\mathrm{tr}_5 = \epsilon(p_1, p_2, p_3, p_4)$. Furthermore, since tr_5^2 is a polynomial in the Mandelstam invariants the dependence on it simplifies

$$r_i(\vec{s}, \mathrm{tr}_5) = r_i^+(\vec{s}) + \mathrm{tr}_5\, r_i^-(\vec{s})\,, \tag{5.30}$$

where the $r_i^\pm$ are rational functions of the Mandelstam invariants. The Mandelstam variables themselves are parity invariant while the pseudo-scalar tr_5 transforms as parity odd. It is therefore clear that we can extract the $r_i^\pm$ by computing the r_i on parity-conjugate phase-space points [218].

$$r^+ = \frac{1}{2}\left(r(\vec{s}, \mathrm{tr}_5) + r(\vec{s}, -\mathrm{tr}_5)\right), \qquad r^- = \frac{1}{2\mathrm{tr}_5}\left(r(\vec{s}, \mathrm{tr}_5) - r(\vec{s}, -\mathrm{tr}_5)\right). \tag{5.31}$$

The split of the remainder into parity even and parity odd parts is in a sense unphysical, because the SM is organised by chirality rather than parity. Therefore, it is sometimes fruitful to not split the amplitude into parity even and odd parts, but directly reconstruct in terms of spinor brackets $[ij]$,$\langle ij\rangle$ (see section 5.6.6).

5.6.2 Denominators from Univariate Slices

The analytic structure of the master integrals in a pure basis is, to a large extent, described by the symbol letters W_k of this basis (see section 3.2). Any unphysical pole in the pentagon function coefficients has to cancel out in the amplitude and thereby requires a degeneracy of the pentagon functions on this pole. It has therefore been conjectured in ref. [57], that the denominators of the $r_i^\pm$ factorize into products of symbol letters raised to some power

$$r_i^\pm = \frac{n_i^\pm}{\prod_{j=1}^n W_j^{q_{ij}^\pm}}, \tag{5.32}$$

where the $q_{ij}^\pm$ are (potentially negative) integers.

The exponents $q_{ij}^{\pm}$ can be determined by reconstructing the amplitude on a (sufficiently generic) univariate slice in the kinematic invariants [57]. The denominators of the resulting coefficients factorize into simple functions which can be mapped to the letters and whose exponents then correspond to the exponents of symbol letters in eqn. (5.32).

To obtain such a reconstruction on a univariate slice, we construct parametrisations of the external momenta in one parameter t which leads to Mandelstam variables which are linear in t and also rationalises tr_5. We achieve this with a generic method based on generalised Britto–Cachazo–Feng–Witten (BCFW)-shifts [221]. Specifically, a multi-line purely holomorphic shift [222] naturally results in Mandelstam variables that are linear in the shift parameter. In order to be sufficiently generic, we shift all of the lines (see e.g. ref. [223]) as proposed in ref. [224]. Starting from a randomly chosen point defined by its spinor-representation $\{\lambda_1, ..., \lambda_n, \tilde{\lambda}_1, ..., \tilde{\lambda}_n\}$, a holomorphic shift adjusts every λ spinor in a way which is proportional to a common reference spinor η

$$\lambda_i \to \lambda_i + t c_i \eta. \tag{5.33}$$

The c_i have to be chosen such that the shifted kinematics satisfy momentum conservation

$$0 = \sum_{i=1}^{n} k_i = \sum_{i=1}^{n} \tilde{\lambda}_i \lambda_i \to \sum_{i=1}^{n} \left(\tilde{\lambda}_i \lambda_i + c_i t \tilde{\lambda}_i \eta \right) = \left(\sum_{i=1}^{n} c_i t \tilde{\lambda}_i \right) \eta = 0, \tag{5.34}$$

which is ensured by choosing

$$\sum_{i=1}^{n} c_i \tilde{\lambda}_i = 0, \tag{5.35}$$

We chose a random set c_i out of the four-dimensional solution space of this equation. Under such a shift the holomorphic spinor products transform linearly in t

$$\langle ij \rangle \to \langle ij \rangle + t \left(c_i \langle \eta j \rangle + c_j \langle i \eta \rangle \right), \tag{5.36}$$

whereas the anti-holomorphic spinor products $[ij]$ are constant, such that the Mandelstam invariants $s_{ij} = \langle ij \rangle [ji]$ become linear in t while tr_5 is quadratic in t. For each point on this slice the parity conjugate point is trivially obtained by $[i| \leftrightarrow \langle i|$, $|i] \leftrightarrow |i\rangle$.

On the univariate slice, given by this shift, we can obtain the coefficients $\tilde{r}_i^{\pm}(t) = \frac{n_i^{\pm}(t)}{d_i^{\pm}(t)}$ by Thieles interpolation formula [225] (see appendix D.1).

The letters W_k become simple univariate rational functions $W_k(t) = \nu_k(t)/\delta_k(t)$ on the slice, which are unique if the slice is chosen sufficiently generic. Due to the conjecture in eqn. (5.32), the denominator $d_i(t)$ factorises into these simple functions. By comparing the degrees of the factors $\nu_k(t)$ and $\delta_j(t)$ in the factorised form of the denominator, the analytic

denominator of the pentagon-function coefficients can be obtained. The reconstructed coefficients on the univariate slice also reveal the exponents $q_{ij}^{\pm}$ in eqn. (5.32). It is also possible to extract letters which appear as a factor in the numerator the same way.

Moreover, the univariate reconstruction gives the polynomial degrees of the $n_i^{\pm}$, giving a measure of the complexity of the ansatz. If the degrees are sufficiently low, we can construct an ansatz with all monomials up to the maximal degree and constrain it from numerical evaluations. For many amplitudes, however, the complexity involved in solving the linear systems required to constrain such an ansatz makes this an inviable approach to determining the analytic form of the $r_i^{\pm}$.

5.6.3 Linear Dependencies of Coefficients

Pentagon functions make many physical properties of the amplitude such as the pole structure and the *transcendentality* (i.e. the number of iterated logarithmic integrals) explicit, which makes them a very suitable basis to expand the amplitude in. However, they still do contain spurious (multi-)logarithmic singularities which have to cancel in the amplitude. In practice this implies that many of the pentagon function coefficients are linearly dependent [226]. We can use this property by sampling the amplitude on a sufficient number of points p_i. This cancellation happens for the even and odd parts individually. We can hence construct two matrices

$$M_{ij}^{+} = r_i^{+}(p_j), \qquad M_{ij}^{-} = r_i^{-}(p_j) \tag{5.37}$$

by sampling over different values of p_j. When choosing a sufficient number of p_j, the reduced row echelon form of this matrix expresses the linear dependencies of the analytic remainder. In practice we increase the number of sampling points until the ranks of the matrices $M^{\pm}$ saturate.

We choose a basis of coefficient functions $r_k^{\pm}, k \in K$ such that the degrees computed via univariate sampling is minimal. This allows to systematically express complicated coefficients in terms of simpler coefficients. The remainder then takes the form [218]

$$\mathcal{R}^{(2)} = \sum_{i \in K, j \in B} r_i L_{ij} h_j, \tag{5.38}$$

where h_j are the pentagon functions, r_i are the independent (rational function) coefficients and L_{ij} is a matrix of rational numbers expressing the linear dependencies.

Furthermore, it is possible to include known analytic functions into this sampling procedure in order to express coefficient functions through them [40]. We find that this is particularly fruitful when including the coefficients of similar but simpler amplitudes. For instance, many of the most complicated coefficients of non-planar amplitudes can be

expressed through the coefficients of planar-amplitudes with the same particles or at least the same kinematic structure.

Often, the ansätze for the r_i have several ten-thousands to several hundred-thousands of free coefficients, while only a few hundred r_i are independent, thus making the sampling to get linear dependencies negligible as compared to the sampling required for the reconstruction. The linear dependencies, however, contain complicated rational numbers. We find it convenient to do the sampling over several finite fields and reconstruct these rational numbers via the Chinese Remainder Theorem (see appendix C).

5.6.4 Partial-Fraction Ansatz

If the polynomial degrees of the numerators of pentagon function coefficients in common-denominator form is too high for simple ansatzing to be feasible, it is necessary to identify simpler polynomials whose reconstruction is possible with moderate computational effort.

In previous computations of two-loop amplitudes it has been observed that pentagon function coefficients greatly simplify in a partial fraction decomposition. This simplification can be exploited by employing a univariate partial-fraction decomposition as suggested in ref. [40], which we will review in the following.

We perform a partial fraction decomposition with respect to one kinematic invariant s_{ij}, where we group the remaining kinematic invariants into some vector $\vec{s}_{\text{rem}}$. For any two distinct letters W_{k_1}, W_{k_2} with powers $Q_{k_1} Q_{k_2}$, Hilberts's Nullstellensatz guarantees the existence of a solution to the equation

$$1 = \frac{n_{k_1}(\vec{s}_{\text{rem}}, s_{ij})}{d_{k_1}(\vec{s}_{\text{rem}})} W_{k_1}^{Q_{k_1}} + \frac{n_{k_2}(\vec{s}_{\text{rem}}, s_{ij})}{d_{k_2}(\vec{s}_{\text{rem}})} W_{k_2}^{Q_{k_2}}, \tag{5.39}$$

where the n and d are polynomials. Note that when only considering s_{ij} as a variable this means that 1 is the Gröbner basis of $W_{k_1}^{Q_{k_1}}$ and $W_{k_2}^{Q_{k_2}}$ and we can use Buchberger's algorithm to obtain the n and d.

Repeatedly inserting such identities into the numerator of a coefficient in common denominator form, the denominator can be decomposed into pieces with only one s_{ij} dependent letter in the denominator.

In general, this procedure will generate spurious poles, i.e. poles which appear for individual terms but cancel in the sum. For example, in

$$\frac{1}{(x-b)\,(cx^2-a)} \overset{\text{part. fract w.r.t } x}{=} \frac{-bc-cx}{(b^2c-a)\,(cx^2-a)} + \frac{1}{(x-b)\,(b^2c-a)} \tag{5.40}$$

the term $(b^2c - a)$ is a spurious pole. In the context of pentagon function coefficients such spurious poles are not necessarily symbol letters themselves. We find, however, that when repeatedly applying the decomposition in eqn. (5.39), such spurious poles can

only occur from pairwise correlations of letters. We can therefore construct all possible spurious factors systematically by solving eqn. (5.39) for all pairs of letters via Gröbner basis methods and taking the denominators d_{j_k}, giving a new set of letter-like objects $\overline{\mathcal{W}} = \{\overline{W}_1(\vec{s}_{\text{rem}}), \ldots, \overline{W}_{|\overline{\mathcal{W}}|}(\vec{s}_{\text{rem}})\}$.

After cancelling the s_{34} dependent polynomials in the numerator via polynomial division, we arrive at a canonical partial fraction decomposition of the coefficients $r^{\pm}$

$$r^{\pm} = \sum_{k=1}^{n_i} \sum_{m} \frac{P^{\pm}_{km}(\vec{s}_{\text{rem}}) s_{ij}^m}{W_k(\vec{s}_{\text{rem}}, s_{ij})^{\beta^{\pm}_k} \prod_l \overline{W}_l(\vec{s}_{\text{rem}})^{\gamma^{\pm}_{kl}}}\,, \tag{5.41}$$

where the $P^{\pm}_{ij}$ are polynomial in $\vec{s}_{\text{rem}}$. The W_k and $\overline{W}_l$ are known fully analytically, while the polynomials $P^{\pm}_{ij}$ and and the exponents $\beta^{\pm}_k$ and $\gamma^{\pm}_{kl}$ have to be determined from numerical samples. We first discuss how to determine the exponents, the contributing degrees s_{ij}^m in the numerator and the total degrees of the polynomials $P^{\pm}_{ij}$. Similarly to the univariate slice, which we have used to determine the denominators and total degrees in common denominator form, we achieve this by reconstructing on a bivariate slice. This slice is chosen such that s_{ij} varies freely while the other Mandelstam variables are chosen as linear in one parameter. Specifically, we set

$$s_{ij} = s, \quad s_{\text{rem},i} = a_i + b_i t, \tag{5.42}$$

where the a_i and b_i are fixed, randomly chosen elements of a finite field. This again raises the problem that Mandelstam invariantes do not rationally parametrize the phase space. For the cases we consider, however, it is always possible to parametrise the n-dimensional phase space by $n-1$ Mandelstam invariants and one twistor parameter x (for the details, see appendix F). We choose such a parametrisation with all Mandelstams but s_{ij} and an additional x. s_{ij} and tr_5 then depend rationally on these variables. It is then trivial to choose $\vec{s}_{\text{rem}}$ with a t dependence as in eqn. (5.42).

To obtain the dependence on s, we apply the methodology of ref. [218], where we sample over values of $\{t, x\}$, and reconstruct the rational functions through their dependence on

$$\{s_{ij}, t\} = \{s_{ij}(t, x), t\}. \tag{5.43}$$

This approach also requires the ability to find parity conjugate phase-space points, which we detail in appendix F as well. With this parametrisation it is possible to reconstruct the numerators of coefficients[4] on the bivariate slice via iterated Newton interpolation (see appendix D.2).

After reconstructing the finite remainder on such a slice, the terms of a partial fraction

[4]Recall that the denominators is known analytically and can hence be multiplied out.

decomposition w.r.t. s are equivalent to the terms in eqn. (5.41) and can be easily identified by their s_{ij} dependence. The maximal degrees of $P^{\pm}_{km}$ and the exponents of the letters in the denominator β_k and γ_{kl} can be identified with the standard univariate analysis, leaving only the explicit form of the $P^{\pm}_{km}$ to be determined.

As a final remark, we note that the partial fraction expansion is disadvantageous when one letter correlates with many others, i.e. they appear together in irreducible denominators. For instance, in the comparably simple function

$$\frac{-xs_{45}+s_{45}+3}{(s_{45}+1)(s_{45}-x)(s_{45}x-2)} \tag{5.44}$$

$$= -\frac{x}{(s_{45}x-2)(x^2-2)} + \frac{1}{(s_{45}+1)(x+1)} + \frac{-x^2+x+3}{(s_{45}-x)(x+1)(x^2-2)}$$

$$= \frac{1}{x-s_{45}}\left(\frac{1}{2-s_{45}x} + \frac{1}{s_{45}+1}\right) \tag{5.45}$$

the letter $(x - s_{45})$ appears together with all other letters. This has the effect that the term with $(s_{45} - x)$ as a denominator factor has, in fact, a higher polynomial degree in x than the common denominator form (see eqn. (5.44)). However, by excluding this factor from the partial fraction expansion a very simple ansatz is found indeed (see eqn. (5.45)).

Such factors could appear e.g. from a badly chosen normalization, but also seem to appear naturally in the coefficients. Since the partial fraction expansion is computationally rather lightweight compared to sampling the amplitude, we can determine by trial an error which factors have to be excluded from the partial fraction expansion for an optimal ansatz for each coefficient. Nevertheless, it would certainly be interesting to study these correlations in more detail.

5.6.5 Vandermonde Sampling Procedure

After reducing the reconstruction problem to sufficiently simple polynomials $P^{\pm}_{km}$, we can use an ansatz consisting of all monomials up to the known total degree and constrain it from numerical evaluations. For $r^{\pm}_i = c^{\pm}_{ik} m_k$, where the m_k are the monomials of the ansatz, this could be realised in the following way:

$$c^{\pm}_{ik} = \{m_k(p_j)\}^{-1} r^{\pm}_i(p_j), \tag{5.46}$$

where the p_j are sampling points in the phase-space of the external kinematics. In practice, however, the ansätze can still have a few hundred-thousands of free coefficients. Therefore, sampling on random points and inverting this linear system is not a viable option. We can overcome this problem, however, by special choices of the sampling points p_j. In this section, we will describe a sampling procedure introduced in ref. [51] which leads to (generalized) Vandermonde matrices whose inversion is possible for very large sizes and

therefore allows for an efficient determination of the $P^{\pm}_{km}$.

To begin with, we discuss how to separate the individual $P^{\pm}_{km}$ from eqn (5.41). We can only directly compute the numerical values of the $r^{\pm}_i$ (using the algorithm outlined in section 5.5) and the numerical values of the denominators (using their analytic expression). We can, however, extract the value of the $P^{\pm}_{km}(\vec{s}^{(k)}_{\text{rem}})$ by sampling eqn. (5.41) over enough values of $s_{ij} = s_{ij,a}$, that is by solving the system

$$\begin{pmatrix} \frac{s^0_{ij,1}}{W_1(\vec{s}_{\text{rem}},s_{ij,1})^{\beta^{\pm}_1}\prod_l \overline{W_l}(\vec{s}_{\text{rem}})^{\gamma^{\pm}_{1l}}} & \cdots & \frac{s^M_{ij,1}}{W_{n_i}(\vec{s}_{\text{rem}},s_{ij,1})^{\beta^{\pm}_n}\prod_l \overline{W_l}(\vec{s}_{\text{rem}})^{\gamma^{\pm}_{nl}}} \\ \vdots & \ddots & \vdots \\ \frac{s^0_{ij,N}}{W_1(\vec{s}_{\text{rem}},s_{ij,N})^{\beta^{\pm}_1}\prod_l \overline{W_l}(\vec{s}_{\text{rem}})^{\gamma^{\pm}_{1l}}} & \cdots & \frac{s^M_{ij,N}}{W_{n_i}(\vec{s}_{\text{rem}},s_{ij,N})^{\beta^{\pm}_n}\prod_l \overline{W_l}(\vec{s}_{\text{rem}})^{\gamma^{\pm}_{nl}}} \end{pmatrix} \begin{pmatrix} P^{\pm}_{11}(\vec{s}_{\text{rem}}) \\ \vdots \\ P^{\pm}_{n_iM}(\vec{s}_{\text{rem}}) \end{pmatrix}$$

$$= \begin{pmatrix} r^{\pm}_i(\vec{s}_{\text{rem}}, s_{ij,1}) \\ \vdots \\ r^{\pm}_i(\vec{s}_{\text{rem}}, s_{ij,N}) \end{pmatrix}. \tag{5.47}$$

The sampling is done in a finite field and the number of sample points, denoted by N, is the number of terms in the partial-fraction decomposition ansatz of eqn. (5.41). This sampling has to be done for each value of $\vec{s}_{\text{rem}}$. For the amplitudes we consider this number is $\mathcal{O}(30)$. The sampling over different values of s_{ij} is realised by sampling over different values of x in our twistor parametrisation (see appendix F).

Having described how to numerically evaluate the $P^{\pm}_{ij}(\vec{s}^{(a)}_{\text{rem}})$ for a given value $\vec{s}^{(a)}_{\text{rem}}$, we describe how these evaluations can be used to determine the analytic form of P_{km}. We begin by considering a polynomial

$$q(\vec{s}_{\text{rem}}) = \sum_{\vec{\alpha}_i \in S} c_{\vec{\alpha}_i} m_{\vec{\alpha}_i}, \quad \text{where} \quad m_{\vec{\alpha}_i} = s_{12}^{\alpha_{i,1}} \cdots s_{n1}^{\alpha_{i,n}}, \tag{5.48}$$

and the sum over exponent vectors $\vec{\alpha}_i$ runs over some finite set S.

We then introduce a so-called *anchor point*,

$$\vec{s}_{\text{rem},(0)} = \left(s_{1,(0)}, ..., s_{n,(0)}\right), \tag{5.49}$$

and choose the further sampling points as powers of the original point

$$\vec{s}_{\text{rem},(a)} = \left(s_1^a, ..., s_n^a\right). \tag{5.50}$$

On these sampling points, the monomials also behave as powers of the monomials on the anchor-point

$$m_{\vec{\alpha}_i}(\vec{s}^{(a)}_{\text{rem}}) = \left[m_{\vec{\alpha}_i}(\vec{s}_{\text{rem},(0)})\right]^a. \tag{5.51}$$

When using these sampling points in the procedure described in eqn. (5.46), the con-

straining linear system is of generalised Vandermonde form [51]

$$\begin{pmatrix} \left[m_{\vec{\alpha}_1}(\vec{s}_{\text{rem},(0)})\right]^0 & \cdots & \left[m_{\vec{\alpha}_{|S|}}(\vec{s}_{\text{rem},(0)})\right]^0 \\ \vdots & \ddots & \vdots \\ \left[m_{\vec{\alpha}_1}(\vec{s}_{\text{rem},(0)})\right]^{|S|} & \cdots & \left[m_{\vec{\alpha}_{|S|}}(\vec{s}_{\text{rem},(0)})\right]^{|S|} \end{pmatrix} \begin{pmatrix} c_{\vec{\alpha}_1} \\ \dots \\ c_{\vec{\alpha}_{|S|}} \end{pmatrix} = \begin{pmatrix} q(\vec{s}_{\text{rem}}^{(1)}) \\ \dots \\ q(\vec{s}_{\text{rem}}^{(|S|)}) \end{pmatrix}. \tag{5.52}$$

Such a Vandermonde matrix has several interesting properties, e.g. it's determinant can easily be computed as

$$\det V(m_{\vec{\alpha}_1}, ..., m_{\vec{\alpha}_{|S|}}) = \prod_{1<a<b\leq|S|} (m_{\vec{\alpha}_a} - m_{\vec{\alpha}_b}). \tag{5.53}$$

The special structure of this system allows it to be efficiently solved in $\mathcal{O}(|S|^2)$ time and $\mathcal{O}(|S|)$ space. A discussion of an efficient algorithm for solving the Vandermonde system can be found in refs. [51, 224, 227]. In practice, Vandermonde systems with a side length $|S|$ of around 10^5 can be solved in just over a minute on a modern laptop computer.

When one of the polynomials $P^{\pm}_{km}$ is fully reconstructed, we can subtract it in eqn. (5.47) such that less evaluations over s_{ij} are needed. This procedure known as "pruning" [51] leads to a siginificant efficiency gain. The maximal number of evaluations needed to reconstruct each $P^{\pm}_{km}$ can be computed before the reconstruction from their total degrees. Therefore, the generation of points which can be done on a laptop-computer, is completely decoupled from the evaluations of the amplitude which are performed on a cluster.

The numeric coefficients in the polynomials $P^{\pm}_{ik}$ are, in general rational, numbers. The reconstruction algorithm, however, returns them in a finite field, making rational reconstruction necessary (see appendix C). In some cases one finite field with cardinality $O(2^{31})$ is not enough to uniquely determine all rational numbers and hence reconstruction in additional finite fields is necessary to use the Chinese Remainder Theorem. In practice, after reconstruction in one finite field, we can identify which coefficients $c_{\vec{\alpha}_i}$ are zero. This makes the reconstruction in additional finite fields significantly more efficient by repeating the procedure with a reduced set S.

5.6.6 Spinor Reconstruction

The reconstruction of analytic master integral coefficients from numerical samples has a developing methodology in recent years. In this section, we discuss a latest advance using spinor variables.

The normalisation of the amplitude as well as the unphysical split of the coefficients into parity even and parity odd parts can be avoided by reconstructing directly in terms of spinor brackets (see appendix E for a review of spinor helicity variables). At first

glance this seems to be disadvantageous, since it doubles the number of variables that the amplitude depends on. Moreover, since every Mandelstam $s_{ij} = \langle i|j\rangle[j|i]$ corresponds to a product of two spinor brackets, one would naively expect the degree in spinor brackets to be much higher than in Mandelstams.

However, the monomials in the ansatz are constrained by the total spinor-weight and Schouten-identities give further dependencies, such that the physical advantages of the spinor parametrisation outweigh the appearent disadvantages. Therefore, ansätze for the coefficients in terms of spinor brackets are often simpler than the ansätze in Mandelstams [54, 228]. Moreover, the reconstruction in spinor variables allows to employ additional physical conjectures about the form of the amplitude.

In common denominator form the pentagon function coefficients are given by

$$r_i = \frac{\mathcal{N}_i}{\prod_j \mathcal{D}_j^{q_{ij}}} \,. \tag{5.54}$$

To obtain the denominators in spinor-brackets we can use the univariate slice discussed in section 5.6.2 to obtain the $\langle ij\rangle$ dependent denominators and the parity conjugate slice to obtain the $[ij]$ dependent denominators, both of which also factorize into (slightly different) letters[5]. The denominator of pentagon function coefficients is then given by their least common multiple. The linear dependencies between the coefficients are found in the same way as described in section 5.6.3. It is well known that the pentagon function coefficients simplify in a partial fraction decomposition

$$r_i = \sum_k \frac{\mathcal{N}_{ik}}{\prod_j \mathcal{D}_j^{q_{ijk}}} \,, \tag{5.55}$$

where $q_{ijk} \leq q_{ij}$.

In previous computations it has been observed that poles of the form $\langle i|j+k|i]^\alpha$ can be separated into different terms in the partial fraction decomposition, i.e.

$$r = \sum_{d \in \{\langle i|j+k|i\rangle^\alpha\}} \frac{\mathcal{N}_d}{d \prod_j \mathcal{D}_j^{q_{jd}}} \tag{5.56}$$

This can be proven for pure bases at one-loop level. At two loops, it is possible to take such a partial fraction decomposition as an ansatz and verify that it reproduces the amplitude later.

In this form it turns out that most of the terms in the partial fraction decomposition of complicated coefficients are linearly dependent on simpler coefficients. Assuming that only one term in the decomposition with respect to the $\langle i|j+k|i]^\alpha$ denominators is independent of simpler coefficients, an ansatz is made containing a basis of simpler coefficients and all

[5]The difference is that letters s_{ij} turn into two letters $[ij]$ and $\langle ij\rangle$

independent spinor brackets allowed by mass-dimension and spinor-weight[6].

$$r = \frac{\mathcal{N}}{\langle i|j+k|i\rangle^{\alpha} \prod_n \mathcal{D}_n n^{q_n}} + \sum_n c_n r_n^{\text{simpler}}. \tag{5.57}$$

This ansatz only works when it is known which of the terms $\frac{\mathcal{N}_d}{d \prod_j \mathcal{D}_j^{q_{jd}}}$ is independent from simpler coefficients. Since the reduction of linear systems is very fast compared to the evaluation of the amplitude, the most efficient way to determine this is trial and error. Compared to the reconstruction in Mandelstams without partial fraction decomposition, this method was found to reduce the number of necessary samples by almost two orders of magnitude.

[6]They should also be independent w.r.t. momentum conservation and Schouten identities (see ref [54]).

Chapter 6

Results

So far, we have outlined the method of combining surface terms from algebraic geometry, multi-loop numerical unitarity and functional reconstruction to compute multi-loop amplitudes. In this chapter, we will present some results that we have calculated with these methods; in particular, the planar helicity amplitudes for vector-boson + two-jet production at the LHC and the full colour NNLO corrections to tri-photon production at the LHC.

6.1 W-Boson + Four Partons

A major success of this approach was the computation of the two-loop helicity amplitudes contributing to the production of an off-shell W-boson (including the leptonic decay-products) in association with two jets at leading colour [229]. This process is an important standard candle which can be used for detector calibration and can contribute to PDF determination (see e.g. [230–232]). Moreover, it is an important background to processes like vector-boson-pair production or vector-boson plus Higgs production [233, 234]. This process is also interesting from a theoretical perspective, since all production channels are present at tree-level and therefore a fast perturbative convergence is expected. It is an interesting question whether this fast convergence is found indeed.

The computation of these amplitudes was carried out using the methods discussed in chapters 4 and 5. In this section we will discuss the details and results of this computation, following the discussion in ref. [229].

In the SM the W couples to left-handed quarks. In this process, at leading colour, the W-boson couples only to external quark-lines and hence the vector and axial contributions are equal up to an overall sign (see section 2.3.1). This allows us to assemble the amplitudes for four partons and a W-boson from amplitudes for four partons and a V boson which couples to the quarks only through vector coupling.

6.1.1 Notation & Conventions

There are two independent partonic processes contributing to the production, one with a single quark line and two external gluons and one with two quark lines. In the latter case, we can assume without loss of generality that the vector boson only couples to one of the quark flavours, which we denote as q. Representative diagrams for the two tree level processes are given in fig. 6.1. According to the notation in ref. [229], the respective amplitudes are denoted as

$$\begin{aligned} &\mathcal{M}_{\mathrm{g}}\left(\bar{\mathrm{q}}^{h_1}_{p_1}, \mathrm{g}^{h_2}_{p_2}, \mathrm{g}^{h_3}_{p_3}, \mathrm{q}^{h_4}_{p_4}; \bar{\ell}^{h_5}_{p_5}, \ell^{h_6}_{p_6}\right) , \\ &\mathcal{M}_{\mathrm{Q}}\left(\bar{\mathrm{q}}^{h_1}_{p_1}, \mathrm{Q}^{h_2}_{p_2}, \bar{\mathrm{Q}}^{h_3}_{p_3}, \mathrm{q}^{h_4}_{p_4}; \bar{\ell}^{h_5}_{p_5}, \ell^{h_6}_{p_6}\right) , \end{aligned} \tag{6.1}$$

where g denotes a gluon, q and Q denote massless quarks which we assume have different flavours[1]. The indices h_i and p_i denote the helicity and the momentum of the ith external particle, respectively. For the physical case under consideration, we have e.g. $\mathrm{q} = u$, $\bar{\mathrm{q}} = \bar{d}$, $\ell = e$ and $\bar{\ell} = \bar{\nu}_e$ and the axial part is equal to the vector-part up to a sign.

Closely following the notation of ref. [235] the amplitudes including the W-boson can be expressed by these amplitudes as

$$\begin{aligned} \mathcal{M}^{W}\left(\bar{u}^{R}_{p_1}, g^{h_2}_{p_2}, g^{h_3}_{p_3}, d^{L}_{p_4}, \bar{e}^{R}_{p_5}, \nu^{L}_{p_6}\right) &= v^2\, \mathcal{P}_W(s_{56})\, \mathcal{M}_{\mathrm{g}}\left(\bar{q}^{+}_{p_1}, g^{h_2}_{p_2}, g^{h_3}_{p_3}, q^{-}_{p_4}; \bar{\ell}^{+}_{p_5}, \ell^{-}_{p_6}\right) , \\ \mathcal{M}^{W}\left(\bar{u}^{R}_{p_1}, c^{h}_{p_2}, \bar{c}^{-h}_{p_3}, d^{L}_{p_4}, \bar{e}^{R}_{p_5}, \nu^{L}_{p_6}\right) &= v^2\, \mathcal{P}_W(s_{56})\, \mathcal{M}_{\mathrm{Q}}\left(\bar{q}^{+}_{p_1}, Q^{h}_{p_2}, \bar{Q}^{-h}_{p_3}, q^{-}_{p_4}; \bar{\ell}^{+}_{p_5}, \ell^{-}_{p_6}\right) , \end{aligned} \tag{6.2}$$

where u and d denote a quark doublet[2] while c denotes any distinct (massless) quark flavour and $v^2 = \frac{e^2}{2\sin^2\theta_w}$ with θ_W the weak mixing angle denotes the vector-coupling of the W boson. The propagator $P_W(s)$ is given by

$$\mathcal{P}_W(s) = \frac{s}{s - M_W^2 + \mathrm{i}\,\Gamma_W M_W} , \tag{6.3}$$

where M_W and Γ_W are the mass and decay width of the W boson, respectively.

These amplitudes also determine the planar gauge-invariant contributions for the amplitudes for four partons plus a Z/γ^* decaying to leptons. For this process, however, the term in the amplitude proportional to N_f/N_c receives contributions from non-planar diagrams (e.g. fig. 6.4). They only contribute to gauge-invariant piece with a distinct coupling structure, however.

We perform the evaluation of the amplitudes in eq. (6.1) in the 't Hooft-Veltman scheme of dimensional regularization with $D = 4 - 2\epsilon$. We compute for the first time the two-loop corrections $\mathcal{M}^{(2)}_{\kappa}$ and also recompute the one-loop corrections [211, 235] up to order ϵ^2 in the dimensional regulator. This is necessary because the $\epsilon^{1,2}$ pieces

[1]The case of equal flavours can be computed as a suitable linear combination of amplitudes where flavours are assumed to be different.

[2]We assume diagonal CKM matrix.

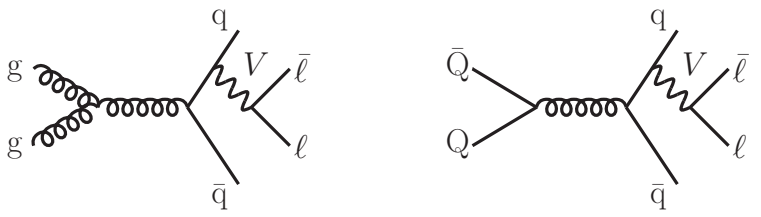

(a) Partonic process with gluons as external particles

(b) Partonic process with only quarks as external particles

Figure 6.1: Representative diagrams for the two partonic processes in eq. (6.1)

together with the universal form-factors in Catani-operators contribute to the ϵ^{-1} and the finite piece. Moreover, in the NNLO cross-section contributions, rhe $\epsilon^{1,2}$ pieces contribute through the squared one-loop amplitude.

We use a colour-trace decomposition (see 5.3)

$$\begin{aligned}\mathcal{M}_{\text{g}}^{(k)} &= \left(\frac{S_\epsilon\, N_c}{2}\right)^k \sum_{\sigma\in S_2} \left(T^{a_{\sigma(3)}} T^{a_{\sigma(2)}}\right)_{i_4}^{\bar{i}_1} \mathcal{A}_g^{(k)}\,, \\ \mathcal{M}_{\text{Q}}^{(k)} &= \left(\frac{S_\epsilon\, N_c}{2}\right)^k \delta_{i_2}^{\bar{i}_1}\delta_{i_4}^{\bar{i}_3} \mathcal{A}_Q^{(k)}\,,\end{aligned} \tag{6.4}$$

where $S_\epsilon = (4\pi)^\epsilon e^{-\epsilon\gamma_E}$. The partial amplitudes $\mathcal{A}_\kappa^{(k)}$ can be further decomposed into powers of N_f and N_c, where N_f denotes the number of massless quark flavors, while N_c denotes the number of colours

$$\mathcal{A}_\kappa^{(k)} = \sum_{k_1}\sum_{k_2} \left(\frac{{N_f}^{k_1}}{{N_c}^{k_2}}\right) \mathcal{A}_\kappa^{(k)[j]}\,, \qquad \text{for } \kappa = \text{g, Q}\,. \tag{6.5}$$

In this decomposition we consider the pieces which receive contributions from planar diagrams only, that is ${N_f}^0/{N_c}^0$, ${N_f}^1/{N_c}^1$ and ${N_f}^2/{N_c}^2$. Compared to these, other contributions are suppressed by $1/{N_c}^2$ or $1/{N_f}^2$. We do not include any loop contributions from massive quark flavours. Figures 6.2 and 6.3 show representative diagrams for the different powers of N_f for the different external states.

6.1.2 Reduction to Five-Point One-Mass Kinematics

The (partonic) amplitudes described in eq. (6.1) depend on six massless momenta, p_1 through p_6. They can be factorised, however, into the production of an off-shell vector boson in association with jets and its decay into a pair of leptons (see eqn. (6.2). While $\mathcal{M}_\kappa$ depends on six massless momenta and thus eight kinematic invariants, the inherently two-loop parts of the amplitude only depend on the five momenta p_1, p_2, p_3, p_4 and $p_{\text{v}} = p_5 + p_6$, with $p_{\text{v}}^2 \neq 0$ and thus six kinematic invariants $\{s_{12}, s_{23}, s_{34}, s_{4V}, s_{1V}, p_V^2\}$.

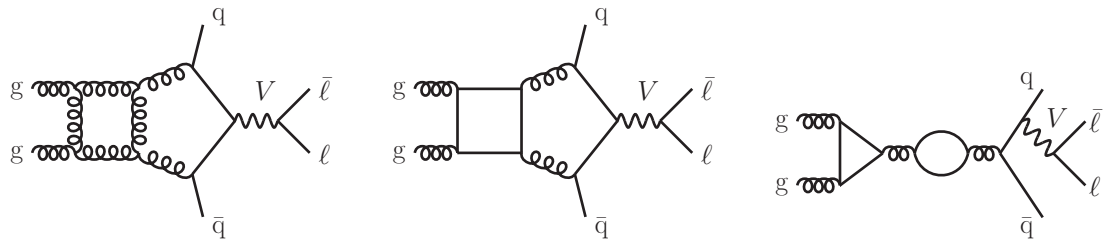

(a) N_f^0/N_c^0 (b) N_f^1/N_c^1 (c) N_f^2/N_c^2

Figure 6.2: Representative diagrams for the different contributions to $\mathcal{M}_{\text{g}}$.

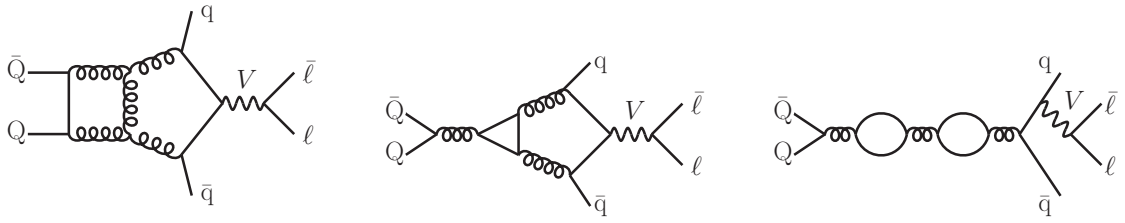

(a) N_f^0/N_c^0 (b) N_f^1/N_c^1 (c) N_f^2/N_c^2

Figure 6.3: Representative diagrams for the different contributions to $\mathcal{M}_{\text{Q}}$.

Since we will obtain analytic expressions via functional reconstruction, it is crucial to express the amplitude dependent on six variables only. For example, a homogeneous polynomial of degree 30 in six variables has $3 \cdot 10^5$ unconstrained parameters while it has 10^7 for eight variables. This implies that functional reconstruction would require roughly 30 times as many evaluations in the eight variable setup. Despite this simplification, the process still is considerably more complex than the five-point massless processes previously considered in the context of numerical unitarity.

In the following, we discuss how we carry out the reduction from six-point kinematics to the underlying set of five-point one-mass kinematics in practice. The amplitudes $\mathcal{A}$ under consideration factorize into a QCD current A^μ and a tree-level leptonic current J^μ

$$\mathcal{A} = A^\mu J_\mu, \quad \text{where} \quad J_\mu = \overline{u}(p_6)\gamma_\mu v(p_5). \tag{6.6}$$

$\overline{u}$ and v are the Dirac spinors associated to the leptons $\bar{\ell}$ and ℓ in fig. 6.1, and A^μ depends only on the five-point one-mass kinematics. In HV scheme, thus A^μ has four components (see e.g. [236]), since external states are four-dimensional. Additionally, both currents satisfy the Ward identity

$$p_{\text{v}}^\mu A_\mu = 0, \qquad \text{and} \qquad p_{\text{v}}^\mu J_\mu = 0, \tag{6.7}$$

thus trivially determining one of the components.

We compute the remaining components by considering sets of six-point kinematic

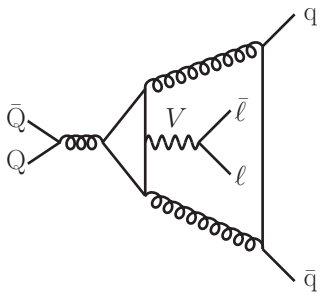

Figure 6.4: A non-planar diagram contributing to Z-boson production at order N_f^1/N_c^1. This type of contribution has a unique coupling structure proportional to the sum over the couplings of the Z to all quarks that can appear in the loop. It is therefore a gauge invariant piece that can be dropped consistently.

configurations that do not introduce new kinematic invariants compared to the five-point case. This is achieved by requiring the first lepton to be collinear to the ith parton, leading to the configurations

$$p_5^{(i)} = \frac{p_{\mathrm{v}}^2}{2p_i \cdot p_{\mathrm{v}}} p_i, \quad p_6^{(i)} = p_{\mathrm{v}} - \frac{p_{\mathrm{v}}^2}{2p_i \cdot p_{\mathrm{v}}} p_i. \tag{6.8}$$

We compute the amplitude in three such collinear configurations, which are arbitrarily chosen as $i = 1, 2, 3$. Other choices, e.g. with p_6 chosen parallel to a parton or linear combinations are possible, however, we did not find them to be advantageous.

We use the leptonic current J^μ evaluated in each collinear configuration to define three reference directions n_i

$$n_i^\mu = J^\mu\left(p_5^{(i)}, p_6^{(i)}\right), \qquad i = 1, 2, 3 \tag{6.9}$$

and we furthermore define $n_4^\mu = p_{\mathrm{v}}^\mu$. These four auxiliary vectors allow to decompose the four-dimensional metric tensor $g_{(4)}^{\mu\nu}$ as

$$g_{(4)}^{\mu\nu} = \sum_{i,j=1}^{4} G_{ij}^{-1} n_i^\mu n_j^\nu, \qquad \text{where} \qquad G_{ij} = n_i \cdot n_j. \tag{6.10}$$

Due to the Ward identity in eq. (6.7), $G_{i4} = G_{4j} = 0$ for $i, j = 1, 2, 3$.

With this decomposition of unity, the QCD current A^μ is given by

$$A^\mu = \sum_{i,j=1}^{3} G_{ij}^{-1} \left(A \cdot n_i\right) n_j^\mu, \tag{6.11}$$

where

$$A \cdot n_i = \mathcal{A}\left(p_1, p_2, p_3, p_4, p_5^{(i)}, p_6^{(i)}\right), \qquad \text{for } i = 1, 2, 3 \tag{6.12}$$

and the Ward identity $A \cdot n_4 = 0$. It is therefore sufficient to compute the on-shell six-point

amplitudes $\mathcal{A}\left(p_1, p_2, p_3, p_4, p_5^{(i)}, p_6^{(i)}\right)$ for $i = 1, 2, 3$ in order to obtain the QCD current A^μ or the six-point amplitude for generic phase-space points. As a side remark, we point out that the amplitude has no spurious or physical poles on the chosen kinematic point.

6.1.3 Analytic Reconstruction

As described in section 5.6, a technical subtlety in applying a functional reconstruction in Mandelstam variables is that the $\mathcal{A}^{\{i\}}$ are not little group invariant. This is easily remedied by factoring out some function with the same little group weights, where we employ a standard spinor weight defined in CARAVEL (see Appendix A.3 of ref. [167]). We shall suppress this normalisation factor in the rest of the discussion and regard $\mathcal{A}^{\{i\}}$ as a rational function of

$$\vec{s} = \{s_{\mathrm{v}1}, s_{12}, s_{23}, s_{34}, s_{4\mathrm{v}}, p_{\mathrm{v}}^2\} \quad \text{and} \quad \mathrm{tr}_5 = 4\,\mathrm{i}\,\varepsilon_{\mu_1\mu_2\mu_3\mu_4} p_1^{\mu_1} p_2^{\mu_2} p_3^{\mu_3} p_4^{\mu_4}. \tag{6.13}$$

To close this discussion, we note that it is straightforward to define an analogue of the form factors $\mathcal{A}^{\{i\}}$ for the finite remainders

$$\mathcal{R}^{\{i\}} = \mathcal{R}\left(p_1, p_2, p_3, p_4, p_5^{(i)}, p_6^{(i)}\right), \qquad i = 1, 2, 3, \tag{6.14}$$

which are implicitly considered to be normalized by the CARAVEL spinor weight.

These remainders $\mathcal{R}^{\{i\}}$ can be decomposed in terms of pentagon functions similarly to eq. (5.29),

$$\mathcal{R}^{\{i\}} = \sum_{i \in B} r_i(\vec{s}, \mathrm{tr}_5) h_i\,, \tag{6.15}$$

where the $r_i(\vec{s}, \mathrm{tr}_5)$ are rational functions of their arguments which we obtain via functional reconstruction. We evaluate these functions numerically via the method of multi-loop numerical unitarity described in section 5.5. These evaluations are performed first for points generated via a purely holomorphic all-line BCFW-shift in order to extract the denominators and total degrees (see section 5.6.2). Having obtained this information, we employ the bivariate reconstruction discussed in section 5.6.4 where we choose s_{34} as one variable, while $\{s_{12}, s_{23}, s_{4V}, s_{1V}, p_V^2\}$ are each chosen as a linear function in some parameter t. This allows to generate ansätze for the coefficients in a partial fraction decomposition with respect to s_{34}, where some letters are excluded from the partial fraction decomposition to achieve simpler ansätze (see section 5.6.4).

We analyse the linear dependencies between the coefficients (see section 5.6.3) and choose a basis of coefficients with the minimal number of terms in the ansatz. Finally, we employ the Vandermonde-based reconstruction strategy discussed in section 5.6.5 to obtain the analytic coefficients. To illustrate the impact of the partial-fraction ansätze, we present the number of free coefficients in the two ansätze in tables 6.1 and 6.2 [229],

$\mathcal{R}_{\mathrm{Q}}$	$p_5 \parallel p_i$	—K—	Max Ansatz Size		Max Non-Zero Terms
			Common Denominator	Partial Fraction	Result
$+-$ N_f^0	1	50	1200 k	53 k	11 k
	2	57	1700 k	210 k	56 k
	3	56	1400 k	240 k	56 k
$+-$ N_f^1	1	18	26 k	13 k	1.5 k
	2	20	140 k	47 k	5.1 k
	3	20	140 k	54 k	8.4 k
$-+$ N_f^0	1	69	2300 k	64 k	14 k
	2	75	2300 k	230 k	57 k
	3	79	5500 k	220 k	48 k
$-+$ N_f^1	1	30	240 k	21 k	3.9 k
	2	31	380 k	52 k	11 k
	3	31	380 k	51 k	9.1 k

Table 6.1: Characterizing information for remainders with $\kappa = \mathrm{Q}$ at various stages of the computation. The remainders are specified by the helicity states of the gluon pair and the power of N_f. $|K|$ is the dimension of the space of rational functions of the corresponding amplitude. We give the maximal Ansatz size in common denominator and partial-fraction form. The last column gives the largest number of non-zero monomial coefficients. Term counts are given to two significant digits for readability.

where we omitted the N_f^2/N_c^2 pieces and the case of two gluons with positive helicity since they are trivial compared to the others.

It can clearly be seen that, for all amplitudes, the univariate partial fraction decomposition has a large effect. In particular, the dimension of the ansatz for the most complicated pentagon function coefficient in common denominator form is almost 50 times larger than the most complicated partial-fraction.

Despite this simplification, we note that there are still contributions with $\mathcal{O}(500\,\mathrm{k})$ undetermined parameters even after partial fractioning, and there is a large number of linear systems with $\mathcal{O}(100\,\mathrm{k})$ side length to be solved. While this would be challenging when using Gaussian elimination, the solutions can be obtained $\mathcal{O}(1\,\mathrm{min})$ on a laptop when these systems are in Vandermonde form.

Furthermore, we point out that once the ansatz has been fit many of the coefficients turn out to be zero (see the last column of tables 6.1 and 6.2), which allows to use smaller ansätze when reconstruction in additional finite fields is necessary.

In practice, we could perform the rational reconstruction employing only two finite fields of cardinality $\mathcal{O}(2^{31})$.

$\mathcal{R}_{\mathrm{g}}$	$p_5 \parallel p_i$	$\lvert K\rvert$	Max Ansatz Size		Max Non-Zero Terms
			Common Denominator	Partial Fraction	Result
$+-\ N_f^0$	1	58	5500 k	180 k	37 k
	2	67	7000 k	480 k	110 k
	3	67	5900 k	380 k	90 k
$+-\ N_f^1$	1	50	4600 k	160 k	33 k
	2	53	5000 k	380 k	87 k
	3	53	4200 k	310 k	75 k
$-+\ N_f^0$	1	75	12000 k	210 k	46 k
	2	85	14000 k	500 k	130 k
	3	85	24000 k	430 k	99 k
$-+\ N_f^1$	1	44	4600 k	120 k	25 k
	2	49	3800 k	210 k	54 k
	3	49	8900 k	270 k	63 k

Table 6.2: Information about the complexity for remainders with $\kappa = \mathrm{g}$ at various stages of the computation. Column headings are identical to table 6.2. Term counts are given to two significant digits for readability.

6.1.4 Results and Validation

The main result presented in this section are the two-loop remainders $\mathcal{R}_\kappa^{(2)[j]}$ in analytic form, which can be obtained from the ancillary files of [229]. We also provide the one-loop amplitudes $\mathcal{A}^{(1)[j]}$ to arbitary orders in ϵ (provided that the integrals are known), thereby extending the results of refs. [211,235]. These one-loop amplitudes can be used to also assemble the two-loop amplitudes $\mathcal{A}^{(2)[j]}$ employing eq. (5.19). In fact, the one-loop amplitudes are presented as a decomposition in terms of the one-loop master integral basis used in [34].

The same ancillary files also include a map from the one-loop integrals to the pentagon functions of ref. [43] up to weight 4, such that the one-loop expressions can be written in the same pentagon-function decomposition as the remainders.

To demonstrate the use of these ancillary files, we include a `Mathematica` script called `amp_eval.m` which assembles the one-loop and two-loop amplitudes and remainders, and evaluates them at a given phase-space point.

We have performed a number of checks on the final results as well as on intermediate steps of our calculation. As discussed in section 4, the surface terms where numerically cross-checked against `FIRE` [134, 237]. The numerical-unitarity code Caravel [167], includes many internal self-consistency checks including the dimensions of master-surface decompositions, the consistency of D_s and D reconstruction among others. The numeri-

cal calculation of the two-loop remainders is also performed within CARAVEL, where the finiteness of the finite remainder at each phase-space point confirms that the amplitude has indeed the pole structure predicted by eqn. (5.19). We have compared the functionally reconstructed results for the analytic one-loop amplitudes and two-loop finite remainders against numerical evaluations obtained from Caravel, thereby confirming the validity of the functional and rational reconstruction.

The final results for the one-loop amplitudes were checked up to order ϵ^0 with the results obtained from the `BlackHat` library [238]. For the two-loop remainders, we have reproduced the numerical table of ref. [239] using CARAVEL to evaluate the master integral coefficients and `DiffExp` [39] to evaluate the master integrals, confirming the correctness of the numerical evaluations within CARAVEL.

By intefering our currents A^μ in eq. (6.6) with the tree amplitudes appropriately and setting the W on-shell, we have reproduced the results of (the revised version of) ref. [40]. The calculation in ref. [40] is performed in the conventional dimensional regularization scheme employing Larin's scheme for the treatment of γ_5 in dimensional regularisation [240], which produces non-trivial differences between vector and axial currents. We find full agreement at the level of the finite remainders, which is a particularly stringent test of our γ_5 treatment and the analytic result as a whole.

Our analytic results as they are given in the ancillary files of [37] are valid for the partonic channels of eqn. (6.1) with momenta p_1 and p_2 incoming. It is, however, straightforward to obtain results in other partonic channels by permutations of the particles' momenta. While the action of permutations on the rational functions $\tilde{r}_i(\vec{s}, \mathrm{tr}_5)$ is obvious, the action of permutations on the one-mass pentagon functions h_i is discussed in section 3.2 of ref. [43], and is explicitly provided in the supplementary materials thereof. We emphasize that this allows us to replace the dedicated analytic continuation procedure which had to be employed, for instance, in ref. [241], by simple substitutions.

We close the discussion of these amplitudes with some comments on the analytic structure of our results. In ref. [40], the pentagon functions involving the letters[3]

$$\{W_{16}, W_{17}, W_{27}, W_{28}, W_{29}, W_{30}\}$$

where observed to drop out for an on-shell $Wb\bar{b}$ production when expanded to finite order in ϵ and summing over polarizations. The same observation was made for the production of a H boson in association with a $b\bar{b}$ pair in ref. [226], where the authors considered the b as massless, but with non-vanishing Yukawa coupling. We observe that the same holds also for the finite remainders with a polarised off-shell W. We also observe that pentagon functions involving the letter tr_5 do not contribute to the finite remainders, a fact that has been previously linked to cluster algebras [242]. We use the pentagon-function basis

[3] using the notation of ref. [34].

of ref. [43], which has been constructed such that these cancellations are manifest.

6.2 Tri-Photon Production

Colour-singlet final states are particularly interesting processes for precision studies, because they have a clear signature over the QCD-background. Moreover, many models for physics beyond the Standard Model couple to the electro-weak or Higgs sector. As of today, NNLO-predictions for the production of two vector bosons are standard (see e.g. [243–272]), while the first computations for the production of three-particle colourless final states have only been performed recently [273, 274].

Both of these calculations targeted the production of three massless photons and have been performed at leading colour. The leading-colour approximation, however, is not necessarily suitable for this process since it ignores contributions where the photons couple to closed fermion loops. These contributions are indeed suppressed by the number of colours, but enhanced by the number of generations of massless quarks which are considered to be running in the loop. We therefore compute for the first time the two-loop amplitudes for tri-photon production to full colour.

6.2.1 Helicity Amplitudes

In principle, there are two partonic processes contributing to the production of three photons, one with two external quarks and one with two external gluons. However, since at NNLO the two-loop amplitudes are always multiplied with the corresponding tree-amplitude (see section 2.70) and there is no tree-level amplitude for two gluons scattering to three photons, only the amplitudes with quarks in the initial state have to be computed. The colour decomposition of this amplitude is given by

$$\begin{aligned}\mathcal{A}^{(1)} &= C_F A^{(1)},\\ \mathcal{A}^{(2)} &= C_F^2 B^{(2,0)} + C_F C_A B^{(2,1)} + C_F T_F N_f A^{(2,N_f)} + C_F T_F \left(\sum_{f=1}^{N_f} Q_f^2\right) \tilde{A}^{(2,N_f)},\end{aligned} \tag{6.16}$$

where N_f is the number of light quarks, and Q_f are the electric charges of the quarks. Note that contributions with an odd number of photons coupling to the quark loop cancel due to the summation over quarks and their antiquarks, while the colour trace of two gluons is symmetric under such an exchange. The non-N_f terms of the amplitude can be organised by their scaling with the number of colours N_c

$$\mathcal{A}^{(2)} = \frac{N_c^2}{4}\left(A^{(2,0)} - \frac{1}{{N_c}^2}(A^{(2,0)} + A^{(2,1)}) + \frac{1}{{N_c}^4}A^{(2,1)}\right) + O(N_f), \tag{6.17}$$

with

$$A^{(2,1)} := B^{(2,0)} + 2B^{(2,1)}, \tag{6.18}$$

$$A^{(2,0)} := B^{(2,0)}. \tag{6.19}$$

We compute, for the first time, the non-planar pieces $A^{(2,1)}$ and $\tilde{A}^{(2,N_f)}$. We also recompute the other pieces in order to compare to ref. [275] and thereby validate our approach. Example diagrams contributing to the different pieces are given in figure 6.5.

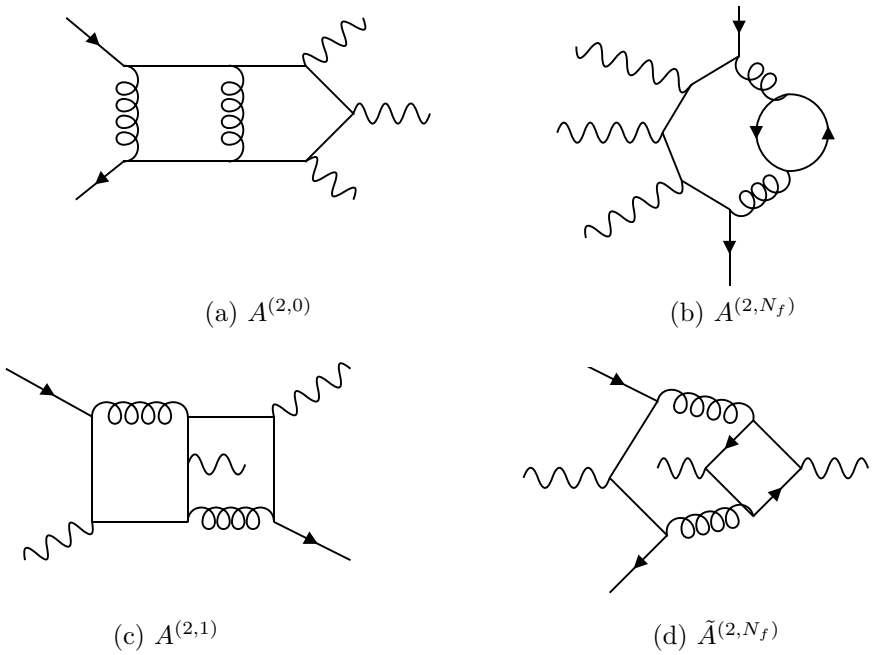

(a) $A^{(2,0)}$ (b) $A^{(2,N_f)}$

(c) $A^{(2,1)}$ (d) $\tilde{A}^{(2,N_f)}$

Figure 6.5: Representative Feynman diagrams for the individual contributions to the $q\bar{q} \to \gamma\gamma\gamma$ amplitude at two loops. These contributions scale differently with the number of colours, the number of light fermions and the charge of the external fermions and are therefore individually gauge invariant. The contribution $A^{(2,1)}$ is the only piece where all non-planar integral topologies contribute.

We have computed a set of surface-terms for all massless non-planar five-point topologies up to a total power-counting of 5 for the top-level topologies, using the methods described in chapter 4. In particular, we have generated linear systems which allow to rapidly generate numeric IBP-vectors for arbitrary phase-space points. For the $A^{(2,N_f)}$ amplitude, to which all topologies contribute, solving these linear systems takes 5 minutes per phase-space point, making it sub-dominant in the 36 minute computation of the amplitude.

For the non-planar topologies, power-counting equations are only solved on-shell and the power-counting of their planar descendants is increased such that the function space of the off-shell terms is covered.

	max. degree		
Contribution	Before lin. dep.	after lin. dep.	max ansatz size
$A^{(2,0)}_{-++}$	30/30	25/25	24k
$A^{(2,0)}_{+++}$	16/13	10/10	1k
$\tilde{A}^{(2,N_f)}_{-++}$	41/41	21/21	13k
$\tilde{A}^{(2,N_f)}_{+++}$	21/18	19/16	9k
$A^{(2,1)}_{-++}$	41/41	32/32	59k
$A^{(2,1)}_{+++}$	20/17	16/13	5k
$A^{(2,N_f)}_{-++}$	13/13	13/13	2k
$A^{(2,N_f)}_{+++}$	12/9	10/7	1k

Table 6.3: Degrees and ansatz size of each the most complex pentagon function coefficient of the 2-quark 3-photon finite remainders at various stages of the computation. The remainders are specified by their coupling structure and the helicities of the photons. Term counts are given to two digits for readability.

We have used these surface-terms and the master integrals expressed in terms of pentagon-functions from ref. [42] as an ansatz which is fitted with the numerical unitarity method (see section 5.5). This allows to evaluate the amplitude or the remainder for finite-field numerical values of the kinematic invariants. We have then used these evaluations to reconstruct the analytic two-loop remainders. First, we have reconstructed the remainders on a univariate slice to obtain analytic denominators and degrees (see section 5.6.2).

Then, we have analysed the linear dependencies (see section 5.6.3) and then reconstructed the numerators via Vandermonde sampling (see section 5.6.5). The maximal degrees of the pentagon function coefficients for the remainder of each amplitude and the sizes of their common denominator ansätze are given in table 6.3.

The ansatz sizes are considerably smaller than for the amplitude considered in the previous section, even when the latter are in their partial-fractioned form. We therefore renounce the bivariate reconstruction and construction of partial fraction ansätze and simply perform the reconstruction in common denominator form.

Spinor Reconstruction

Complementary to this approach, the non-planar contributions have also been reconstructed using a spinor reconstruction method (see section 5.6.6). After reconstruction on a univariate slice and removal of linear dependencies, the sizes of the ansätze are given in table 6.4.

Evidently, the ansatz sizes of the remainder coefficients are smaller than for the parity split Mandelstam reconstruction[4]. For the contributions with positive helicity these

[4]We emphasize that the number of evaluations needed in Mandelstam reconstruction is two times the size of the ansatz, since the amplitude is evaluated on pairs of parity conjugate points. In spinor-reconstruction, this is not necessary.

ansätze are directly constrained in common denominator form via numerical samples. When employing the decomposition w.r.t. to the $\langle i|j+k|i]$ terms described in section 5.6.6, the size of the ansätze is again cut in half.

Contribution	Numerator mass dimension	Numerator spinor weight	Common Den. Ansatz Size
$\tilde{A}^{(2,N_f)}_{+++}$	20	[2, 4, 6, 6, 6]	535
$A^{(2,1)}_{+++}$	21	[5, 4, 3, 3, 3]	1092
$\tilde{A}^{(2,N_f)}_{-++}$	47	[4, 4, -5, 3, 4]	24582
$A^{(2,1)}_{-++}$	48	[1, -3, -6, 2, 2]	29059

Table 6.4: Information about non-planar amplitude coefficients in spinor form.

For the most complicated pentagon coefficients, there are seven terms with each a different factor $\langle i|j+k|i]$ factor in the denominator, out of which six are dependent on simpler remainder coefficients. Additionally, the symmetry of the amplitude under an exchange of the two positive helicity gluons can be exploited, further reducing the Ansatz size. The last terms can then be constrained with slightly over 2000 evaluations.

6.2.2 Results & Validation

The main result presented in this section are the finite remainders of the non-planar two-loop contributions $A^{(2,1)}_{h_1h_2h_3}, \tilde{A}^{(2,N_f)}_{h_1h_2h_3}$ to the amplitudes contributing to three-photon production. By sampling these remainders over random points in the phase-space, it turns out that the full colour two-loop remainder is $0-40\%$ smaller than the leading colour two-loop remainder, with a peak at 30%. This confirms the expectations of ref. [273] and would be significant, if the contribution of the finite-remainder to the cross-section was not small.

To validate our calculation, we performed several checks on intermediate steps, as well as on the final result. The surface terms where numerically cross-checked against `FIRE` [134, 237]. The numerical unitarity method was carried out by the well-tested code Caravel [167], which furthermore includes many internal self-consistency checks.

We have verified that the result reproduces the pole structure predicted by eqn. (5.19). We have compared the analytic results against Caravel evaluations in a different finite-field, thereby confirming the validity of the functional and rational reconstruction. The analytic results of the two reconstruction approaches are in full agreement with each other. Furthermore, the planar amplitudes match with the results previously obtained in ref. [275].

6.3 Surface-Terms for Higgs + Four Partons

One of the main objectives of Run 3 and the high-luminosity phase of the LHC is a detailed analysis of the Higgs-sector. One of the key observables, in this regard, is the transverse momentum distribution of the Higgs boson, $p_{T,H}$ which probes many models in BSM physics [276–285]. At high $p_{T,H}$ vector-boson fusion (VBF) contributes significantly to Higgs production while at lower energies the production is dominated by gluon fusion [286]. Given the connection of the Higgs and the electro-weak sector, the electroweak couplings of the Higgs are of particular interest. Precise studies of Higgs-production via VBF are therefore important.

In this regard, one of the dominant uncertainties to this process is the production of a Higgs with two associated light partons via gluon fusion. When considering the full theory including mass-effects, higher order corrections to this process are notoriously difficult to compute due to the loop-induced nature.

Indeed, Higgs and Higgs+jet production are currently only known at NLO [287–290], [291] while Higgs plus dijet production is only known at leading order [292–296]. For momentum transfers below the top-quark threshold, however, it is possible to obtain higher precision in the heavy-top-loop approximation (see section 5.2). In this approximation, Higgs plus jet production is known at NNLO [297–301] and Higgs plus dijet production at NLO [302, 303].

A bottleneck of the computation of Higgs+dijet production at NNLO is the calculation of the analytic two-loop amplitudes. We provide some important steps towards the computation of the leading terms of this amplitude in the N_f/N_c expansion.

6.3.1 Notation and Conventions

There are three partonic processes contributing to the production of a Higgs boson in association with jets with zero, two or four quarks as external particles, respectively. We denote the respective helicity amplitudes as

$$M_{4g}(g_{p_1}^{h_1}, g_{p_2}^{h_2}, g_{p_3}^{h_3}, g_{p_4}^{h_4}, H_{p_5}), \tag{6.20}$$

$$M_{ggqq}(q_{p_1}^{h_1}, \bar{q}_{p_2}^{h_2}, g_{p_3}^{h_3}, g_{p_4}^{h_4}, H_{p_5}) \tag{6.21}$$

$$M_{qqQQ}(q_{p_1}^{h_1}, \bar{q}_{p_2}^{h_2}, Q_{p_3}^{h_3}, \bar{Q}_{p_4}^{h_4}, H_{p_5}), \tag{6.22}$$

where g denotes a gluon, while q and Q are massless quarks which we again assume to have different flavours, while H denotes the Higgs-boson. The indices p_i, h_i denote the momenta and helicities, respectively. As before, the amplitude can be decomposed by the

numbers of colours and light fermions

$$A_\kappa^{(k)} = \sum_{k_1} \sum_{k_2} \left(\frac{N_f^{k_1}}{N_c^{k_2}} \right) A_\kappa^{(k,k_1,k_2)}. \tag{6.23}$$

In this decomposition for each power of N_f we only consider the leading power in N_c, i.e. $\frac{N_f^0}{N_c^0}$, $\frac{N_f^1}{N_c^1}$, $\frac{N_f^2}{N_c^2}$. Figures 6.6 - 6.8 show representative diagrams for each contribution. By contrast to $W+$ 4 partons, the terms proportional to $\frac{N_f^0}{N_c^0}$ do contain non-planar integral topologies. However, they do not contain all non-planar topologies, since diagrams with each a quark or gluon on every rung are colour suppressed (see figure 6.9).

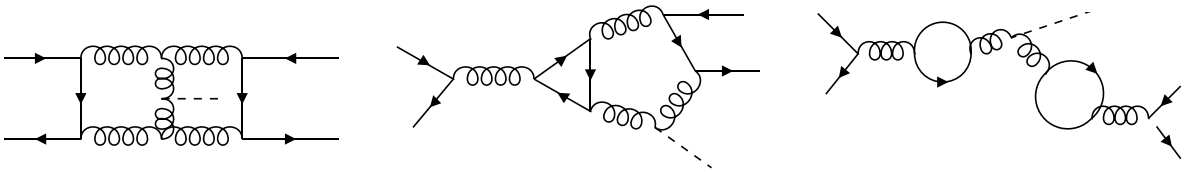

(a) N_f^0/N_c^0 (b) N_f^1/N_c^1 (c) N_f^2/N_c^2

Figure 6.6: Representative diagrams of $\mathcal{M}_{qqQQ}$ at two loops.

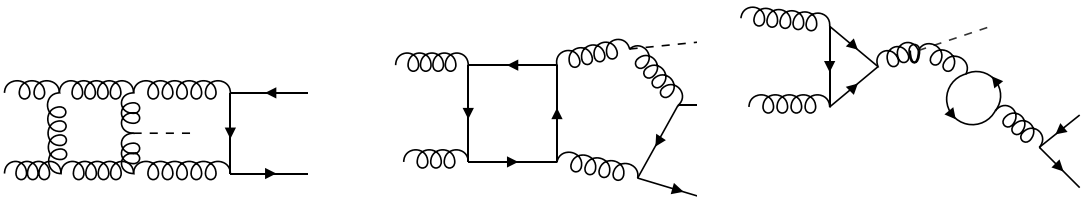

(a) N_f^0/N_c^0 (b) N_f^1/N_c^1 (c) N_f^2/N_c^2

Figure 6.7: Representative diagrams of $\mathcal{M}_{ggqq}$ at two loops.

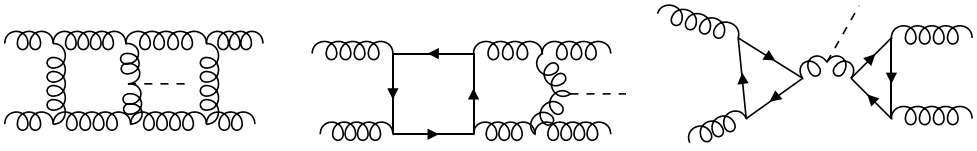

(a) N_f^0/N_c^0 (b) N_f^1/N_c^1 (c) N_f^2/N_c^2

Figure 6.8: Representative diagrams of $\mathcal{M}_{4g}$ at two loops.

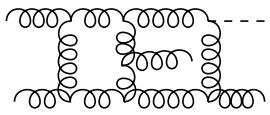

Figure 6.9: A non-planar diagram contributing to N_f^0/N_c^1.

6.3.2 Surface Terms & Master-Integral Decomposition

We have constructed a set of surface terms which allow the reduction of these amplitudes, using the methods described in chapter 4. In particular, we have generated linear equation systems that can be solved on every phase-space point to get IBP-generators and expressed analytic surface terms in terms of these generators. The set covers the function space up to degree six for all non-planar topologies. The surface terms are validated against numeric reductions with FIRE5.

We have employed these surface terms within the numerical unitarity method, implemented in the framework Caravel. The reduction to a basis of integrals takes 4:51 hours on a single core per phase-space point. Given the efficiency of the spinor approach described in section 5.6.6, we estimate that we will need $\lesssim 10^5$ evaluations to constrain pentagon function coefficients, which would be feasible on a mid-size cluster. A pure basis of non-planar five-point master integrals has recently become available [304]. This basis has been implemented in Caravel and we have evaluated decompositions of leading colour amplitudes in this basis. We find that the ϵ-dependent denominators factorize from the kinematically dependent denominators, which is a non-trivial check of the master-surface decomposition. For the planar-pieces, where pentagon functions are available, we have formulated Catani-operators and verified that the ϵ poles of the two-loop amplitude take the predicted form. As can be seen by considering the full theory, the renormalised amplitudes are thus obtained by taking eqn. (5.17) with $q = 2$.

We presume that when a pentagon function decomposition of the master-integrals becomes available, the functional reconstruction of the finite remainders will be within reach.

Chapter 7

Conclusions and Outlook

7.1 Conclusions

In this thesis, we have demonstrated advances in the computation and analysis of unitarity compatible Integration-by-Parts (IBP) relations and their application in the framework of numerical unitarity and functional reconstruction. These techniques were applied to cutting-edge case of multi-loop amplitude computation. The numerical unitarity approach circumvents the inversion of large IBP-systems that appear in Laporta-reduction, directly targeting the simpler final result.

We have generated unitarity compatible IBP-relations via suitable polynomial vector fields (IBP generators), which we have computed with methods from computational algebraic geometry. We have used a formulation of this problem in a conformal embedding space and have used numerical solutions to generate linear systems that can quickly be solved on different phase-space points. In particular, we have used Gröbner-basis methods to solve the syzygy problem at highest order in loop-momentum space and then solved the lower degrees numerically via linear algebra. This approach allowed to compute sets of surface-terms for non-planar five-point-massless topologies as well as the (previously unknown) planar and non-planar five-point-one-mass topologies.

We have observed several interesting properties of IBP-generating vectors. In particular, we have demonstrated that IBP-vector components vanish on critical points of the Baikov-polynomial, while their divergence vanishes on its extrema. This can be used to identify these points and count master-integrals. We have also observed that a large class of unitarity compatible IBP-relations vanishes on the critical points of the Baikov polynomial, which allowed us to deduce a criterion that a set of IBP-vectors has to fulfill in order to produce all surface-terms necessary for the reduction of a topology.

We have used the unitarity compatible IBP-relations in the framework of numerical unitarity to numerically compute master-integral decompositions of cutting-edge two-loop amplitudes, in particular the helicity amplitudes necessary for three-photon production

at full colour, the production of a W-boson in association with two jets at leading order in N_c for each N_f contribution and the production of a Higgs-boson in association with two jets in the heavy-top-loop approximation and at leading colour for (finite-field) numeric phase space point. This method of reducing amplitudes to a master-integral basis is very flexible, robust and less sensitive to additional scales than standard multi-loop techniques.

We have used the numerical evaluations of the master-integral coefficients of the W+2-jet amplitude to reconstruct analytic expressions for this amplitude. We have developed a rational parametrisation of the five-point one-mass phase-space and a method to handle the W-boson polarisations based on different choices for the momenta of its decay-products. These expressions allow to compute leading colour two-loop QCD corrections to amplitudes for four partons and an off-shell W-boson decaying into a lepton pair. They also determine the gauge-invariant planar contributions to Z/γ^*-production in association with two jets (in this case the N_f^1/N_c^1 contributions involve non-planar diagrams). For their reconstruction, we have used an approach based on partial-fraction ansätze and a sampling procedure that gives constraining systems for them in Vandermonde-form.

We have applied similar methods to compute the scattering amplitudes contributing to the production of three photons at full colour. The computation relied on linear systems that, for every phase-space point, give surface terms that can be used for numerical unitarity. The reconstruction of the amplitude was carried out using the univariate analysis and the reconstruction method based on Vandermonde sampling. Complementary to this, the reconstruction was also carried out using a novel approach based on spinor variables. It has been demonstrated that this approach allows to constrain an ansatz with very few evaluations.

We have constructed a set of IBP-relations for non-planar five-point-one-mass integral topologies with sufficient power-counting for the production of a Higgs-boson in association with two jets. These surface terms have been used together with numerical unitarity to compute master-integral decompositions for this amplitude for a few phase-space points in a finite field. The analytic computation of these amplitudes is work in progress.

7.2 Outlook

Given the recent progress in handling the real-radiation contributions (see e.g. [27]), we expect that our results can be used to compute NNLO QCD predictions for W-boson plus two-jet production at hadron colliders in the near future. In fact, for the special case $d\bar{u} \to b\bar{b}W(\ell\bar{\nu})$, such a calculation has recently been carried out [305].

For 3γ-productions, full colour NNLO QCD predictions using our amplitudes are also possible. However, the numerical contribution of the non-planar remainders is relatively small.

Given the efficiency of the spinor-reconstruction technique and the moderate computational effort required for the numerical computation of the master-integral decomposition of the Higgs plus four parton amplitude, we expect that the reconstruction of the analytic amplitudes will be feasible.

We expect that our method of generating linear systems can be used to compute surface terms for integral topologies with more loops and/or mass-scales. In combination with the efficient spinor-reconstruction technology, we assume that this will allow to compute analytic multi-loop amplitudes for many interesting processes.

Appendix A

QCD Feynman-Rules

The diagramatic objects and their corresponding analytic expressions employed in this thesis, expressed in momentum space and 't Hooft-Feynman-gauge, are [306]:

Gluon propagator:

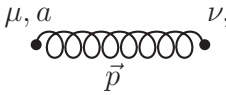

$$= \frac{-ig_{\mu\nu}\delta^{ab}}{p^2 + i\varepsilon}$$

Fermion propagator:

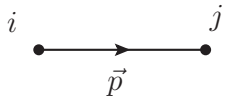

$$= \frac{\delta^{ij}}{\gamma^\mu p_\mu - m + i\varepsilon'} = \frac{\delta^{ij}\gamma^\mu p_\mu + m}{p^2 - m^2 + i\varepsilon}$$

Ghost propagator:

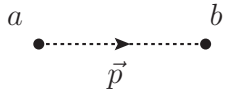

$$= \frac{-i\delta^{ab}}{p^2 + i\varepsilon}$$

Gluon-quark vertex:

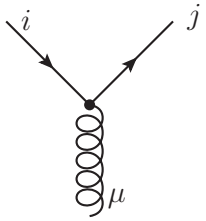

$$= ig_s\gamma^\mu T^a_{ij}$$

Three-gluon vertex:

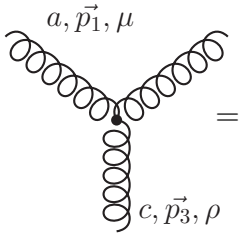

$$= -g_s f^{abc}\big[g^{\mu\nu}(p_1 - p_2)^\rho + g^{\nu\rho}(p_2 - p_3)^\mu + g^{\rho\mu}(p_3 - p_1)^\nu\big]$$

Four-gluon vertex:

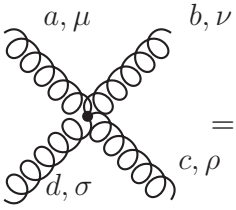

$$= -ig_s^2 \begin{bmatrix} f^{abe}f^{ecd}\big(g^{\mu\rho}g^{\nu\sigma} - g^{\nu\rho}g^{\mu\sigma}\big) \\ +f^{bce}f^{ead}\big(g^{\mu\nu}g^{\rho\sigma} - g^{\mu\rho}g^{\nu\sigma}\big) \\ +f^{cae}f^{ebd}\big(g^{\nu\rho}g^{\mu\sigma} + g^{\sigma\rho}g^{\mu\nu}\big) \end{bmatrix}$$

Gluon-ghost vertex:

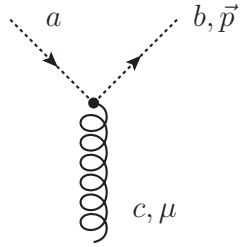

$$= -f^{abc} p^{\mu}$$

Quark-$W^{\pm}$ vertex with an incoming up-type and outgoing down-type field:

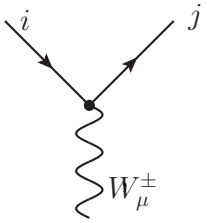

$$= \frac{-ig_2}{\sqrt{2}^3}\gamma^{\mu}(1-\gamma_5)V_{CKM}^{f_1,f_2}$$

Lepton-neutrino-$W^{\pm}$ vertex with an incoming lepton and an outgoing neutrino:

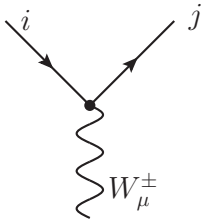

$$= \frac{-ig_2}{\sqrt{2}^3}\gamma^{\mu}(1-\gamma_5)$$

Quark-γ vertex:

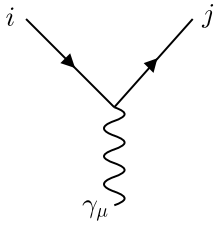

$$= \frac{-ig_2}{\sqrt{2}^3}\gamma^{\mu}(1-\gamma_5)$$

Quark-Z vertex:

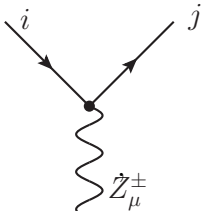

$$= \frac{-ig_z}{2}\gamma^{\mu}(v_f - a_f\gamma_5),$$

abbreviating $g_z = i\frac{g_2}{\sqrt{g_1^2+g_2^2}}$, $a_f = 1$ and $v_f = 1 - 2Y_f\frac{g_1^2}{g_1^2+g_2^2}$, where Y_f denotes the hypercharge of the quark q_f

Top-Higgs vertex

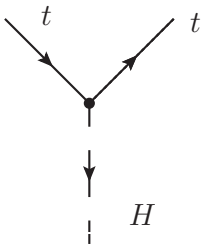

$$= -i\frac{m_t}{v}$$

We consider all external momenta as incoming. We consider all quarks except the top-quark as massless, which is a good approximation at the TeV scale.

Appendix B

Treatment of γ_5 in Dimensional Regularisation

Complications with Dimensional Regularization arise from quantities which are only defined for fixed dimensions, in particular the additional Dirac-matrix γ_5.

Since we will compute amplitudes involving bosons of the electroweak interaction, we will briefly review why the treatment of γ_5 is problematic and how it can be dealt with consistently. The Clifford-algebra of $\gamma-$matrices carries over to D dimensions, hence formally it is possible to define γ^μ in arbitrary dimensions. We distinguish these form the four-dimensional $\gamma_\mu^{[4]}$. The canonical four-dimensional γ_5 matrix is defined to be anticommuting

$$\{\gamma_\mu^{[4]}, \gamma_5^{[4]}\} = 0. \tag{B.1}$$

Considering the trace with seven Dirac matrices $\mathrm{Tr}\left[(\prod_{i=0}^{4}\gamma^{\mu_i})\gamma_5\gamma^\alpha\right]$, using cyclicity of the trace and anti-commuting γ_α with $\gamma_{\mu_0}, ..., \gamma_{\mu_4}$, the following identity is obtained:

$$\mathrm{Tr}\left[\left(\prod_{i=0}^{4}\gamma^{\mu_i}\right)\{\gamma_5,\gamma^\alpha\}\right] + 2\sum_{i=0}^{4} g^{\alpha\mu_i}\mathrm{Tr}\left[\left(\prod_{j=0,j\neq i}^{4}\gamma^{\mu_j}\right)\gamma_5\right] = 0. \tag{B.2}$$

Contracting with $g_{\mu_0\alpha}$ gives

$$\mathrm{Tr}\left[\left(\prod_{i=1}^{4}\gamma^{\mu_i}\right)\{\gamma_5,\gamma^\alpha\}\gamma_\alpha\right] + 2(D-4)\,\mathrm{Tr}\left[\left(\prod_{i=1}^{4}\gamma^{\mu_i}\right)\gamma_5\right] = 0. \tag{B.3}$$

If the first term is set to zero, the second term also has to be set to zero.

Therefore, it is not possible to define a γ_5 which is anti-commuting in D-dimensions

and has the conventional γ_5 as a limit[1], since this would require

$$\mathrm{Tr}(\gamma^\mu\gamma^\nu\gamma^\rho\gamma^\sigma\gamma_5) \xrightarrow{D\to 4} i\varepsilon^{\mu\nu\rho\sigma}. \tag{B.4}$$

The standard procedure to deal with this problem is to employ Larin's scheme [240], where the anti-commutativity is given up, while the condition in eqn. (B.4) is kept. This can be achieved for example by using the four-dimensional γ_5 in the lowest four dimensions and zero else. Giving up the anti-commutation, however, leads to a violation of Ward-Takahashi identities. Therefore, γ_5 is equipped with an additional renormalisation constant which is used to restore these identities. Alternatively, one can use Keimer's scheme where an anti-commuting $\tilde{\gamma}$ is introduced together with a prescription to translate traces with γ_5 to traces with $\tilde{\gamma}$ [307, 308].

In this thesis, however, we can employ a simpler approach: We define block-diagonal γ_μ matrices that equal the four-dimensional definitions in the lowest 4×4 block. For all amplitudes discussed in this thesis, γ_5 only appears within spinor traces involving external fermions. Carrying these out in HV-scheme, the spinor-algebra beyond four-dimensions vanishes and we can therefore treat γ_5 as anti-commuting[2]. When considering Z-bosons or (multiple) W-bosons coupled to closed quark loops, however, this problem has to be dealt with. Physical observables, defined as a four-dimensional limit do not depend on the chosen scheme, however.

[1] In fact, such a prescription is possible when redefining the $D-$dimensional spinor trace to be non-cyclic; an option which we will however not discuss in this work.

[2] In fact, this is equivalent to a trivial application of Kreimer's scheme

Appendix C

Finite Fields

In this thesis, we heavily rely on the use of finite fields which we use to analyse the structure of the coefficients and for functional reconstruction [49, 50]. We will therefore briefly review the concepts of finite fields and rational reconstruction in this section.

A finite field with *cardinality* F is given by all integer numbers $\{0, 1, ..., F-1\}$. Among these numbers, arithmetic operations are defined modulo the prime number F. For addition, subtraction and multiplication this is straightforward. The multiplicative inverse (with a prime number chosen as cardinality) is usually implemented via the Extended Euclidean Algorithm:

Algorithm 3 Extended Euclidean Algorithm

Input: cardinality F, number n

$r_0 = -F \quad r_1 = n$
$(s_0 = 1 \quad s_1 = 0)$
$t_0 = 0 \quad t_1 = 1$
$i = 1$
while $r_i \neq 0$ **do**
    $r_{i+1} = r_{i-1} - q r_i$, where q is (uniquely) chosen such that $0 \leq r_{i+1} < |r_i|$
    $(s_{i+1} = s_{i-1} - q s_i)$
    $t_{i+1} = t_{i-1} - q s_i$
    $i = i + 1$
end while
return t_i

This algorithm is constructed such that the remainder $r_i = s_i F - t_i n$ is monotonously decreasing. If r_{i+1} and r_i are both divisible by a number m, then all previous numbers $r_1, ..., r_{i-1}$ are also divisible by this number. It follows that for a prime cardinality the last $r_n = 1$ and hence the algorithm indeed gives a solution for $t_i n = 1 + s_i F$.

This algorithm is of complexity $O(\log(F))$ and hence allows for fast determination of quotients. Note that for operations with rational numbers, the greatest common divisor of the numerator and denominator have to be found with the same algorithm, hence finite-field operations are not any slower than operations with rational numbers where the numerator and denominator are numbers $\lessapprox F$. Since the parts proportional to s are always omitted in finite-field computations, we can drop the variable (which is why the corresponding lines are written in brackets).

C.1 Rational Reconstruction

The Extended Euclidean Algorithm can also be used to obtain rational numbers that correspond to a value in a finite-field [309]. This *rational reconstruction* is needed because after functional reconstruction the rational numbers appearing in the master integral coefficients are only given in the finite field. Such rational numbers arise e.g. from symmetry factors or summations over diagrams and are therefore difficult to avoid.

The rational reconstruction employing the Extended Euclidean Algorithm is based on the observation that

$$r_i = -s_i F + t_i n \tag{C.1}$$

$$\Rightarrow \frac{r_i}{t_i} \bmod F = n. \tag{C.2}$$

If a solution with $2|r_i| \cdot |t_i| < F$, exists, then it is unique in the sense that for all other solutions $|n| \cdot |d| > F$. Moreover, one can show that if such a solution exists, it will be found by the Extended Euclidean Algorithm [309]. After one has constructed such a guess for a rational number, it is usually verified by comparing to a computation in a different finite-field.

C.1.1 The Chinese Remainder Theorem

If a rational number cannot be extracted from it's value in one finite field, it can be extracted from several computations using the Chinese Remainder Theorem, discovered by the third century Chinese mathematician Sun-Tzu. Given a rational number a and k finite fields with cardinalities $F_1, ..., F_k$ such that

$$\begin{aligned} a \bmod F_1 &= n_1, \\ &\vdots \\ a \bmod F_k &= n_k, \end{aligned} \tag{C.3}$$

one can compute the number in a larger cardinality

$$a \bmod \prod_{i=1}^{k} F_i = \sum_j n_j \left(\left(\prod_{i=1, i\neq j}^{k} F_i \right)^{-1} \bmod F_j \right). \tag{C.4}$$

Thus for $a = \frac{n}{d}$, one can reconstruct a result which is unique for $2|n| \cdot |d| < \prod_i F$, as long as n and d are not divisible by any of the cardinalities.

C.1.2 Denominator Guessing & Integer Reconstruction

The rational reconstruction algorithm described above does not include any knowledge about the structure of the numbers. In the case of master-integral coefficients (or pentagon function coefficients), however, the rational numbers after functional reconstruction are not generic. When shifting all rational numbers to the numerator of the coefficients, the denominators of rational numbers originate only in symmetry factors and rational numbers in the definition of pentagon functions. In principle, it would therefore be possible to trace back the greatest possible denominator for each rational number from this information.

In practice, however, we find it more convenient to experimentally determine this denominator by using the rational reconstruction described above and computing the greatest common denominator of all reasonable results, that is all results whose denominators factorise into small prime numbers[1]. Then, for a finite-field number n, two guesses for the rationally reconstruction number are

$$a_1 = \frac{nd \bmod F}{d}, \quad a_2 = -\frac{F - nd \bmod F}{d}, \tag{C.5}$$

and we take the one with the smaller absolute value. This approach gives unique results for $|a| \cdot |d| < F/2$ and thus has a much larger range than the algorithm described before. This approach can also be combined with the Chinese Remainder Theorem. With this reconstruction method, we were able to determine all rational numbers in the $W + 2j$ amplitude by reconstructing it in two finite-fields and the numbers in the γ amplitudes with one finite-field.

The rational numbers in the linear relations between pentagon coefficients, however, do not have such simple denominators in general. Therefore, there we rely on the Extended Euclidean Algorithm and the Chinese Remainder Theorem to obtain the numbers from evaluations in several fields. In particular, for the non-planar amplitudes contributing to three-photon production, we evaluated the linear relations in four finite fields to rationally reconstruct them and verified the results in a fifth.

[1]What *small* means in this context is decided case-by-case. For $W + 2$jet production, prime numbers up to 17 appear.

Appendix D

Interpolation Formulae

We obtain analytic amplitudes by functional reconstruction over finite-field evaluations [50]. We will therefore review two important interpolation formulae in this appendix.

D.1 Thieles Interpolation Formula

We use Thieles interpolation formula [225] to reconstruct univariate rational functions or multivariate rational functions on univariate slices. In this section, we will therefore review the interpolation formula. The basic idea is to represent a rational function as a continued fraction

$$r_i(t) = r_i(t_1) + \cfrac{t - t_1}{\rho(t_1,t_2) + \cfrac{t - t_2}{\rho_2(t_1,t_2,t_3) - r_i(t_1) + \cfrac{t - t_3}{\rho_3(t_1,t_2,t_3,t_4) - \rho(t_1,t_2) + \cdots}}}, \tag{D.1}$$

with the reciprocal differences

$$\rho_1(t_0,t_1) = \frac{t_0 - t_1}{r_i(t_0) - r_i(t_1)} \tag{D.2}$$

$$\rho_2(t_0,t_1,t_2) = \frac{t_0 - t_2}{\rho_1(t_0,t_1) - \rho_1(t_1,t_2)} + r_i(t_1) \tag{D.3}$$

$$\rho_n(t_0,t_1,\ldots,t_n) = \frac{t_0 - t_n}{\rho_{n-1}(t_0,t_1,\ldots,t_{n-1}) - \rho_{n-1}(t_1,t_2,\ldots,t_n)} + \rho_{n-2}(t_1,\ldots,t_{n-1}). \tag{D.4}$$

The interpolation is finished when the nth reciprocal difference $\rho_n(t)$ is zero. For a rational function with numerator degree R_n and denominator degree R_d, the interpolation finishes after $2\max(R_n, R_d)$ steps.

D.2 Multivariate Newton Interpolation

We use iterated Newton interpolation to reconstruct pentagon function coefficients on bivariate slices. We will therefore review the interpolation formula in this section. In particular, we focus on the special case where we want to interpolate in a variable which we cannot choose freely, but that is expressed as a rational function of other variables. Suppose a polynomial $f(s,t)$ where $s(x,t)$ is a rational function of x and t. First, for each value of $t = t_j$ we can reconstruct $f(x,t_j)$ by simple Newton interpolation

$$f_0(s,t_j) = f(s(x_0),t_j), \tag{D.5}$$

$$f_i(s,t_j) = f_{i-1}(s,t_j) + \frac{f(s(x_i t_j),t_j) - f_{i-1}(f(s(x_i,t_j),t_j)}{(s(x_i,t_j) - s(x_{i-1},t_j))^i}(s - s(x_{i-1,t_j}))^i, \tag{D.6}$$

$$f(s,t_j) = f_{m_j}(s,t_j). \tag{D.7}$$

$$\tag{D.8}$$

Then, we reconstruct the dependence on t, for which we again use univariate Newton interpolation

$$.f_0(s,t) = f(s,t_0), \tag{D.9}$$

$$f_j(s,t) = f_{j-1}(s,t) + \frac{f(s,t_j) - f_{j-1}(s,t_j)}{(t_j - t_{j-1})^j}(t - t_{j-1})^j, \tag{D.10}$$

$$f(s,t) = f_N(s,t). \tag{D.11}$$

The points of this interpolation $f(s,t_i)$ are obtained as D.5. When we use this interpolation, the maximal degree of the numerator R_f is usually known from a previous univariate interpolation. Therefore, in the expansion

$$f(s,t) = \sum_{i,j=0,i+j\leq R_f} c_{ij} s^i t^j, \tag{D.12}$$

the coefficients $c_{i=R,j\leq R_f-R}$ are known after evaluating $f_(s,t_j)$ for $R_f - R + 1$ values of t_j. This allows to systematically subtract them from f, such that for the $(n+1)$th evaluation of $f(s,t_k)$, we can interpolate $f(s,t_k) - \sum_{i=R_f-n}^{R_n} \sum_{j=0}^{R_n-i} c_{ij} s^i t_k^j$ by evaluating $f(s(x_i,t_k),t_k)$ for $R_n - n$ values of x_n. This procedure known as *pruning* leads to a considerable efficiency gain. As a side remark, we note that it is straightforward to extend this interpolation method to more than two variables, which we will not need in this thesis, however.

Appendix E

Spinor Helicity Formalism

As described in section 1.2.1 any four-vector can be decomposed into a pair of left- and right-handed Weyl spinors

$$A^{\mu} = \sigma^{\mu}_{a\tilde{b}} \xi^{a} \chi^{\tilde{b}}. \tag{E.1}$$

This decomposition can be used as a particularly useful decomposition of massless four-momenta, where

$$\chi \propto (\xi)^{*}. \tag{E.2}$$

Conventionally, for a massless momentum p_j, these are described in a bra-ket notation

$$\{\xi^{a}_{j}\} = |j\rangle, \quad \{\xi^{j}_{a}\} = \langle j| \tag{E.3}$$

$$\{\chi^{\tilde{a}}_{j}\} = |j], \quad \{\chi^{j}_{\tilde{a}}\} = [j|, \tag{E.4}$$

such that the momenta are written as

$$p^{\mu}_{j} = \sigma^{\mu}|j\rangle[j|, \quad (p^{*}_{j})^{\mu} = \sigma^{\mu}|j]\langle j|, \quad s_{ij} = \langle ij\rangle[ij], \tag{E.5}$$

with the Pauli-matrices $\{\sigma_{\mu}\} = (\mathbb{1}, \sigma^{i})$. The spinors are only defined modulo a global rescaling $|j\rangle \to e^{-i\lambda}|j\rangle$, $|j] \to e^{i\lambda}|j]$, as such a transformation leaves the momenta and Mandelstam variables invariant. Amplitudes in a helicity basis, however, are chiral objects and, thus, not invariant under such a rescaling. The rescaling property of an amplitude with each such redefinition is referred to as *spinor weight*. When computing cross-sections, the spinor weights cancel when taking $|\mathcal{M}|^2$.

A clear advantage of this parametrisation is that it is trivial to construct on-shell massless momenta p_{μ} employing eq. E.2. Note that such momenta are in general complex, however. Moreover, this parametrisation of momenta allows to distinguish left-handed

from right-handed objects, which is often advantageous since the SM is indeed a chiral theory.

Appendix F

Rationalization of Momenta & tr_5

In this work we have used rational parametrizations of the five-point zero-mass and the five-point one-mass phase-space, as was described in section 5.6.4, were we required that all but one variables are Mandelstam-variables. In this appendix, we detail the explicit form of the rational phase-space parametrisations.

F.1 Five-Point Zero-Mass

Following reference [218], we use the phase-space parameters

$$\{s_{12}, s_{23}, s_{45}, s_{15}, x\}, \tag{F.1}$$

where the remaining Mandelstams and tr_5 are given by

$$s_{34} = \frac{(s_{45} - s_{12})s_{15}x - s_{23}(s_{23} - s_{45} - s_{15} - xs_{12})}{(s_{45} - s_{23} + x)x}, \tag{F.2}$$

$$\mathrm{tr}_5 = \frac{-s_{23}^2 + (-s_{12} + s_{45})s_{15}x + s_{23}(s_{45} + s_{15} + s_{12}x)}{x(-s_{23} + s_{45} + s_{12}x)}. \tag{F.3}$$

In this parameters, parity conjugation is given by

$$x \to \bar{x} = \frac{s_{23}(s_{23}s_{45} - s_{15})}{s_{12}s_{34}(s_{12}, s_{23}, s_{45}, s_{15}, x)x}, \tag{F.4}$$

which leads to

$$s_{34} \to s_{34}, \quad \mathrm{tr}_5 \to -\mathrm{tr}_5\,. \tag{F.5}$$

F.2 Five-Point One-Mass

We use the variables

$$\{s_{\mathrm{v}1}, s_{12}, s_{23}, s_{4\mathrm{v}}, p_{\mathrm{v}}^2, x\}. \tag{F.6}$$

This allows to choose $s_{34}(x)$ and $\mathrm{tr}_5(x)$ as rational functions

$$\begin{aligned}\mathrm{tr}_5(s_{\mathrm{v}1}, s_{12}, s_{23}, s_{4\mathrm{v}}, p_{\mathrm{v}}^2, x) = &\frac{s_{\mathrm{v}1}(s_{4\mathrm{v}} - s_{12}) + (s_{12} - p_{\mathrm{v}}^2)s_{23}}{4\left((s_{4\mathrm{v}} - s_{23})^2 - [s_{\mathrm{v}1}(s_{4\mathrm{v}} - s_{12}) + (s_{12} - p_{\mathrm{v}}^2)s_{23}]^2 x^2\right)}\\ &\times \Big[(s_{4\mathrm{v}} - s_{23})^2 + \\ &2\big(s_{\mathrm{v}1}s_{4\mathrm{v}}(s_{12} - s_{4\mathrm{v}}) + [p_{\mathrm{v}}^2(s_{4\mathrm{v}} - 2s_{12}) + s_{4\mathrm{v}}s_{12} + s_{\mathrm{v}1}(s_{4\mathrm{v}} + s_{12})]s_{23} - (p_{\mathrm{v}}^2 + s_{12})s_{23}^2\big)x\\ &+ (s_{\mathrm{v}1}(s_{4\mathrm{v}} - s_{12}) + (s_{12} - p_{\mathrm{v}}^2)s_{23})^2 x^2\Big],\end{aligned} \tag{F.7}$$

$$\begin{aligned}s_{34}(s_{\mathrm{v}1}, s_{12}, s_{23}, s_{4\mathrm{v}}, p_{\mathrm{v}}^2, x) = &\frac{2}{(s_{\mathrm{v}1}(s_{4\mathrm{v}} - s_{12}) + (s_{12} - p_{\mathrm{v}}^2)s_{23})^2 x^2 - (s_{4\mathrm{v}} - s_{23})^2}\\ &\times \Big[(s_{\mathrm{v}1}s_{4\mathrm{v}}s_{12} - s_{\mathrm{v}1}s_{4\mathrm{v}}^2 + p_{\mathrm{v}}^2 s_{4\mathrm{v}}s_{23} + s_{\mathrm{v}1}s_{4\mathrm{v}}s_{23} - 2p_{\mathrm{v}}^2 s_{12}s_{23} + s_{\mathrm{v}1}s_{12}s_{23}\\ &+ s_{4\mathrm{v}}s_{12}s_{23} - p_{\mathrm{v}}^2 s_{23}^2 - s_{12}s_{23}^2 + (s_{\mathrm{v}1}(s_{4\mathrm{v}} - s_{12}) + (s_{12} - p_{\mathrm{v}}^2)s_{23})^2 x)\Big].\end{aligned} \tag{F.8}$$

The parity conjugate point $\{s_{\mathrm{v}1}, s_{12}, s_{23}, s_{4\mathrm{v}}, p_{\mathrm{v}}^2, \bar{x}\}$ to such a point is defined by the same kinematic-invariants, but a sign-flip for tr_5

$$\begin{aligned}\mathrm{tr}_5(s_{\mathrm{v}1}, s_{12}, s_{23}, s_{4\mathrm{v}}, p_{\mathrm{v}}^2, \bar{x}) &= -\mathrm{tr}_5(s_{\mathrm{v}1}, s_{12}, s_{23}, s_{4\mathrm{v}}, p_{\mathrm{v}}^2, x),\\ s_{34}(s_{\mathrm{v}1}, s_{12}, s_{23}, s_{4\mathrm{v}}, p_{\mathrm{v}}^2, \bar{x}) &= s_{34}(s_{\mathrm{v}1}, s_{12}, s_{23}, s_{4\mathrm{v}}, p_{\mathrm{v}}^2, x).\end{aligned} \tag{F.9}$$

Solving for $\bar{x}$, we find

$$\begin{aligned}\bar{x} = &\Big[-(s_{4\mathrm{v}} - s_{23})^2 + (s_{\mathrm{v}1}s_{4\mathrm{v}}(s_{4\mathrm{v}} - s_{12}) - (p_{\mathrm{v}}^2(s_{4\mathrm{v}} - 2s_{12})\\ &+ s_{4\mathrm{v}}s_{12} + s_{\mathrm{v}1}(s_{4\mathrm{v}} + s_{12}))s_{23} + (p_{\mathrm{v}}^2 + s_{12})s_{23}^2)x\Big] \Big/ \Big[s_{\mathrm{v}1}s_{4\mathrm{v}}s_{12}\\ &- s_{\mathrm{v}1}s_{4\mathrm{v}}^2 + p_{\mathrm{v}}^2 s_{4\mathrm{v}}s_{23} + s_{\mathrm{v}1}s_{4\mathrm{v}}s_{23} - 2p_{\mathrm{v}}^2 s_{12}s_{23} + s_{\mathrm{v}1}s_{12}s_{23}\\ &+ s_{4\mathrm{v}}s_{12}s_{23} - p_{\mathrm{v}}^2 s_{23}^2 - s_{12}s_{23}^2 + (s_{\mathrm{v}1}(s_{4\mathrm{v}} - s_{12}) + (-p_{\mathrm{v}}^2 + s_{12})s_{23})^2 x\Big].\end{aligned} \tag{F.10}$$

Thus we provide a rational parametrisation of the phase-space with the possibility to compute parity-conjugate points.

Appendix G

Bibliography

[1] Particle Data Group collaboration, M. Tanabashi, K. Hagiwara, K. Hikasa, K. Nakamura, Y. Sumino, F. Takahashi et al., *Review of particle physics*, *Phys. Rev. D* **98** (2018) 030001.

[2] V. C. Rubin and J. Ford, W. Kent, *Rotation of the Andromeda Nebula from a Spectroscopic Survey of Emission Regions*, *Astrophys. Journal* **159** (1970) 379.

[3] K. C. Freeman, *On the Disks of Spiral and S0 Galaxies*, *Astrophys. Journal* **160** (1970) 811.

[4] Super-Kamiokande collaboration, Y. Fukuda et al., *Evidence for oscillation of atmospheric neutrinos*, *Phys. Rev. Lett.* **81** (1998) 1562 [hep-ex/9807003].

[5] A. D. Sakharov, *Violation of CP Invariance, C asymmetry, and baryon asymmetry of the universe*, *Pisma Zh. Eksp. Teor. Fiz.* **5** (1967) 32.

[6] G. W. Bennett, B. Bousquet, H. N. Brown, G. Bunce, R. M. Carey, P. Cushman et al., *Final report of the e821 muon anomalous magnetic moment measurement at BNL*, *Physical Review D* **73** (2006) .

[7] G. Hooft, *Symmetry breaking through bell-jackiw anomalies*, *Physical Review Letters* **37** (1976) .

[8] J. R. Ellis, M. K. Gaillard and D. V. Nanopoulos, *A Phenomenological Profile of the Higgs Boson*, *Nucl. Phys. B* **106** (1976) 292.

[9] V. V. Sudakov, *Vertex parts at very high-energies in quantum electrodynamics*, *Sov. Phys. JETP* **3** (1956) 65.

[10] C. F. Berger, Z. Bern, L. J. Dixon, F. Febres Cordero, D. Forde, H. Ita et al., *One-Loop Calculations with BlackHat*, *Nucl. Phys. Proc. Suppl.* **183** (2008) 313 [0807.3705].

[11] T. Hahn, *Generating Feynman diagrams and amplitudes with FeynArts 3, Comput, Phys. Commun. 140(2001) 418-431, [hep-ph/0012260]* **140** .

[12] T. Hahn, S. Pa-ehr and C. Schappacher, *Formcalc 9 and extensions, PoS LL2016* **068** (2016) 04611.

[13] V. Shtabovenko, R. Mertig and F. Orellana, *New developments in FeynCalc 9, 0, Comput. Phys. Commun. 207 (2016) 432-444* .

[14] V. Shtabovenko, *Feynhelpers: Connecting FeynCalc to FIRE and package-x, Comput. Phys. Commun. 218 (2017) 48-65, [1611* .

[15] G. Cullen, N. Greiner, G. Heinrich, G. Luisoni, P. Mastrolia et al., *Automated one-loop calculations with GoSam, Eur. Phys. J. C72 (2012) 1889* .

[16] G. Cullen et al., *Gosam-2.0: a tool for automated one-loop calculations within the Standard Model and beyond,, Eur. Phys. J. C74 (2014)* .

[17] G. Bevilacqua, M. Czakon, M. V. Garzelli, A. van Hameren, A. Kardos, C. G. Papadopoulos et al., *Helac-nlo, Comput. Phys. Commun. 184 (2013) 986-997* .

[18] V. Hirschi, R. Frederix, S. Frixione, M. V. Garzelli, F. Maltoni and R. Pittau, *Automation of one-loop QCD corrections, JHEP 05* **044** (2011) .

[19] J. Alwall, R. Frederix, S. Frixione, V. Hirschi, F. Maltoni, O. Mattelaer et al., *The automated computation of tree-level and next-to-leading order differential cross sections, and their matching to parton shower simulations, JHEP 07* **079** (2014) .

[20] F. Cascioli, P. Maierhofer and S. Pozzorini, *Scattering amplitudes with open loops, Phys. Rev. Lett. 108 (2012)* .

[21] S. Actis, A. Denner, L. Hofer and J. N., *Lang, A. Scharf and S. Uccirati, RECOLA: REcursive Computation of One-Loop Amplitudes, Comput. Phys. Commun. 214 (2017) 140-173, [1605* .

[22] F. Caola, K. Melnikov, R. Röntsch and L. Tancredi, *QCD corrections to W^+W^- production through gluon fusion, Phys. Lett.* **B754** (2016) 275 [1511.08617].

[23] F. Caola, M. Dowling, K. Melnikov, R. Röntsch and L. Tancredi, *QCD corrections to vector boson pair production in gluon fusion including interference effects with off-shell Higgs at the LHC, JHEP* **07** (2016) 087 [1605.04610].

[24] F. Cascioli, T. Gehrmann, M. Grazzini, S. Kallweit, P. Maierhöfer, A. von Manteuffel et al., *ZZ production at hadron colliders in NNLO QCD, Phys. Lett.* **B735** (2014) 311 [1405.2219].

[25] T. Gehrmann, M. Grazzini, S. Kallweit, P. Maierhöfer, A. von Manteuffel, S. Pozzorini et al., *W^+W^- Production at Hadron Colliders in Next to Next to Leading Order QCD*, *Phys. Rev. Lett.* **113** (2014) 212001 [1408.5243].

[26] N. A. Lo Presti, T. Gehrmann and J. Henn, *Two-loop five-point integrals in massless QCD*, *PoS* **LL2016** (2016) 051.

[27] M. Czakon, A. Mitov and R. Poncelet, *Next-to-Next-to-Leading Order Study of Three-Jet Production at the LHC*, *Phys. Rev. Lett.* **127** (2021) 152001 [2106.05331].

[28] H. A. Chawdhry, M. Czakon, A. Mitov and R. Poncelet, *Nnlo qcd corrections to diphoton production with an additional jet at the lhc*, *Journal of High Energy Physics* (2021) .

[29] A. V. Kotikov, *Differential equations method: New technique for massive Feynman diagrams calculation*, *Phys. Lett. B* **254** (1991) 158.

[30] E. Remiddi, *Differential equations for Feynman graph amplitudes*, *Nuovo Cim. A* **110** (1997) 1435 [hep-th/9711188].

[31] J. M. Henn, *Multiloop integrals in dimensional regularization made simple*, *Phys. Rev. Lett.* **110** (2013) 251601 [1304.1806].

[32] S. Abreu, B. Page and M. Zeng, *Differential equations from unitarity cuts: nonplanar hexa-box integrals*, *JHEP* **01** (2019) 006 [1807.11522].

[33] C. G. Papadopoulos, D. Tommasini and C. Wever, *The Pentabox Master Integrals with the Simplified Differential Equations approach*, *JHEP* **04** (2016) 078 [1511.09404].

[34] S. Abreu, H. Ita, F. Moriello, B. Page, W. Tschernow and M. Zeng, *Two-Loop Integrals for Planar Five-Point One-Mass Processes*, *JHEP* **11** (2020) 117 [2005.04195].

[35] D. D. Canko, C. G. Papadopoulos and N. Syrrakos, *Analytic representation of all planar two-loop five-point Master Integrals with one off-shell leg*, *JHEP* **01** (2021) 199 [2009.13917].

[36] C. G. Papadopoulos and C. Wever, *Internal Reduction method for computing Feynman Integrals*, *JHEP* **02** (2020) 112 [1910.06275].

[37] S. Abreu, H. Ita, B. Page and W. Tschernow, *Two-loop hexa-box integrals for non-planar five-point one-mass processes*, *JHEP* **03** (2022) 182 [2107.14180].

[38] F. Moriello, *Generalised power series expansions for the elliptic planar families of Higgs + jet production at two loops*, *JHEP* **01** (2020) 150 [1907.13234].

[39] M. Hidding, *DiffExp, a Mathematica package for computing Feynman integrals in terms of one-dimensional series expansions*, *Comput. Phys. Commun.* **269** (2021) 108125 [2006.05510].

[40] S. Badger, H. B. Hartanto and S. Zoia, *Two-Loop QCD Corrections to $Wb\bar{b}$ Production at Hadron Colliders*, *Phys. Rev. Lett.* **127** (2021) 012001 [2102.02516].

[41] T. Gehrmann, J. M. Henn and N. A. Lo Presti, *Pentagon functions for massless planar scattering amplitudes*, *JHEP* **10** (2018) 103 [1807.09812].

[42] D. Chicherin and V. Sotnikov, *Pentagon Functions for Scattering of Five Massless Particles*, *JHEP* **12** (2020) 167 [2009.07803].

[43] D. Chicherin, V. Sotnikov and S. Zoia, *Pentagon functions for one-mass planar scattering amplitudes*, *JHEP* **01** (2022) 096 [2110.10111].

[44] K. G. Chetyrkin and F. V. Tkachov, *Integration by Parts: The Algorithm to Calculate beta Functions in 4 Loops*, *Nucl. Phys. B* **192** (1981) 159.

[45] S. Laporta, *High precision calculation of multiloop Feynman integrals by difference equations*, *Int. J. Mod. Phys. A* **15** (2000) 5087 [hep-ph/0102033].

[46] J. Gluza, K. Kajda and D. A. Kosower, *Towards a Basis for Planar Two-Loop Integrals*, *Phys. Rev.* **D83** (2011) 045012 [1009.0472].

[47] K. J. Larsen and Y. Zhang, *Integration-by-parts reductions from unitarity cuts and algebraic geometry*, *Phys. Rev.* **D93** (2016) 041701 [1511.01071].

[48] H. Ita, *Two-loop Integrand Decomposition into Master Integrals and Surface Terms*, *Phys. Rev.* **D94** (2016) 116015 [1510.05626].

[49] A. von Manteuffel and R. M. Schabinger, *A novel approach to integration by parts reduction*, *Phys. Lett. B* **744** (2015) 101 [1406.4513].

[50] T. Peraro, *Scattering amplitudes over finite fields and multivariate functional reconstruction*, *JHEP* **12** (2016) 030 [1608.01902].

[51] J. Klappert and F. Lange, *Reconstructing rational functions with FireFly*, *Comput. Phys. Commun.* **247** (2020) 106951 [1904.00009].

[52] J. Klappert, S. Y. Klein and F. Lange, *Interpolation of dense and sparse rational functions and other improvements in FireFly*, *Comput. Phys. Commun.* **264** (2021) 107968 [2004.01463].

[53] T. Peraro, *FiniteFlow: multivariate functional reconstruction using finite fields and dataflow graphs*, *JHEP* **07** (2019) 031 [1905.08019].

[54] G. De Laurentis and B. Page, *Ansätze for scattering amplitudes from p-adic numbers and algebraic geometry*, *arXiv preprint arXiv:2203.04269* (2022) .

[55] S. Abreu, F. Febres Cordero, H. Ita, M. Jaquier, B. Page and M. Zeng, *Two-Loop Four-Gluon Amplitudes from Numerical Unitarity*, *Phys. Rev. Lett.* **119** (2017) 142001 [1703.05273].

[56] S. Abreu, F. Febres Cordero, H. Ita, B. Page and M. Zeng, *Planar Two-Loop Five-Gluon Amplitudes from Numerical Unitarity*, *Phys. Rev. D* **97** (2018) 116014 [1712.03946].

[57] S. Abreu, J. Dormans, F. Febres Cordero, H. Ita and B. Page, *Analytic Form of Planar Two-Loop Five-Gluon Scattering Amplitudes in QCD*, *Phys. Rev. Lett.* **122** (2019) 082002 [1812.04586].

[58] D. V. Schroeder and M. E. Peskin, *Introduction to quantum field theory*, 1995.

[59] S. Weinberg, *The Quantum Theory of Fields*, vol. 1. Cambridge University Press, 1995, 10.1017/CBO9781139644167.

[60] H. Weyl, *Electron and Gravitation. 1. (In German)*, *Z. Phys.* **56** (1929) 330.

[61] R. Brauer and H. Weyl, *Spinors in n dimensions*, *American Journal of Mathematics* **57** (1935) 425.

[62] P. A. M. Dirac, *The quantum theory of the electron*, *Proc. Roy. Soc. Lond. A* **117** (1928) 610.

[63] W. Pauli, *Relativistic Field Theories of Elementary Particles*, *Reviews of Modern Physics* **13** (1941) 203.

[64] C. N. Yang and R. L. Mills, *Conservation of Isotopic Spin and Isotopic Gauge Invariance*, *Physical Review* **96** (1954) 191.

[65] R. Peccei and H. Quinn, *Cp conservation in the presence of pseudoparticles*, *Physical Review Letters - PHYS REV LETT* **38** (1977) 1440.

[66] M. Gell-Mann, *A Schematic Model of Baryons and Mesons*, *Phys. Lett.* **8** (1964) 214.

[67] S. L. Glashow, *Partial symmetries of weak interactions*, *Nuclear Physics* **22** (1961) 579.

[68] S. Tomonaga, *On a Relativistically Invariant Formulation of the Quantum Theory of Wave Fields*, *Progress of Theoretical Physics* **1** (1946) 27.

[69] J. Schwinger, *On Quantum-Electrodynamics and the Magnetic Moment of the Electron*, *Physical Review* **73** (1948) 416.

[70] R. P. Feynman, *Space-Time Approach to Quantum Electrodynamics*, *Physical Review* **76** (1949) 769.

[71] S. Weinberg, *A model of leptons*, *Phys. Rev. Lett.* **19** (1967) 1264.

[72] A. Salam, *Weak and Electromagnetic Interactions*, *Conf. Proc. C* **680519** (1968) 367.

[73] F. Englert and R. Brout, *Broken Symmetry and the Mass of Gauge Vector Mesons*, *Phys. Rev. Lett.* **13** (1964) 321.

[74] P. W. Higgs, *Broken symmetries, massless particles and gauge fields*, *Phys. Lett.* **12** (1964) 132.

[75] P. W. Higgs, *Broken symmetries and the masses of gauge bosons*, *Phys. Rev. Lett.* **13** (1964) 508.

[76] C. Q. Geng and R. E. Marshak, *Uniqueness of Quark and Lepton Representations in the Standard Model From the Anomalies Viewpoint*, *Phys. Rev. D* **39** (1989) 693.

[77] B. Pontecorvo, *Mesonium and Antimesonium*, *Soviet Journal of Experimental and Theoretical Physics* **6** (1958) 429.

[78] Z. Maki, M. Nakagawa and S. Sakata, *Remarks on the Unified Model of Elementary Particles*, *Progress of Theoretical Physics* **28** (1962) 870.

[79] P. Dirac, *The fundamental equations of quantum mechanics*, *Proceedings of the Royal Society of London A: Mathematical, Physical and Engineering Sciences* **109** (1925) 642 [`http://rspa.royalsocietypublishing.org/content/109/752/642.full.pdf`].

[80] L. Faddeev and V. Popov, "Feynman diagrams for the yang-mills field.." Phys. Lett. B. Band 25, Nr. 1,, 1967.

[81] C. Becchi, A. Rouet and R. Stora, *Renormalization of gauge theories*, *Annals of Physics* **98** (1976) 287.

[82] I. V. Tyutin, *Gauge Invariance in Field Theory and Statistical Physics in Operator Formalism*, 0812.0580.

[83] M. Flory, R. C. Helling and C. Sluka, *How i learned to stop worrying and love qft*, 2012. 10.48550/ARXIV.1201.2714.

[84] R. P. Feynman, "Space-time approach to non-relativistic quantum mechanics." Rev. Mod. Phys. 20, 367, Apr., 1948.

[85] G. C. Wick, *The evaluation of the collision matrix*, *Phys. Rev.* **80** (1950) 268.

[86] H. Lehmann, K. Symanzik and W. Zimmermann, *Zur Formulierung quantisierter Feldtheorien*, *Nuovo Cimento Serie* **1** (1955) 205.

[87] T. D. Lee and M. Nauenberg, *Degenerate Systems and Mass Singularities*, *Physical Review* **133** (1964) B1549.

[88] T. Kinoshita, *Mass Singularities of Feynman Amplitudes*, *Journal of Mathematical Physics* **3** (1962) 650.

[89] J. R. Oppenheimer, "Note on the theory of the interaction of field and matter." Phys. Rev. 35, 461, 1930.

[90] F. J. Dyson, "The radiation theories of tomonaga, schwinger, and feynman." Phys. Rev. 75, 486, 1949.

[91] C. G. Bollini and J. J. Giambiagi, *Dimensional renorinalization : The number of dimensions as a regularizing parameter*, *Il Nuovo Cimento B (1971-1996)* **12** (1972) 20.

[92] M. V. G. 't Hooft, "Regularisation and renormalisation of gauge fields."

[93] W. Heisenberg, "über die in der theorie der elementarteilchen auftretende universelle lange.." Annalen der Physik 32: 20-33, 1936.

[94] W. P. F. Villars, "On the invariant regularization in relativistic quantum theory." Rev. Mod. Phys. 21, 434, 1949.

[95] J. C. Ward, *An Identity in Quantum Electrodynamics*, *Physical Review* **78** (1950) 182.

[96] Y. Takahashi, *On the generalized ward identity*, *Il Nuovo Cimento* **6** (1957) 371.

[97] G. 't Hooft and M. J. G. Veltman, *Regularization and Renormalization of Gauge Fields*, *Nucl. Phys.* **B44** (1972) 189.

[98] E. Egorian and O. V. Tarasov, *Two Loop Renormalization of the QCD in an Arbitrary Gauge*, *Teor. Mat. Fiz.* **41** (1979) 26.

[99] S. J. Brodsky, G. P. Lepage and P. B. Mackenzie, *On the elimination of scale ambiguities in perturbative quantum chromodynamics*, *Phys. Rev. D* **28** (1983) 228.

[100] D. J. Gross and F. Wilczek, *Ultraviolet behavior of non-abelian gauge theories*, *Phys. Rev. Letters* **30** (1973) 1343.

[101] H. D. Politzer, *Reliable Perturbative Results for Strong Interactions?*, *Phys. Rev. Letters* **30** (1973) 1346.

[102] P. A. M. Dirac, *Quantum theory of emission and absorption of radiation*, *Proc. Roy. Soc. Lond. A* **114** (1927) 243.

[103] J. Orear and E. Fermi, *Nuclear Physics: A Course Given by Enrico Fermi at the University of Chicago*. University of Chicago Press, 1950.

[104] T. Kinoshita, "Mass singularities of feynman amplitudes." Journal of Mathematical Physics 3, 650, 1962.

[105] G. Somogyi, Z. Trócsányi and V. D. Duca, *A subtraction scheme for computing QCD jet cross sections at NNLO: regularization of doubly-real emissions*, *Journal of High Energy Physics* **2007** (2007) 070.

[106] G. Somogyi and Z. Trocsanyi, *A new subtraction scheme for computing qcd jet cross sections at next-to-leading order accuracy*, 2006. 10.48550/ARXIV.HEP-PH/0609041.

[107] A. Aude Gehrmann-De Ridder, T. Gehrmann and E. N. Glover, *Antenna subtraction at NNLO*, *Journal of High Energy Physics* **2005** (2005) 056.

[108] J. Gaunt, M. Stahlhofen, F. J. Tackmann and J. R. Walsh, *N-jettiness subtractions for nnlo qcd calculations*, 2015. 10.48550/ARXIV.1505.04794.

[109] M. Czakon, *A novel subtraction scheme for double-real radiation at NNLO*, *Physics Letters B* **693** (2010) 259.

[110] M. Czakon, *Double-real radiation in hadronic top quark pair production as a proof of a certain concept*, *Nuclear Physics B* **849** (2011) 250.

[111] J. Currie, E. W. N. Glover and S. Wells, *Infrared structure at NNLO using antenna subtraction*, *Journal of High Energy Physics* **2013** (2013) .

[112] S. Catani and M. Grazzini, *Next-to-next-to-leading-order subtraction formalism in hadron collisions and its application to higgs-boson production at the large hadron collider*, *Physical Review Letters* **98** (2007) .

[113] C. Anastasiou, K. Melnikov and F. Petriello, *A new method for real radiation at next-to-next-to-leading order*, *Physical Review D* **69** (2004) .

[114] R. P. Feynman, *Very high-energy collisions of hadrons*, *Phys. Rev. Lett.* **23** (1969) 1415.

[115] J. D. Bjorken and E. A. Paschos, *Inelastic electron-proton and γ-proton scattering and the structure of the nucleon*, *Phys. Rev.* **185** (1969) 1975.

[116] X. Ji, Y. Liu, Y.-S. Liu, J.-H. Zhang and Y. Zhao, *Large-momentum effective theory*, *Reviews of Modern Physics* **93** (2021) .

[117] K. Cichy and M. Constantinou, *A guide to light-cone PDFs from lattice QCD: An overview of approaches, techniques, and results*, *Advances in High Energy Physics* **2019** (2019) 1.

[118] V. N. Gribov and L. N. Lipatov, *Deep inelastic e p scattering in perturbation theory*, *Sov. J. Nucl. Phys.* **15** (1972) 438.

[119] G. Altarelli and G. Parisi, *Asymptotic freedom in parton language*, *Nuclear Physics B* **126** (1977) 298.

[120] Y. L. Dokshitzer, *Calculation of the Structure Functions for Deep Inelastic Scattering and e+ e- Annihilation by Perturbation Theory in Quantum Chromodynamics.*, *Sov. Phys. JETP* **46** (1977) 641.

[121] G. Marchesini and B. R. Webber, *Simulation of QCD Jets Including Soft Gluon Interference*, *Nucl. Phys. B* **238** (1984) 1.

[122] P. Ilten, T. Menzo, A. Youssef and J. Zupan, *Modeling hadronization using machine learning*, 2022. 10.48550/ARXIV.2203.04983.

[123] S. Ferreres-Solé and T. Sjöstrand, *The space–time structure of hadronization in the lund model*, *The European Physical Journal C* **78** (2018) .

[124] G. S. Chahal and F. Krauss, *Cluster hadronisation in sherpa*, *SciPost Physics* **13** (2022) .

[125] G. Passarino and M. J. Veltman, "One-loop corrections for e^+e^- annihilation into $\mu^+\mu^-$ in the weinberg model." Nucl. Phys. B160, 151, 1979.

[126] R. P. G. Ossola, C. Papadopoulos, "Reducing full one-loop amplitudes to scalar integrals at the integrand level.." Nucl.Phys. , B763:147–169, 2007.

[127] V. Sotnikov, *Scattering amplitudes with the multi-loop numerical unitarity method*, Ph.D. thesis, Freiburg U., 9, 2019. 10.6094/UNIFR/151540.

[128] F. V. T. K. G. Chetyrkin, "Integration by parts: The algorithm to calculate β-functions in 4 loops." Nuclear Physics B, 192, Nov., 1981.

[129] J. Collins, "Renormalization." Cambridge Monographs on Math. Phy., 1984.

[130] A. Georgoudis and Y. Zhang, *Two-loop integral reduction from elliptic and hyperelliptic curves*, *JHEP Volume 2015, Issue 12* (2015) .

[131] S. Laporta, *High-precision calculation of multi-loop feynman integrals by difference equations*, Feb., 2001.

[132] C. Anastasiou and A. Lazopoulos, *Automatic integral reduction for higher order perturbative calculations*, *JHEP* **07** (2004) 046 [hep-ph/0404258].

[133] P. Maierhöfer and J. Usovitsch, *Kira 1.2 release notes*, 2018. 10.48550/ARXIV.1812.01491.

[134] A. V. Smirnov, *FIRE5: a C++ implementation of Feynman Integral REduction*, *Comput. Phys. Commun.* **189** (2015) 182 [1408.2372].

[135] A. von Manteuffel and C. Studerus., *Reduze 2 - distributed feynman integral reduction*, 2012.

[136] R. N. Lee, *LiteRed 1.4: a powerful tool for reduction of multiloop integrals*, *Journal of Physics: Conference Series* **523** (2014) 012059.

[137] P. U. P. Maierhoefer, J. Usovitsch, *Kira - a feynman integral reduction program*, arXiv:1705.05610 [hep-ph].

[138] E. Panzer, *Algorithms for the symbolic integration of hyperlogarithms with applications to feynman integrals*, *Computer Physics Communications* **188** (2015) 148–166.

[139] A. Smirnov, *Fiesta4: Optimized feynman integral calculations with gpu support*, *Computer Physics Communications* **204** (2016) 189–199.

[140] I. Dubovyk, J. Gluza, T. Riemann and J. Usovitsch, *Numerical integration of massive two-loop mellin-barnes integrals in minkowskian regions*, 2016. 10.48550/ARXIV.1607.07538.

[141] G. Heinrich, S. Jahn, S. P. Jones, M. Kerner, F. Langer, V. Magerya et al., *Expansion by regions with pysecdec*, 2021.

[142] Z. Capatti, V. Hirschi, D. Kermanschah, A. Pelloni and B. Ruijl, *Numerical loop-tree duality: contour deformation and subtraction*, *Journal of High Energy Physics* **2020** (2020) .

[143] F. Driencourt-Mangin, G. Rodrigo, G. F. R. Sborlini and W. J. T. Bobadilla, *On the interplay between the loop-tree duality and helicity amplitudes*, 2021.

[144] A. V. Kotikov, *Differential equation method: The Calculation of N point Feynman diagrams*, *Phys. Lett. B* **267** (1991) 123.

[145] T. Gehrmann and E. Remiddi, *Differential equations for two-loop four-point functions*, *Nuclear Physics B* **580** (2000) 485–518.

[146] Z. Bern, L. Dixon and D. A. Kosower, *Dimensionally-regulated pentagon integrals*, *Nuclear Physics B* **412** (1994) 751–816.

[147] N. Arkani-Hamed, J. Bourjaily, F. Cachazo and J. Trnka, *Local integrals for planar scattering amplitudes*, *Journal of High Energy Physics* **2012** (2012) .

[148] S. Bloch, M. Kerr and P. Vanhove, *A feynman integral via higher normal functions*, *Compositio Mathematica* **151** (2015) 2329–2375.

[149] S. Bloch, M. Kerr and P. Vanhove, *Local mirror symmetry and the sunset feynman integral*, 2018.

[150] J. L. Bourjaily, Y.-H. He, A. J. McLeod, M. von Hippel and M. Wilhelm, *Traintracks through calabi-yau manifolds: Scattering amplitudes beyond elliptic polylogarithms*, *Physical Review Letters* **121** (2018) .

[151] J. L. Bourjaily, A. J. McLeod, M. von Hippel and M. Wilhelm, *Bounded collection of feynman integral calabi-yau geometries*, *Physical Review Letters* **122** (2019) .

[152] A. Klemm, C. Nega and R. Safari, *The l-loop banana amplitude from gkz systems and relative calabi-yau periods*, *Journal of High Energy Physics* **2020** (2020) .

[153] K. Bönisch, F. Fischbach, A. Klemm, C. Nega and R. Safari, *Analytic structure of all loop banana integrals*, *Journal of High Energy Physics* **2021** (2021) .

[154] K. Bönisch, C. Duhr, F. Fischbach, A. Klemm and C. Nega, *Feynman integrals in dimensional regularization and extensions of calabi-yau motives*, 2021.

[155] J. Broedel, C. Duhr and N. Matthes, *Meromorphic modular forms and the three-loop equal-mass banana integral*, 2021.

[156] J. Broedel, N. Matthes, G. Richter and O. Schlotterer, *Twisted elliptic multiple zeta values and non-planar one-loop open-string amplitudes*, *Journal of Physics A: Mathematical and Theoretical* **51** (2018) 285401.

[157] J. Broedel, C. Duhr, F. Dulat, B. Penante and L. Tancredi, *Elliptic symbol calculus: from elliptic polylogarithms to iterated integrals of eisenstein series*, *Journal of High Energy Physics* **2018** (2018) .

[158] M. Walden and S. Weinzierl, *Numerical evaluation of iterated integrals related to elliptic feynman integrals*, *Computer Physics Communications* **265** (2021) 108020.

[159] S. Weinzierl, *Modular transformations of elliptic feynman integrals*, *Nuclear Physics B* **964** (2021) 115309.

[160] H. Frellesvig, C. Vergu, M. Volk and M. von Hippel, *Cuts and isogenies*, *Journal of High Energy Physics* **2021** (2021) .

[161] C. Bogner and F. Brown, *Feynman integrals and iterated integrals on moduli spaces of curves of genus zero*, 2015.

[162] J. L. Bourjaily, A. J. McLeod, M. von Hippel and M. Wilhelm, *Bounded collection of feynman integral calabi-yau geometries*, *Physical Review Letters* **122** (2019) .

[163] L. Adams and S. Weinzierl, *The ϵ-form of the differential equations for feynman integrals in the elliptic case*, *Physics Letters B* **781** (2018) 270–278.

[164] A. Levin and G. Racinet, *Towards multiple elliptic polylogarithms*, .

[165] F. C. S. Brown and A. Levin, *Multiple elliptic polylogarithms*, 2013.

[166] J. Ablinger, J. Blümlein, A. De Freitas, M. van Hoeij, E. Imamoglu, C. G. Raab et al., *Iterated elliptic and hypergeometric integrals for feynman diagrams*, *Journal of Mathematical Physics* **59** (2018) 062305.

[167] S. Abreu, J. Dormans, F. Febres Cordero, H. Ita, M. Kraus, B. Page et al., *Caravel: A C++ framework for the computation of multi-loop amplitudes with numerical unitarity*, *Comput. Phys. Commun.* **267** (2021) 108069 [2009.11957].

[168] D. A. Kosower, "Direct solution of integration-by-parts systems." arXiv:1804.00131 [hep-ph], Mar., 2018.

[169] R. E. Cutkosky, *Singularities and discontinuities of Feynman amplitudes*, *J. Math. Phys.* **1** (1960) 429.

[170] P. A. Baikov, "Explicit solutions of the three loop vacuum integral recurrence relations." Phys. Lett. B385:404–410, 1996.

[171] O. V. Tarasov, *Connection between feynman integrals having different values of the space-time dimension*, *Physical Review D* **54** (1996) 6479.

[172] D. J. Broadhurst, "Summation of an infinite series of ladder diagrams." Physics Letters B 307 1-2, 1993.

[173] D. Simmons-Duffin, "Projectors, shadows, and conformal blocks." arXiv:1204.3894 [hep-th], 2012.

[174] S. Abreu, R. Britto, C. Duhr and E. Gardi, *Cuts from residues: the one-loop case*, *JHEP* **06** (2017) 114 [1702.03163].

[175] Z. Bern, M. Enciso, H. Ita and M. Zeng, *Dual Conformal Symmetry, Integration-by-Parts Reduction, Differential Equations and the Nonplanar Sector*, *Phys. Rev.* **D96** (2017) 096017 [1709.06055].

[176] B. Buchberger, "Theoretical basis for the reduction of polynomials to canonical forms." ACM SIGSAM Bulletin. ACM. 10 (3): 19–29., Aug., 1976.

[177] L. E. Dickson, *Finiteness of the odd perfect and primitive abundant numbers with n distinct prime factors*, *American Journal of Mathematics* **35** (1913) 413.

[178] W. Decker, G.-M. Greuel, G. Pfister and H. Schönemann, SINGULAR *4-1-0 — A computer algebra system for polynomial computations*, 2016.

[179] J.-C. Faugère, "A new efficient algorithm for computing gröbner bases (f4)." Journal of Pure and Applied Algebra. Elsevier Science. 139 (1): 61–88, June, 1999.

[180] F.-O. Schreyer, "Die berechnung von syzygien mit dem verallgemeinerten weierstrass'schen divisionssatz." Diplom Thesis, University of Hamburg, Germany.

[181] R. M. Schabinger, *A New Algorithm For The Generation Of Unitarity-Compatible Integration By Parts Relations*, *JHEP* **01** (2012) 077 [1111.4220].

[182] D. Hilbert, *Ueber die vollen invariantensysteme*, *Mathematische Annalen* **42** (1893) 313.

[183] H. Ita, *Two-loop integrand decomposition into master integrals and surface terms*, *arXiv:1510.05626v1 [hep-th]* (2015) .

[184] S. Caron-Huot and K. J. Larsen, *Uniqueness of two-loop master contours*, *JHEP* **10** (2012) 026 [1205.0801].

[185] R. N. Lee and A. A. Pomeransky, *Critical points and number of master integrals*, *JHEP* **11** (2013) 165 [1308.6676].

[186] H. Frellesvig, F. Gasparotto, M. K. Mandal, P. Mastrolia, L. Mattiazzi and S. Mizera, *Vector space of feynman integrals and multivariate intersection numbers*, *Phys. Rev. Lett.* **123** (2019) 201602.

[187] P. Mastrolia and S. Mizera, *Feynman integrals and intersection theory*, *Journal of High Energy Physics* **2019** (2019) .

[188] H. Frellesvig, F. Gasparotto, S. Laporta, M. K. Mandal, P. Mastrolia, L. Mattiazzi et al., *Decomposition of Feynman Integrals on the Maximal Cut by Intersection Numbers*, *JHEP* **05** (2019) 153 [1901.11510].

[189] S. Mizera and A. Pokraka, *From infinity to four dimensions: higher residue pairings and feynman integrals*, *Journal of High Energy Physics* **2020** (2020) .

[190] S. Mizera, *Status of Intersection Theory and Feynman Integrals*, *PoS* **MA2019** (2019) 016 [2002.10476].

[191] H. Frellesvig, F. Gasparotto, S. Laporta, M. K. Mandal, P. Mastrolia, L. Mattiazzi et al., *Decomposition of feynman integrals by multivariate intersection numbers*, *Journal of High Energy Physics* **2021** (2021) .

[192] Y. Z. K. J. Larsen, "ntegration-by-parts reductions from unitarity cuts and algebraic geometry." Phys. Rev. , D93(4):041701, 2016.

[193] A. V. Smirnov, *FIESTA4: Optimized Feynman integral calculations with GPU support*, *Comput. Phys. Commun.* **204** (2016) 189 [1511.03614].

[194] M. L. Mangano, *The Color Structure of Gluon Emission*, *Nucl. Phys. B* **309** (1988) 461.

[195] F. A. Berends and W. T. Giele, *Recursive Calculations for Processes with n Gluons*, *Nucl. Phys.* **B306** (1988) 759.

[196] N. Bohr, R. Peierls and G. Placzek, *Nuclear Reactions in the Continuous Energy Region*, *Nature* **144** (1939) 200.

[197] R. Britto, F. Cachazo, B. Feng and E. Witten, *Direct proof of the tree-level scattering amplitude recursion relation in yang-mills theory*, *Physical Review Letters* **94** (2005) .

[198] R. K. Ellis and G. Zanderighi, "Scalar one-loop integrals for qcd." arXiv:0712.1851 [hep-ph], Dec., 2007.

[199] R. V. Harlander, *Virtual corrections to gg→h to two loops in the heavy top limit*, *Physics Letters B* **492** (2000) 74.

[200] G. 't Hooft, "A planar diagram theory for strong interactions." Nuclear Physics B. 72 (3): 461., 1974.

[201] S. Catani, *The Singular behavior of QCD amplitudes at two loop order*, *Phys. Lett.* **B427** (1998) 161 [hep-ph/9802439].

[202] T. Becher and M. Neubert, *Infrared singularities of scattering amplitudes in perturbative QCD*, *Phys. Rev. Lett.* **102** (2009) 162001 [0901.0722].

[203] E. Gardi and L. Magnea, *Factorization constraints for soft anomalous dimensions in QCD scattering amplitudes*, *JHEP* **03** (2009) 079 [0901.1091].

[204] A. Broggio, C. Gnendiger, A. Signer, D. Stöckinger and A. Visconti, *SCET approach to regularization-scheme dependence of QCD amplitudes*, *JHEP* **01** (2016) 078 [1506.05301].

[205] S. Weinzierl, *Does one need the O(epsilon)- and O(epsilonˆ2)-terms of one-loop amplitudes in an NNLO calculation ?*, *Phys. Rev. D* **84** (2011) 074007 [1107.5131].

[206] A. B. Goncharov, M. Spradlin, C. Vergu and A. Volovich, *Classical Polylogarithms for Amplitudes and Wilson Loops*, *Phys. Rev. Lett.* **105** (2010) 151605 [1006.5703].

[207] C. Duhr, H. Gangl and J. R. Rhodes, *From polygons and symbols to polylogarithmic functions*, *JHEP* **10** (2012) 075 [1110.0458].

[208] C. Duhr, *Hopf algebras, coproducts and symbols: an application to Higgs boson amplitudes*, *JHEP* **08** (2012) 043 [1203.0454].

[209] S. Abreu, F. Febres Cordero, H. Ita, B. Page and V. Sotnikov, *Planar Two-Loop Five-Parton Amplitudes from Numerical Unitarity*, *JHEP* **11** (2018) 116 [1809.09067].

[210] Z. Bern, L. J. Dixon, D. C. Dunbar and D. A. Kosower, *Fusing gauge theory tree amplitudes into loop amplitudes*, *Nucl. Phys.* **B435** (1995) 59 [hep-ph/9409265].

[211] Z. Bern, L. J. Dixon, D. A. Kosower and S. Weinzierl, *One loop amplitudes for e+ e- —> anti-q q anti-Q Q*, *Nucl. Phys. B* **489** (1997) 3 [hep-ph/9610370].

[212] Z. Bern, L. J. Dixon and D. A. Kosower, *Two-loop $g \to gg$ splitting amplitudes in QCD*, *JHEP* **08** (2004) 012 [hep-ph/0404293].

[213] R. K. Ellis, W. T. Giele and Z. Kunszt, *A Numerical Unitarity Formalism for Evaluating One-Loop Amplitudes*, *JHEP* **03** (2008) 003 [0708.2398].

[214] W. T. Giele, Z. Kunszt and K. Melnikov, *Full one-loop amplitudes from tree amplitudes*, *JHEP* **04** (2008) 049 [0801.2237].

[215] A. Ochirov and B. Page, *Full Colour for Loop Amplitudes in Yang-Mills Theory*, *JHEP* **02** (2017) 100 [1612.04366].

[216] A. Ochirov and B. Page, *Multi-Quark Colour Decompositions from Unitarity*, *JHEP* **10** (2019) 058 [1908.02695].

[217] F. R. Anger and V. Sotnikov, *On the Dimensional Regularization of QCD Helicity Amplitudes With Quarks*, 1803.11127.

[218] S. Abreu, J. Dormans, F. Febres Cordero, H. Ita, B. Page and V. Sotnikov, *Analytic Form of the Planar Two-Loop Five-Parton Scattering Amplitudes in QCD*, *JHEP* **05** (2019) 084 [1904.00945].

[219] A. Hodges, *Eliminating spurious poles from gauge-theoretic amplitudes*, *JHEP* **05** (2013) 135 [0905.1473].

[220] M. Heller and A. von Manteuffel, *MultivariateApart: Generalized Partial Fractions*, 2101.08283.

[221] R. Britto, F. Cachazo and B. Feng, *Generalized unitarity and one-loop amplitudes in N=4 super-Yang-Mills*, *Nucl. Phys.* **B725** (2005) 275 [hep-th/0412103].

[222] K. Risager, *A direct proof of the csw rules*, *Journal of High Energy Physics* **2005** (2005) 003–003 [hep-th/0508206].

[223] H. Elvang, D. Z. Freedman and M. Kiermaier, *Proof of the MHV vertex expansion for all tree amplitudes in N=4 SYM theory*, *JHEP* **06** (2009) 068 [0811.3624].

[224] B. Page, "Sagex mathematica and maple schools: Lectures on finite fields and large ansätze." January, 2021.

[225] T. Thiele, *Interpolationsrechnung*, Cornell University Library historical math monographs. B.G. Teubner, 1909.

[226] S. Badger, H. B. Hartanto, J. Kryś and S. Zoia, *Two-loop leading-colour QCD helicity amplitudes for Higgs boson production in association with a bottom-quark pair at the LHC*, 2107.14733.

[227] W. H. Press, S. A. Teukolsky, W. T. Vetterling and B. P. Flannery, *Numerical recipes: the art of scientific computing*. Cambridge University Press, 3rd ed., 2007.

[228] G. De Laurentis and B. Page, *Constructing compact ansätze for scattering amplitudes*, 2022. 10.48550/ARXIV.2207.10125.

[229] S. Abreu, F. F. Cordero, H. Ita, M. Klinkert, B. Page and V. Sotnikov, *Leading-color two-loop amplitudes for four partons and a w boson in QCD*, *Journal of High Energy Physics* **2022** (2022) .

[230] D. M. Walker, *Higher Order QCD Corrections to Electroweak Boson Production at Colliders*, Ph.D. thesis, Durham U., 2019.

[231] A. G.-D. Ridder, T. Gehrmann, N. Glover, A. Huss and D. Walker, *Nnlo qcd corrections to w+jet production in nnlojet*, 2018. 10.48550/ARXIV.1807.09113.

[232] A. Gehrmann-De Ridder, T. Gehrmann, E. W. N. Glover, A. Huss and D. M. Walker, *Vector boson production in association with a jet at forward rapidities*, 2019. 10.48550/ARXIV.1901.11041.

[233] A. Collaboration, *Measurement of $ww/wz \to \ell\nu qq'$ production with the hadronically decaying boson reconstructed as one or two jets in pp collisions at $\sqrt{s} = 8$ tev with atlas, and constraints on anomalous gauge couplings*, *The European Physical Journal C* **77** (2017) .

[234] ATLAS collaboration, G. Aad et al., *Measurements of WH and ZH production in the $H \to b\bar{b}$ decay channel in pp collisions at 13 TeV with the ATLAS detector*, *Eur. Phys. J. C* **81** (2021) 178 [2007.02873].

[235] Z. Bern, L. J. Dixon and D. A. Kosower, *One-loop amplitudes for e^+ e^- to four partons*, *Nucl. Phys.* **B513** (1998) 3 [hep-ph/9708239].

[236] C. Gnendiger et al., *To d, or not to d: recent developments and comparisons of regularization schemes*, *Eur. Phys. J. C* **77** (2017) 471 [1705.01827].

[237] A. V. Smirnov, *Algorithm FIRE – Feynman Integral REduction*, *JHEP* **10** (2008) 107 [0807.3243].

[238] C. F. Berger, Z. Bern, L. J. Dixon, F. Febres Cordero, D. Forde, H. Ita et al., *An Automated Implementation of On-Shell Methods for One-Loop Amplitudes*, *Phys. Rev.* **D78** (2008) 036003 [0803.4180].

[239] H. B. Hartanto, S. Badger, C. Brønnum-Hansen and T. Peraro, *A numerical evaluation of planar two-loop helicity amplitudes for a W-boson plus four partons*, *JHEP* **09** (2019) 119 [1906.11862].

[240] S. Larin, *The Renormalization of the axial anomaly in dimensional regularization*, *Phys. Lett. B* **303** (1993) 113 [hep-ph/9302240].

[241] S. Abreu, F. Febres Cordero, H. Ita, B. Page and V. Sotnikov, *Leading-color two-loop QCD corrections for three-jet production at hadron colliders*, *JHEP* **07** (2021) 095 [2102.13609].

[242] D. Chicherin, J. M. Henn and G. Papathanasiou, *Cluster algebras for Feynman integrals*, *Phys. Rev. Lett.* **126** (2021) 091603 [2012.12285].

[243] G. Ferrera, M. Grazzini and F. Tramontano, *Associated higgs- w -boson production at hadron colliders: A fully exclusive qcd calculation at nnlo*, *Physical Review Letters* **107** (2011) .

[244] G. Ferrera, M. Grazzini and F. Tramontano, *Associated ZH production at hadron colliders: The fully differential NNLO QCD calculation*, *Physics Letters B* **740** (2015) 51.

[245] G. Ferrera, G. Somogyi and F. Tramontano, *Associated production of a higgs boson decaying into bottom quarks at the LHC in full NNLO QCD*, *Physics Letters B* **780** (2018) 346.

[246] J. M. Campbell, R. K. Ellis, Y. Li and C. Williams, *Predictions for diphoton production at the LHC through NNLO in QCD*, *Journal of High Energy Physics* **2016** (2016) .

[247] R. V. Harlander and W. B. Kilgore, *Higgs boson production in bottom quark fusion at next-to-next-to-leading order*, *Physical Review D* **68** (2003) .

[248] R. V. Harlander, H. Mantler, S. Marzani and K. J. Ozeren, *Higgs production in gluon fusion at next-to-next-to-leading order QCD for finite top mass*, *The European Physical Journal C* **66** (2010) 359.

[249] S. Buehler, F. Herzog, A. Lazopoulos and R. Mueller, *The fully differential hadronic production of a higgs boson through bottom-quark fusion at NNLO*, *Journal of High Energy Physics* **2012** (2012) .

[250] S. Marzani, R. D. Ball, V. D. Duca, S. Forte and A. Vicini, *Higgs production via gluon–gluon fusion with finite top mass beyond next-to-leading order*, *Nuclear Physics B* **800** (2008) 127.

[251] R. V. Harlander and K. J. Ozeren, *Finite top mass effects for hadronic higgs production at next-to-next-to-leading order*, *Journal of High Energy Physics* **2009** (2009) 088.

[252] A. Pak, M. Rogal and M. Steinhauser, *Finite top quark mass effects in NNLO higgs boson production at LHC*, *Journal of High Energy Physics* **2010** (2010) .

[253] T. Neumann and M. Wiesemann, *Finite top-mass effects in gluon-induced higgs production with a jet-veto at NNLO*, *Journal of High Energy Physics* **2014** (2014) .

[254] S. Catani, L. Cieri, D. de Florian, G. Ferrera and M. Grazzini, *Diphoton production at hadron colliders: A fully differential QCD calculation at next-to-next-to-leading order*, *Physical Review Letters* **108** (2012) .

[255] M. Grazzini, S. Kallweit, D. Rathlev and A. Torre, *$Z\gamma$ production at hadron colliders in NNLO QCD*, *Physics Letters B* **731** (2014) 204.

[256] M. Grazzini, S. Kallweit and D. Rathlev, *Wgamma and zgamma production at the lhc in nnlo qcd*, 2015. 10.48550/ARXIV.1504.01330.

[257] J. M. Campbell, T. Neumann and C. Williams, *$Z\gamma$ production at NNLO including anomalous couplings*, *Journal of High Energy Physics* **2017** (2017) .

[258] T. Gehrmann, N. Glover, A. Huss and J. Whitehead, *Scale and isolation sensitivity of diphoton distributions at the LHC*, *Journal of High Energy Physics* **2021** (2021) .

[259] F. Cascioli, T. Gehrmann, M. Grazzini, S. Kallweit, P. Maierhöfer, A. von Manteuffel et al., *ZZ production at hadron colliders in NNLO QCD*, *Physics Letters B* **735** (2014) 311.

[260] M. Grazzini, S. Kallweit and D. Rathlev, *ZZ production at the LHC: Fiducial cross sections and distributions in NNLO QCD*, *Physics Letters B* **750** (2015) 407.

[261] G. Heinrich, S. Jahn, S. P. Jones, M. Kerner and J. Pires, *NNLO predictions for z-boson pair production at the LHC*, *Journal of High Energy Physics* **2018** (2018) .

[262] S. Kallweit and M. Wiesemann, *ZZ production at the LHC: NNLO predictions for $2\ell 2\nu$ and 4ℓ signatures*, *Physics Letters B* **786** (2018) 382.

[263] T. Gehrmann, M. Grazzini, S. Kallweit, P. Maierhöfer, A. von Manteuffel, S. Pozzorini et al., *w^+w^--production at hadron colliders in next to next to leading order qcd*, *Physical Review Letters* **113** (2014) .

[264] M. Grazzini, S. Kallweit, S. Pozzorini, D. Rathlev and M. Wiesemann, *$W + w$ - production at the LHC: fiducial cross sections and distributions in NNLO QCD*, *Journal of High Energy Physics* **2016** (2016) .

[265] M. Grazzini, S. Kallweit, D. Rathlev and M. Wiesemann, *$W^{\pm}z$ production at hadron colliders in NNLO QCD*, *Physics Letters B* **761** (2016) 179.

[266] M. Grazzini, S. Kallweit, D. Rathlev and M. Wiesemann, *$W \pm z$ production at the LHC: fiducial cross sections and distributions in NNLO QCD*, *Journal of High Energy Physics* **2017** (2017) .

[267] D. de Florian and J. Mazzitelli, *Higgs boson pair production at next-to-next-to-leading order in QCD*, *Physical Review Letters* **111** (2013) .

[268] D. de Florian, M. Grazzini, C. Hanga, S. Kallweit, J. M. Lindert, P. Maierhöfer et al., *Differential higgs boson pair production at next-to-next-to-leading order in QCD*, *Journal of High Energy Physics* **2016** (2016) .

[269] M. Grazzini, G. Heinrich, S. Jones, S. Kallweit, M. Kerner, J. M. Lindert et al., *Higgs boson pair production at NNLO with top quark mass effects*, *Journal of High Energy Physics* **2018** (2018) .

[270] J. Baglio, A. Djouadi, R. Gröber, M. Mühlleitner, J. Quevillon and M. Spira, *The measurement of the higgs self-coupling at the LHC: theoretical status*, *Journal of High Energy Physics* **2013** (2013) .

[271] H. T. Li and J. Wang, *Fully differential higgs pair production in association with a w boson at next-to-next-to-leading order in QCD*, *Physics Letters B* **765** (2017) 265.

[272] D. de Florian, I. Fabre and J. Mazzitelli, *Triple higgs production at hadron colliders at NNLO in QCD*, *Journal of High Energy Physics* **2020** (2020) .

[273] S. Kallweit, V. Sotnikov and M. Wiesemann, *Triphoton production at hadron colliders in NNLO QCD*, *Physics Letters B* **812** (2021) 136013.

[274] H. A. Chawdhry, M. Czakon, A. Mitov and R. Poncelet, *NNLO QCD corrections to three-photon production at the LHC*, *Journal of High Energy Physics* **2020** (2020) .

[275] S. Abreu, B. Page, E. Pascual and V. Sotnikov, *Leading-color two-loop QCD corrections for three-photon production at hadron colliders*, *Journal of High Energy Physics* **2021** (2021) .

[276] C. Arnesen, I. Z. Rothstein and J. Zupan, *Smoking Guns for On-Shell New Physics at the LHC*, *Phys. Rev. Lett.* **103** (2009) 151801 [0809.1429].

[277] A. Banfi, A. Martin and V. Sanz, *Probing top-partners in Higgs+jets*, *JHEP* **08** (2014) 053 [1308.4771].

[278] A. Azatov and A. Paul, *Probing Higgs couplings with high p_T Higgs production*, *JHEP* **01** (2014) 014 [1309.5273].

[279] C. Grojean, E. Salvioni, M. Schlaffer and A. Weiler, *Very boosted Higgs in gluon fusion*, *JHEP* **05** (2014) 022 [1312.3317].

[280] R. V. Harlander and T. Neumann, *Probing the nature of the Higgs-gluon coupling*, *Phys. Rev. D* **88** (2013) 074015 [1308.2225].

[281] S. Dawson, I. M. Lewis and M. Zeng, *Effective field theory for Higgs boson plus jet production*, *Phys. Rev. D* **90** (2014) 093007 [1409.6299].

[282] U. Langenegger, M. Spira and I. Strebel, *Testing the Higgs Boson Coupling to Gluons*, 1507.01373.

[283] M. Grazzini, A. Ilnicka, M. Spira and M. Wiesemann, *Modeling BSM effects on the Higgs transverse-momentum spectrum in an EFT approach*, *JHEP* **03** (2017) 115 [1612.00283].

[284] N. Deutschmann, C. Duhr, F. Maltoni and E. Vryonidou, *Gluon-fusion Higgs production in the Standard Model Effective Field Theory*, *JHEP* **12** (2017) 063 [1708.00460].

[285] M. Battaglia, M. Grazzini, M. Spira and M. Wiesemann, *Sensitivity to BSM effects in the Higgs p_T spectrum within SMEFT*, 2109.02987.

[286] K. Becker et al., *Precise predictions for boosted Higgs production*, 2005.07762.

[287] S. P. Jones, M. Kerner and G. Luisoni, *Next-to-Leading-Order QCD Corrections to Higgs Boson Plus Jet Production with Full Top-Quark Mass Dependence*, *Phys. Rev. Lett.* **120** (2018) 162001 [1802.00349].

[288] J. M. Lindert, K. Kudashkin, K. Melnikov and C. Wever, *Higgs bosons with large transverse momentum at the LHC*, *Phys. Lett. B* **782** (2018) 210 [1801.08226].

[289] T. Neumann, *NLO Higgs+jet production at large transverse momenta including top quark mass effects*, *J. Phys. Comm.* **2** (2018) 095017 [1802.02981].

[290] M. Kerner, *Top mass effects in HJ and HH production*, *PoS* **RADCOR2019** (2019) 020.

[291] X. Chen, A. Huss, S. P. Jones, M. Kerner, J.-N. Lang, J. M. Lindert et al., *Top-quark mass effects in h+jet and h+2 jets production*, *Journal of High Energy Physics* **2022** (2022) .

[292] V. Del Duca, W. Kilgore, C. Oleari, C. Schmidt and D. Zeppenfeld, *Higgs + 2 jets via gluon fusion*, *Phys. Rev. Lett.* **87** (2001) 122001 [hep-ph/0105129].

[293] V. Del Duca, W. Kilgore, C. Oleari, C. Schmidt and D. Zeppenfeld, *Gluon fusion contributions to H + 2 jet production*, *Nucl. Phys. B* **616** (2001) 367 [hep-ph/0108030].

[294] T. Neumann and C. Williams, *The Higgs boson at high p_T*, *Phys. Rev. D* **95** (2017) 014004 [1609.00367].

[295] J. R. Andersen, J. D. Cockburn, M. Heil, A. Maier and J. M. Smillie, *Finite Quark-Mass Effects in Higgs Boson Production with Dijets at Large Energies*, *JHEP* **04** (2019) 127 [1812.08072].

[296] L. Budge, J. M. Campbell, G. De Laurentis, R. K. Ellis and S. Seth, *The one-loop amplitudes for Higgs + 4 partons with full mass effects*, *JHEP* **05** (2020) 079 [2002.04018].

[297] R. Boughezal, F. Caola, K. Melnikov, F. Petriello and M. Schulze, *Higgs boson production in association with a jet at next-to-next-to-leading order in perturbative QCD*, *JHEP* **06** (2013) 072 [1302.6216].

[298] X. Chen, T. Gehrmann, E. W. N. Glover and M. Jaquier, *Precise QCD predictions for the production of Higgs + jet final states*, *Phys. Lett. B* **740** (2015) 147 [1408.5325].

[299] R. Boughezal, F. Caola, K. Melnikov, F. Petriello and M. Schulze, *Higgs boson production in association with a jet at next-to-next-to-leading order*, *Phys. Rev. Lett.* **115** (2015) 082003 [1504.07922].

[300] R. Boughezal, C. Focke, W. Giele, X. Liu and F. Petriello, *Higgs boson production in association with a jet at NNLO using jettiness subtraction*, *Phys. Lett. B* **748** (2015) 5 [1505.03893].

[301] X. Chen, J. Cruz-Martinez, T. Gehrmann, E. W. N. Glover and M. Jaquier, *NNLO QCD corrections to Higgs boson production at large transverse momentum*, *JHEP* **10** (2016) 066 [1607.08817].

[302] J. M. Campbell, R. K. Ellis and G. Zanderighi, *Next-to-Leading order Higgs + 2 jet production via gluon fusion*, *JHEP* **10** (2006) 028 [hep-ph/0608194].

[303] H. van Deurzen, N. Greiner, G. Luisoni, P. Mastrolia, E. Mirabella, G. Ossola et al., *NLO QCD corrections to the production of Higgs plus two jets at the LHC*, *Phys. Lett. B* **721** (2013) 74 [1301.0493].

[304] S. Abreu, D. Chicherin, H. Ita, B. Page, V. Sotnkikov, W. Tschernow et al., *Two-Loop Master Integrals for Five-Point One-Mass Scattering (to appear)*, *???* **??** (2022) ???

[305] H. B. Hartanto, R. Poncelet, A. Popescu and S. Zoia, *Nnlo qcd corrections to $wb\bar{b}$ production at the lhc*, 2022. 10.48550/ARXIV.2205.01687.

[306] M. Mangano, "Introduction to qcd." Cern, TH Division, 1999.

[307] D. Kreimer, *The $\gamma(5)$ Problem and Anomalies: A Clifford Algebra Approach*, *Phys. Lett. B* **237** (1990) 59.

[308] J. G. Korner, D. Kreimer and K. Schilcher, *A Practicable gamma(5) scheme in dimensional regularization*, *Z. Phys. C* **54** (1992) 503.

[309] P. S. Wang, *A p-adic algorithm for univariate partial fractions*, in *SYMSAC '81*, 1981.

List of Abbreviations

- BCFW - Britto–Cachazo–Feng–Witten
- BSM - Beyond the Standard Model
- CDR - conventional dimensional regularisation
- CKM - Cabibbo-Kobayashi-Maskawa (in the context of flavour physics)
- CP - Charge-Parity conjugation
- DGLAP - Dokshitzer-Gribatov-Lipatow-Altarelli-Parisi
- eqn. - equation
- EW - Electroweak theory
- HV - 't Hooft Veltman-scheme
- HTL - heavy-top-loop
- IBP - integration-by-parts (used in the context of integration-by-parts relations)
- iff - if and only if
- IR - infrared
- ISP - irreducible scalar product
- LHC - Large Hadron Collider
- LSZ - Lehman-Symanzik-Zimmermann (used to describe the relation between amplitudes and correlation functions)
- MPL - multiple polylogarithms
- MS - minimal subtraction (in the context of renormalisation)
- $\overline{\text{MS}}$ - modified minimal subtraction (in the context of renormalisation)

- NLO - next-to-leading order
- NNLO - next-to-next-to-leading order
- PDF - parton distribution function
- SM - Standard Model of Particle Physics
- QCD - Quantum Chromodynamics
- QED -Quantum Electrodynamics
- QFD - Quantum Flavourdynamics
- QFT - Quantum field theory
- ref. -reference
- UV - ultraviolet (used to describe divergencies originating from the large loop momentum region)
- VBF - vector boson fusion
- VEV - vacuum expectation value

List of Figures

2.1 Examples for the different classes of Feynman diagrams. 18
(a) A disconnected diagram 18
(b) A connected tree-level diagram 18
(c) A connected loop-level diagram 18
2.2 One-loop corrections to the gluon propagator 26
(a) Quark bubble insertion 26
(b) Gluon bubble insertion 26
(c) Gluon tadpole insertion 26
(d) Ghost bubble insertion 26

3.1 Examples of our naming convention for topologies. 35
(a) Simple planar BoxBox 35
(b) Semi-simple non-planar BoxPentagon 35
(c) Generic factorizing TriangleBox 35
3.2 Two seemingly different integral topolgies which turn out to be equivalent. 36

4.1 The planar double-box with momentum space coordinates and region-space coordinates. 51

5.1 Visualization of the Berends-Giele recursion [195]. 79
5.2 Approximation of a gluon using two quark colour indices 82
(a) Leading-colour approximation for a simple gluon propagator: The colour flow is described by $\delta_{ik}\delta_{jl}$, omitting the factor $\frac{1}{N_c}\delta_{ij}\delta_{kl}$. 82
(b) Leading-colour approximation for the one-loop gluonic box diagram. . 82
5.3 Planar and non-planar gluonic diagrams with colour-flow lines. 82
(a) A colour planar one-loop box diagram. Every internal and external colout line yields a sum over fundamental colour indices. 82
(b) A colour non-planar diagram. Only external colour lines yield a sum over fundamental colour indices, because no closed colour line is present. Therefore, the diagram is supressed by $1/N_c$ compared to (a). 82

(c) A kinematically non-planar two-loop diagram. There is no colour configuration such that two closed colour lines appear, hence the diagram is automatically subleading in colour. 82
5.4 A kinematically non-planar diagram for Higgs production via gluon fusion. 83

6.1 Representative diagrams for the two partonic processes in eq. (6.1) 101
(a) Partonic process with gluons as external particles 101
(b) Partonic process with only quarks as external particles 101
6.2 Representative diagrams for the different contributions to $\mathcal{M}_{\mathrm{g}}$. 102
(a) N_f^0/N_c^0 102
(b) N_f^1/N_c^1 102
(c) N_f^2/N_c^2 102
6.3 Representative diagrams for the different contributions to $\mathcal{M}_{\mathrm{Q}}$. 102
(a) N_f^0/N_c^0 102
(b) N_f^1/N_c^1 102
(c) N_f^2/N_c^2 102
6.4 A non-planar diagram contributing to Z-boson production at order N_f^1/N_c^1. This type of contribution has a unique coupling structure proportional to the sum over the couplings of the Z to all quarks that can appear in the loop. It is therefore a gauge invariant piece that can be dropped consistently. 103
6.5 Representative Feynman diagrams for the individual contributions to the $q\bar{q} \to \gamma\gamma\gamma$ amplitude at two loops. These contributions scale differently with the number of colours, the number of light fermions and the charge of the external fermions and are therefore individually gauge invariant. The contribution $A^{(2,1)}$ is the only piece where all non-planar integral topologies contribute. 109
(a) $A^{(2,0)}$ 109
(b) $A^{(2,N_f)}$ 109
(c) $A^{(2,1)}$ 109
(d) $\tilde{A}^{(2,N_f)}$ 109
6.6 Representative diagrams of $\mathcal{M}_{qqQQ}$ at two loops. 113
(a) N_f^0/N_c^0 113
(b) N_f^1/N_c^1 113
(c) N_f^2/N_c^2 113
6.7 Representative diagrams of $\mathcal{M}_{ggqq}$ at two loops. 113
(a) N_f^0/N_c^0 113
(b) N_f^1/N_c^1 113
(c) N_f^2/N_c^2 113
6.8 Representative diagrams of $\mathcal{M}_{4g}$ at two loops. 113

(a) N_f^0/N_c^0 . . . 113
(b) N_f^1/N_c^1 . . . 113
(c) N_f^2/N_c^2 . . . 113
6.9 A non-planar diagram contributing to N_f^0/N_c^1. . . . 114

List of Tables

1.1 Fermion field content of the SM. The fermions are organized into left-chiral doublets with and without strong interaction, which are called quarks and leptons, resepectively. Additionally, there are two types of strongly interacting right-chiral fermions and one type of right-chiral fermions without strong interaction. Each of these particles appears in three generations which differ by their Yukawa interactions. Remarkably, the values of the hypercharge cannot be chosen arbitrarily but are constrained by requiring a cancellation of $U(1)_y$ anomalies [76]. 9

6.1 Characterizing information for remainders with $\kappa = \mathrm{Q}$ at various stages of the computation. The remainders are specified by the helicity states of the gluon pair and the power of N_f. $|K|$ is the dimension of the space of rational functions of the corresponding amplitude. We give the maximal Ansatz size in common denominator and partial-fraction form. The last column gives the largest number of non-zero monomial coefficients. Term counts are given to two significant digits for readability. 105

6.2 Information about the complexity for remainders with $\kappa = \mathrm{g}$ at various stages of the computation. Column headings are identical to table 6.2. Term counts are given to two significant digits for readability. 106

6.3 Degrees and ansatz size of each the most complex pentagon function coefficient of the 2-quark 3-photon finite remainders at various stages of the computation. The remainders are specified by their coupling structure and the helicities of the photons. Term counts are given to two digits for readability. 110

6.4 Information about non-planar amplitude coefficients in spinor form. 111

List of Publications

S. Abreu, F. Febres Cordero, H. Ita, M. Klinkert, B. Page, & V. Sotnikov (2022). Leading-color two-loop amplitudes for four partons and a W boson in QCD. *Journal of High Energy Physics, 2022(4).*

Abreu, S., De Laurentis, G., Ita, Klinkert, M., Page, B., & Sotnikov, V.. Full-Colour Two-Loop Helicity Amplitudes for 3-γ Production at the LHC *(to appear).*

Kurzzusammenfassung

In dieser Arbeit werden Methoden zur Berechnung von Zwei-Schleifen-Streumplituden weiterentwickelt und angewendet. Diese Amplituden werden benötigt, um für die Streuprozesse am Large Hadron Collider Korrekturen zu berechnen, welche in der starken Kopplungskonstante α_s zwei Ordnungen über der führenden Ordnung liegen (NNLO QCD Korrekturen).

Zur Berechnung von Streuamplituden werden Feynman-Integrale mit Hilfe von Relationen, welche durch partielle Integration gewonnen werden (IBP-Relationen) auf Master-Integrale reduziert. Wir präsentieren neue Methoden zur Berechnung solcher unitaritätskompatibler IBP-Relationen welche mit Hilfe bestimmter Vektorfelder (IBP-Vektoren) generiert werden. Wir verwenden eine Formulierung in einem konformen Einbettungsraum und kombinieren Methoden der algebraischen Geometrie mit linearer Algebra um solche Vektorfelder zu berechnen. Auf diese Weise werden Relationen erhalten, mit denen planare und nicht-planare Streuamplituden mit zwei schleifen und insgesamt fünf Teilchen in Anfangs- und Endzustand, von denen eines massiv sein kann auf Master-Integrale reduziert werden können.

In der numerischen Unitaritätsmethode werden die Integranden von Streuamplituden durch Master-Integrale und kompatible IBP-Relationen ausgedrückt. Diese Methode wird verwendet um die planaren Amplituden zu berechnen, welche zur Produktion eines W-Bosons (welches in ein Lepton und ein Neutrino zerfällt) zusammen mit zwei leichten Partonen beitragen, sowie die nicht-planaren Amplituden, welche zur Produktion von drei Photonen am LHC beitragen. Die analytische Form dieser Amplituden wird mittels funktioneller Rekonstruktion in einem Primzahlkörper erhalten. Dabei werden analyitsche Informationen über die Form der Amplitude verwendet um die Effizienz der Rekonstruktion zu steigern. Für die (nicht-planaren) Amplituden, die zur Produktion eines Higgs-Bosons zusammen mit zwei leichten Partonen in der Näherung schwerer Top-Quark-Schleifen beitragen wurden erste Phasenraumpunkte berechnet.

Wir erwarten, dass mit den vorhandenen Methoden die Higgs-Amplitude bald analytisch rekonstruiert werden kann und dass die analytischen Amplituden für Präzisionsvorhersagen genutzt werden können.

Acknowledgements

First, I would like to thank my first supervisor Harald Ita for giving me the opportunity to be part of his group and participate in the fascinating field of multi-loop amplitude computation. Thank you for your guidance, your advice and support. I am also thankful to my second supervisor Stefan Dittmaier for his consultations and his incentives to strive for higher standards. I am very grateful to all my colleagues for patiently mentoring me, for giving me the opportunity to collaborate with them and for sharing their insights with me. In particular I would like to thank Ben Page, Vasily Sotnikov, Samuel Abreu and Giuseppe de Laurentis.

My thanks go to Evgenij Pascual, Wladimir Tschernow, Jerry Dormans, Giuseppe de Laurentis and Claudia and Alfred Buhl for carefully reading parts of the manuscript and giving me the most valuable suggestions. I would like to thank my friends and family for their continuous assistance and encouragement and for supporting me in the moments of deepest frustration.

Finally, I would like to thank the "Graduiertenkolleg 2044" for supporting my work, but also for providing a unique and supportive environment of learning and sharing knowledge between different areas of particle physics.